

**Examination of IpLITR-mediated signal transduction events: the
cross-talk regulation of phagocytosis**

by

Myron Anthony Zwozdesky

A thesis submitted in partial fulfillment of the requirements for the degree of

Doctor of Philosophy
in
Physiology, Cell and Developmental Biology

Department of Biological Sciences
University of Alberta

© Myron Anthony Zwozdesky, 2019

ABSTRACT

Cells perceive their environment through cell surface-expressed transmembrane (TM) receptors. TM receptors transduce extracellular cues to highly sophisticated intracellular signaling pathways. Transduction of multiple signaling inputs fine-tunes the regulation of vital effector responses, such as phagocytosis. All metazoan species possess an innate immune system, which is critical for host protection and maintaining homeostasis. Multiple innate immune cell-types constantly sense the extracellular micro-environment through immunoregulatory receptors and several immunoregulatory receptor families have been identified in vertebrates. Members of the immunoglobulin superfamily (IgSF) are conserved throughout mammalian, avian, amphibian and fish species. Although some families contain highly diversified members in teleost fish, they operate via evolutionarily conserved principles of signaling for regulating effector responses. This has allowed the study of conserved signaling events and novel immunoregulatory receptor-mediated signal transduction capabilities using fish receptor models.

Channel catfish (*Ictalurus punctatus*) leukocyte immune-type receptors (IpLITRs) are a polygenic and polymorphic immunoregulatory receptor family that share structural and phylogenetic relationships with a number of vertebrate IgSF receptor-types. This family contains stimulatory and inhibitory forms that regulate several innate immune cell effector responses via classical as well as novel cytoplasmic tail (CYT)-dependent signaling capabilities. My thesis is focused on using an IpLITR model to better understand how receptor CYT signaling versatility affects the regulation of innate effector responses. Previous functional and biochemical characterizations were performed in innate immune cell-types. The stimulatory IpLITR 2.6b directly associated with the ITAM-containing adaptor molecule IpFcR γ -L and activated phagocytosis, cytokine secretion and degranulation in rat mast cells through highly conserved

pathways. Conversely, the inhibitory IpLITR 1.1b abrogated cytotoxicity via a predictable ITIM-dependent SHP pathway in mouse natural killer (NK) cells. Uniquely, IpLITR 1.1b could also use an ITIM-independent Csk pathway to abrogate cytotoxicity. Surprisingly, IpLITR 1.1b activated a unique ITAM-independent phagocytic phenotype in rat mast cells that occurs in two distinct actin polymerization-dependent stages to capture and then internalize targets. This functional plasticity placed IpLITR 1.1b into a growing category of ITIM-containing vertebrate receptors with versatile CYT-dependent signaling capabilities. Importantly, IpLITR 1.1b evokes different functional outcomes by switching its signaling potential between cell-types (i.e. NK cell vs. mast cell), however, detailed mechanistic studies of this potential had not been performed.

Non-immune epithelial cell-types do not express IgSF immune receptors, however, they express sub-membrane proximal signaling molecules and downstream effectors of actin polymerization. In other words, these cells only lack expression of a cell surface receptor capable of orchestrating sub-membrane signaling events to transduce extracellular target recognition into internalization. This effectively offers a cellular background for isolating receptor CYT-specific sub-membrane proximal signaling events away from co-activated pathway interference. This reductionist strategy for studying receptor signaling was used to define CYT signaling requirements of ITAM-containing receptors in mammals. Therefore, the overall objective of my thesis is to establish a non-immune epithelioid cell system to examine details of IpLITR CYT-dependent signaling versatility. My specific research aims were: (1) to characterize signaling molecule recruitment to the CYT of IpLITR 1.1b; (2) to examine IpLITR 1.1b CYT-dependent phagocytic signaling potential; (3) to establish an assay for measuring IpLITR CYT-dependent cross-talk signaling potential; and (4) to examine IpLITR 1.1b CYT requirements for down-regulating IpFcR γ -L CYT ITAM-driven phagocytosis.

My research has demonstrated that although IpLITR CYTs recruit various stimulatory signaling molecules, the functional outcome is predicted by the presence of canonical CYT motifs when expressed in epithelioid cells. Specifically, IpLITR 1.1b recruited Nck and Syk to the proximal and distal CYT segments, respectively, in GST pulldown assays. However, while IpFcR γ -L CYT ITAM activated phagocytosis in epithelioid cells, IpLITR 1.1b CYT did not. Furthermore, co-immunoprecipitation showed that the IpLITR 1.1b CYT recruited the inhibitory molecules Csk and SHP2 in physiologically activated cells using pervanadate. This facilitated a shift in my objectives based on previous IpLITR characterizations to assess a novel aspect of IpLITR signaling potential. IpLITRs contain highly conserved extracellular domains that may bind common targets and catfish immune cells co-express IpLITRs. Since the IpFcR γ -L CYT ITAM orchestrated sub-membrane signaling events that activated phagocytosis in epithelioid cells, I examined IpLITR 1.1b CYT-dependent sub-membrane proximal cross-talk signaling potential. Using a novel imaging flow cytometry-based phagocytosis assay, I demonstrated IpLITR 1.1b CYT-dependent cross-talk down-regulation of ITAM-driven phagocytic signaling upon co-cross-linking with bead targets. To examine the details of this down-regulation, I used site-directed mutagenesis, dominant-negative signaling molecule constructs and shRNA-mediated protein knockdown techniques. I showed that IpLITR 1.1b CYT-dependent down-regulation of phagocytosis requires both Y⁴⁵³ and Y⁴⁷⁷ for maximum inhibition, however, neither SHP2 nor Csk were critically involved. These results indicate that IpLITR 1.1b uses a novel proximal and distal CYT-dependent co-operative inhibitory signaling mechanism to down-regulate ITAM-driven phagocytosis. Overall, I have demonstrated novel inhibitory signaling capabilities for IpLITR 1.1b, including the first report of cross-talk signaling potential within a teleost immunoregulatory

receptor family. My work shows that teleost immunoregulatory receptors are excellent models to advance the understanding of innate immunoregulatory processes in vertebrates.

PREFACE

This thesis is the original work of Myron Anthony Zwozdesky. No animals were used during the completion of this research, therefore no ethics committee approval was required.

Chapter IV herein is published in part as Zwozdesky MA, Fei C, Lillico DME & Stafford JL (2017). Imaging flow cytometry and GST pulldown assays provide new insights into channel catfish leukocyte immune-type receptor-mediated phagocytic pathways. *Developmental & Comparative Immunology* **67**: 126-38.

Chapter V herein is published in part as Zwozdesky MA, Fei C & Stafford JL (2019). An imaging flow cytometry protocol for studying immunoregulatory receptor-mediated regulation of phagocytosis. *Methods in Molecular Biology*, accepted.

I collected and analyzed all data and wrote this book. Dr. James Stafford contributed philosophical, conceptual and technical guidance and edited this book. I supervised a number of undergraduate students: Julianna Deutscher (BIOL 499); Brittney Loney (BIOL 298); Lena Jones (BIOL 498); Ting Wang (BIOL 298); Samantha DeChamplain (BIOL 298); Sharon Rao (BIOL 298); Nicole Herbers (BIOL 298); Payal Kumar (BIOL 398); Pramalkumar Patel (BIOL 298); Hima Gurupalli (BIOL 499); Ifeoluwa Odeleye (BIOL 399).

DEDICATED

До пам'яті мого героя and #1 fan;

Тато,

you gave me the best advice and always said:

“Learn everything!”

Here's what I've learned, so far

ACKNOWLEDGEMENTS

This thesis was easier to accomplish because of the support of several people.

To James Stafford, who took on an undergraduate student who used two keywords while applying to labs: “cell signaling”. You embody several intangibles that make you a great supervisor; genuine enthusiasm, curiosity, passion and encouragement. You are a model of professionalism and scientific excellence that a young scientist should emulate while also balancing camaraderie and friendship, making you a great boss to work for and the lab a pleasant place to be. I was, am and always will be a sucker for a mechanism because of it. Thank you!

To my examining and committee members: Bart Hazes and Kathy Magor for taking the time to meet with me, letting me work in your lab, offer your insights on my project, but also identify weaknesses. Although some meetings are deliberately confrontational, it is part of the process; you made me a better scientist and thinker. Thank you! To Robert Ingham for participating in my examinations and providing reagents. Thank you! To Declan Ali, David Pilgrim and Keith Tierney; thank you for participating in my candidacy exam. To our sister lab supervisor Deborah Burshtyn: thank you for listening and engaging at our lab meetings. Your knowledge, passion and curiosity for science are evident but also accompanied by a welcoming, collegial aura that makes you easier to approach and a model to emulate. I hope to be colleagues with all of you going forward!

To my fellow co-workers, graduate and undergraduate students: Herman, Dustin, Harry, Hima, Enezi, Yemaya, Josh, Jacob, Danyel, Emmanuel, Michelle, Sydney, Kinola, Heather (for the YTS cells!), Chelsea, Marco, Ben, Li, Arashdeep (for the GTPase activation reagents!), Cameron (for the plasmids and cells!), Zuoqiao Wu (for the shRNA reagents and protocol!); thank you all for the scientific talks. I hope we collaborate someday. Good luck! To the unsung heroes of shipping/receiving: thank you Shelley, Ben, Debbie, Troy, Cheryl and other Bio Sci Store/MBSU employees for tracking down orders, following up on details and keeping my lab fully stocked, especially over loooong weekends 😊. Cheers!

To the Seahawks: my bro, Johnny Bridges! I am so thankful to have a team of lads with a love for hockey as great as mine. Being at the rink is one of my favourite places on Earth and after a long day/week at work, skating with you kept me relaxed, focused and fit. Is this the year?

To my family: my Мама, for prompting me to reconsider a graduate program at the U of A; for years of upbringing in such a supportive and loving home; I hope we stay close over the coming years and that I have made you proud. My thesis is dedicated to you too. To Ariana, Joe, Joshua and Talka Whitlow; Elizabeth, Nic, Olivia and Norah Moffatt; Баба and Gido Kinhnicki: seeing all of you and watching our families grow is the best. To my extended family, past and present: Баба Ана, Баба й дідо Kit, Bridgeses, Cionas, Farynas, Zwozdeskys, Michalaks, Browns, Olineks, Rudukes, Deptucks, Gulutsans, Pelechs, Bohonoses, Lazaruks. I cannot wait to celebrate birthdays, Christmas, Різдо, Easter and all of our traditions for years to come.

To my wife Krystal and son Charlie: You were by my side through the most challenging times of my life so far. I cannot imagine the past ten years nor the rest without you. My academic priority is finally done; you are my priority forever. I hope to repay the patience, understanding, support and inspiration that you gave me. I cannot wait to watch you grow up! Люблю!

TABLE OF CONTENTS

ABSTRACT.....	i
PREFACE.....	vi
DEDICATION	vii
ACKNOWLEDGEMENTS	viii
TABLE OF CONTENTS.....	ix
LIST OF TABLES	xiv
LIST OF FIGURES	xv
LIST OF ABBREVIATIONS.....	xviii

CHAPTER I INTRODUCTION

1.1 Introduction.....	1
1.2 Thesis objectives.....	3
1.3 Thesis overview	4

CHAPTER II LITERATURE REVIEW

2.1 Overview of innate immunity	10
2.1.1 Physical/chemical barriers.....	12
2.1.2 Cellular barriers.....	13
2.1.3 Innate immune cell effector responses	15
2.2 Immunoregulatory receptor-mediated control of effector responses.....	16
2.2.1 Currencies of signal transduction.....	17
2.2.2 Paired receptor paradigm.....	18
2.2.3 SH2 domains confer selective activation of phosphotyrosine-driven signaling pathways.....	20
2.2.3.1 Non-SH2 domain-mediated phosphotyrosine-dependent signaling	22
2.2.4 ITAM-dependent signaling	22
2.2.5 ITIM-dependent signaling.....	25
2.2.6 Immunoregulatory receptor-mediated signaling versatility and functional plasticity..	28
2.2.6.1 Non-ITAM- or ITIM-dependent signaling versatility	32
2.3 Diverse cytoplasmic tail (CYT)-dependent molecular mechanisms regulate effector responses	34
2.3.1 SFKs mediate activation of specific pathways.....	35
2.3.2 CYT requirements for differential signaling pathway activation.....	37
2.3.3 CYT-membrane interactions limit CYT motif availability	38
2.3.4 Pre-formed signaling molecule complexes	39
2.3.5 Transmembrane signaling complexes and actin polymerization control synapse formation	39

2.3.6	Sub-membrane organization controls receptor dynamics before and after phosphotyrosine-dependent cellular activation	41
2.3.6.1	Serine/threonine motifs and protein kinase A and C	41
2.3.6.2	Inside-out integrin activation	41
2.3.6.3	Actin-dependent sub-membrane receptor trafficking	42
2.4	Summary of receptor CYT-mediated regulation of signaling events	43
2.4.1	Immunoregulatory receptor cross-talk	44
2.4.2	Early and late progression of signaling events	46
2.4.3	Thesis objectives and aims	47

CHAPTER III

MATERIALS AND METHODS

3.1	Cell lines and antibodies	54
3.1.1	Cells	54
3.1.2	Antibodies	54
3.2	Cloning SH2 domain-containing signaling molecules into the FLAG epitope tag-encoding p3XFLAG-CMV14 expression vector	55
3.2.1	Generating dominant-negative Csk-FLAG and SHP2-FLAG signaling molecule constructs	56
3.3	Generating GST-CYT fusion protein constructs	56
3.3.1	Sub-cloning receptor CYT sequences into the GST vector, pFN2A	56
3.3.2	Synthesis and affinity purification of GST-CYT fusion proteins from <i>E. coli</i>	57
3.4	Generating HA epitope-tagged IpLITR 1.1b CYT receptor constructs	59
3.4.1	A chimeric IpLITR 1.1b/IpFcR γ -L WT _{CYT} phagocytic receptor construct	59
3.4.2	Site-directed mutagenesis to generate IpLITR 1.1b CYT YF mutant receptor constructs	59
3.4.3	Generating eGFP-tagged IpLITR 1.1b CYT receptor constructs	60
3.5	Generating stable IpLITR 1.1b CYT construct-expressing AD293 cell lines	61
3.6	Generating lentiviral shRNA-mediated signaling molecule protein knockdowns in stable IpLITR 1.1b/IpFcR γ -L WT _{CYT} -expressing AD293 cells	62
3.6.1	Producing lentiviral particle-containing supernatants from HEK293T cells	62
3.6.2	Lentiviral titering and generation of stable Csk and SHP2 knockdown IpFcR γ -L WT _{CYT} -expressing AD293 cell lines	62
3.7	Biochemical signaling molecule recruitment to IpLITR 1.1b CYT segments and motifs ..	63
3.7.1	Transient transfection of FLAG-tagged molecules into AD293 cells to generate FLAG-containing lysates	63
3.7.2	GST-CYT fusion protein pulldowns from FLAG-containing lysates	64
3.7.3	Co-immunoprecipitation and Western blotting from pervanadate-stimulated cells transiently transfected with FLAG-tagged signaling molecules	65
3.8	Imaging flow cytometry-based assays to assess IpLITR-mediated phagocytosis in AD293 cells	66

3.8.1	Measuring IpLITR-mediated phagocytosis of α HA-coated yellow green (YG) bead targets by component masking analysis	66
3.8.2	IpLITR 1.1b CYT construct-mediated cross-talk regulation of phagocytosis in co-transfected parental cells	67
3.8.3	Measuring eGFP-tagged IpLITR-mediated phagocytosis of α HA-coated light yellow (LY) bead targets by component masking analysis.....	67
3.8.4	Transient eGFP-tagged IpLITR 1.1b CYT construct transfection into stable IpLITR 1.1b/IpFcR γ -L WT _{CYT} - or IpLITR 2.6b/IpFcR γ -L WT _{CYT} -expressing cells.....	68
3.8.5	Transient eGFP-tagged IpLITR 1.1b CYT (IpLITR 1.1b CYT-eGFP) and dominant-negative FLAG-tagged Csk (Δ Csk-FLAG) or SHP2 (Δ SHP2-FLAG) construct co-transfection into stable IpFcR γ -L WT _{CYT} -expressing cells.....	68
3.8.6	Transient transfection of eGFP-tagged IpLITR 1.1b CYT constructs into stable Csk or SHP2 knockdown IpFcR γ -L WT _{CYT} -expressing cell lines	69
3.8.7	Statistical analysis	69

CHAPTER IV

BIOCHEMICAL AND FUNCTIONAL EXAMINATION OF IpLITR CYT-DEPENDENT PHAGOCYTOTIC SIGNALING POTENTIAL

4.1	INTRODUCTION	76
4.2	RESULTS	79
4.2.1	Synthesis and purification of GST-CYT fusion proteins in <i>E. coli</i>	79
4.2.2	Generation of cellular lysates containing FLAG-tagged SH2 domain-containing signaling molecules	80
4.2.3	Differential phosphotyrosine-dependent recruitment of C-terminal FLAG-tagged signaling molecules to the proximal and distal CYT segments of IpLITR 1.1b.....	80
4.2.4	α HA-coated bead-induced cross-linking of IpFcR γ -L WT _{CYT} , but not IpLITR 1.1b WT _{CYT} , induces CYT-dependent phagocytic signaling	82
4.2.5	Co-expressing IpLITR 1.1b WT _{CYT} with vSrc does not evoke phagocytic signaling .	84
4.2.6	Over-expressing Syk or SAP in IpLITR 1.1b WT _{CYT} -expressing cells does not activate phagocytic signaling.....	85
4.2.7	Pervanadate stimulation followed by co-immunoprecipitation show that IpLITR 1.1b WT _{CYT} recruits Csk and SHP2 to the proximal CYT motif Y ⁴⁵³ and distal CYT motif ITIM Y ⁴⁷⁷ , respectively	86
4.3	DISCUSSION	89

CHAPTER V

DEVELOPING NOVEL IMAGING FLOW CYTOMETRY-BASED PHAGOCYTOSIS ASSAYS TO CHARACTERIZE IpLITR 1.1b WT_{CYT}-MEDIATED CROSS-TALK INHIBITION OF ITAM-DRIVEN PHAGOCYTOTIC SIGNALING

5.1	INTRODUCTION	135
-----	--------------------	-----

5.2	RESULTS	138
5.2.1	IpLITR 1.1b WT _{CYT} mediates cross-talk inhibition of IpFcR γ -L WT _{CYT} -driven phagocytosis in transiently co-transfected AD293 cells	138
5.2.2	eGFP-tagged IpLITR 1.1b WT _{CYT} (IpLITR 1.1b WT _{CYT} -eGFP) mediates inhibition of IpFcR γ -L WT _{CYT} -driven phagocytosis through its proximal and distal CYT segment motifs.....	140
5.2.3	eGFP-tagged IpLITR 1.1b WT _{CYT} (IpLITR 1.1b WT _{CYT} -eGFP) mediates CYT motif-dependent cross-talk inhibition of ITAM-driven phagocytosis in IpFcR γ -L-expressing AD293 stable cells.....	142
5.2.4	Effect of receptor expression levels on eGFP-tagged IpLITR 1.1b WT _{CYT} (IpLITR 1.1b WT _{CYT} -eGFP)-mediated cross-talk inhibition of IpFcR γ -L WT _{CYT} -driven phagocytosis	144
5.3	DISCUSSION	146

CHAPTER VI

MOLECULAR CHARACTERIZATION OF IpLITR 1.1b WT_{CYT}- MEDIATED CROSS-TALK INHIBITION OF ITAM-DRIVEN PHAGOCYTTIC SIGNALING

6.1	INTRODUCTION	176
6.2	RESULTS	179
6.2.1	eGFP-tagged IpLITR 1.1b WT _{CYT} segments differentially modulate cross-talk inhibition of IpFcR γ -L WT _{CYT} -driven phagocytosis via proximal CYT Y ⁴⁵³ and distal CYT ITIM Y ⁴⁷⁷	179
6.2.2	Co-expressing IpLITR 1.1b Y ^{dist} _{FCYT} -eGFP with dominant-negative Csk does not restore IpFcR γ -L WT _{CYT} -driven phagocytosis.....	180
6.2.3	Co-expressing IpLITR 1.1b Y ^{prox} _{FCYT} with dominant-negative SHP2 partially restores phagocytic signaling through IpFcR γ -L WT _{CYT}	181
6.2.4	Csk knockdown does not reverse IpLITR 1.1b WT _{CYT} -mediated cross-talk inhibition of IpFcR γ -L WT _{CYT} -driven phagocytosis	182
6.2.5	SHP2 knockdown partially reverses IpLITR 1.1b WT _{CYT} -mediated cross-talk inhibition of IpFcR γ -L WT _{CYT} -driven phagocytosis.....	184
6.2.6	Effect of receptor expression levels on eGFP-tagged IpLITR 1.1b WT _{CYT} -mediated cross-talk inhibition of IpLITR 2.6b/IpFcR γ -L WT _{CYT} -driven phagocytosis.....	185
6.2.7	eGFP-tagged IpLITR 1.1b WT _{CYT} segments synergistically down-regulate IpLITR 2.6b/IpFcR γ -L WT _{CYT} -driven phagocytosis through distinct CYT motif Y ⁴⁵³ - and Y ⁴⁷⁷ -dependent pathways	186
6.3	DISCUSSION	187

CHAPTER VII

GENERAL DISCUSSION AND FUTURE DIRECTIONS

7.1	Summary of thesis findings	227
-----	----------------------------------	-----

7.2	Future directions	234
7.2.1	Mechanism(s) of IpLITR 1.1b WT _{CYT} segment-mediated cross-talk down-regulation of ITAM-driven phagocytosis	235
7.2.2	Potential roles for IpLITR signaling in channel catfish immune cells	236
7.2.3	Potential impact of LITR research on vaccine development and aquaculture	239
7.2.4	Establishing LITR-based <i>in/ex vivo</i> immune models in zebrafish and goldfish	241
7.2.5	Identification of LITR ligands	243
7.3	Concluding remarks	244
	REFERENCES.....	250

LIST OF TABLES

Table 3.1. Primers used to generate human FLAG-tagged SH2 domain-containing signaling molecules, including truncated (Δ) Csk-FLAG, SHP2-FLAG and Syk-FLAG, from AD293 cells and Avian sarcoma virus (ASV) FLAG-tagged vSrc _____	73
Table 3.2. Primers used to generate GST-CYT fusion protein constructs _____	74
Table 3.3. Primers used to generate IpLITR 1.1b CYT receptor constructs, including IpLITR 1.1b/IpFcR γ -L WT _{CYT} chimeric receptor, IpLITR 1.1b CYT YF mutant receptors and eGFP-tagged receptors _____	75

LIST OF FIGURES

Figure 1.1. Versatility of IpLITR cytoplasmic tail (CYT)-mediated signal transduction capabilities _____	7
Figure 1.2. Cytoplasmic tail (CYT) ITAM-dependent phagocytic signal transduction pathways _____	9
Figure 2.1. Tertiary crystal structure schematic of the cellular Src kinase SH2 domain bound to a phospho-YEEI peptide ligand _____	51
Figure 2.2. SH2 domain residues that co-ordinate peptide ligand residues and determine binding specificity are highly conserved throughout vertebrates _____	53
Figure 3.1. Schematic representations of all FLAG-tagged SH2 domain-containing signaling molecule constructs _____	72
Figure 4.1. Schematic representations of the N-terminal tagged GST-CYT fusion proteins and overview of the GST pulldown assay _____	98
Figure 4.2. Generation of N-terminal tagged GST-CYT fusion protein ‘bait’ and C-terminal FLAG-tagged signaling molecule ‘prey’-containing cellular lysates _____	101
Figure 4.3. GST-IpLITR 1.1b WT _{CYT} and GST-IpLITR 1.1b PROX _{CYT} fusion proteins cross-react with α FLAG M2 monoclonal blotting antibody _____	103
Figure 4.4. Differential phosphotyrosine-dependent recruitment of C-terminal FLAG-tagged signaling molecules to the proximal and distal CYT segments of IpLITR 1.1b WT _{CYT} by GST pulldown _____	107
Figure 4.5. Differential phosphotyrosine-dependent recruitment of C-terminal FLAG-tagged signaling molecules to the proximal and distal CYT segments of IpLITR 1.1b WT _{CYT} by GST pulldown _____	111
Figure 4.6. Schematic representation of the Image Stream-based phagocytosis assay _____	113
Figure 4.7. Generation and stable expression of N-terminal HA epitope-tagged IpLITR 1.1b CYT constructs in AD293 cells _____	115
Figure 4.8. α HA-coated bead-induced cross-linking of IpFcR γ -L WT _{CYT} , but not IpLITR 1.1b WT _{CYT} , mediates CYT-dependent phagocytic signaling _____	117
Figure 4.9. Co-expressing IpLITR 1.1b WT _{CYT} with a promiscuous Src kinase, vSrc, does not activate phagocytic signaling _____	120
Figure 4.10. Over-expressing Syk or SAP in IpLITR 1.1b WT _{CYT} -expressing cells does not activate phagocytic signaling _____	123

Figure 4.11. Schematic representation of pervanadate-mediated cellular activation and signaling molecule recruitment _____	125
Figure 4.12. Generation and stable expression of N-terminal HA epitope-tagged IpLITR 1.1b CYT YF mutant constructs in AD293 cells for co-immunoprecipitation assays _____	128
Figure 4.13. Wild-type IpLITR 1.1b recruits the inhibitory signaling molecules Csk and SHP2 to the proximal CYT segment Y ⁴⁵³ and distal CYT segment ITIM Y ⁴⁷⁷ , respectively _____	132
Figure 4.14. Schematic representation of the ITAM-dependent phagocytic signaling networks of IpFcR γ -L WT _{CYT} , highlighting hypothetical sites for molecular alteration of signaling _____	134
Figure 5.1. Schematic representations of IpLITR CYT-mediated signaling potential in AD293 cells _____	154
Figure 5.2. Schematic representation of IpLITR 1.1b WT _{CYT} -mediated cross-talk regulation of IpFcR γ -L WT _{CYT} -driven phagocytosis by an Image Stream-based yellow green (YG) bead assay in transiently co-transfected parental AD293 cells _____	156
Figure 5.3. IpLITR 1.1b WT _{CYT} appears to mediate cross-talk inhibition of IpFcR γ -L WT _{CYT} -driven phagocytosis in transiently co-transfected AD293 cells _____	158
Figure 5.4. Schematic representation of IpLITR 1.1b WT _{CYT} -mediated cross-talk regulation of IpFcR γ -L WT _{CYT} -driven phagocytosis by an Image Stream-based light yellow (LY) bead assay in transiently co-transfected parental AD293 cells _____	160
Figure 5.5. eGFP-tagged IpLITR 1.1b WT _{CYT} appears to mediate inhibition of IpFcR γ -L WT _{CYT} -driven phagocytosis through both proximal and distal CYT segment tyrosine-based motifs _____	163
Figure 5.6. Schematic representation of eGFP-tagged IpLITR 1.1b WT _{CYT} -mediated cross-talk regulation of ITAM-driven phagocytosis in stable IpFcR γ -L WT _{CYT} -expressing AD293 cells via imaging cytometry-based light yellow (LY) bead phagocytosis assay _____	165
Figure 5.7. Gating strategy for Image Stream-based analysis of cells with phagocytosed and/or surface-bound light yellow (LY) beads _____	168
Figure 5.8. eGFP-tagged IpLITR 1.1b WT _{CYT} mediates CYT motif-dependent cross-talk inhibition of ITAM-driven phagocytosis in stable IpFcR γ -L-expressing AD293 cells _____	171
Figure 5.9. Gating strategy for eGFP-tagged IpLITR 1.1b CYT construct expression level during Image Stream-based analysis of cells with phagocytosed and/or surface-bound light yellow (LY) beads _____	173

Figure 5.10. Effect of receptor expression levels on eGFP-tagged IpLITR 1.1b WT _{CYT} -mediated cross-talk inhibition of IpFcR γ -L WT _{CYT} -driven phagocytosis _____	175
Figure 6.1. Schematic representations of 8 IpLITR cytoplasmic tail (CYT) constructs used in chapter VI _____	196
Figure 6.2. Schematic representation of IpLITR 1.1b WT _{CYT} -mediated mechanisms of cross-talk inhibition of IpFcR γ -L WT _{CYT} -driven phagocytic signaling explored in chapter VI _____	197
Figure 6.3. eGFP-tagged IpLITR 1.1b WT _{CYT} segments differentially modulate cross-talk inhibition of IpFcR γ -L WT _{CYT} -driven phagocytosis via proximal CYT Y ⁴⁵³ and distal CYT ITIM Y ⁴⁷⁷ _____	200
Figure 6.4. Co-expressing IpLITR 1.1b WT _{CYT} with dominant-negative Csk does not restore IpFcR γ -L WT _{CYT} -driven phagocytosis _____	204
Figure 6.5. Co-expressing IpLITR 1.1b WT _{CYT} with dominant-negative SHP2 partially restores phagocytic signaling through IpFcR γ -L WT _{CYT} _____	209
Figure 6.6. Csk knockdown does not reverse IpLITR 1.1b WT _{CYT} -mediated cross-talk inhibition of IpFcR γ -L WT _{CYT} -driven phagocytosis _____	214
Figure 6.7. SHP2 knockdown partially reverses IpLITR 1.1b WT _{CYT} -mediated cross-talk inhibition of IpFcR γ -L WT _{CYT} -driven phagocytosis _____	219
Figure 6.8. Schematic representation of IpLITR 1.1b WT _{CYT} -mediated cross-talk inhibition of IpLITR 2.6b/IpFcR γ -L WT _{CYT} -driven phagocytic signaling _____	221
Figure 6.9. Effect of receptor expression levels on eGFP-tagged IpLITR 1.1b WT _{CYT} -mediated cross-talk inhibition of IpFcR γ -L WT _{CYT} -driven phagocytosis _____	223
Figure 6.10. eGFP-tagged IpLITR 1.1b WT _{CYT} segments synergistically down-regulate IpLITR 2.6b/IpFcR γ -L WT _{CYT} -driven phagocytosis through distinct CYT motif Y ⁴⁵³ - and Y ⁴⁷⁷ - dependent pathways _____	226
Figure 7.1. Select inhibitory IpLITR isoforms contain an inserted proximal cytoplasmic tail (CYT) segment signaling cassette _____	247
Figure 7.2. Versatility of IpLITR cytoplasmic tail (CYT)-mediated signal transduction capabilities includes cross-talk potential _____	249

LIST OF ABBREVIATIONS

- AF647 AlexaFluor 647
- Akt AK thymoma
- AMP anti-microbial peptide
- Arp actin-related protein
- ATP adenosine triphosphate
- BCR B cell receptor
- BL21 *E. coli* B F⁻ *dcm ompT hsdS(rb⁻mb⁻) galλ*
- BLAST basic local alignment search tool
- Blk B lymphocyte kinase
- Btk Bruton's tyrosine kinase
- C1 protein kinase C conserved region 1
- C3G Crk SH3-binding guanine nucleotide-releasing protein
- c-Abl cellular Abelson murine leukemia viral oncogene homolog
- CARD caspase activation and recruitment domain
- c-Cbl cellular casitas B-lineage lymphoma proto-oncogene
- CCR chemokine receptor
- CD cluster of differentiation
- cdc42 cell division cycle 42
- cDMEM complete Dulbecco's minimum essential medium
- cDNA complementary deoxyribonucleic acid
- CEACAM carcinoembryonic antigen-related cell adhesion molecule
- CH calponin homology
- CHIR chicken Ig-like receptor
- CIN85 Cbl-interacting protein of 85 kDa
- CLEC C-type lectin
- CO₂ carbon dioxide
- co-IP co-immunoprecipitation
- Crk chicken tumour virus regulator of kinase

- Csk C-terminal Src kinase
- cSMAC central supramolecular activation cluster
- CTL cytotoxic T lymphocyte
- CYT cytoplasmic tail
- DAP DNAX-activation protein
- dectin dendritic cell-associated C-type lectin
- DIST distal
- DN dominant-negative
- DNA deoxyribonucleic acid
- Dok downstream of tyrosine kinase
- dSMAC distal supramolecular activation cluster
- EAT2 EWS/FLI1-activated transcript 2
- ED extracellular domain
- EDTA ethylenediaminetetraacetic acid
- eGFP enhanced green fluorescent protein
- ERK extracellular signal-regulated kinase
- ERM ezrin-radixin-moesin
- EV empty vector
- F-actin filamentous actin
- FBS fetal bovine serum
- FcR fragment crystallizable receptor
- FcRL fragment crystallizable receptor-like
- Fer/Fps feline encephalitis virus-/Fujinami poultry sarcoma virus-related kinase
- Fgr feline Gardner-Rasheed sarcoma viral oncogene homolog
- Frk Fyn-related kinase
- Fwd forward
- Fyn Src/Yes-related novel oncogene homolog
- G418 geneticin
- Gab Grb2-associated-binding protein
- GALT gut-associated lymphoid tissue

- GAP GTPase activating protein
- GEF guanine exchange factor
- gg *Gallus gallus*
- gp49 glycoprotein 49
- Grb growth factor receptor-bound
- GST glutathione S-transferase
- GTPase guanosine triphosphatase
- HA hemagglutinin
- Hck hematopoietic cell kinase
- HEK human embryonic kidney
- hemITAM partial immunoreceptor tyrosine-based activating motif
- HLA human leukocyte antigen
- HRP horseradish peroxidase
- IFN interferon
- Ig immunoglobulin
- IgSF immunoglobulin superfamily
- IL interleukin
- ILR Ig-like receptor
- IP immunoprecipitation
- IP₃ inositol 1,4,5-trisphosphate
- IpLITR *Ictalurus punctatus* leukocyte immune-type receptor
- IS immunological synapse
- ITAM immunoreceptor tyrosine-based activating motif
- ITAMi inhibitory immunoreceptor tyrosine-based activating motif
- ITIM immunoreceptor tyrosine-based inhibitory motif
- Itk IL2-inducible T cell kinase
- ITSM immunoreceptor tyrosine-based switch motif
- ITT Ig tail tyrosine
- Jun ju-nana
- KD knockdown

- kDa kilo-Dalton
- KIR killer cell Ig-like receptor
- LAT linker for activation of T cells
- Lck lymphocyte cell-specific protein tyrosine kinase
- LILR leukocyte Ig-like receptor
- LPS lipopolysaccharide
- LRC leukocyte receptor complex
- LY light yellow
- Lyn Lck/Yes-related novel protein tyrosine kinase
- mAb monoclonal antibody
- MAPK mitogen-activated protein kinase
- MCP monocyte chemoattractant protein
- MHC major histocompatibility
- MIP macrophage inflammatory protein
- mRNA messenger ribonucleic acid
- MUT mutant
- MyD88 myeloid differentiation primary response protein 88
- NALT nasopharynx-associated lymphoid tissue
- Nck non-catalytic region of tyrosine kinase adaptor protein
- NCR natural cytotoxicity receptor
- NF- κ B nuclear factor kappa in B cells
- NILT novel Ig-like transcript
- NITR novel immune-type receptor
- NK natural killer
- NKG natural killer gene
- NKIS natural killer cell immunological synapse
- O₂ oxygen
- pAb polyclonal antibody
- PAK p21-activated kinase
- PAMP pathogen-associated molecular pattern

- PBS phosphate buffered saline
- PCR polymerase chain reaction
- PD1 programmed cell death protein 1
- PECAM platelet endothelial cell adhesion molecule
- PH pleckstrin homology
- PI-_{3,4,5}-P₃ phosphatidylinositol-(3,4,5)-trisphosphate
- PI-_{3,4}-P₂ phosphatidylinositol-(3,4)-bisphosphate
- PI3K phosphoinositide 3-kinase
- PI-_{4,5}-P₂ phosphatidylinositol-(4,5)-bisphosphate
- PIR paired Ig-like receptor
- PKA protein kinase A
- PKC protein kinase C
- PLC phospholipase C
- PLD phospholipase D
- PROX proximal
- PRR pattern recognition receptor
- PSGL P-selectin glycoprotein ligand
- pSMAC peripheral supramolecular activation cluster
- PTB phosphotyrosine binding
- PTM post-translational modification
- Pyk protein tyrosine kinase
- Rac Ras-related C3 botulinum toxin substrate
- Rap Ras-related protein
- Ras rat sarcoma viral oncogene homolog
- RBC red blood cell
- RBL rat basophilic leukemia
- Rho Ras homolog
- ROS reactive oxygen species
- Rvs reverse
- SAP SLAM-associated protein

- SDM site-directed mutagenesis
- SDS-PAGE sodium dodecyl sulfate polyacrylamide gel electrophoresis
- SFK Src family kinase
- SH2 Src homology 2
- SH3 Src homology 3
- Shc SH2 domain-containing transforming protein
- SHIP SH2 domain-containing inositol 5'-phosphatase
- SHP SH2 domain-containing phosphatase
- shRNA short hairpin ribonucleic acid
- SIRP signal regulatory protein
- SLAMF signaling lymphocytic activation molecule family
- SLP SH2 domain-containing leukocyte protein
- Sos son of sevenless
- Src sarcoma viral oncogene homolog
- Syk spleen tyrosine kinase
- TBS tris buffered saline
- TCR T cell receptor
- TK tyrosine kinase
- TKB1 tyrosine kinase derivative of BL21
- TLR Toll-like receptor
- TM transmembrane
- TNF tumor necrosis factor
- TRIF TIR domain-containing adaptor inducing interferon
- TSAd T cell-specific adaptor
- USD United States dollar
- Vav the 6th letter of the Hebrew alphabet
- VO₃ pervanadate
- vSrc viral Src kinase
- WASp Wiskott Aldrich syndrome protein
- WAVE WASp family verprolin homologous

- WT wild-type
- XFL *Xenopus* FcR-like
- Yes Yamaguchi sarcoma viral oncogene homolog
- YF tyrosine-phenylalanine
- YG yellow green
- Yrk Yes-related kinase
- Δ truncated

CHAPTER I

INTRODUCTION

1.1 Introduction

Animals are composed of cells which are the smallest fundamental living units on Earth. Part of their classification as living is based on their ability to perceive the environment, allowing them to detect nutrients or avoid stressful conditions. Perceiving environmental cues is important for single cells, but multicellular organisms have evolved sophisticated networks for coordinating the activities of many individual cells (1). Multiple immune cell-types like natural killer (NK) cells and granulocytes (e.g. mast cells) coordinate the detection and elimination of invading microbes, repairing tissue damage, removing debris and restoring homeostasis. Importantly, immune cells sense and respond to their environment through cell surface-expressed immunoregulatory receptors that communicate extracellular stimuli to complex intracellular signaling pathways. Characteristic modifications of the phosphorylation status of tyrosine-based motifs allow cells to balance inputs and select appropriate responses. Although these immune cell signal transduction events are highly conserved throughout the animal kingdom, information from earlier vertebrate models is relatively limited.

A family of immunoregulatory receptors, called leukocyte immune-type receptors (LITRs), were originally discovered in the channel catfish (*Ictalurus punctatus*) over a decade ago (2). These receptors have ancestral relationships with several amphibian, avian and mammalian receptor families. Since 2007, the Stafford lab has employed IpLITRs as tools to study immunoregulatory receptor-mediated functional and signaling potential to address gaps in the understanding of innate immunoregulatory processes in vertebrates. Specifically, very limited descriptions of immunoregulatory receptor-mediated control of signal transduction in fish immune cells were available and our work has since revealed expected as well as unique aspects

of immunoregulatory receptor signaling. For example, the stimulatory receptor IpLITR 2.6b features conserved functional and signaling capabilities with mammalian receptors, including associations with stimulatory adaptor molecules such as IpFcR γ -L, that allow it to activate degranulation, cytokine secretion and phagocytosis (Figure 1.1; 3–5). Conversely, the inhibitory receptor IpLITR 1.1b has demonstrated predictable as well as versatile signaling capabilities. Originally, IpLITR 1.1b blocked mouse NK cell-mediated cytotoxicity using both conserved SHP-dependent pathways and a novel SHP-independent pathway (6). More recently, IpLITR 1.1b was shown to stimulate the phagocytic process when expressed in a mammalian myeloid cell line (Figure 1.1; 5, 7). This response was not inhibited by pharmacological inhibitors of conserved phagocytic signaling pathways nor decreased temperatures (i.e. 17°C). However, removing the cytoplasmic tail (CYT) region, which contains proximal and distal segment signaling modules, blocked phagocytosis. Microscopic examinations also revealed a unique phagocytic phenotype whereby wild-type IpLITR 1.1b CYT (IpLITR 1.1b WT_{CYT})-expressing cells captured targets on actin-rich membranous protrusions. IpLITR 1.1b WT_{CYT}-mediated phagocytic signaling is driven by recruitment of stimulatory signaling molecules to distinct CYT regions (8). Importantly, this is the first characterization of functional plasticity for an ITIM-containing teleost immunoregulatory receptor, revealing conserved principles of innate immune signal transduction events across vertebrate lineages. However, details of signaling versatility within teleost immunoregulatory receptor families have not been studied. Due to the ancestral relationship between LITRs and receptor families in descendant vertebrates, this work may uncover novel signaling capabilities that are conserved throughout vertebrate lineages. Therefore, to advance the understanding of versatile signaling capabilities in vertebrates, my thesis research focuses on IpLITR CYT-dependent signaling events.

1.2 Thesis objectives

Previous characterizations of IpLITR 1.1b WT_{CYT} were performed using transfected immune cells, however, detailed phagocytic signaling mechanisms can be studied in non-immune epithelial cell-types. Epithelial cells are the main cell-types that comprise the anatomical barrier separating external and internal environments which prevents microbial entry to host tissues. Their primary functions do not include internalization of particulate antigen and they do not constitutively express cell-surface immunoglobulin superfamily (IgSF) innate immune receptors. However, epithelial cells do express sub-membrane proximal signaling molecules as well as the downstream actin polymerization machinery (9, 10). By expressing a receptor capable of orchestrating sub-membrane proximal signaling events that link to the actin polymerization machinery, phagocytic signaling pathways can be re-constituted without interference from co-activated immune pathways. Heterologous expression systems typically use plasmid vectors (e.g. pDisplay) that drive constitutive expression of the proteins they encode resulting in over-expression of target protein. However, in the case of phagocytic receptor protein targets, the purpose of these systems is to detect a cellular response downstream of receptor activation to be able to study underlying signal transduction events, not match *in vivo* levels of receptor protein expression. This represents a reductionist approach for studying receptor CYT-dependent sub-membrane proximal signaling events and was successfully used to define CYT requirements of ITAM-driven phagocytosis in mammals (Figure 1.2; 11–18). Therefore, my overall thesis objective was to establish a non-immune epithelioid cell system to examine the events underlying IpLITR 1.1b WT_{CYT}-mediated sub-membrane proximal signaling versatility. The specific aims of my research were: (1) to characterize the signaling molecule recruitment potential of IpLITR 1.1b WT_{CYT} proximal and distal segments and (2) to examine

IpLITR 1.1b WT_{CYT}-mediated phagocytic signaling potential. Since these aims showed that IpFcR γ -L CYT activated phagocytosis but IpLITR 1.1b WT_{CYT} appeared to mediate inhibitory signaling, the next aims of my research were: (3) to establish an assay for measuring IpLITR CYT-dependent cross-talk signaling potential; and (4) to examine IpLITR 1.1b WT_{CYT} requirements for down-regulating IpFcR γ -L-driven phagocytosis.

1.3 Thesis overview

Chapter II begins by reviewing paradigms of immunoregulatory receptor-mediated control of effector responses, including detailed examples of dynamic signaling events. In addition, chapter II will discuss conserved details of signaling versatility and functional plasticity across vertebrate lineages and establish LITRs as an excellent model for examining novel signaling capabilities. Chapter III describes the materials and methods used to complete my thesis research. In chapter IV, I test hypotheses of signaling molecule recruitment and phagocytic signaling potential of IpLITR CYTs using co-precipitation and imaging flow cytometry-based approaches. My results show that while IpLITR 1.1b WT_{CYT} differentially recruits several stimulatory signaling molecules to distinct CYT region segments from cellular lysates, only inhibitory molecules are recruited from intact, physiologically stimulated cells. IpLITR 1.1b WT_{CYT} was shown to not mediate phagocytic signaling likely due to the recruitment of inhibitory signaling molecules, while IpFcR γ -L was phagocytic. These observations formed the basis for testing hypotheses of IpLITR-mediated cross-talk signaling potential. Chapter V details the development of a novel imaging flow cytometry-based phagocytosis assay involving the transient transfection of eGFP-tagged IpLITR 1.1b WT_{CYT} constructs into stable IpFcR γ -L-expressing cells. My results show that IpLITR 1.1b WT_{CYT} down-regulates IpFcR γ -L-driven phagocytic signaling via tyrosine-based motif-dependent mechanisms. In chapter VI, I examine

IpLITR 1.1b WT_{CYT} requirements of the down-regulatory mechanism revealed in chapter V. This involved site-directed IpLITR 1.1b WT_{CYT} YF mutant constructs, dominant-negative signaling molecule constructs and shRNA-mediated signaling molecule knockdown techniques in combination with the phagocytosis assay developed in chapter V. I show that IpLITR 1.1b WT_{CYT} requires proximal and distal CYT segment motifs to optimally inhibit IpFcR γ -L-driven phagocytosis. This down-regulation uses novel inhibitory signaling pathways compared to those previously demonstrated for IpLITR 1.1b WT_{CYT}. In summary, my research has demonstrated a novel inhibitory signaling mechanism for down-regulating phagocytosis in vertebrates and is the first report of cross-talk signaling potential within a teleost immunoregulatory receptor family. Chapter VII discusses the main findings of this thesis in relation to immunoregulatory receptor-mediated regulation of immune cell effector responses in vertebrates as well as the potential utility of other teleost LITR models to expand the current understanding of innate immune processes in the future. Chapter VIII is a bibliography of thesis references.

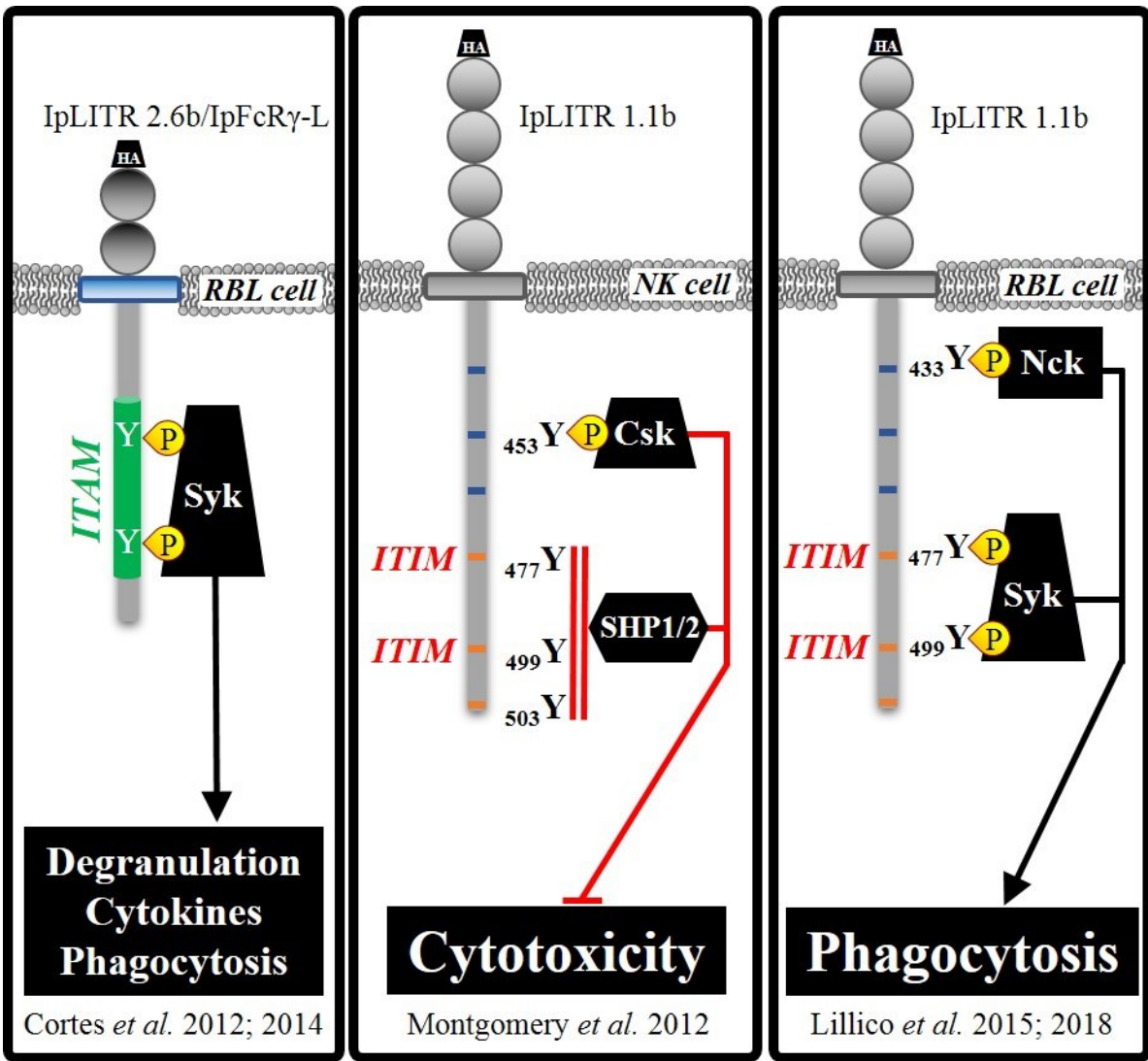


Figure 1.1. Versatility of IpLITR cytoplasmic tail (CYT)-mediated signal transduction capabilities. Heterologous expression of N-terminal hemagglutinin (HA) epitope-tagged IpLITRs in mammalian immune cells allows receptor-specific activation of signal transduction by α HA antibody-mediated cross-linking. Conserved aspects of IpLITR-mediated control of effector responses include the activation of stimulatory responses (e.g. phagocytosis, left panel) and the inhibition of cytotoxicity (middle panel) through ITAM (green) Syk-dependent and ITIM (red) SHP-dependent pathways, respectively. Two unique aspects of IpLITR-mediated control of effector responses include: 1) inhibitory signaling plasticity through an ITIM-independent, Csk-dependent membrane proximal cytoplasmic tail (CYT) segment pathway (middle panel) and 2) functional plasticity via activation of phagocytosis through a co-operative ITAM-independent Nck- and Syk-dependent pathway (right panel).

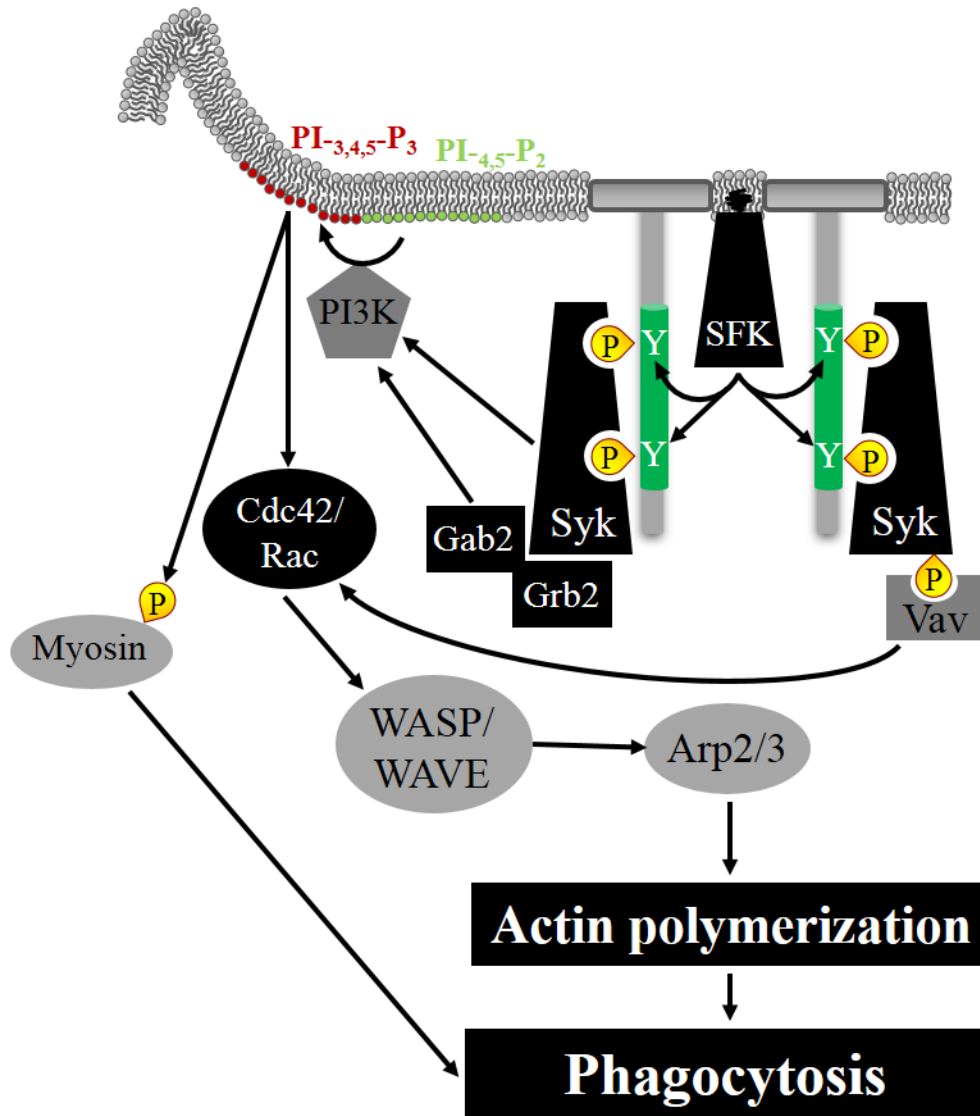


Figure 1.2. Cytoplasmic tail (CYT) ITAM-dependent phagocytic signal transduction pathways. Receptor-mediated target recognition leads to receptor clustering and the activation of phosphotyrosine-dependent signaling events, resulting in membrane remodeling and target internalization. CYT ITAMs (green) are phosphorylated by membrane-associated Src family kinases (SFKs) leading to recruitment of Syk. Syk can recruit the guanine exchange factor Vav or the adaptor proteins Grb2 and Gab2, leading to the activation of phosphoinositide 3-kinase (PI3K). PI3K catalyzes the phosphorylation of membrane lipids, leading to the accumulation of phosphatidylinositol-(3,4,5)-trisphosphate (PI-_{3,4,5}-P₃) which activates myosin and recruits the small GTPases cdc42 and Rac that are activated by Vav. Small GTPases activate effectors of actin polymerization, WASP/WAVE and Arp2/3. Arp2/3 facilitates actin polymerization leading to membrane remodeling and target internalization.

CHAPTER II

LITERATURE REVIEW

2.1 Overview of innate immunity

All multi-cellular animals possess an innate immune system broadly composed of anatomical barriers and underlying cellular components (19). While anatomical barriers present a formidable and hostile obstacle, invading microbes must then evade various innate immune cell-types that actively search for and destroy them (20). The study of innate immune cell-types across vertebrate models established evolutionarily conserved phenotypes and functional responses activated during microbial encounters. Seminal observations in a number of organisms, including starfish larvae in 1883, but also reptiles, birds and primates made by Elie Metchnikoff, contributed to the development of cellular defense theories in animals and the awarding of the 1908 Nobel Prize in Physiology and Medicine (21–23). Indeed, mammals, birds, reptiles, amphibians and fish all possess innate immune cell-types that execute conserved cellular responses. These responses serve to maintain anatomical barriers by secreting anti-microbial peptides, kill infected or stressed host cells via cytotoxicity, eliminate microbes by phagocytosis, influence inter-cellular communication by secreting and responding to cytokines and chemokines, and guide adaptive immune responses by presenting antigen. Collectively, these cell-mediated processes eradicate infections, orchestrate tissue repair, and re-establish host homeostasis (20, 24–26). Overall, these outcomes rely on the ability of cells to sense and respond to their micro-environments.

Cell surface-expressed innate immune cell receptor proteins (called immunoregulatory receptors) communicate extracellular stimuli to complex, highly conserved intracellular signaling networks that control cellular responses. These events are collectively known as signal transduction. Several immunoregulatory receptor families discovered in mammals have helped

define key molecular principles of innate immune cell signal transduction (27). In general, receptor ligation leads to clustering and activation of receptor cytoplasmic tail (CYT)-dependent signaling cascades (28, 29). The integration of signaling cascade inputs balances cellular activation and inhibition (30–33). Molecular signal transduction events are highly conserved throughout vertebrate lineages, however, detailed mechanistic information from earlier vertebrate models (i.e. teleost fish) is relatively limited. The Stafford lab has focused on biochemical and functional characterizations of a family of immunoregulatory receptors originally discovered in the channel catfish (*Ictalurus punctatus*) called leukocyte immune-type receptors (IpLITRs; 2). The research described in this thesis is a continuation of these characterizations with a focus on expanding novel receptor CYT-dependent regulatory capabilities of two representative IpLITR family members.

In this review, I will first provide an overview of innate immunity components, highlighting select innate immune cell-types and their effector responses in vertebrates, with a focus on teleost fish. I will then introduce concepts of immunoregulatory receptor-mediated control of effector responses and biochemical currencies of signal transduction. Next, I will integrate these two concepts by reviewing historical aspects of the paired (i.e. stimulatory/inhibitory) receptor paradigm. I will then review detailed molecular mechanisms of specific stimulatory and inhibitory receptor-types, including examples from select vertebrate species, which I will then contrast with more recent characterizations that exemplify receptor CYT signaling versatility (e.g. inhibitory receptor-types that activate functions). These contrasting examples provide a basis for reviewing underlying dynamics of receptor CYT-mediated integration of biochemical signal transduction currencies during immune cell-target interactions. In doing so, I will highlight recent advances in our understanding of how receptor

CYT activate specific intracellular signaling pathways and the central role that actin polymerization plays in organizing membrane structure and consequently, sub-membrane proximal signaling events.

Throughout this review, I will primarily discuss evolutionary relationships between vertebrate innate immune cell-types and the immunoregulatory receptors they express, focusing on IpLITRs and their counterparts in birds and mammals. However, when discussing mechanisms of receptor CYT signaling dynamics and the role of actin polymerization, I will include select adaptive immune cell receptor examples (e.g. CD28). Since theories that adaptive immune cells are evolutionary descendants of innate cell-types (e.g. B cells are specialized macrophages and T cells are specialized cytotoxic cells; 32, 33) have been proposed, the CYT phosphotyrosine- and actin-dependent nature of mechanisms downstream of adaptive immune receptors likely also operate during innate immunoregulatory receptor signaling.

2.1.1 Physical/chemical barriers

The first barrier that microbes interact with during invasion is the skin, which includes a continuous external (i.e. skin) and internal (i.e. digestive tract) lining. Although macroscopically the external lining appears much different in terrestrial versus marine animals (e.g. feathers/fur versus scales), both linings are generally composed of two major microscopic cellular layers: the dermis and the epidermis, along with their associated connective and immunological tissues.

In fish, constant contact with potentially pathogenic microbes in aquatic environments facilitated the evolution of robust epidermal defenses, including mineralized scales supported by actin-, collagen- and keratin-rich filaments (36, 37). In addition, this penetration-resistant barrier is bathed in a gel-like mucous secreted by specialized goblet cells within the epidermis and it contains various glycoproteins, anti-microbial peptides and immunoglobulins (i.e. protective

antibodies). Furthermore, the epidermis contains multiple secondary lymphoid tissues that combat infection by housing interaction sites between various immune cell-types. These include the gill-associated lymphoid tissue, gut-associated lymphoid tissue (GALT), mucosae-associated lymphoid tissue, nasopharynx-associated lymphoid tissue (NALT), and skin-associated lymphoid tissue. Lymphoid tissues contain several resident immune cell-types including T and B cells (which are adaptive immune cells), macrophages, dendritic cells, non-specific cytotoxic cells and neutrophils. Within these tissues, innate and adaptive immune cell-types interact directly to influence immune responses. Specifically, dendritic cells and macrophages present antigen to resident T and B cells thereby inducing antigen-specific adaptive immune responses. All vertebrates possess a GALT and NALT indicating that communication between innate and adaptive cell-types is highly conserved throughout vertebrate lineages (38–41). If these initial barriers fail, the next line of defense depends upon the induction of cellular effector responses by various innate immune cell-types.

2.1.2 Cellular barriers

Invading microbes can establish infections in virtually any tissue of the host. Innate immune responses are activated immediately and include the mobilization of specific cell-types to sites of infection where they activate effector responses to combat the infection. In mammals, the major cellular participants during innate responses include innate-like lymphoid cells (e.g. natural killer cells), dendritic cells, monocytes/macrophages and the granulocytes (e.g. neutrophils, basophils and eosinophils; 40, 41).

Traditionally, innate cell-types have been identified using a combination of cyto- and histo-chemical staining, ultrastructural morphology and broad functional assessments. These functions include increased adhesion after immune stimulation, cell migration into particular

tissues after immune challenge or proliferation during *in vitro* mixed leukocyte reactions in the presence of allo- or xeno-geneic cells. Innate immune cell-types have been identified in several vertebrate species including birds, reptiles, amphibians, jawed fishes and jawless fishes. In fact, additional granulocytic cell-types have been identified in earlier vertebrates called heterophils and azurophils (44–46). More advanced molecular techniques have supported the evolutionary conservation of innate cell-types.

The development of techniques to characterize cells at the transcriptional (i.e. DNA and RNA) and translational (i.e. protein) levels has deepened our understanding of evolutionary relationships. Vertebrate innate cell-types not only appear morphologically, cytochemically and functionally similar, they express evolutionarily conserved genes including various cytokines, chemokines and cell surface-expressed receptors, some of which are extensively characterized in teleost fish. For example, orthologous mammalian interferon- γ , colony stimulating factor and interleukin (IL) cytokine genes, like IL1 β , IL6, IL8, IL10, have been characterized in teleost fish (47, 48). The expression of conserved receptors has greatly facilitated studies of innate immunity by enabling the isolation of specific cell-types through antibody staining of molecular markers on their surfaces. For example, early vertebrate (i.e. fish, amphibian, reptile and chicken) T and B cells are functionally similar and express orthologs of mammalian T cell receptor (TCR), B cell receptor (BCR), major histocompatibility complex (MHC) class I and II, CD4, CD8 and CD28 IgSF genes (49–53). Likewise, early vertebrate monocyte/macrophages express mammalian-like markers such as scavenger receptors (54) and are highly efficient phagocytic cells (55). However, molecular characterizations have also started to explain differences between vertebrate innate cell-types.

2.1.3 Innate immune cell effector responses

Common effector responses include cytotoxicity, phagocytosis, degranulation, cytokine secretion and netosis, which have been demonstrated in chicken, reptiles, frogs and fishes (56, 57, 66–68, 58–65). In fishes, cytotoxic responses can be activated by several cell-types including natural killer (NK)-like cells, macrophages, cytotoxic T cells and non-specific cytotoxic cells (69–72). While mammalian innate-like NK cells target allogeneic cells, non-specific cytotoxic cells have the ability to recognize and kill allo- and xeno-geneic targets spontaneously (i.e. without prior activation) and cells with similar abilities have been described in cartilaginous fishes (73). Internalization of opsonized and/or microbial targets has been observed for multiple phagocytic cell-types in fishes (74, 75). In fact, goldfish macrophages are thoroughly characterized and have a unique ability to proliferate in *in vitro* cultures and differentiate into distinct activation states (76, 77). In mammals, macrophages and neutrophils were thought to be the predominant tissue resident phagocytic cells. However, phagocytic B cells, originally observed in teleost fish and frogs (78), have been observed in mammals as well (79). These contrasting capabilities in fish have facilitated molecular investigations to identify the genes and proteins involved and, consequently, have informed our understanding of immune-related gene evolution. In the case of B cells, the IgM and IgD isotypes are conserved throughout vertebrate lineages (80). Although not thoroughly tested, it would be interesting to know which mammalian immune genes are ancestral gene homologs of fish genes that have since, evolved specialized cell-type-specific roles. In comparison, innate cell-types of earlier vertebrates evolved several highly diversified gene families that likely confer unique phenotypic but similar functional capabilities (19). For example, several teleost fish contain conserved adaptive cell markers yet adaptive responses like affinity maturation are not as efficient compared to mammals (81–83).

Conversely, teleost fish cytotoxic cells exhibit broader target specificity and higher potency in killing targets after alloantigen stimulation (69, 84). This may be explained in part, by expanded immunoregulatory receptor families involved in mediating cytotoxic cell function (71, 85–88). These trade-offs between adaptive and innate responses may be a consequence of an additional whole genome duplication event in teleost (89). Specifically, the apparent lack of co-evolution between MH class I and II genes (called MHC class I and II in mammals) and NK cell receptors (e.g. like the LRC complex in mammals) in fish, along with the preservation of large families of immune genes that give rise to diverse immunoregulatory proteins by mechanisms of alternative splicing may also underlie some of these trade-offs (52, 90, 91).

In any event, highly diversified immunoregulatory receptor families in teleost offer an opportunity to expand the current understanding of fundamental principles of regulatory signaling pathways. Immunoregulatory receptor proteins fall into several structurally related categories and this review will focus on the IgSF receptors which have evolved vital roles in vertebrates.

2.2 Immunoregulatory receptor-mediated control of effector responses

Cell surface-expressed immunoregulatory receptors transduce extracellular stimuli into intracellular signaling cascades and these events are governed largely by the CYT regions of the receptors. Several immunoregulatory receptor families have been identified in teleost fish including the leukocyte immune-type receptors (LITRs; 2), novel immune-type receptors (NITRs; 77) and novel Ig-like transcripts (NILTs; 78). While some appear to be present in fish only (e.g. NITRs and NILTs), the LITRs represent an immunoregulatory receptor family with relatives in frogs (XFLs), chickens (CHIRs) and mammals (KIRs, LILRs, FcRs and FcRLs; 79, 80). Immunoregulatory receptor CYT-dependent mechanisms of cellular activation and

inhibition were originally identified for mammalian KIRs (called the paired receptor paradigm) and involve a balance between kinase- and phosphatase-driven pathways. By integrating opposing stimulatory and inhibitory signaling inputs, innate immune cells can tightly regulate various potent effector responses.

In this section, I will review biochemical currencies of signaling transduction and use the paired receptor paradigm to establish phosphotyrosine-dependent currency models. The categorization of stimulatory and inhibitory receptor-types based on structural features and their phosphotyrosine-dependent signaling capabilities will then be discussed in detail. Finally, I will discuss recent examples that show how functional outcomes of receptor engagement do not always correspond with the presence of canonical structural features as versatile signaling capabilities contributing to functional plasticity have emerged.

2.2.1 Currencies of signal transduction

Transmission of information across the cellular membrane via intracellular pathways is dependent on sequential changes in the states of specific proteins. Signaling proteins act like switches that change states in response to an input signal (e.g. ligand binding), generating a signaling output that is ‘read’ by the next switch. Wiring several switches together in a ‘circuit’ allows cells to transform receptor ligations into signaling-dependent antimicrobial responses. In general, innate immune cells contain several co-operating circuits, allowing them to integrate co-incident input information to effect appropriate output responses (96–98).

Signaling proteins can change their states in four general ways: association/dissociation, conformation, localization and post-translational modification (PTM). It is very important to note that protein state changes virtually never occur in isolation and this can generate multiple outputs. For example, phosphorylation of a molecule can provide a binding site for another

molecule while simultaneously causing conformational changes that reveal multiple binding sites for additional interactions. Protein tyrosine phosphorylation (i.e. a PTM) is an energetically cheap, rapid and reversible currency of immunoregulatory receptor-mediated signaling vital for the control of a range of immune cell effector responses (1).

2.2.2 Paired receptor paradigm

Natural killer (NK) cell-mediated cytotoxicity was originally observed in 1975 (99, 100), however, the receptors and molecular mechanisms involved were not described for nearly two decades. An allogeneic target-specific NK cell-type expressing novel surface markers was identified by monoclonal antibody (i.e. α GL183 and α EB6) staining (101, 102). The cytotoxic function of these NK cells could be inhibited by specific MHC class I expression on target cells (103, 104). Subsequently, a direct relationship for activating or inhibitory signals provided by α EB6/ α GL183 staining surface markers (named p50/58 molecules) after binding MHC class I (i.e. HLA-C) on target cells was demonstrated (105, 106). P50/58 family receptors, re-named killer cell Ig-like receptors (KIRs; 92), were cloned along with additional p70 receptor members (108) revealing their polymorphic molecular structures (109–113). KIRs contain two or three extracellular immunoglobulin-like domains, a neutral or charged transmembrane (TM) segment and variable length CYT regions (114). In addition, genomic mapping localized ~10 KIR genes to chromosome 19q13.4 (115), a region known as the leukocyte receptor complex (LRC). The LRC also contains genes for other polygenic immunoregulatory receptor families, including leukocyte Ig-like receptors (LILRs), carcinoembryonic antigen-related cell adhesion molecules (CEACAMs) and leukocyte-associated Ig-like receptors (LAIRs).

Several key observations of regulatory signaling in NK and B cells supported the hypothesis that KIRs mediated SHP-dependent down-regulation of cytotoxicity. NK cell

activation involved Fc γ RIIIA-induced phosphorylation events while KIRs utilized FcR γ and the tyrosine kinase Lck (116–120). In B cells, the protein tyrosine phosphatase SHP1 opposed kinase-driven signaling and inhibited cellular activation (121–124). Antibody-mediated cross-linking of KIR2DL1 resulted in receptor phosphorylation and recruitment of SHP1, leading to inhibition of NK cell-mediated cytotoxicity and the definition of a new CYT motif later named the immunoreceptor tyrosine-based inhibitory motif (ITIM; 110–112). In general, stimulatory receptor-types contain short CYT regions devoid of signaling motifs and a positively charged TM segment that facilitates association with the negatively charged TM segment of adaptor signaling molecules (e.g. FcR γ , DAP12) containing cytoplasmic immunoreceptor tyrosine-based activating motifs (ITAMs; defined by a YxxL_{x6-8}YxxL sequence; 126–128). Upon receptor-ligand engagement, ITAMs are phosphorylated and recruit kinases that activate various signaling pathways. Conversely, inhibitory receptors have long CYT regions that contain one or more ITIMs (defined by a S/L/I/VxYxxL/I/V sequence) that are also phosphorylated after receptor engagement. The phosphorylated ITIM recruits Src homology 2 (SH2) domain-containing cytoplasmic phosphatases (e.g. SHP1/2) that dephosphorylate signaling pathway intermediates, thereby down-regulating cellular activation. Altogether, these studies established a model for the regulation of immune cell activation that depends on a balance of phosphorylation signals from polygenic families of co-expressed stimulatory and inhibitory receptors, called the paired receptor paradigm (131, 132).

This signaling paradigm has been applied to predict the biochemical recruitment potential of a number of vertebrate receptors, some of which are described in sections 2.2.4 and 2.2.5 below. Importantly, the selective activation of phosphotyrosine-dependent signaling pathways is

largely dependent on the modular SH2 protein domain and the molecular determinants of this selectivity have been reported.

2.2.3 SH2 domains confer selective activation of phosphotyrosine-driven signaling pathways

The organization and prevailing activities of molecules (e.g. kinase, phosphatase, scaffolding) within receptor CYT region-associated signaling complexes, or signalosomes, determine the stimulatory or inhibitory outcome of signaling. SH2 domains are protein modules that recognize specific linear tyrosine-based motifs thereby mediating specific protein-protein interactions (133).

The SH2 domain was originally identified by multiple sequence alignment of viral and mammalian kinases that contained an ~100 residue segment with a highly conserved FLVRES motif (134). High through-put peptide binding microarray approaches have since identified consensus binding motif requirements of several human SH2 domains (and a handful from other organisms like *Drosophila* and *C. elegans*; 117–119). Crystallization has revealed that the tertiary structure of an SH2 domain is composed of three central anti-parallel β -sheets with a single α -helix on each side. This structure resembles a two-pronged electrical socket and each inlet or groove binds to a different peptide ligand residue, defining SH2 domain binding specificity (Figure 2.1).

Overall, the ability of SH2 domains to recognize negatively charged phosphotyrosine (pY) residues is dependent on: (1) the depth of the phosphotyrosine binding groove, which prevents recognition of shorter phospho-serine or -threonine side chains; and (2) a positively charged arginine residue at the base of the pY binding groove contained within the signature SH2 domain FLVRES motif. Fine-tuned binding specificity depends on critical residues at

positions minus 2 and plus 3 relative to tyrosine (e.g. LxYxxV, ITIM described in section 2.2.2). Alternatively, for other SH2 domains, the plus 1 and/or 2 positions may also be involved. For example, in comparison to ideal ligand binding affinity (e.g. K_D ranging from 3 nM to 5 μ M), the presence of non-ideal flanking residues reduces affinity (i.e. \sim 20 μ M; 120, 121). However, binding affinity can drop up to 10,000-fold between phosphorylated and unphosphorylated ligands containing identical flanking residues (1) but, recognition of unphosphorylated ligands may influence signaling. For example, the Grb2 cytoplasmic adaptor molecule facilitates stimulatory pathways downstream of growth factor receptors. Interestingly, the Grb2 SH2 domain is capable of binding unphosphorylated peptide ligands and this unique interaction may play a role in downstream epidermal growth factor receptor signaling and oncogenic transformation (140).

SH2 domains are present within all eukaryotic genomes, including single-celled protists like *Acanthamoeba castellanii* (141) and *Monosiga brevicollis* (142), indicating that SH2 domain-mediated phosphotyrosine signaling networks are ancient (143). The channel catfish genome contains genes for most, if not all, SH2 domain-containing signaling molecules that play major roles in immune signaling in mammals (6, 95). The highly conserved specificity of SH2 domain-mediated signaling networks in vertebrates is apparent after analyzing SH2 domain-peptide ligand crystal structures. While the residues flanking tyrosine on ligands are important for specificity, additional SH2 domain residues outside of the FLVRES motif also interact with peptide ligands and are highly conserved in vertebrates (Figure 2.2). While SH2 domains are by far the most studied phosphotyrosine-binding modules, a second phosphotyrosine-binding (PTB) domain has also been characterized.

2.2.3.1 Non-SH2 domain-mediated phosphotyrosine-dependent signaling

The PTB (a.k.a. SAIN) domain was first discovered in the SH2 domain-containing transforming protein (Shc) downstream of epidermal growth factor receptor signaling (144, 145). Shc phosphorylation downstream of B cell receptor activation requires binding of SHIP to the PTB of Shc (146). In contrast to SH2 domains, PTB domain binding specificity is more dependent on N-terminal (i.e. Y minus 5) rather than C-terminal (i.e. Y plus 1, 2 and 3) residues flanking the tyrosine residue. Approximately 60 PTB domains have been identified in the human genome, compared to ~120 SH2 domains (129; 121).

2.2.4 ITAM-dependent signaling

Clearly, phosphotyrosine recognition domains are critical for selective activation of cellular signal transduction pathways. Cells must respond rapidly to activate downstream functions to facilitate immune processes. Stimulatory signaling is organized both temporally and spatially into membrane proximal and/or distal events by the association and dissociation of signaling complexes. This discussion will focus on common principles of stimulatory signaling and describe the downstream intracellular ITAM-dependent pathways used by select vertebrate receptors (27, 148).

In general, receptor engagement by ligand- or antibody-induced cross-linking results in the clustering of receptors on the cell surface. These receptor clusters form segregated microdomains within specialized membrane lipid rafts. Lipid rafts are enriched with signal transducing molecules including Src family kinases (SFKs) that are critical for initiating intracellular signaling. Immune cells contain several hematopoietic (e.g. Lyn, Lck) and ubiquitous (e.g. Src, Yes) SFKs. During cluster formation, stimulatory receptors associate with ITAM-containing adaptor molecules (e.g. FcR γ , DAP12) through charged transmembrane (TM)

segments. In humans and mice, several activating receptors associate with adaptor molecules including KIRs and natural cytotoxicity receptors (NCRs) such as NKp30, NKp44 and NKp46 (148). Chicken CHIR-A contains a charged arginine TM segment and associates with the ITAM-containing adaptor FcR γ to activate phosphotyrosine signaling (149). Two families of LRC-related receptors have been identified in amphibians. The *Xenopus* FcR-like (XFL) receptor Ig-like domains are related to FcRLs, KIRs and CHIRs, however, XFL proteins may contain one of two unrelated TM segments, TM1 or TM2. TM1 facilitates associations with FcR γ (150). A second family of receptors in amphibians are the Ig-like receptors (ILRs). ILRs appear to be activating receptors and *Xenopus* ILR1 may associate with FcR γ due to increases in cell surface expression when the two are co-expressed (151). ITAMs are phosphorylated by SFKs and recruit the cytoplasmic tyrosine kinase spleen tyrosine kinase (Syk). Sites of sustained signaling between targets and cells are called synapses (152–156). The formation of different types of synapses leads to the activation of different effector responses like cytotoxicity, degranulation or phagocytosis.

Phagocytosis is a vital effector response with well-defined spatio-temporal signaling dynamics. This receptor-mediated process involves the recognition of targets, activation of specific intracellular pathways, actin polymerization, membrane remodeling and target internalization. While phagocytic signaling may alter gene expression or endosomal trafficking, the pathways responsible for target internalization occur exclusively at the membrane. Phagocytic signaling involves the activation of kinases (e.g. Syk, protein kinase C), intermediate molecules (e.g. Grb2, PI3K), guanine nucleotide exchange factors (e.g. Vav1, Sos), small GTPases (e.g. cdc42, Rac, Ras) and actin nucleating machinery (e.g. WAVE, WASp, Arp2/3). The exact pathway involved depends on the receptor being triggered. In the case of ITAM-

containing Fc γ Rs, a Syk-PI3K-Vav-Rho/Rac/cdc42-WASp/WAVE2-Arp2/3 pathway polymerizes actin and remodels the membrane to internalize the target. Mammalian phagocytic signaling molecules share 44-96% sequence identity with their teleostean homologs, including channel catfish (6, 95). Additional pathways are simultaneously activated, for example, by recruitment of Btk and PLC γ to PI3K-generated PI-_{3,4,5}-P₃ membrane lipids, resulting in Ca²⁺ influx and PKC α activation which up-regulate cytokine gene transcription and secretion (21, 157–160).

Cell-mediated cytotoxicity is a primary function of natural killer cells and results in the targeted exocytic release of cytoplasmic granules. This function can be activated by antibody-dependent mechanisms or alternative mechanisms, but both use ITAM-dependent FcR γ /DAP12-Syk-LAT-SLP76-PLC γ -Ca²⁺ pathways (161, 162). Activating receptors include KIR2DS and several NCRs in humans (131, 163). Cytokines are simultaneously induced by several co-operating pathways downstream of PLC γ or Vav-MAPK including Ras-ERK and PKC-NF- κ B/NFAT or p38 and JNK, respectively (164–166). Lastly, degranulation is activated by human Fc ϵ RI and a chimeric mouse receptor CYT-containing construct Fc γ RIII/PIR-A, which associate with FcR γ and Syk when cross-linked in mast cells and activate Ca²⁺ mobilization (167).

ITAM-dependent signaling potential has also been reported in fish. For example, zebrafish NITR9 associates with the ITAM-containing DAP12 adaptor (168). In channel catfish, the putative stimulatory receptor, IpLITR 2.6b, recruits ITAM-containing adaptor molecules like IpFcR γ -L, which activates degranulation, cytokine secretion and phagocytosis (3–5). Several pharmacological inhibitors that effectively block Fc γ R-mediated phagocytosis also inhibited IpLITR 2.6b-mediated phagocytosis. In addition, temperatures below 37°C inhibited this response and the cellular phenotype during target internalization resembled that of Fc γ R-

expressing cells (7). Furthermore, the cross-linking of IpLITR 2.6b induced phosphorylation of downstream intermediates of ITAM-dependent pathways such as ERK1/2 and Akt (5).

2.2.5 ITIM-dependent signaling

The ability for cells to down-regulate responses is equally important to avoid aberrant immune cell activation and cellular phosphatases play critical roles. This includes the dephosphorylation of signaling intermediates by the cytoplasmic SH2 domain-containing protein tyrosine phosphatases (SHPs) but also the dephosphorylation of membrane lipids by SH2 domain-containing inositol 5'-polyphosphatases (SHIPs). Additional inhibitory mechanisms also operate downstream of ITIMs and rely on specialized kinase pathways. Temporally and spatially organized recruitment of phosphatases to forming signalosomes and synapses affects target recognition and adhesion and can occur during early or late stages of signaling. KIR family inhibitory mechanisms have been extensively characterized.

The paired receptor paradigm studies, described in section 2.2.2, revealed inhibitory receptors block early activation because downstream IP_3 and Ca^{2+} influx were not detected in cells (169). This is explained by recruiting and activating SHP1 to receptor CYT ITIMs at the plasma membrane (31, 126). This is further supported by observations that activating and inhibitory receptors must be co-cross-linked within the same signalosome to effect inhibition (170). Co-cross-linking of CD16 with an inhibitory receptor results in decreased phosphorylation of $FcR\gamma$, Syk and $PLC\gamma$ (169). In fact, SHP1 directly targets Vav1 (171), LAT and $PLC\gamma$ for dephosphorylation downstream of KIR2DL1. KIRs contain one (e.g. KIR2DL5, KIR3DL3) or two (e.g. KIR2DL1/2/3, KIR3DL1/2) CYT ITIMs. It appeared that dual ITIMs were required for recruiting and activating SHP1, while single ITIMs favor SHP2 binding. Indeed, KIR N-terminal and C-terminal CYT ITIMs play distinct roles in inhibiting cytotoxicity. When co-

cross-linked with FcεRI or BCR, an N-terminal ITIM only-containing KIR and wild-type KIR inhibited activation via SHP2 and SHP1/2, respectively (172). In support of differential SHP signaling by KIRs, KIR2DL5 contains one CYT ITIM and an ITSM, recruits SHP1/2 and inhibits NK mediated cytotoxicity. While a dominant-negative SHP2 restores cytotoxicity downstream of FcγRII/III in the presence of KIR2DL5, a dominant-negative SHP1 has no effect. In contrast, KIR3DL1 recruits SHP1/2 and blocks NK cell-mediated cytotoxicity, which is restored by both dominant-negative SHP1 and SHP2 (173). These characterizations established early inhibitory signaling that prevents signalosome and synapse formation. In fact, KIRs do not require adhesion or cytoskeletal dynamics to recruit SHP1 and inhibit early NK activation and cytotoxicity (174).

More advanced imaging techniques allowed for visualization of KIR signaling dynamics. Ligand binding to KIR2DL3 causes translocation to the centre of a forming NK cell immunological synapse (NKIS), recruitment and activation of SHP1 and a dissolution of the forming NKIS, leading to inhibited NK responses. In cytolytic NKISs, KIR2DL3 is non-specifically distributed and eventually displaced from the centre of the NKIS, where exocytic vesicles accumulate (175). However, ITIM phosphorylation is not required in all cases of SHP-mediated inhibitory pathways nor is SHP required by all inhibitory pathways initiated by KIRs.

Alternative SHP-independent inhibitory mechanisms also contribute to balancing cellular activation. LAT phosphorylation occurs downstream of FcRγ-Syk activation and provides docking sites for several SH2 domain-containing signaling molecules. However, the ubiquitin ligases c-Cbl and Cbl-b also associate with and ubiquitinate phosphorylated LAT, leading to its degradation and inhibition of cytotoxicity (176). KIR engagement leads to c-Abl-mediated phosphorylation of Crk (177). Since unphosphorylated Crk is required for activation downstream

of CD16, the phosphorylation of Crk inhibits cytotoxicity (177, 178). Interestingly, KIR2DL4 inhibits NK cell-mediated cytotoxicity via CYT ITIM-dependent recruitment of SHP2, not SHP1. In this case, cytotoxicity and recruitment of SHP2 was not phosphotyrosine-dependent and a non-phosphorylated KIR2DL4 ITIM peptide weakly recruited SHP2, which correlated with inhibition (179). Several additional LRC family members, LILRB1, LILRB2 and LILRB4 inhibit activation by recruiting and activating SHPs (180).

ITIM-dependent inhibitory signaling has been characterized using several vertebrate models including mouse, chicken and fish receptors. The human LRC homolog gp49B is expressed by mouse NK cells and inhibits NK cytotoxicity (181, 182) and mast cell degranulation (183). Phosphorylated gp49B CYT ITIM peptides recruit SHP1/2 and SHIP (184). Another LRC homolog, mouse PIR-B, contains ITIMs and recruits SHP1 to inhibit mast cell and BCR-evoked activation of mouse B cells when co-cross-linked with antibodies (185). Inhibitory LRC homologs called CHIRs have been identified in chicken. Three inhibitory CHIRs (B2, B3 and B4) have been identified. CHIR-B2 contains two CYT ITIMs, associates with SHP2 constitutively, recruits SHP1/2 when cross-linked with antibody and inhibits immune cell proliferation (186). In teleost fish, NITR3 contains a CYT ITIM which down-regulates MAPK/ERK activation when cross-linked in NK cells exposed to allogeneic target cells (187). In channel catfish, the putative inhibitory receptor, IpLITR 1.1b, contains two CYT ITIMs that recruit SHP1/2 to inhibit NK cell-mediated cytotoxicity (6, 188).

It is clear that ITAM-ITIM signaling is an effective system for regulating immune cell responses. In support of the utility of this system, paired receptor families are a highly conserved immunoregulatory feature throughout vertebrates. However, versatile signaling capabilities of ITAM- and ITIM-containing receptors have also emerged.

2.2.6 Immunoregulatory receptor-mediated signaling versatility and functional plasticity

A stimulatory/inhibitory signaling paradigm over-simplifies the regulation of immune cell responses as strictly an on/off phenomenon. In reality, receptor CYT signaling events are less restricted and more dynamic in fine-tuning intracellular signaling events. A growing category of receptors demonstrate versatile ITAM or ITIM signaling capabilities that result in inhibitory or stimulatory signaling outcomes, respectively. This is known as functional plasticity and in this section, I will discuss examples of inhibitory ITAM (ITAMi) signaling and stimulatory ITIM signaling. Furthermore, a number of receptors contain additional tyrosine-based motifs: the hemITAM, immunoreceptor tyrosine-based switch motif (ITSM) and Ig tail tyrosine (ITT) motif, that uniquely regulate effector responses and contribute to signaling versatility.

ITAMi signaling was first observed during low and high affinity hapten triggering of FcεR in mast cells, which showed an inhibition and activation of cells, respectively (189). A subsequent study showed low affinity anti-FcαRI Fab fragments partially activate FcαR and inhibit FcγR-mediated phagocytosis in transfected macrophages (190). In addition, monovalent FcαRI activation inhibits MCP1- and TNF-guided chemotaxis of immune cells via SHP1-dependent mechanisms, attenuating tissue damage in an antibody-induced glomerulonephritis model (191). Furthermore, ITAM-dependent pathways can down-regulate TLR-evoked signaling. Specifically, FcRγ- and DAP12-deficient mice display increased TLR-evoked responses to CpG, LPS or zymosan (192). In fact, ITAM-TLR cross-talk may occur during an early sub-membrane proximal stage via Syk since β2 integrin activation through DAP12/FcRγ-Syk pathways makes macrophages and dendritic cells resistant to TLR stimulation (193, 194). TLRs require the adaptors MyD88 and TRIF to initiate signaling (195). However, Syk also

activates the c-Cbl ubiquitin ligase which ubiquitinates Syk, MyD88 and TRIF, causing their degradation and accounting for a TLR signaling refractory period (196). Collectively, these studies demonstrated an ITAMi signaling capability. Conversely, ITIM-containing receptors can activate instead of inhibit functions and the following section features mammalian (i.e. KIRs, PECAM and CD300), chicken (i.e. CHIR-AB) and teleost (i.e. IpLITR 1.1b) receptor examples of functional plasticity.

KIR2DL1 contains two CYT ITIMs and mediates opposite modulatory effects on CD4+ T cell TCR-evoked activation if co-ligated. Ligated KIR2DL1 CYT ITIMs are phosphorylated and recruit SHP1/2, which inhibits IL2 secretion. However, unligated KIR2DL1 CYT ITIMs are phosphorylated and activate a SHP2-PKC θ pathway that enhances IL2 secretion (197).

KIR2DL4, expressed in NK and some T cells, contains one CYT ITIM but also a charged TM segment arginine. It activates NK cell-mediated cytotoxicity by the classic Fc γ pathway resulting in Ca²⁺ influx, cytotoxicity and secretion of IFN γ , IL8 and MIP1 α . However, a TM mutant fails to activate cytotoxicity, but still activates MIP1 α cytokine secretion. This example shows that distinct TM and CYT modules can activate multiple signaling pathways (198, 199).

Platelet-endothelial cell adhesion molecule (PECAM) 1 is expressed by platelets and leukocytes and contains 4 tyrosine-based motifs including a CYT Y⁶⁶³ ITIM and Y⁶⁸⁶ ITSM with extensively characterized signaling potential. Initial inhibitory characterizations showed that PECAM1 CYT ITIM and ITSM were the only targets of kinase-mediated phosphorylation and that these residues recruit SHP2. While an ITIM or ITSM phosphopeptide stimulates similar SHP2 phosphatase activity, the ITIM phosphopeptide shows 10-fold higher affinity for SHP2. A detailed SH2 binding assessment revealed differences in binding specificity such that the ITIM prefers the N-terminal SH2 domain of SHP2, while the ITSM only binds the C-terminal SH2

domain of SHP2 (200). The functional consequences of SHP recruitment were subsequently demonstrated. An Fc γ RIIB/PECAM1 CYT chimeric receptor construct inhibited BCR-evoked Ca²⁺ influx via phosphorylated ITIM- and ITSM-dependent SHP1/2 activation upon co-cross-linking (201). PECAM1 attenuates mast cell activation, which is dependent on Fer/Fps kinase-mediated phosphorylation of Y⁷⁰¹ followed by Lyn-mediated ITIM/ITSM phosphorylation resulting in SHP1/2 recruitment (202). In platelets, PECAM1 activates a SHP2-PI3K pathway to decrease Gab1-LAT signaling and reduce GPVI-evoked platelet responses (203). However, PECAM1 also binds stimulatory signaling molecules. For example, antibody cross-linked PECAM1 triggers Syk phosphorylation and a dually phosphorylated ITIM-ITSM phosphopeptide binds and activates Syk. This PECAM1-Syk pathway may mediate macrophage spreading (204). In addition, the PECAM1 ITIM binds SAP, which mediates adhesion in T-like cells (205). Finally, the PECAM1 CYT ITIM and ITSM bind Nck, coupling the receptor to activation of p21-activated kinase and NF- κ B during oxidative stress in endothelial cells (206). Overall, these examples demonstrate that an ITIM-containing receptor PECAM1 activates functional plasticity due to signaling versatility and differential signaling molecule recruitment in different cell-types.

The CD300 family of IgSF receptors play multiple regulatory roles in human and mouse immune cells and also exhibit signaling versatility. For example, human CD300f binds sphingomyelin and ceramide, preventing anaphylaxis in a mouse model by inhibiting mast cell degranulation. Inhibition by human CD300f is dependent on two CYT ITIMs or an ITSM via SHP1. Interestingly, when CYT ITIMs and ITSM are mutated (i.e. converted from tyrosine to phenylalanine to abolish phosphorylation and therefore signaling and function), cross-linking human CD300f activates mast cell degranulation via PI3K-dependent pathways (207, 208). The

mouse CD300f contains two ITIMs and an ITSM and binds ceramide *in vivo* to prevent activation of mast cells via ITIM/ITSM-dependent inhibitory signals (209), which plays a role in preventing ATP-induced experimental colitis in mice (210). In addition, co-cross-linking with FcεRI inhibits cytokine production via ITIM/ITSM-dependent pathways in mast cells. However, cross-linking an ITIM/ITSM mutant alone induces IL6 cytokine secretion, which depended on FcRγ-PI3K signaling. In mice, CD300f co-cross-linking with TLR4 enhanced cytokine production while suppressing activation through other TLRs (211). Finally, mouse CD300f binds phosphatidylserine and mediates apoptotic cell phagocytosis by macrophages via a PI3K-Rac/cdc42 pathway (212). Four CD300 genes have been identified in chickens, but only one, ggCD300L-B1, contains recognizable tyrosine-based motifs in the form of an ITIM and ITSM and none have been characterized further (213). In teleost, three CD300-like proteins (i.e. CD300a, CD300b and CD300f) were identified in salmon and CD300a and CD300f transcript expression increased in the skin of fish after infection, indicating a role in mucosal immunity (214).

Similar to KIR2DL4, chicken CHIR-AB1 contains a CYT ITIM and a charged TM segment. While no inhibitory signaling has been described for the ITIM, the positively charged TM segment facilitates FcRγ association and activates Ca²⁺ influx in B cells when cross-linked by heat-aggregated IgY. In fish, the IpLITR 1.1b CYT contains six tyrosine-based motifs, including two ITIMs and an ITSM, and inhibits NK cell-mediated cytotoxicity using two distinct pathways: an ITIM-dependent SHP mechanism and an ITIM-independent Csk mechanism (6). Furthermore, IpLITR 1.1b demonstrated an ability to activate actin-rich protrusions and phagocytosis when expressed in a rat basophilic cell line that was not inhibited by pharmacological inhibitors of ITAM pathways (7, 8). Collectively, these examples demonstrate

that ITIM-containing receptors can trigger stimulatory signaling pathways leading to activation of cellular responses.

2.2.6.1 Non-ITAM- or ITIM-dependent signaling versatility

Since the identification of ITAMs and ITIMs, three additional CYT motifs have been defined: hemITAM, ITSM and ITT (28). HemITAMs are partial ITAMs (i.e. only one tyrosine) with additionally conserved N-terminal residues (i.e. defined by DEDGYxxL sequence) present in the CYTs of multiple receptors including carcinoembryonic antigen-related cell adhesion molecule 3 (CEACAM3) and dectin1. CEACAM3 is strictly expressed in activated human neutrophils where it mediates bacterial recognition and phagocytosis. While Fc γ R-mediated phagocytosis progresses to Vav via Syk-PI3K signaling upstream, the CEACAM3 CYT binds directly to a complex of Nck-WAVE2 and the guanine exchange factor Vav (215, 216). These components activate the actin polymerization machinery without the need for Syk. However, production of reactive oxygen species (ROS) for target degradation requires both PI3K and Syk which are activated during later stages of phagocytic signaling (217, 218). Interestingly, the adaptor molecule Grb14, a relative of Grb2, binds the CEACAM3 CYT directly, but attenuates phagocytic signaling (219).

Dectin1 is a type II TM receptor belonging to the C-type lectin superfamily that forms non-covalent homodimers (220–223). It is expressed by dendritic cells, macrophages, neutrophils and a $\gamma\delta$ T cell subset in mice (224, 225), but also by B cells, eosinophils and mast cells in humans (226, 227). Dectin1 synergizes with TLR2-dependent signaling via Syk and MyD88 (228), while ligation on dendritic cells allows cross-priming of CTLs by a CARD9 pathway (229). Dectin1 activates phagocytosis (230, 231), ROS production (232) and IL2 and IL10 secretion that promote adaptive cell differentiation (233, 234). Interestingly, dectin1 binds

zymosan (a component of fungal cell walls) which activates phagocytosis. However, the mechanism of internalization depends on the availability of signaling molecules within the cytoplasm, which differs between cell-type due to differential signaling molecule gene expression (i.e. the cellular context). In fibroblasts, phagocytosis depends on SFKs and Syk, but in macrophages, phagocytosis depends only on SFKs (231). A subsequent study characterized a detailed molecular mechanism of dectin1-mediated phagocytosis in which Syk is recruited to the signalosome via phosphorylation of a cryptic ITAM in the C-terminus of SHP2 (235).

Collectively, the hemITAM-containing receptor dectin1 demonstrates cell context-dependent signaling versatility upstream of the same functional outcome (i.e. phagocytosis). In addition, the activation of Syk can occur in the absence of a dectin1 CYT ITAM via phosphorylation of tandem tyrosine residues (i.e. a cryptic ITAM) within an upstream signaling molecule.

The ITSM was first identified in a family of immunoregulatory receptors expressed by NK cells called the SLAM family receptors (236). Subsequently, the functions of these receptors were thoroughly investigated due to a causal link with X-linked lymphoproliferative (XLP) syndrome in humans (237–239). In general, SLAMF receptors homodimerize *in trans* with target cells (except SLAMF4 which binds SLAMF2) and activate NK cell-mediated cytotoxicity through CYT ITSM-dependent pathways. However, the versatility of SLAMF receptor CYT signaling is exemplified by SLAMF4 (a.k.a. 2B4, CD244). For example, SLAMF4 binds SLAMF2 on target cells resulting in CYT ITSM phosphorylation and activation of a SAP-Fyn-PLC γ -LAT-Vav1 pathway for cytotoxicity (240, 241). In the absence of SAP (e.g. in patients with XLP syndrome) phosphorylated ITSMs recruit SHIP, SHP1/2 and Csk resulting in cellular inhibition (236, 242, 243). SLAMF receptors have also been identified in chickens (244) where

SLAMF4, expressed by platelets, monocytes, NK cells, some T and B cells, binds to SLAMF2 on target cells just like its mammalian counterpart (245).

Finally, the ITT motif (defined by a YxNM sequence) is present in the CYT of DAP10 and CD28. DAP10 is an adaptor molecule that, like DAP12, associates with multiple activating receptors via charged TM segment interactions, however unlike DAP12, it activates a PI3K-Grb2-Vav pathway downstream of the NK cell receptor NKG2D (246). CD28 is a co-stimulatory receptor expressed by T cells that enhances TCR-evoked T cell activation by a Grb2-PI3K pathway (247).

Clearly, receptor CYT regions are important and dynamic regulatory components of immunoregulatory receptor-mediated responses due to their signaling capabilities and earlier vertebrate models have not been studied in as much detail as mammalian models. In the next section, I will extend these discussions to highlight detailed temporal and spatial receptor CYT sub-membrane dynamics and the recently appreciated role that actin polymerization plays in organizing signaling dynamics.

2.3 Diverse cytoplasmic tail (CYT)-dependent molecular mechanisms regulate effector responses

While extracellular domains and TM segments of receptors may influence signaling, the CYT regions of receptors are directly involved in activating specific signaling pathways. However, the presence of canonical CYT motifs does not always predict the stimulatory or inhibitory signaling outcome. In addition, immunoregulatory receptor-mediated regulation of effector responses progresses through temporally and spatially organized signaling events.

To gain a better understanding of signaling dynamics the following discussion will highlight detailed molecular examples of sub-membrane proximal signaling events. Roles for Src

family kinases (SFks), CYT requirements for differential signaling pathway activation and pre-formed signaling molecule complexes will be discussed. An emergent appreciation for actin should be apparent throughout these examples due to recent studies that show direct links between receptors and the actin cytoskeleton via actin-binding adaptors. The study of individual receptors and pharmacological inhibitors of actin dynamics are providing a refined understanding of membrane organization and its impact on signal transduction during, but also before and after, formation of cell-target synapses.

2.3.1 SFks mediate activation of specific pathways

SFks are critical regulators of phosphotyrosine-dependent signaling pathways because they initiate and facilitate phosphorylation events.

SFks are conserved throughout vertebrate lineages (248) and nine family members are expressed in humans (248, 249). Broadly expressed SFks include Fyn, Src, Yes, while Blk, Fgr, Hck, Lck, Lyn and Yrk are restricted to immune cells. SFks contain 3 or 4 modular domains that include an SH2 domain and a catalytic kinase domain. In general, kinase activity is regulated by intramolecular interactions involving Y⁴¹⁶ (within the catalytic domain) and Y⁵²⁷ (at the C-terminus). Inactive SFks are phosphorylated at Y⁵²⁷ by the C-terminal Src kinase (Csk), causing an auto-inhibited phospho-Y⁵²⁷-SH2 domain 'closed' conformation. Removal of auto-inhibition by dephosphorylating Y⁵²⁷ allows the kinase domain to unfold into an 'open' conformation. Subsequent phosphorylation of Y⁴¹⁶ activates kinase activity. Interestingly, sequential phosphorylation of the catalytic domain Y³⁹⁶ then C-terminal Y⁵⁰⁷ in Lyn SFK (homologous to Y⁴¹⁶ and Y⁵²⁷, respectively) stabilize an active conformation (250).

Co-expression of multiple isoforms of SFks and their regulation by Csk allows cells to differentially regulate signaling pathways. For example, differential activation of phagocytic

signaling by SFKs was investigated in mouse macrophages. Phagocytosis-negative cell lines were generated by co-expressing a membrane-bound form of Csk (mCsk). In mCsk-expressing cells, constitutively active (i.e. lack C-terminal regulatory Y⁵²⁷) Lyn, Hck and c-Src SFKs restore Vav and c-Cbl phosphorylation downstream of FcγR cross-linking. However, only Lyn and Hck, but not c-Src, associated with lipid rafts and restored phagocytosis. This demonstrates that SFKs are differentially involved in FcγR-mediated signaling pathways (251).

SFK-mediated activation of specific pathways also depends, in part, on substrate specificity of the kinase enzyme (252). For example, SFKs specifically phosphorylate tyrosine residues using an F_P⁴²⁵IKWTA motif within the kinase active site. P⁴²⁵ co-ordinates tyrosine residues within the active site but does not co-ordinate serine or threonine. Residues flanking the target tyrosine also influence substrate phosphorylation. Src and Lck prefer EEEIYG/EFD and xExIYGVFF substrate sequences, respectively (253). Furthermore, an HRDLA/R³⁸⁸AA/RN motif within the catalytic domains of Src and Lck contributes to a preference for N-terminal acid-rich sequences relative to the targeted tyrosine in substrates (254).

Finally, since SFKs require close proximity to phosphorylate substrates, the binding specificity of SFK SH2 domains also impacts the selection and progression of signaling pathway activation. In some cases, SFK recruitment via their own SH2 domains, to specific substrates that are then phosphorylated by their kinase activity, facilitates signaling through ‘processive’ phosphorylation (255). On top of this, detailed mechanistic investigations have shown that after initial SFK recruitment, SFK SH2 domains can be phosphorylated, changing binding specificity, altering protein-protein interaction to facilitate signaling. Specific examples include phosphorylation of Lck and Lyn SH2 domains. An elegant study of TCR signaling showed that Lck Y¹⁹² is critical for facilitating TCR-evoked actin polymerization and maintaining

immunological synapses (IS). Specifically, CD4⁺ T cells that lack an adaptor protein, TSAd, display impaired actin polymerization at the IS and reduced phosphorylation of downstream signaling molecules, Pyk2 and Itk. After TCR-evoked signaling, Itk-TSAd promote Lck Y¹⁹² phosphorylation resulting in recruitment of Pyk2. In other words, Lck Y¹⁹² phosphorylation changes the binding specificity of the Lck SH2 domain to release CD3-contained ITAMs and bind and activate Pyk2, which sustains IS formation (256). Upon inspecting Lck Y¹⁹², this residue is adjacent to the SH2 domain ligand binding grooves and is conserved in several human SFKs (257). Indeed, phosphorylation of the Lyn SH2 domain Y¹⁹⁴ (homologous to Lck Y¹⁹²) also alters its SH2 domain binding specificity (258). These examples demonstrate dynamic mechanisms of SFK-mediated regulation of selective signaling pathway activation.

2.3.2 CYT requirements for differential signaling pathway activation

In some cases, receptors contain more than one signaling motif or exist as isoforms with differing CYT compositions. This allows receptors to facilitate independent signaling pathways often resulting in co-activation of pathways and functions.

For example, the co-stimulatory molecule CD28 contains four tyrosine residues (i.e. Y¹⁷³ ITT, Y¹⁸⁸, Y¹⁹¹ and Y²⁰⁰) that it uses to activate various signaling pathways via distinct CYT motifs. CD28 cross-linking results in Vav and p62^{Dok} phosphorylation that depend on a Y¹⁷³ ITT Grb2-PI3K pathway and an intact Y²⁰⁰, respectively (259). CD28 also evokes IL2 secretion, which is reduced in a Y²⁰⁰F mutant receptor and blocked when the receptor is truncated after Y¹⁹¹. This indicates that the CD28 C-terminus activates IL2 secretion that is enhanced by an intact Y²⁰⁰ (260). Another example involves FcγRIIB, which is expressed in two isoforms (e.g. 1 and 2) that appear to be CYT region splice variants. FcγRIIB2 activates endocytosis and

phagocytosis but Fc γ RIIB1 only activates endocytosis. While phagocytosis requires both CYT Y²⁷² ITIM and Y²⁸⁹, endocytosis requires only CYT ITIM Y²⁷² (261).

In contrast with these examples, a single pathway may require distinct CYT segments for recruiting and activating a signaling molecule. The integrin $\alpha_M\beta_2$ activates phagocytosis of C3bi-opsonized targets by a RhoA pathway. The β_2 CYT recruits RhoA via C-terminal residues 758-760, while 16 residues in the membrane proximal CYT segment are necessary for activating RhoA (262). Similarly, inhibitory SHIP signaling pathways mediated by Fc γ RIIB require the C-terminal 16 residues for detection of SHIP association *in vivo* and catalytic activity (263). Altogether, CYTs display versatile recruitment and activation capabilities to selectively activate intracellular signaling pathways.

2.3.3 CYT-membrane interactions limit CYT motif availability

Another dynamic regulatory mechanism involves CYT associations with the inner leaflet of the membrane, which can limit CYT motif accessibility.

During TCR-mediated signaling, both CD3 ϵ and CD3 ζ ITAM-containing adaptor molecules must be released from the membrane by phosphorylation for full stimulatory signaling (264–266). Downstream of TCR activation, a basic residue-rich sequence within CD28 binds to the SHK Lck and the negatively charged inner membrane leaflet. The phosphorylation of Y¹⁹¹ (reported as Y²⁰⁷) causes CYT dissociation from the membrane allowing Lck to bind via its SH2 domain. Mutating the basic residues reduces Lck binding and downstream PKC θ activation, reducing T cell activation (267). A final example of an elegant mechanism involving the PECAM1 CYT, which contains an N-terminal ITIM and C-terminal ITSM, has been reported. At rest, the PECAM1 CYT adopts a helical conformation that begins with serine residue 673 (S⁶⁷³) and encompasses the C-terminal ITSM. Upon activation, S⁶⁷³ and the C-terminal ITSM are

phosphorylated, releasing the CYT-membrane association and allowing N-terminal ITIM phosphorylation (268). Overall, interactions between the inner leaflet of the membrane and receptor CYTs can influence signaling by limiting motif access.

2.3.4 Pre-formed signaling molecule complexes

Signaling molecules can exist as pre-formed complexes. Upon receptor cross-linking, these pre-formed complexes localize to a receptor. For example, an SLP65/CIN85 pre-formed heterodimer is necessary for BCR-evoked signaling (269). The ITAM-devoid PSGL1 receptor activates a Syk-dependent pathway. In this case, the actin-binding adaptor molecule ERM contains a constitutively phosphorylated C-terminal cryptic ITAM-like sequence that associates with Syk. By binding to a membrane proximal CYT segment of PSGL1, ERM localizes Syk to the receptor allowing its activation (270). Syk also associates with the fifth Ig domain of filamin A, an actin-binding adaptor molecule, and activates Syk-dependent pathways downstream of GPVI and CLEC2 platelet receptors (271). Intriguingly, pre-formed signaling complexes may interact with the actin cytoskeleton via actin-binding adaptors. These actin-binding adaptors are gaining more attention recently, and this concept will be revisited in section 2.3.6 below. Next, I will discuss integrated examples of transmembrane receptors, signalosomes and the underlying role of actin polymerization in forming cell-target contacts.

2.3.5 Transmembrane signaling complexes and actin polymerization control synapse formation

Depending on the cell-type and receptors being triggered, immune cells form different types of synapses with targets. These synapses are called the immunological synapse (IS), the natural killer/cytotoxic immunological synapse (NKIS), the phagocytic synapse and the mast cell synapse (152, 154, 272–275).

In general, synapse formation involves the recruitment of several receptors, co-receptors and cytoplasmic signaling complexes that organize its structure. IS dynamics are extensively characterized and its formation requires sustained signaling through multimolecular complexes involving the T cell receptor (TCR), CD3, CD4/8, CD80/86 and CD28, for example. These complexes form microclusters across the membrane that are constantly remodeled as actin mediates trafficking of molecules to and from different regions of the synapse. Three regions of the IS are the central supramolecular activation cluster (cSMAC), peripheral supramolecular activation cluster (pSMAC) and distal supramolecular activation cluster. Sustained signaling in the cSMAC involves intracellular signaling hubs like Gab2, LAT and SLP76/65 that function as scaffolding platforms for signalosome formation while the pSMAC is enriched with cell-cell adhesion molecules (276–280). Investigations of the NKIS have revealed the formation of inhibitory microclusters which dissociate activating receptor clusters by collapsing the pSMAC-associated actin cytoskeleton (281). The phagocytic synapse is also a highly organized structure. In fact, after Fc γ R is triggered, an outwardly diffusing integrin barrier excludes membrane-associated phosphatases (e.g. CD45, CD148) from the forming cSMAC, allowing underlying signaling complexes to form. While Fc γ R recruits and activates Syk-PI3K-SLP76/LAT pathways, the downstream formation of a PLD₂-Grb2-WASp heterotrimeric complex appears to dissociate from the receptor while facilitating actin polymerization and target internalization (282). These events exemplify the dynamics underlying immune cell-target contact sites. The next section will focus on the role of actin before and after synapse formation during signaling.

2.3.6 Sub-membrane organization controls receptor dynamics before and after phosphotyrosine-dependent cellular activation

The preceding examples demonstrate some dynamics underlying immunoregulatory receptor-mediated signaling. While phosphotyrosine-driven cascades predominate at formed synapses, the trafficking of receptors before and after synapse formation has gained much attention in recent years. In this section, I will highlight examples of sub-membrane receptor dynamics, including serine phosphorylation, inside-out receptor activation and actin-mediated receptor trafficking, and how they impact phosphotyrosine-dependent cellular activation.

2.3.6.1 Serine/threonine motifs and protein kinase A and C

FcR γ contains an ITAM containing two tyrosine residues at positions 47 and 58 that are critical for activating Syk-dependent pathways. However, within the ITAM is a serine residue at position 51 that can be phosphorylated by two kinases, protein kinase A and protein kinase C δ . S⁵¹ phosphorylation blocks dual ITAM tyrosine phosphorylation, resulting in decreased Syk recruitment and cellular activation (283).

2.3.6.2 Inside-out integrin activation

Integrins are well-characterized vertebrate receptors that mediate several biological functions including cell-cell adhesion and phagocytosis. Integrins are composed of heterodimeric $\alpha\beta$ complexes and at least ten are expressed by immune cells, including eight integrins that activate phagocytosis (e.g. $\alpha_M\beta_2$).

The ability to mediate ligand recognition requires cytoplasmic recruitment events to ‘open’ the receptor (i.e. inside-out activation), which then binds ligands and activates phagocytosis (i.e. outside-in signaling). Inside-out activation is mediated by signals from other receptors that activate the small GTPase Rap1 which promotes the recruitment of the adaptor

molecule talin to CYT NPxY motifs of integrin β subunits. In other words, participation in signaling through some immunoregulatory receptors may be controlled by conformational changes that turn on ligand recognition.

2.3.6.3 Actin-dependent sub-membrane receptor trafficking

The preceding sections have alluded to underlying roles that actin plays during dynamic regulation of immunoregulatory receptor signaling. Recent imaging studies have implicated direct roles for actin in these processes and provide mechanistic explanations for the heterogenous structure of membranes. By tracking single particle movement on the membrane in the presence of pharmacological inhibitors of actin polymerization, it appears that membrane components are segregated into microdomains by CD44-dependent ‘picket fences’, for example, that restrict lateral diffusion through the membrane (284–286). Not only have these observations highlighted the importance of alternative receptor CYT motifs that participate in receptor-actin adaptor molecule associations, they have also complemented previous observations of the effects of receptor-actin associations. For example, CYT motifs that link receptors to actin-binding adaptors include: basic residue-rich juxta-membrane sequences (287), L/IRRRY of 4.1 family proteins (288), SRRRC and QKKKL of CD44 (289) and Φ xxBxxxBB (where Φ is a hydrophobic residue and B is a basic residue) of Fc γ RI (290).

Several receptors demonstrate actin-dependent dynamics. For example, CD44-spectrin-actin linkages facilitate CD44 clustering after it binds E-selectin on activated endothelial cells during neutrophil extravasation (291). A poly-lysine motif within the CD86 CYT is necessary to re-organize CD86 within the immunological synapse during T cell stimulation (292). A number of studies have also focused on examination of phagocytic synapse dynamics. For example, Fc γ RI is constitutively serine phosphorylated and associates with the actin adaptor 4.1G,

tethering Fc γ RI to lipid rafts allowing rapid clustering upon receptor engagement (293). In addition, Fc γ RI segregates from inhibitory receptors upon IgG cross-linking, facilitating phagocytic synapse formation (294). The control of Fc γ R diffusion depends on CD44 picket fences and SFK-Syk pathways. Specifically, at the leading edges of advancing membrane protrusions during phagocytosis, actin branching facilitates lateral diffusion of Fc γ R, enhancing target avidity and signaling (284). SFKs and Syk induce cytoskeletal rearrangements that facilitate Fc γ R engagement and control phagocytic signaling (295). Finally, the scavenger receptor CD36 is confined to linear diffusion channels. This restricts perpendicular diffusion which effectively increases local receptor density 5-fold, compared to unrestricted diffusion, in resting cells. Upon target contact, linear diffusion channels accelerate receptor clustering and signal transduction (296). Clearly, receptor-actin linkages affect signaling dynamics and studying diverse receptor CYTs may lead to the identification of alternative receptor CYT motifs for actin-binding adaptors.

2.4 Summary of receptor CYT-mediated regulation of signaling events

The phosphotyrosine-dependent regulation of immune cell effector responses is critically dependent on receptor CYT motifs that activate specific pathways. Receptor CYT dynamics fine-tune the integration of input signaling and recent evidence has established the importance of non-canonical CYT motifs and the role of actin polymerization in controlling receptor trafficking. Signal transduction pathways often require inputs from several receptors, especially in organizing synapse formation, which effectively restricts signaling to sites of cell-target interaction.

To conclude this chapter, I will discuss two intrinsic themes of this review, cross-talk and the temporal stages of signaling, before addressing the utility of teleost models in expanding the

understanding of immune cell signal transduction, which sets the stage for the specific research objectives and aims of my thesis.

2.4.1 Immunoregulatory receptor cross-talk

A central theme of the examples presented in this review has been the co-ordinated signaling events of multiple receptor-types. Although signal transduction is most commonly studied by activating a single receptor within a reductionist system, mechanisms of signaling never involve a single receptor. In fact, immune cells co-express multiple immunoregulatory receptor-types, including related and unrelated families. Paired receptor families contain highly related extracellular domains, suggesting they bind similar targets, which has been demonstrated for LRC members that interact with MHC class I. However, in mammals, certain receptor families have evolved cell-type-specific regulatory functions like the FcR-like (FcRL) family in mammalian B cells.

The seven human and six mouse FcRL members are structurally diverse proteins containing up to nine extracellular Ig-like domains and variable combinations of CYT ITIMs or ITAMs or even composite CYTs with both ITIMs and ITAMs (297). FcRL-like genes are present in many different vertebrates including mammals, birds, frogs, and fish, but extensive molecular characterizations demonstrating FcRL cross-talk have only been conducted using mammalian models. For example, both FcRL2 and FcRL3 CYTs contain combinations of ITIMs and putative ITAM-like sequences. While FcRL2 is preferentially expressed in memory B cells, FcRL3 expression increases as B cells mature. Both FcRL2 and FcRL3 inhibit BCR-evoked signaling through CYT ITIM or ITIM-like-dependent SHIP/SHP pathways (298–300). FcRL3 promotes TLR9-mediated B cell proliferation, activation and survival but it suppresses the final stage of B cell maturation into plasma cells. Underlying these effects, FcRL3 amplified NF- κ B

and MAPK activation but inhibited the activation of a transcription factor for plasma cell differentiation BLIMP1 (301). FcRL4 CYT contains ITIM and ITAM-like motifs and has demonstrated functional versatility in B cells. While FcRL4 reduces BCR-evoked early activation signals (i.e. blocks PLC γ 2 and Vav phosphorylation, and Ca²⁺ influx) via SHP1/2 recruitment, it also localizes to endosomes and enhances CpG-evoked TLR9-mediated activation. Interestingly, the inhibitory function requires all three CYT tyrosines (one ITSM, two ITIMs) but not receptor ligation (302). In a second study, FcRL4 differentially regulated B cell function in the presence of Hck or Fgr SFKs. In MAPK activation reporter assays, Fgr co-expression caused inhibition while Hck caused activation upon FcRL4 co-cross-linking with BCR. However, FcRL4 co-expression with either Hck or Fgr promoted IL10 and IFN γ secretion in human memory B cells (303). FcRL5 CYT contains an ITAM-like motif and two ITIMs and enhances proliferation when co-activated with BCR and TLR9 during B cell activation (304). Cell-type-specific regulation by FcRL5 differs in marginal zone B cells and peritoneal B1 cells where it inhibits BCR signaling via SHP1 recruitment to a phosphorylated CYT ITIM and has no effect on BCR activation due to decreased SHP1 expression levels, respectively (305). Finally, FcRL6 is expressed by natural killer cells and CD8⁺ cytotoxic T lymphocytes (CTLs) and its expression increases during cell differentiation. Although FcRL6 recruits inhibitory signaling molecules SHP1/2 and SHIP1/2, it can also recruit a stimulatory signaling molecule Grb2. However, FcRL6 does not affect cytotoxicity nor cytokine secretion in NK cells and CD8⁺ CTLs (306, 307).

These studies show that expression of FcRLs increases during maturation of immune cells. In fact, the innate-like B cell known as a B1 cell was described nearly three decades ago and thanks to the works above, the molecular mechanisms and immunoregulatory receptors

governing their innate-like functions have been revealed (308–310). In other words, not only do fully differentiated adaptive B cell-types fine-tune their activation thresholds by regulating the expression of cell-type-specific FcRL immunoregulatory receptors, but expression of these receptors also controls innate-like capabilities of B1 cell-types.

2.4.2 Early and late progression of signaling events

Another central theme of this chapter has been the temporal progression of signaling. Immunoregulatory receptors activate different signaling pathways during receptor engagement by recruiting molecules at different times. Two studies have demonstrated early and late signaling events during platelet activation and NK immunological synapse (NKIS) formation.

Platelet activation occurs via two waves of phosphorylation involving recruitment of molecules by three receptors. IgG-opsonized *S. sanguis* first activates an Fc γ RIIA-Syk-LAT-PLC γ phagocytic pathway. PECAM1 then localizes SHP1 to this complex, deactivating signaling via dephosphorylation. Subsequent localization of $\alpha_{IIb}\beta_3$ integrin re-phosphorylates Syk-LAT-PLC γ 2 pathway leading to granule exocytosis (311).

During NK cell activation, the ITIM-containing KIR2DL1 mediates inhibitory signaling by recruiting cellular phosphatases, like SHP1. However, NKISs contain activating receptors centrally and adhesion receptors peripherally that stabilize cell-target adhesion. The efficient inhibition of NKIS formation may involve differential inhibitory pathways that target centrally and peripherally forming complexes. Indeed, SHP1-mediated inhibitory signaling dephosphorylates cSMAC signaling complexes including Syk and Vav. An additional inhibitory pathway involves the phosphorylation of an adaptor molecule Crk, which no longer associates with the Rap1 GTPase C3G, thereby inhibiting the inside-out activation of the adhesion molecule

$\alpha_L\beta_2$ integrin which no longer binds intercellular adhesion molecule 1 in the pSMAC (177).

These examples demonstrate early and late signaling events during signaling.

2.4.3 Thesis objectives and aims

The regulation of immune cell effector functions depends in large part on dynamic signaling of cell surface-expressed immunoregulatory receptors. In particular, emergent details are revealing how ITIM-containing receptor CYT regions fine-tune signaling pathway activation across vertebrate lineages. Importantly, the teleost LITR family is evolutionarily related not only to LRC members, but also to FcRLs, which are traceable throughout amphibian, avian and mammalian lineages (297). In other words, LITRs may represent an ancestral family of receptors in fish that occupy important functional niches in descendant vertebrate lineages. Importantly, LITRs and their evolutionary homologs have maintained conserved and divergent phosphotyrosine-dependent CYT signaling capabilities, making them a valuable model.

The engineering of chimeric and epitope-tagged receptor constructs has allowed for heterologous expression of IpLITRs in mammalian cells. In combination with hemagglutinin (HA) epitope-tagging, commercially-available α HA antibodies trigger cellular activation through these receptors in the absence of natural ligands allowing for functional and biochemical characterizations of IpLITR signaling. This approach has revealed predictable ITAM-dependent signaling capabilities, as described in section 2.2.4, as well as unexpected details of IpLITR signaling potential. In particular, the ITIM-containing IpLITR 1.1b WT_{CYT} inhibited mouse NK cell-mediated cytotoxicity via ITIM-dependent SHP1/2 pathways, but also using an ITIM-independent Csk pathway (6). Subsequently, IpLITR 1.1b WT_{CYT} activated a unique ITAM-independent mode of phagocytic signaling that evokes actin-rich membrane protrusions to capture and internalize targets in rat myeloid RBL-2H3 cells (5, 7, 8). Clearly, IpLITR 1.1b

WT_{CYT} mediates versatile signaling and functional plasticity that depend on the cellular context of receptor expression (i.e. NK cell vs. RBL). The basis for my research came from observations of IpLITR 1.1b WT_{CYT}-mediated functional plasticity, however I aimed to establish a system for detailed molecular characterizations in a reductionist non-immune cell context.

Non-immune epithelial cells comprise the anatomical barrier to infection, separating the external environment from host tissues and preventing microbial entry and tissue damage. Maintaining this barrier requires multiple additional cell-types. For example, goblet cells secrete protective mucous and M cells sample and present particulate antigen to underlying sub-mucosal lymphoid tissues and immune cells. Epithelial cells express certain innate immune receptors (e.g. Toll-like receptors) that trigger constitutive cytokine release which stimulates underlying tissues and cells and maintains barrier integrity. Importantly, they do not typically bind, internalize nor process microbial antigen because they do not express the appropriate immune recognition receptors (e.g. certain IgSF members; 9, 282–284), except for specialized retinal pigment epithelium that express immune scavenger receptors (315). However, epithelial cells do require dynamic actin polymerization signaling pathways to polarize their membranes (i.e. apical and basolateral sides; 285). As such, resting epithelial cells express SH2 domain-containing sub-membrane proximal signaling molecules and effectors of actin polymerization but do not express a receptor capable of linking sub-membrane signaling events to transduce extracellular target recognition into internalization (9, 10, 313, 317). This provides a cellular context for isolating receptor CYT-specific sub-membrane proximal signaling events while mitigating interference from co-activated signaling pathways. This reductionist strategy successfully defined CYT requirements of mammalian ITAM-dependent signaling pathways (12, 14–18), which were

described in detail in section 2.2.4. Therefore, my primary objective was to establish a non-immune AD293 epithelioid cell system to examine IpLITR 1.1b WT_{CYT} signaling versatility.

Specifically, I generated GST-IpLITR CYT fusion proteins to characterize signaling molecule recruitment to IpLITR CYT regions (outlined in Figure 4.1). My results showed several stimulatory molecules were recruited to IpLITR 1.1b WT_{CYT}. Next, I generated stable IpLITR-expressing AD293 cell lines (outlined in Figure 4.7) to test IpLITR-mediated phagocytic signaling potential (outlined in Figure 4.6). While the ITAM-containing IpFcR γ -L WT_{CYT} activated phagocytosis, IpLITR 1.1b WT_{CYT}-mediated phagocytosis observed in RBL-2H3 cells could not be re-constituted in AD293 cells. This led me to examine gain-of-function re-constitution hypotheses (outlined in Figure 4.14), including co-expression with the promiscuous vSrc SFK and over-expression of Syk or SAP signaling molecules, to restore IpLITR 1.1b WT_{CYT}-mediated phagocytosis. My results showed that IpLITR 1.1b WT_{CYT} was not capable of 'bona fide' phagocytic signaling, suggesting that while it can evoke phagocytosis in RBL-2H3 cells, it may revert to an inhibitory signaling potential, similar to previous mouse NK cell characterizations, when expressed in AD293 cells. Subsequent biochemical characterizations revealed an inhibitory signaling molecule recruitment profile in physiologically stimulated cells using pervanadate (outlined in Figure 4.11), indicating an inhibitory signaling potential. Since innate cell-types co-express paired receptor families, IpLITRs are co-expressed in channel catfish immune cell-types and IpLITR extracellular domains are highly similar (i.e. may bind common ligands), I pursued two main objectives. First, I established a novel phagocytosis assay to measure IpLITR-mediated cross-talk signaling potential using fluorescent bead targets and transiently transfected eGFP-tagged IpLITR 1.1b CYT constructs into stable IpFcR γ -L WT_{CYT}-expressing cells (outlined in Figure 5.6). Next, I used site-directed IpLITR 1.1b CYT YF mutant

constructs, dominant-negative signaling molecule constructs and shRNA-mediated signaling molecule knockdown techniques to characterize IpLITR 1.1b WT_{CYT} requirements for down-regulating ITAM-dependent phagocytosis (outlined in Figure 6.2). My results show a novel IpLITR 1.1b WT_{CYT}-mediated inhibitory signaling capability for down-regulating ITAM-driven phagocytosis. Interestingly, this inhibitory down-regulation required co-operativity between the proximal and distal CYT segments of IpLITR 1.1b WT_{CYT} for maximal effect. Altogether, this represents a new inhibitory signaling capability for IpLITR 1.1b WT_{CYT} and the first functional and biochemical assessments of signaling cross-talk potential within a teleost immunoregulatory receptor family.

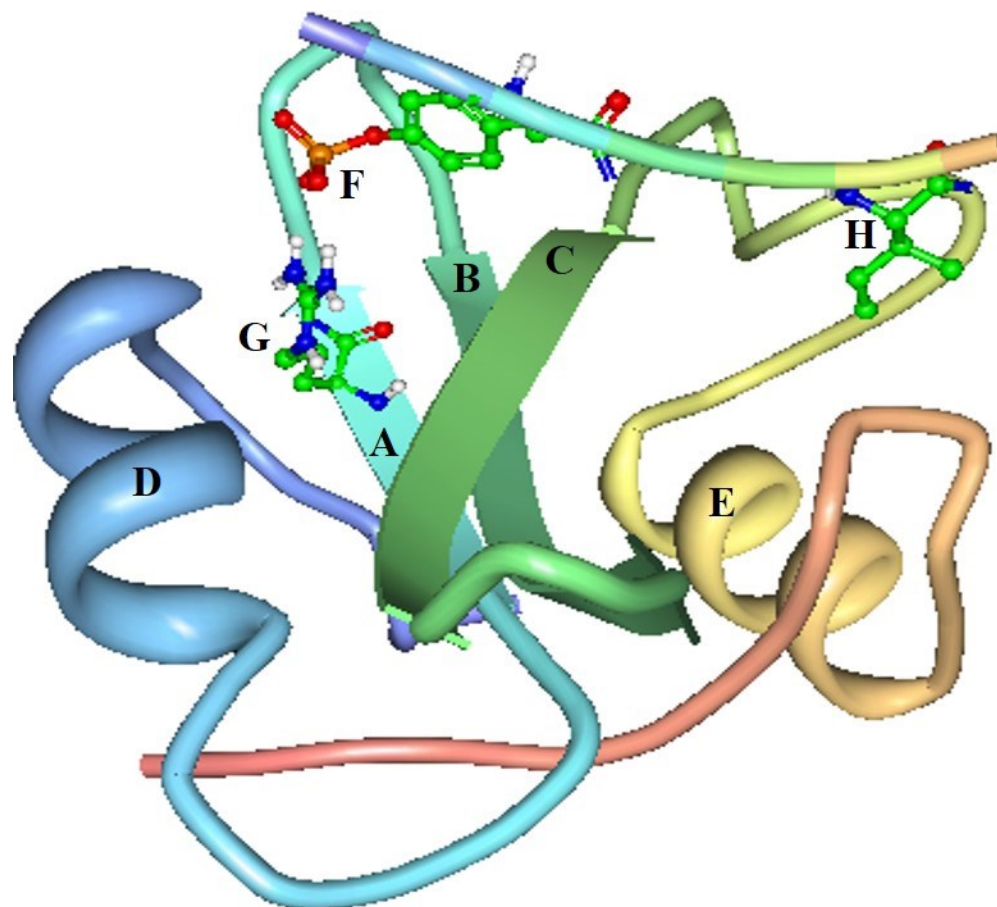


Figure 2.1. Tertiary crystal structure schematic of the cellular Src kinase SH2 domain bound to a phospho-YEEI peptide ligand. The SH2 domain is composed of three anti-parallel β -sheets (A, B, C) in between two α -helices (D, E), one on each side. The peptide ligand phosphotyrosine residue (F) co-ordinates the arginine residue (G; of the signature SH2 domain FLVRES motif) of β -sheet A within the phosphotyrosine binding groove. SH2 domain binding specificity is dependent on phosphotyrosine + 1, 2 and/or 3 C-terminal position residues. Isoleucine (H) at position + 3 within the binding specificity groove. Protein Data Bank ID for this crystal structure is 1SPS. Each chain is colour-coded purple to red from N- to C-terminus, respectively.

Figure 2.2. SH2 domain residues that co-ordinate peptide ligand residues and determine binding specificity are highly conserved throughout vertebrates.

Crystal structures of SH2 domains complexed with phosphopeptide ligands were analyzed in RCSB Protein Workshop. By visualizing specificity-determining ligand residue side chains, closely coordinating SH2 domain residue side chains were identified (red boxes). Consensus sequence similarity is indicated by ‘*’ or ‘.’ symbols. Black or grey shading indicates identical or similar (e.g. hydrophobic, polar, charged) residues in a column, respectively. Protein Data Bank IDs for the crystal structures analyzed include: Csk (2RSY); SHP1 (2YU7); SHP2 (3TL0, 4JEG, 4QSY); Syk (1A81). GenBank accessions for the N- and C-terminal (N- and C-, respectively) SH2 domain sequences used include: Csk (NP_004374.1, JAA38735.1, NP_001291690.1, NP_001025210.1, NP_990756.1, NP_001079062.1, NP_001071067.1, AHH39155.1); SHP1 (AAA36610.1, PNI21144.1, AAC36009.1, NP_446360.1, NP_001026655.1, AAI60526.1, NP_956254.1); SHP2 (Q06124.2, JAA44247.1, AAH59278.1, P41499.4, NP_990299.1, NP_001084076.1, NP_956140.1); Syk (P43405.1, XP_016816611.1, AAA87462.1, Q64725.1, NP_001026601.1, NP_001086665.1, NP_998008.1).

CHAPTER III

MATERIALS AND METHODS

3.1 Cell lines and antibodies

3.1.1 Cells

Human embryonic kidney HEK293T cells (ATCC #CRL-3216) and an adhesion-enhanced derivative of HEK293 cells called AD293 cells (Stratagene #240085) were grown at 37°C and 5% CO₂ in complete Dulbecco's minimal essential medium (cDMEM; Gibco #12800017) containing 10% (v/v) heat-inactivated fetal bovine serum (FBS; Sigma #F1051), 44 mM NaHCO₃ (Sigma #S5761), 50 U/mL penicillin (Gibco #15070-063) and 50 µg/mL streptomycin (Gibco #15070-063).

Human natural killer YTS cells (provided by Heather Eaton, Dept. of Medical Microbiology & Immunology, University of Alberta) were grown at 37°C and 5% CO₂ in complete Iscove's modified Dulbecco's medium (Sigma #I3390) containing 15% FBS, 50 µM β-mercaptoethanol (Bio-Rad #161-0710) and 4 mM L-glutamine (Gibco #25030-081).

3.1.2 Antibodies

The following blotting antibodies were used: mouse THE™ αFLAG HRP-conjugated monoclonal antibody (mAb; Genscript Corp. #A01428), goat anti-β-actin IgG polyclonal antibody (pAb; Santa Cruz #sc-1616), rabbit αCsk IgG pAb (Santa Cruz #sc-286), rabbit αSHP2 IgG mAb (Cell Signaling #3397S), mouse αGST IgG mAb (Thermo Scientific #MA4-004), mouse PY20 α-phosphotyrosine HRP-conjugated mAb (Thermo Scientific #MA1-12445), mouse THE™ α-hemagglutinin (HA) HRP-conjugated mAb (Genscript Corp. #A01296), bovine α-goat IgG HRP-conjugated secondary antibody (Santa Cruz #sc-2350), goat α-mouse IgG(H+L) HRP-conjugated secondary antibody (Bio-Rad #170-6516) and goat α-rabbit IgG(H+L) HRP-conjugated secondary antibody (Bio-Rad #172-1019).

The following antibodies were used for flow cytometric staining of cell surface-expressed IpLITR constructs: mouse α HA IgG3 mAb HA.C5 (ABM #G036), mouse IgG3 isotype control antibody MG3-35 (BioLegend #401302) and goat α -mouse IgG(H+L) phycoerythrin-conjugated secondary antibody (Beckman Coulter #731849).

The following antibodies were used in bead-based phagocytosis assays: mouse α HA IgG3 mAb HA.C5 (ABM #G036) and rabbit α -mouse IgG(H+L) AlexaFluor647-conjugated secondary antibody (Invitrogen #A21239).

3.2 Cloning SH2 domain-containing signaling molecules into the FLAG epitope tag-encoding p3XFLAG-CMV14 expression vector

To generate C-terminal FLAG-tagged recombinant proteins, AD293 and YTS cell mRNA was isolated using TRIzol™ reagent (Invitrogen #15596026) and full-length cDNA was prepared using the SuperScript® VILO™ cDNA synthesis kit (Invitrogen #11754-050), according to the manufacturer's protocol. The cDNA was then used in polymerase chain reactions (PCRs) to amplify the various SH2 domain-containing signaling molecules and adaptors listed in Table 3.1. A pRS316 plasmid encoding the Avian sarcoma virus vSrc was a gift from Dr. Robert Ingham (Dept. of Medical Microbiology and Immunology, Faculty of Medicine and Dentistry, University of Alberta). All PCR reactions were performed using Phusion High-Fidelity DNA polymerase (Thermo Scientific #F530S) and the following cycling parameters: 98°C for 5 min, then 30 cycles @ [98°C for 10 s, 60°C for 30 s, and 72°C for 30 s], with a final extension step at 72°C for 5 min. Amplified products were gel purified and cloned into pJET1.2/blunt using the blunt-end protocol (CloneJET Thermo Scientific #PMK1231). pJET1.2/blunt plasmids were digested with the restriction enzymes indicated in Table 3.1 and the inserts ligated into the p3XFLAG-CMV14 eukaryotic expression vector (Sigma #E7908). All p3XFLAG-CMV14 expression

constructs were sequenced (Molecular Biology Services Unit, University of Alberta) prior to expression studies. See Figure 3.1 for schematic representations of all SH2 domain-containing signaling molecules.

3.2.1 Generating dominant-negative Csk-FLAG and SHP2-FLAG signaling molecule constructs

Sequenced p3XFLAG-CMV14 vectors encoding Csk and SHP2 were re-amplified with the same forward primers as above, in combination with dominant-negative reverse primers (denoted by Δ in Table 3.1) and the same cycling parameters and sub-cloning procedures described in the previous section. See Figure 3.1 for schematic representations of all SH2 domain-containing signaling molecules.

3.3 Generating GST-CYT fusion protein constructs

3.3.1 Sub-cloning receptor CYT sequences into the GST vector, pFN2A

The cDNA templates for generating GST-CYT fusion proteins include pDisplay expression constructs encoding IpLITR 2.6b/IpFcR γ -L and IpLITR 1.1b (5) as well as a commercially synthesized pUC vector encoding human carcinoembryonic antigen-related cell adhesion molecule 3 (CEACAM3; ACCN# BC106728.1, Genscript Corp). GST-IpLITR 1.1b WT_{CYT} contains the full-length CYT region of IpLITR 1.1b (i.e. residues 393-510; ACCN# ABI16050) including Y⁴³³, Y⁴⁵³, Y⁴⁶³, Y⁴⁷⁷, Y⁴⁹⁹, and Y⁵⁰³. GST-IpLITR 1.1b PROX_{CYT} contains the proximal CYT segment of IpLITR 1.1b (i.e. residues 389-474) including Y⁴³³, Y⁴⁵³, and Y⁴⁶³, and GST-IpLITR 1.1b DIST_{CYT} contains the distal CYT segment of IpLITR 1.1b (i.e. residues 464-510) including Y⁴⁷⁷, Y⁴⁹⁹, and Y⁵⁰³. In addition, GST-IpFcR γ -L WT_{CYT} contains the full-length CYT region of IpFcR γ -L (i.e. residues 50-87; ACCN# AF543420), GST-CEACAM3 WT_{CYT} contains the full-length CYT of human CEACAM3 (i.e. residues 182-252), and the GST

control construct contains only the GST epitope tag encoded by the bacterial GST expression vector pFN2A (Promega #C8461). All CYT cDNA sequences were amplified using primers listed in Table 3.2 and PCR reactions were performed with Phusion High-Fidelity DNA polymerase (Thermo Scientific #F530S) and the following cycling parameters: 98°C for 3 min, then 30 cycles @ [98°C for 10 s, 60°C for 15 s, and 72°C for 30 s], with a final extension step at 72°C for 5 min. Amplified products were gel purified and cloned into pJET1.2/blunt using the blunt-end protocol (CloneJET Thermo Scientific #PMK1231). PJET1.2/blunt plasmids were then digested with *SgfI* (Promega #R7103) and *PmeI* (New England BioLabs #R0560S) restriction enzymes and the inserts ligated into the GST expression vector pFN2A according to the manufacturer's protocol. All GST-CYT fusion protein construct vectors were sequenced (Molecular Biology Services Unit, University of Alberta) prior to expression studies.

3.3.2 Synthesis and affinity purification of GST-CYT fusion proteins from *E. coli*

The sequenced GST-CYT fusion protein construct vectors were transformed for 30 min on ice, followed by a 30 s heat shock at 42°C and a 45 min incubation in 250 µL SOC outgrowth medium (New England BioLabs #B9020S) at 37°C in a shaking incubator into both BL21(DE3) (New England Biolabs #C2527H) and TKB1 (Agilent Technologies #200134) competent *E. coli* strains for the production of control (i.e. non-phosphorylated) and tyrosine-phosphorylated recombinant GST-CYT fusion proteins, respectively, as previously described (198, 318). Briefly, the production of GST, GST-IpLITR 1.1b WT_{CYT}, GST-IpLITR 1.1b PROX_{CYT}, GST-IpLITR 1.1b DIST_{CYT}, GST-IpFcR γ -L WT_{CYT} and GST-CEACAM3 WT_{CYT} fusion proteins was performed by inducing 100 mL of transformed bacterial cultures in lysogeny broth (171 mM NaCl, 10 g/L tryptone, 5 g/L yeast) with 0.2 mM isopropyl 1- β -D-thiogalactopyranoside and incubating them for 2 h at 37°C in a shaking incubator. BL21(DE3) *E. coli* were centrifuged

(5000 x g, 5 min) and the bacterial pellets were frozen at -80°C overnight prior to lysis and purification. TKB1 *E. coli* contain a tryptophan starvation-induced tyrosine kinase (TK), Elk1 (319, 320), so these transformed bacteria were pelleted and re-suspended in 200 mL TK induction media containing casamino acids (42.3 mM Na₂HPO₄, 22.0 mM KH₂PO₄, 18.7 mM NH₄Cl, 8.56 mM NaCl, 27.0 mM CaCl₂, 1 mM MgSO₄•7H₂O, 0.2% w/v glucose, 0.1% w/v casamino acids, 1.5 mM thiamine HCl and 53.4 mM 3-indoleacrylic acid), according to the manufacturer's protocol. Protein phosphorylation proceeded for 1 h at 37°C after which, cells were pelleted and frozen at -80°C. For affinity purification of the various GST-tagged recombinant proteins, BL21(DE3) and TKB1 pellets were first lysed in 10 mL of 1% Triton-X Tris-buffered saline (TBS) lysis buffer (50 mM Tris, 150 mM NaCl supplemented with EDTA-free protease inhibitor cocktail tablets; Roche #11836170001, pH 7.4) by sonication on wet ice for 1 min (Braun sonicator 1510; 33Hz, 110W). Bacterial lysates were then centrifuged at 17000 x g for 10 min and supernatants were collected in 1 mL aliquots and stored at -80°C. To affinity purify GST-CYT fusion proteins, 100 µL of a 50% glutathione-conjugated sepharose bead slurry (Molecular Probes #G2879), washed 3x in lysis buffer, was mixed with 2 mL of clarified bacterial lysate for 10 min at 4°C on a rotating mixer. Beads were then washed 3x with lysis buffer and re-suspended as a 50% slurry in lysis buffer containing 10% glycerol and stored at -20°C. Affinity protein purifications were visualized by adding 10 µL of purified 50% slurry to 100 µL of 2X reducing buffer (Bio-Rad #161-0747) containing 5% β-mercaptoethanol (Bio-Rad #161-0710), which were boiled at 95°C for 10 min prior to loading 10 µL of sample on a 12% SDS-PAGE gel. Separated proteins were transferred to nitrocellulose membranes (Bio-Rad #162-0112) and visualized with Ponceau S solution (Sigma #P7170), a non-specific protein stain.

3.4 Generating HA epitope-tagged IpLITR 1.1b CYT receptor constructs

3.4.1 A chimeric IpLITR 1.1b/IpFcR γ -L WT_{CYT} phagocytic receptor construct

The cDNA templates for generating the IpLITR 1.1b/IpFcR γ -L WT_{CYT} (referred to as IpFcR γ -L WT_{CYT}) phagocytic chimeric receptor construct included pDisplay expression constructs encoding IpLITR 2.6b/IpFcR γ -L and IpLITR 1.1b used previously (5). To generate a pDisplay-encoded IpLITR 1.1b/IpFcR γ -L WT_{CYT} construct, the ectodomain and transmembrane segments of IpLITR 1.1b were fused with the CYT region of IpFcR γ -L by splice overlap extension (SOE) polymerase chain reaction using the primers indicated in Table 3.3, adapted from a previously published procedure (4). All sequences were sub-cloned using *SmaI/SalI* restriction digests into the pDisplay eukaryotic expression vector (Invitrogen Life Technologies #V660-20), which adds an N-terminal HA epitope tag to the protein. See Figure 4.12 and Figure 6.1 for schematics of the IpLITR constructs.

3.4.2 Site-directed mutagenesis to generate IpLITR 1.1b CYT YF mutant receptor constructs

The pDisplay-*IpLITR 1.1b* expression construct synthesized previously (5) was used as a template for generating *IpLITR 1.1b* CYT tyrosine to phenylalanine (YF) mutant receptor constructs using site-directed mutagenesis (SDM) essentially as described elsewhere (3, 6). Mutant constructs containing a single YF mutation (i.e. *IpLITR 1.1b* Y⁴⁵³F_{CYT}, *IpLITR 1.1b* Y⁴⁷⁷F_{CYT} and *IpLITR 1.1b* Y⁴⁹⁹F_{CYT}) were subjected to a single SDM polymerase chain reaction (PCR) using the corresponding primers from Table 3.3 and the following cycling parameters: 95°C for 2 min, then 35 cycles @ [95°C for 20 s, 59°C for 20 s, and 72°C for 3.5 min], with a final extension step at 72°C for 5 min. PCR products were visualized on 0.8% agarose (BioShop #AGA001) gels and a band was gel purified and subjected to T4 ligase (Thermo Scientific

#K1231)-mediated ligation. Ligation reactions were directly transformed into DH5 α *E. coli* (New England BioLabs #C2987H) and positive colonies were inoculated into 10 mL lysogeny broth (171 mM NaCl, 10 g/L tryptone, 5 g/L yeast) and grown up at 37°C overnight. Plasmids were purified by mini-prep (BioBasic kit #SD5005) and sequenced (Molecular Biology Services Unit, University of Alberta) to confirm specific SDM YF mutations. Successive SDM PCRs, using the sequenced template from the previous round of SDM PCR, were performed to generate mutant constructs with accumulated YF mutations (i.e. IpLITR 1.1b Y^{prox}F_{CYT} and IpLITR 1.1b Y^{dist}F_{CYT}). For example, to generate IpLITR 1.1b Y^{prox}F_{CYT}, in which all three proximal tyrosine-based motifs (i.e. Y⁴³³, Y⁴⁵³ and Y⁴⁶³) are mutated, three successive SDM PCRs were conducted, first using primer pairs targeting Y⁴⁵³, then Y⁴³³ and finally Y⁴⁶³. See Figure 4.12 and Figure 6.1 for schematics of the IpLITR constructs.

3.4.3 Generating eGFP-tagged IpLITR 1.1b CYT receptor constructs

CDNA templates for generating eGFP-tagged IpLITR 1.1b CYT receptor constructs include those generated in section 3.4.2 above as well as the pDisplay-encoded IpLITR 1.1b WT_{CYT} synthesized previously (5). Adding a C-terminal eGFP tag was accomplished by sub-cloning receptors into the eGFP expression vector pEGFP-N1 (Clontech #6085-1) and then re-cloning the IpLITR-eGFP sequences back into the pDisplay eukaryotic expression vector (Invitrogen #V660-20). Initial polymerase chain reactions (PCRs) were performed using the *NheI* Fwd and *BamHI* Rvs primers listed in the bottom box of Table 3.3 and the following cycling parameters: 98°C for 5 min, then 25 cycles @ [98°C for 10 s, 60°C for 30 s, and 72°C for 30 s], with a final extension step at 72°C for 5 min. Amplified products were gel purified and sub-cloned into pJET1.2/blunt using the blunt-end protocol (CloneJET Thermo Scientific #PMK1231). pJET1.2/blunt plasmids were digested with *NheI* (Thermo Scientific

#FD0974)/*Bam*HI (Thermo Scientific #FD0054) restriction enzymes and the inserts ligated into the pEGFP-N1 vector. PCRs using the same parameters just described were performed with the *Sma*I Fwd and *Sall* Rvs primers listed in the bottom box of Table 3.3. Amplified products were gel purified and sub-cloned into pJET1.2/blunt using the blunt-end protocol. PJET1.2/blunt plasmids were digested with *Sma*I (Fermentas #ER0665) and *Sall* (Thermo Scientific #FD0644) restriction enzymes and the inserts ligated into the pDisplay eukaryotic expression vector. All eGFP-tagged IpLITR 1.1b CYT receptor constructs were sequenced (Molecular Biology Services Unit, University of Alberta) before expression studies. See Figure 4.12 and Figure 6.1 for schematics of the IpLITR constructs.

3.5 Generating stable IpLITR 1.1b CYT construct-expressing AD293 cell lines

1 µg of pDisplay-IpLITR 1.1b CYT construct expression vector (i.e. the constructs generated in sections 3.4.1 and 3.4.2) was transfected into AD293 cells cultured in 24-well plates using TurboFECT *in vitro* transfection reagent (Thermo Scientific #R0531), according to the manufacturer's protocol. Transfected cells were then cultured in cDMEM to which 800 µg/mL G418 disulfate salt solution (BioBasic Canada Inc. #GDJ958) was added 2 days post-transfection and cells were maintained under selection until ~80-90% confluent. Viable cells were cloned as single cells in round bottom 96-well tissue culture plates by serial limiting dilutions, as described previously (7). Individual clones were then screened for IpLITR surface expression levels by flow cytometry (Beckman Coulter Cell Lab Quanta™ SC) as previously described (5). Briefly, ~2x10⁵ cells were incubated with αHA mAb or mouse IgG3 isotype control antibody, followed by the addition of the goat α-mouse IgG phycoerythrin-conjugated polyclonal secondary antibody (Figure 4.12). Positive clones were cultured at 37°C and 5% CO₂ in cDMEM with 400 µg/mL G418.

3.6 Generating lentiviral shRNA-mediated signaling molecule protein knockdowns in stable IpLITR 1.1b/IpFcR γ -L WT_{CYT}-expressing AD293 cells

MISSION[®] short hairpin RNA (shRNA) lentiviral system was used for generating knockdowns. The protocol for generating lentiviral shRNA-containing particles and transducing AD293 cells was adapted from an Ingham lab protocol (courtesy of Zuoqiao Wu, Dept. of Medical Microbiology & Immunology, University of Alberta) essentially as previously described (321, 322).

3.6.1 Producing lentiviral particle-containing supernatants from HEK293T cells

Pre-mixed lentiviral packaging vectors (Sigma #SHP001) were co-transfected with pLKO.1 vector containing an SH2 domain-containing signaling molecule targeting shRNA sequence using TurboFECT *in vitro* transfection reagent (Thermo Scientific #R0531). The shRNA sequences used include: three different Csk (TRCN0000000805, TRCN0000000806, TRCN0000000807) or SHP2 (TRCN0000005002, TRCN0000005003, TRCN0000005006) targeting shRNAs and one non-targeting scramble control shRNA (SHC002). Media was refreshed at 24 h post-transfection, and lentiviral particle-containing supernatants were collected 48 h post-transfection and frozen in 0.5 mL aliquots at -80°C.

3.6.2 Lentiviral titering and generation of stable Csk and SHP2 knockdown IpFcR γ -L WT_{CYT}-expressing AD293 cell lines

Lentiviral particle-containing supernatants were thawed to room temperature and prepared as 1:3, 1:9 and 1:27 dilutions in cDMEM with 400 μ g/mL G418 to a final volume of 500 μ L. 1 μ L of a 4 mg/mL stock solution of polybrene (EMD Millipore #TR-1003-G) in 0.9% NaCl was then added to each dilution to enhance viral transduction efficiency (323, 324). Cells were incubated in 500 μ L diluted solutions for 12-16 h, washed 3x with cDMEM and incubated in 3

mL of fresh cDMEM with 400 $\mu\text{g}/\text{mL}$ G418 plus 2 $\mu\text{g}/\text{mL}$ puromycin to select for positively transduced cells. The dilution with optimized transduction efficiency and cell viability reaches 80-90% confluence first, and these cells were propagated for downstream phagocytosis experiments. SH2 domain-containing signaling molecule protein knockdowns were confirmed by Western blotting using rabbit αCsk polyclonal antibody (pAb) or αSHP2 mAb followed by goat $\alpha\text{-rabbit IgG(H+L)}$ HRP-conjugated secondary antibody. A goat anti- $\beta\text{-actin}$ pAb followed by bovine $\alpha\text{-goat IgG}$ HRP-conjugated secondary antibody was used as a loading control. Bands were analyzed by densitometry using Fiji v1.52i (325) to quantify protein-targeted knockdowns relative to non-targeting scramble control. ShRNA clones exhibiting the greatest reduction of target expression (i.e. Csk TRCN0000000805 and SHP2 TRCN0000005003) were used in phagocytosis assays (control blots shown in Figure 6.6EF and Figure 6.7EF).

3.7 Biochemical signaling molecule recruitment to IpLITR 1.1b CYT segments and motifs

3.7.1 Transient transfection of FLAG-tagged molecules into AD293 cells to generate FLAG-containing lysates

Transfections were accomplished using $\sim 10^5$ AD293 cells seeded in 6-well tissue culture plates. Cells were seeded in 3 mL cDMEM per well 48 h prior to transfection with plasmid DNA. For each expression construct, DNA was first diluted in 300 μL of reduced serum Opti-MEM (Gibco #31985-070) and then 4 μL of TurboFECT *in vitro* transfection reagent (Thermo Scientific #R0531) was added. For all studies, 2 μg of p3XFLAG-CMV14 plasmid DNA was used. The Opti-MEM-plasmid-TurboFECT solution was evenly layered onto the cells, which were then incubated for 24-48 h at 37°C to allow for protein production. Cells were then lysed in 400 μL of ice-cold 1% Triton-X TBS lysis buffer (50 mM Tris, 150 mM NaCl supplemented with EDTA-free protease inhibitor cocktail tablets; Roche #11836170001, pH 7.4) for 30 min

and lysates were collected after centrifuging the samples at 16000 x g for 10 min at 4°C. Protein expression was confirmed by Western blotting using the mouse HRP-conjugated M2 α FLAG mAb (1:5000), as previously described (3).

3.7.2 GST-CYT fusion protein pulldowns from FLAG-containing lysates

Pulldown assays were essentially performed according to a previously described protocol (246). Briefly, the affinity purified GST-CYT fusion proteins were used as ‘bait’ for the capture of C-terminal FLAG-tagged SH2 domain-containing protein ‘prey’. Ten μ L of a 50% slurry containing the bead-conjugated GST-CYT fusion proteins were mixed with 70-100 μ L of AD293 cellular lysates expressing FLAG-tagged SH2 domain-containing proteins in 900 μ L 1% Triton-X TBS lysis buffer (50 mM Tris, 150 mM NaCl supplemented with EDTA-free protease inhibitor cocktail tablets; Roche #11836170001, pH 7.4). The bait and prey mixtures were then incubated at 4°C for 30 min on a rotating mixer. The GST-CYT protein-conjugated GST beads were then washed 3x with lysis buffer and boiled at 95°C for 10 min in 100 μ L of 2X reducing buffer (Bio-Rad #161-0747) containing 5% β -mercaptoethanol (Bio-Rad #161-0710) to elute proteins. Finally, eluted protein samples were separated by 12% SDS-PAGE gel, transferred to nitrocellulose membranes (Bio-Rad #162-0112) and probed with mouse α FLAG M2 HRP-conjugated mAb (1:5000) to detect any prey proteins captured by the GST-CYT fusion bait proteins. Mouse α GST IgG mAb followed by goat α -mouse IgG(H+L) HRP-conjugated secondary antibody and mouse α -phosphotyrosine HRP-conjugated mAb were controls for GST-CYT fusion protein re-capture and phosphorylation status, respectively.

3.7.3 Co-immunoprecipitation and Western blotting from pervanadate-stimulated cells transiently transfected with FLAG-tagged signaling molecules

Stable IpLITR 1.1b CYT construct-expressing AD293 cells were transfected with 1 μ g p3XFLAG-CMV14 encoding Csk-, Δ SHP2- or Δ Syk-FLAG constructs using TurboFECT *in vitro* transfection reagent (Thermo Scientific #R0531) according to the manufacturer's protocol. After 48 h, media was aspirated and cells were incubated at 37°C for 5 min in 500 μ L of pre-warmed 100 μ M sodium pervanadate in phosphate-buffered saline (PBS; 137 mM NaCl, 2.7 mM KCl, 10 mM Na₂HPO₄, 1.8 mM KH₂PO₄, pH 7.4), essentially as described previously (5). Cells were then lysed in 100 μ L/well of 1% Triton-X TBS lysis buffer (50 mM Tris, 150 mM NaCl supplemented with EDTA-free protease inhibitor cocktail tablets; Roche #11836170001, pH 7.4) for 30 min on ice, after which they were centrifuged at 16000 x g for 10 min at 4°C. Twelve μ L of the resulting supernatant was diluted 1 in 5 with 2X reducing buffer (Bio-Rad #161-0747) containing 5% β -mercaptoethanol (Bio-Rad #161-0710) and boiled at 95°C for 10 min while the rest was topped up to 1 mL with lysis buffer and incubated with 15 μ L of pre-washed α HA-coated magnetic sepharose beads (Pierce™ #PI88836) overnight at 4°C on a rotating mixer. Beads were washed 3x with lysis buffer and boiled at 95°C in 100 μ L 2X reducing buffer for 10 min to elute proteins. Proteins were then separated via 12% SDS-PAGE gel and transferred to nitrocellulose membranes (Bio-Rad #162-0112) that were probed with mouse α FLAG M2 HRP-conjugated monoclonal antibody (mAb; 1:2000) to detect co-precipitating FLAG-tagged signaling molecules. Probing with mouse THE™ α HA HRP-conjugated mAb (1:2000) and mouse α -phosphotyrosine HRP-conjugated mAb (1:2000) were controls for IpLITR 1.1b CYT construct precipitation and phosphorylation status after pervanadate treatment, respectively.

3.8 Imaging flow cytometry-based assays to assess IpLITR-mediated phagocytosis in AD293 cells

3.8.1 Measuring IpLITR-mediated phagocytosis of α HA-coated yellow green (YG) bead targets by component masking analysis

A bead-based phagocytosis assay was performed essentially as previously described (5, 7, 326), except that cells were adherent. Briefly, 4.5 μ m YG beads (Polysciences #16592-5) pre-absorbed with protein A (Sigma-Aldrich #P6031) were coated with 10 μ g/mL of α -hemagglutinin (HA) mAb. 9×10^5 α HA mAb-coated YG beads were added to $\sim 10^6$ stable IpLITR-expressing AD293 cells in 500 μ L cDMEM and incubated for 60 min at 37°C. After aspirating supernatant, 200 μ L of cDMEM containing 2 μ g rabbit α -mouse IgG(H+L) AlexaFluor647-conjugated secondary antibody at 4°C for 30 min to stain the cell surface-exposed beads. Cells were incubated at 37°C for 5 min in 200 μ L of ice-cold harvest PBS containing 0.05% trypsin (Gibco #25200-056) and 1.2 mM EDTA (Fisher #S311) to loosen cells for harvest and remove non-specifically cell-adsorbed beads. After 5 min, 500 μ L ice-cold cDMEM was added, the cells were collected and centrifuged at 500 x g for 2 min at 4°C and re-suspended in 20 μ L of 1% paraformaldehyde in PBS fixative prior to data collection using an ImageStream^x Mark II instrument (Amnis Corporation). For each sample, ~ 5000 events were collected and the data was analyzed using IDEAS software v.6.2 (Amnis Corporation) with connected component masks allowing for the accurate discrimination of phagocytosed versus surface-bound beads as described elsewhere in detail (327). Component masking allowed for the accurate gating of cell populations with only surface-bound beads, only phagocytosed beads, or both surface-bound and phagocytosed beads. Analysis was limited to cells associated with up to 3 beads, as cells with ≥ 4 beads are not as accurately gated by component masking.

3.8.2 IpLITR 1.1b CYT construct-mediated cross-talk regulation of phagocytosis in co-transfected parental cells

Pilot experiments to assess IpLITR-mediated cross-talk during phagocytosis were performed by co-transfecting IpLITR constructs into parental AD293. Approximately 8.5×10^4 parental AD293 cells were seeded in a 6-well plate containing 3 mL cDMEM 24 h before co-transfection. All cells were transfected with 0.625 μ g of pDisplay-IpFcR γ -L WT_{CYT} construct expression vector plus 0.625 μ g of empty pDisplay vector (mock) or the indicated expression construct vector (i.e. 1.25 μ g total plasmid) using TurboFECT *in vitro* transfection reagent (Thermo Scientific #R0531), according to the manufacturer's protocol. After 48 h incubations at 37°C, cells were subjected to the imaging flow cytometry-based YG bead phagocytosis assay described in the previous section.

3.8.3 Measuring eGFP-tagged IpLITR-mediated phagocytosis of α HA-coated light yellow (LY) bead targets by component masking analysis

To assess IpLITR 1.1b CYT construct-mediated cross-talk during bead-based phagocytosis, an alternative assay was developed using light yellow (LY) bead targets (Spherotech Inc. #FP-3042-2) and eGFP-tagged IpLITR 1.1b CYT (IpLITR 1.1b CYT-eGFP) constructs and analyzed with a novel gating strategy. Assays were performed essentially as described in section 3.8.1 above. Briefly, stable IpFcR γ -L WT_{CYT}-expressing cells were transfected with IpLITR 1.1b CYT-eGFP constructs using TurboFECT *in vitro* transfection reagent (Thermo Scientific #R0531). After 48 h, α HA-coated LY bead targets were added to plate-adherent cells for 30 min at 37°C and then counter-stained with rabbit α -mouse IgG(H+L) AlexaFluor647-conjugated secondary antibody for 20 min at 4°C on a rocking mixer. Cells were harvested after trypsinization and fixed in 1% paraformaldehyde PBS before data collection on

the ImageStream^x Mark II instrument (Amnis Corporation). By transfecting eGFP-tagged constructs into stable IpFcR γ -L WT_{CYT}-expressing cells and gating for eGFP fluorescence, eGFP positive (i.e. IpFcR γ -L WT_{CYT} and IpLITR 1.1b CYT-eGFP co-expressing) and eGFP negative (i.e. only IpFcR γ -L WT_{CYT}-expressing) cell populations could be separated and phagocytic phenotypes determined. Cells associating with up to three target beads with only surface-bound beads, only phagocytosed beads, or cells with both surface-bound and phagocytosed beads were determined by component masking analysis, described in detail elsewhere (327).

3.8.4 Transient eGFP-tagged IpLITR 1.1b CYT construct transfection into stable

IpLITR 1.1b/IpFcR γ -L WT_{CYT}- or IpLITR 2.6b/IpFcR γ -L WT_{CYT}-expressing cells

Approximately 8.5×10^4 cells were seeded in a 6-well plate containing 3 mL cDMEM + 400 μ g/mL G418 24 h before transfection. One μ g of pDisplay expression vector encoding an eGFP-tagged IpLITR 1.1b CYT construct was transfected using TurboFECT *in vitro* transfection reagent (Thermo Scientific #R0531), according to the manufacturer's protocol. After 48 h at 37°C, cells were subjected to the imaging flow cytometry-based LY bead phagocytosis assay described in section 3.8.3.

3.8.5 Transient eGFP-tagged IpLITR 1.1b CYT (IpLITR 1.1b CYT-eGFP) and

dominant-negative FLAG-tagged Csk (Δ Csk-FLAG) or SHP2 (Δ SHP2-FLAG) construct co-transfection into stable IpFcR γ -L WT_{CYT}-expressing cells

Approximately 8.5×10^4 cells were seeded in a 6-well plate containing 3 mL cDMEM + 400 μ g/mL G418 24 h before transfection. 0.5 μ g of pDisplay-*IpLITR 1.1b CYT-eGFP* construct expression vector plus 0.75 μ g of p3XFLAG-CMV14 encoding Δ Csk- or Δ SHP2-FLAG construct using TurboFECT *in vitro* transfection reagent (Thermo Scientific #R0531), according

to the manufacturer's protocol. After 48 h at 37°C, cells were subjected to the imaging flow cytometry-based LY bead phagocytosis assay described in section 3.8.3. Duplicate wells were lysed as described in section 3.7.3, except that after centrifuging lysates at 16000 x g for 10 min at 4°C, supernatants were combined 1:1 with 2X reducing buffer and boiled for 10 min at 95°C. Proteins were then separated via 12% SDS-PAGE gel and transferred to nitrocellulose membranes (Bio-Rad #162-0112) that were probed with mouse α FLAG M2 HRP-conjugated mAb (1:2000) to detect transfected dominant-negative FLAG-tagged signaling molecules. A goat anti- β -actin polyclonal antibody followed by bovine α -goat IgG HRP-conjugated secondary antibody was used as a loading control.

3.8.6 Transient transfection of eGFP-tagged IpLITR 1.1b CYT constructs into stable Csk or SHP2 knockdown IpFcR γ -L WT_{CYT}-expressing cell lines

Approximately 9×10^4 cells were seeded in a 6-well plate containing 3 mL cDMEM + 400 μ g/mL G418 and 2 μ g/mL puromycin 24 h before transfection. Half a μ g of pDisplay expression vector encoding an eGFP-tagged IpLITR 1.1b CYT construct was transfected using TurboFECT® *in vitro* transfection reagent (Thermo Scientific #R0531), according to the manufacturer's protocol. After 48 h incubations at 37°C, cells were subjected to the imaging flow cytometry-based LY bead phagocytosis assay described in section 3.8.3. Duplicate wells were used as controls to quantify signaling molecule protein knockdown, as described in section 3.6.2.

3.8.7 Statistical analysis

Means were first compared by ANOVA to determine if any one mean differed significantly from the rest. If a difference was found, individual means were tested against one

another using a post-hoc Tukey analysis. Significantly different means were denoted with alphabetically assigned letters, as described in the figure captions.

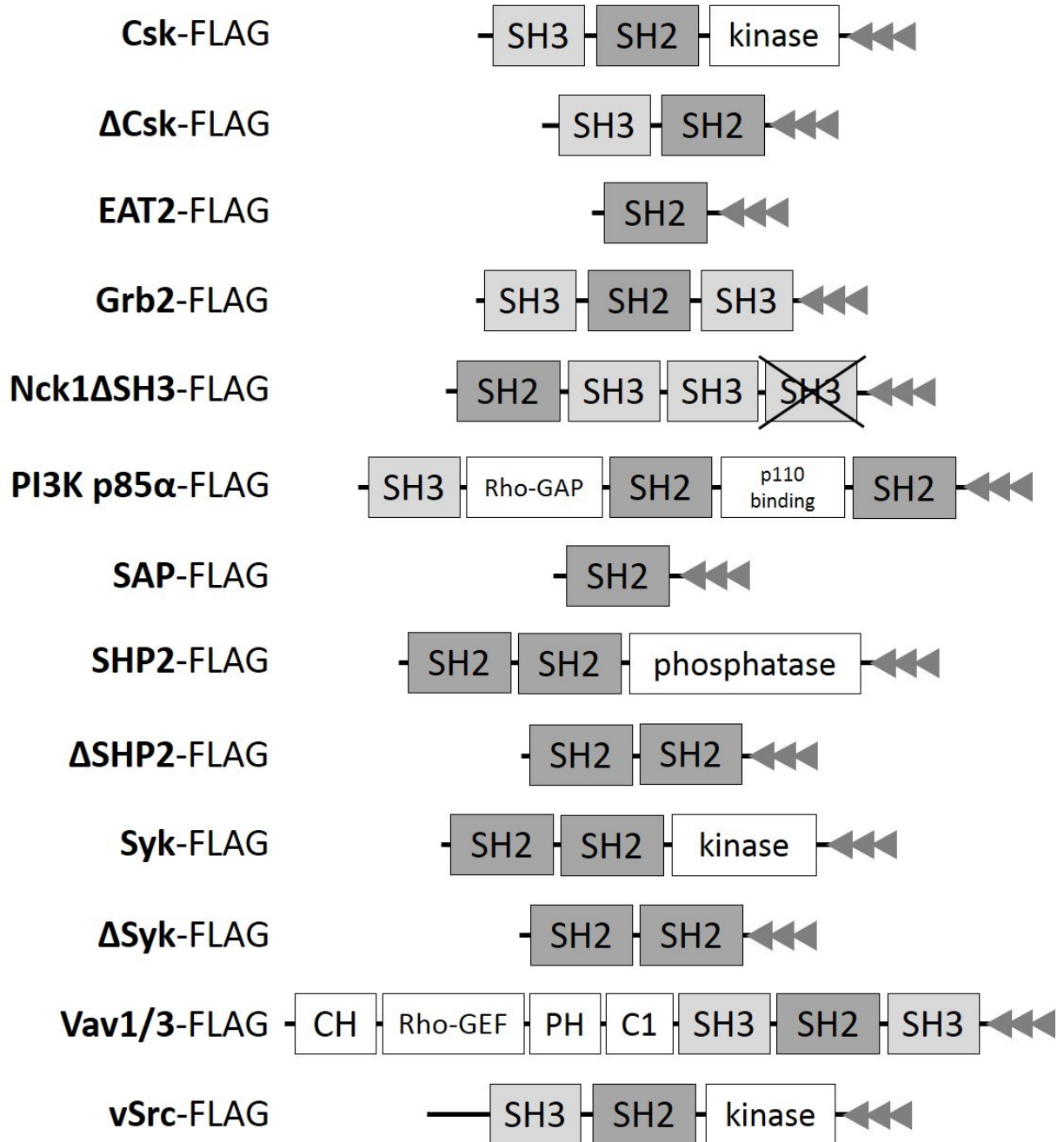


Figure 3.1. Schematic representations of all FLAG-tagged SH2 domain-containing signaling molecule constructs. Full-length signaling molecules and truncated (Δ) forms of Csk, Nck1, SHP2 and Syk that were used in biochemical signal molecule recruitment assays and/or dominant-negative phagocytosis assays are depicted here. “X” through the C-terminal SH3 domain of Nck1 indicates that this domain is not contained within the FLAG-tagged construct. Modular domains of each molecule are labeled as follows: SH2, phosphotyrosine binding domain that mediates protein-protein interactions; SH3, polyproline binding domain that mediates protein-protein interactions; kinase, enzymatic domain that phosphorylates targets; phosphatase, enzymatic domain that dephosphorylates targets; Rho-GAP, GTPase activating protein domain that deactivates Rho family GTPases; Rho-GEF, guanine exchange factor domain that activates Rho family GTPases; p110-binding, protein domain that mediates interaction with the p110 PI3K catalytic subunits; C1, protein kinase C conserved region 1 domain that mediates various interactions, e.g. Ras-GTP; CH, calponin homology domain that mediates protein-actin interactions; PH, pleckstrin homology domain that mediates protein-phospholipid interactions; \blacktriangleleft , FLAG epitope tag.

Primer Name	Primer Sequence 5' to 3'
Csk HindIII Fwd	AAGCTTATGTCAGCAATACAGGCCGCC
Csk BamHI Rvs	GGATCCCAGGTGCAGCTCGTGGGTTTT
ΔCsk BamHI Rvs	GGATCCCTGGGCCGCCACTGTGCCCTC
EAT2 HindIII Fwd	AAGCTTATGGATCTGCCTTACTACCATGGAC
EAT2 BamHI Rvs	GGATCCAGGCAAGACATCCACATAATCGCTGT
Grb2 HindIII Fwd	AAGCTTATGGAAGCCATCGCCAAATAT
Grb2 BamHI Rvs	GGATCCGACGTTCCGGTTCACGGGGGT
Nck1ΔSH3 HindIII Fwd	AAGCTTATGAACATGCCCGCTTATGTGAAA
Nck1ΔSH3 BamHI Rvs	GGATCCTGATAAATGCTTGACAAGATA
PI3K p85α EcoRI Fwd	GAATTCATGAGTGCTGAGGGGTAC
PI3K p85α BamHI Rvs	GGATCCTCGCCTCTGCTGTGCATATACTGG
SAP HindIII Fwd ¹	AAGCTTATGGACGCAGTGGCTGTGTAT
SAP BamHI Rvs ¹	GGATCCTGGGGCTTTCAGGCAGACATC
SHP2 HindIII Fwd	AAGCTTATGACATCGCGGAGATGGTTT
SHP2 BamHI Rvs	GGATCCTCTGAAACTTTTCTGCTGTTG
ΔSHP2 BamHI Rvs	GGATCCAGCAGCATTTATACGAGTCGTGTT
Syk HindIII Fwd	AAGCTTATGGCCAGCAGCGGCATGGCT
Syk BamHI Rvs	GGATCCGTTACCACGTCATAGTAGTA
ΔSyk BamHI Rvs	GGATCCAACATTTCCCTGTGTGCCGAT
Vav1 HindIII Fwd	AAGCTTATGGAGCTGTGGCGCCAA
Vav1 BamHI Rvs	GGATCCGCAGTATTCAGAATAATCTTCC
Vav3 HindIII Fwd	AAGCTTATGGAGCCGTGGAAGCAGTG
Vav3 KpnI Rvs	GGTACCCGTTTCATCCTCTTCCACATATGTGGATGG
ASV vSrc HindIII Fwd ²	AAGCTTATGGGGAGTAGCAAGAGCAAG
ASV vSrc BamHI Rvs ²	GGATCCCTCAGCGACCTCCAACAC

GenBank accessions for the sequences used are: Csk (NM_004383.2); EAT2 (AF484964.1); Grb2 (CR541942.1); Nck1 (NM_001291999.1); PI3K p85α (NM_181523.2); SAP (NM_001114937.2); SHP2 (D13540.1); Syk (Z29630.1); Vav1 (NM_005428.3); Vav3 (NM_006113.4); Avian sarcoma virus (ASV, V01169.1).

¹Cloned from human natural killer YTS cells.

²Sub-cloned from pRS316 vector provided by Dr. Robert Ingham (Dept. of Medical Microbiology & Immunology, University of Alberta).

Table 3.1. Primers used to generate human FLAG-tagged SH2 domain-containing signaling molecules, including truncated (Δ) Csk-FLAG, SHP2-FLAG and Syk-FLAG, from AD293 cells and Avian sarcoma virus (ASV) FLAG-tagged vSrc.

Primer Name	Primer Sequence 5' to 3'
GST SgfI Fwd	GCGATCGCCTAGAAAGGAAAGGAC
IpLITR 1.1b WT_{CYT} SgfI Fwd	GCGATCGCCAAAGGAAAGGAC
IpLITR 1.1b WT_{CYT} PmeI Rvs	GTTTAAACCTATGTGTTCTGCTT
IpLITR 1.1b PROX_{CYT} PmeI Rvs	GTTTAAACCTAATCACTGGGTCC
IpLITR 1.1b DIST_{CYT} SgfI Fwd	GCGATCGCCAAGAATAAAGAT
IpLITR IpFcRγ-L WT_{CYT} SgfI Fwd	GCGATCGCCCGTTCTGGAAATAAT
IpLITR IpFcRγ-L WT_{CYT} PmeI Rvs	GTTTAAACTTATGCCAAAGGTTTCCTT
CEACAM3 WT_{CYT} SgfI Fwd	GCGATCGCCACCAGCATCCAGCGT
CEACAM3 WT_{CYT} PmeI Rvs	GTTTAAACCTAAGAAGCCACTTCTGC

GenBank accessions for the sequences used are: IpLITR 1.1b (ABI16050); IpFcR γ -L (AF543420); CEACAM3 (BC106728.1).

Table 3.2. Primers used to generate GST-CYT fusion protein constructs.

Primer Name	Primer Sequence 5' to 3'
IpLITR 1.1b WT_{CYT} SmaI Fwd	CCCGGGGTTCTGTCTGTGGAGCCG
3' IpFcRγ-L CYT Overhang Rvs	CTCATTATTTCCAGAACGCCACCAAAGCAGGAT
5' IpLITR 1.1b TM Overhang Fwd	ATCCTGCTTTGGTGGCGTTCTGGAAATAATGAG
IpFcRγ-L WT_{CYT} Sall Rvs	GTCGACTTATGCCAAAGGTTCCCTTCTT
IpLITR 1.1b Y433F Fwd	AGACCGATGAGCACATTTTTGACACTGTGGAGAACGC
IpLITR 1.1b Y433F Rvs	GCGTTCTCCACAGTGTCAAAAATGTGCTCATCGGTCT
IpLITR 1.1b Y453F Fwd	AACTCAGTGGGGCCGTTTTTGCACAGGTCATGAAGAA
IpLITR 1.1b Y453F Rvs	TTCTTCATGACCTGTGCAAAAACGGCCCCACTGAGTT
IpLITR 1.1b Y463F Fwd	TGAAGAAAAAGGAGTCATTCAAGAATAAAGATGATGA
IpLITR 1.1b Y463F Rvs	TCATCATCTTTATTCTTGAATGACTCCTTTTTCTTCA
IpLITR 1.1b Y477F Fwd	GACCCAGTGATGTGATTTTCACTGAGCTTGAATCAA
IpLITR 1.1b Y477F Rvs	TTGATTTCAAGCTCAGTGAAAATCACATCACTGGGTC
IpLITR 1.1b Y499F Fwd	TGAAGGCCAGTGTAGAGTTTGAAACTATTTATTCA
IpLITR 1.1b Y499F Rvs	TGAATAAATAGTTTCAAACCTCTACACTGGCCTTCA
IpLITR 1.1b Y499,503F Fwd	TAGAGTTTGAAACTATTTTTTTCACAGCTGAAGCAGAA
IpLITR 1.1b Y499,503F Rvs	TTCTGCTTCAGCTGTGAAAAAATAGTTTCAAACCTCA
Igκ NheI Fwd	GCTAGCATGGAGACAGACACAC
IpLITR 1.1b WT_{CYT} BamHI Rvs	GGATCCCGTGTGTTCTGCTTCAGCTG
IpLITR 1.1b WT_{CYT} SmaI Fwd	CCCGGGGTTCTGTCTGTGGAGCCG
eGFP Sall Rvs	GTCGACTTACTTGTACAGCTCGTCCATGCCGAG

GenBank accessions for the sequences used are: IpLITR 1.1b (ABI16050); IpFcR γ -L (AF543420).

Table 3.3. Primers used to generate IpLITR 1.1b CYT receptor constructs, including IpLITR 1.1b/IpFcR γ -L WT_{CYT} chimeric receptor (top box), IpLITR 1.1b CYT YF mutant receptors (middle box) and eGFP-tagged receptors (bottom box).

CHAPTER IV

BIOCHEMICAL AND FUNCTIONAL EXAMINATION OF IpLITR CYT-DEPENDENT PHAGOCYTTIC SIGNALING POTENTIAL

Parts of this chapter are published:

Zwozdesky et al., 2017. Imaging flow cytometry and GST pulldown assays provide new insights into channel catfish leukocyte immune-type receptor-mediated phagocytic pathways. *Dev Comp Immunol* 67: 126-38

4.1 INTRODUCTION

The classification of immunoregulatory receptors as inhibitory or stimulatory has depended primarily on whether they contain key signaling motifs within the CYT region such as ITAMs (stimulatory receptors) or ITIMs (inhibitory receptors). However, the functional outcome of receptor engagement does not always coincide with the presence of these canonical motifs as versatility in the mechanisms of ITAM- or ITIM-dependent signaling events may contribute to functional plasticity. Details of molecular signaling versatility that underlie receptor function are well-defined in mammalian models. Information from earlier vertebrate models has implicated these receptors in the control of phagocytosis, cytokine secretion and degranulation but also unique cytotoxic effector responses (63, 328). However, detailed molecular signaling versatility data from earlier vertebrate models such as fish is lacking.

To gain an understanding of immunoregulatory receptor signaling versatility in fish, our lab has focused on characterizing two IpLITR members. These efforts have revealed both predictable ITAM-dependent functional signaling and unexpected details of ITIM-dependent functional plasticity. Most recently, the ITIM-containing IpLITR 1.1b activated a phagocytic response in RBL-2H3 myeloid cells (5, 7, 8). This is in direct contrast to initial characterizations of IpLITR 1.1b in mouse NK cells where it recruited the cytoplasmic phosphatases SHP1/2 and abrogated NK cell-mediated cellular cytotoxicity (6). In both cases, the functional outcomes

were dependent on an intact CYT. The IpLITR 1.1b CYT region contains six tyrosine residues, evenly distributed between its membrane proximal and distal CYT segments. The distal CYT segment contains two ITIMs located at Y⁴⁷⁷ and Y⁴⁹⁹ and one overlapping ITSM at Y⁵⁰³. Both ITIMs were implicated in a potent SHP-dependent inhibitory signaling pathway activity.

Surprisingly, an IpLITR 1.1b construct containing only the proximal CYT segment also inhibited NK cell-mediated killing responses despite being devoid of ITIMs. This revealed a novel SHP-independent inhibitory pathway for IpLITR 1.1b that was likely facilitated by one of the tyrosine residues present within its proximal CYT segment. Upon closer examination, the linear CYT motif A-V-Y⁴⁵³-A-Q-V of IpLITR 1.1b closely matched the consensus binding motif of C-terminal Src kinase (Csk); a cellular kinase known to potently abrogate immune cell signaling. Subsequently, Csk recruitment was demonstrated at IpLITR 1.1b Y⁴⁵³ and provided a plausible explanation for its SHP-independent inhibitory activities. The unique proximal and distal CYT segment-dependent inhibitory mechanisms suggested that variable signaling modules exist within the CYT region of IpLITR 1.1b, but even so, a stimulatory function was not predicted before testing IpLITR 1.1b phagocytosis in RBL-2H3 cells. This cell context-dependent shift in function facilitated detailed imaging and pharmacological studies to examine what appeared to be a novel ITAM-independent mode of phagocytosis.

Detailed phenotypic examination by confocal microscopy revealed that IpLITR 1.1b-expressing cells often formed extended membranous protrusions that captured their targets in phagocytic cup-like structures but failed to completely internalize them. Although the capture and partial engulfment phenotype was common during IpLITR 1.1b-mediated phagocytosis, ~30% of the analyzed cells fully internalized at least one target in contrast to ~60% for IpLITR 2.6b/IpFcR γ -L- (i.e. ITAM)-expressing cells. Surprisingly, while incubations at 22°C completely

inhibited IpLITR 2.6b/IpFcR γ -L-mediated phagocytosis, this temperature had little effect on the ability of IpLITR 1.1b-expressing cells to capture and partially engulf beads. Furthermore, while small molecule inhibitors of major kinase and GTPase signaling systems had significant inhibitory effects on the IpLITR 2.6b/IpFcR γ -L-mediated phagocytic pathway, IpLITR 1.1b-induced phagocytosis was insensitive to many of these pharmacological inhibitors. Importantly, a CYT-deficient IpLITR 1.1b did not evoke a response. Collectively, these observations indicated that IpLITR 1.1b operates independently of several of the key components of the ITAM-dependent signaling machinery, suggesting that the CYT region of IpLITR 1.1b may participate in the recruitment and activation of distinct phagocytic effector molecules. Most importantly, these studies provided an opportunity to explore molecular details of IpLITR 1.1b CYT-dependent phagocytic signaling events.

The main research objectives of this thesis chapter are the biochemical and functional characterization of IpLITR 1.1b (referred to as IpLITR 1.1b WT_{CYT})-mediated phagocytic signaling potential. This will be conducted in the non-immune AD293 epithelioid cell line, an established cell system for studying phagocytosis (329). Specifically, I performed detailed CYT segment- and motif-specific signaling molecule recruitment profiles and imaging cytometry-based phagocytosis assays. My results show that IpLITR 1.1b WT_{CYT} differentially recruits several stimulatory signaling molecules to either CYT segment in GST pulldown assays. However, stable IpLITR 1.1b WT_{CYT}-expressing cells activated with pervanadate showed only inhibitory molecules are physiologically recruited to the CYT. My functional results show that while a CYT ITAM-containing (i.e. IpFcR γ -L WT_{CYT}) receptor activates phagocytosis, IpLITR 1.1b WT_{CYT} is not capable of activating phagocytosis in AD293 cells. Indeed, molecular manipulations designed to re-constitute IpLITR 1.1b WT_{CYT}-mediated phagocytic signaling were

also unsuccessful. Collectively, these data reveal that IpLITR 1.1b WT_{CYT} is not a phagocytic receptor and have led to the formulation of new hypotheses regarding the utility of an AD293 cell system in studying IpLITR signaling potential, which will be explored further in chapters V and VI.

4.2 RESULTS

4.2.1 Synthesis and purification of GST-CYT fusion proteins in *E. coli*

To characterize phosphotyrosine-dependent IpLITR CYT signaling molecule recruitment potential by GST pulldown, I generated unphosphorylated and phosphorylated GST-CYT fusion protein ‘bait’ and FLAG-tagged signaling molecule ‘prey’-containing cellular lysates. The GST-CYT fusion proteins used in this assay include three IpLITR 1.1b-derived proteins (i.e. WT_{CYT}, PROX_{CYT} and DIST_{CYT}), one IpFcR γ -L-derived protein, one human CEACAM3-derived protein and a GST only protein (Figure 4.1A). ‘Bait’ and ‘prey’ reagents were subsequently combined to perform GST pulldown assays as outlined in the schematic shown in Figure 4.1B.

BL21 and TKB1 *E. coli* were induced to express GST-CYT fusion proteins with 1- β -D-thiogalactopyranoside. Affinity purification of ‘bait’ was verified by Ponceau staining as bands for each GST-CYT fusion protein appear at their expected weights: lane 1 – GST 26 kDa, lane 2 – GST-*IpLITR* 1.1b WT_{CYT} at 40 kDa, lane 3 – GST-*IpLITR* 1.1b PROX_{CYT} at 36 kDa, lane 4 – GST-*IpLITR* 1.1b DIST_{CYT} at 32 kDa, lane 5 – GST-*IpFcR γ -L* WT_{CYT} at 31 kDa and GST-CEACAM3 WT_{CYT} at 35 kDa (Figure 4.2A). In all lanes, the largest visualized band corresponds to the expected weight of the full-length GST-CYT fusion protein, however, some apparent degradation or partially synthesized products can also be seen as smaller bands.

4.2.2 Generation of cellular lysates containing FLAG-tagged SH2 domain-containing signaling molecules

Sequenced p3XFLAG-CMV14-encoded signaling molecules were transiently transfected into parental AD293 cells for 24–48 h. Bands for each signaling molecule can be seen at their expected weights: Csk at 54 kDa, Grb2 at 28 kDa, PI3K p85 α at 85 kDa, Nck1 Δ SH3 at 34 kDa, SHP2 at 70 kDa, Syk at 72 kDa, Vav1 at 101 kDa, Vav3 at 94 kDa and EAT2 at 15 kDa (Figure 4.2B). No bands are present in cells transfected with an empty p3XFLAG-CMV14 vector (EV). In most lanes, the largest band present corresponds with the expected weight of the signaling molecule indicated, while smaller bands are likely degradation or partially synthesized FLAG-reactive products. However, an unknown \sim 70 kDa band is visible in the Grb2 lane. The Nck1 Δ SH3 lane represents a truncated Nck1 molecule that lacks its N-terminal SH3 domain, resulting in the observed size down-shift from 47 kDa (of endogenous Nck1) to 34 kDa (for Nck1 Δ SH3). Ensuring that no ‘prey’ targets were similar in size to the GST-IpLITR 1.1b WT_{CYT} and GST-IpLITR 1.1b PROX_{CYT} was necessary due to the unexpected technical coincidence that the α FLAG M2 monoclonal blotting antibody cross-reacts with these ‘bait’ proteins (Figure 4.3).

4.2.3 Differential phosphotyrosine-dependent recruitment of C-terminal FLAG-tagged signaling molecules to the proximal and distal CYT segments of IpLITR 1.1b

The potential to recruit SH2 domain-containing signaling molecules to the CYT regions of IpLITR 1.1b, IpFcR γ -L and CEACAM3 were qualitatively assessed using GST pulldowns. In these assays, the unphosphorylated and phosphorylated GST, GST-IpLITR 1.1b WT_{CYT}, GST-IpLITR 1.1b PROX_{CYT}, GST-IpLITR 1.1b DIST_{CYT}, GST-IpFcR γ -L WT_{CYT} and GST-CEACAM3 WT_{CYT} were used as ‘bait’ to capture C-terminal FLAG-tagged signaling molecule ‘prey’ from AD293 cellular lysates. Figure 4.4A and Figure 4.5A demonstrate α GST reactive

bands at their expected weights: lane 1 – GST at ~26 kDa, lane 2 – IpLITR 1.1b WT_{CYT} at ~40 kDa, lane 3 – IpLITR 1.1b PROX_{CYT} at ~36 kDa, lane 4 – IpLITR 1.1b DIST_{CYT} at ~32 kDa, lane 5 – IpFcR γ -L WT_{CYT} at ~31 kDa and lane 6 – CEACAM3 WT_{CYT} at ~35 kDa. I also observed additional α GST reactive bands in some lanes, but none of them were larger than the expected sizes of the corresponding ‘bait’ proteins (similar to Ponceau stains in Figure 4.2A). Next, I probed the blots with a mouse α -phosphotyrosine mAb. Reactive bands were only detected in TKB1-derived lanes (Figure 4.4B and Figure 4.5B), indicating that these ‘bait’ proteins were successfully phosphorylated while BL21-derived ‘bait’ proteins were not. Finally, I probed pulldown samples with an HRP-conjugated mouse α FLAG M2 mAb to identify signaling molecule ‘prey’ that co-precipitated with various GST-CYT fusion protein ‘bait’.

I observed the differential phosphotyrosine-dependent recruitment of signaling molecules to the proximal and distal CYT segments of IpLITR 1.1b WT_{CYT} (Figure 4.4C and Figure 4.5C). Importantly, no α FLAG reactive bands were detected in pulldown lanes using unphosphorylated, BL21-derived fusion proteins, nor were there any such bands in the GST only lanes even though TKB1-derived GST was phosphorylated (Figure 4.4B and Figure 4.5B). Specifically, the phosphorylated TKB1-derived GST-*IpLITR 1.1b WT_{CYT}* ‘bait’ co-precipitated SHP2, Csk, Syk, Grb2, EAT2, Nck1, PI3K p85 α and Vav1, but not Vav3 (Figure 4.4C and Figure 4.5C). In comparison, TKB1-derived GST-*IpLITR 1.1b PROX_{CYT}* co-precipitated Csk, Grb2, EAT2, Nck1, PI3K p85 α (albeit a considerably fainter band) and Vav1, but not SHP2, Syk, or Vav3 (Figure 4.4C and Figure 4.5C). When TKB1-derived GST-*IpLITR 1.1b DIST_{CYT}* was used as ‘bait’, it co-precipitated SHP2, Syk, EAT2 and PI3K p85 α , but not Csk, Grb2, Nck1, Vav1 or Vav3 (Figure 4.4C and Figure 4.5C). Additional ‘bait’ included the ITAM-containing GST-*IpFcR γ -L WT_{CYT}*, which co-precipitated Syk, PI3K p85 α and Vav1, but none of the other ‘prey’

molecules tested (Figure 4.4C and Figure 4.5C). Furthermore, the CYT region of CEACAM3 is known to associate with Nck1, Vav1 and PI3K p85 α (215–217) and when used as a positive control in these assays, it co-precipitated these ‘prey’ molecules, as well as Vav3 (Figure 4.5C). Taken together, these data strongly suggest that IpLITR 1.1b WT_{CYT} is capable of binding several AD293 cell-expressed signaling molecules to each CYT segment that may participate in activating phagocytosis.

4.2.4 α HA-coated bead-induced cross-linking of IpFcR γ -L WT_{CYT}, but not IpLITR 1.1b WT_{CYT}, induces CYT-dependent phagocytic signaling

Based on the biochemical pulldown data above (section 4.2.3), I hypothesized several models for IpLITR 1.1b WT_{CYT}-mediated phagocytic signaling, including the coordinated proximal and distal CYT segment recruitment of Nck1 and Syk, respectively. To test this hypothesis, I employed an Image Stream^X flow cytometry-based phagocytosis assay (outlined in Figure 4.6), developed previously in our lab (327). This assay uses green fluorescent (YG) beads as phagocytic targets and a counter-staining step which allows discrimination of internalized (i.e. phagocytosed) vs. surface-bound targets. I performed phagocytosis assays using stable IpLITR-expressing AD293 cell lines. The IpLITR CYT constructs tested all contain an HA epitope tag and the four extracellular Ig-like domains and TM segment of IpLITR 1.1b fused to different CYT regions: the ITAM-containing IpFcR γ -L CYT (IpFcR γ -L WT_{CYT}), a mutant IpFcR γ -L CYT in which both ITAM tyrosines are converted to phenylalanines (IpFcR γ -L MUT_{CYT}) and the IpLITR 1.1b WT_{CYT} (Figure 4.7A). Similar construct expression levels in stably expressing cell lines were indicated by α HA mAb staining (Figure 4.7B). In comparison, parental AD293 cells show very little α HA staining, similar to IgG3 isotype control antibody staining (Figure 4.7B).

This allows me to specifically cross-link N-terminal HA-tagged IpLITR CYT constructs with α HA antibody-coated YG beads to trigger phagocytic signaling.

To begin assessing IpLITR CYT-mediated phagocytic signaling in AD293 cells, I established the phagocytic phenotypes of a positive and negative control by cross-linking a known phagocytic CYT-containing receptor (i.e. IpFcR γ -L WT_{CYT}) and a mutant knockout receptor (i.e. IpFcR γ -L MUT_{CYT}), that were expected to display a phagocytic phenotype (i.e. at least one YG bead is inside the cell) and a surface-bound phenotype (i.e. no beads are internalized), respectively. As shown in Figure 4.8A, 47.9% of IpFcR γ -L WT_{CYT}-expressing cells associated with at least one bead, with 42.1% and 5.8% displaying a phagocytic and surface-bound phenotype, respectively. In contrast, 41.2% of IpFcR γ -L MUT_{CYT}-expressing cells associated with at least one bead, with 6.6% and 34.6% displaying a phagocytic and surface-bound phenotype, respectively. After establishing these controls, I tested IpLITR 1.1b WT_{CYT}-mediated phagocytosis. While IpLITR 1.1b WT_{CYT}-expressing cells showed a 52.9% bead association, only 4.5% had internalized at least one bead (i.e. phagocytic cells; Figure 4.8A). To simplify visualization of the phagocytic vs. surface-bound phenotypes, the bead-associated cell population data was indexed by normalizing % phagocytic or surface-bound cells to % bead associated cells (Figure 4.8B). Overall, these data show that while IpFcR γ -L WT_{CYT} invokes CYT-dependent phagocytic signaling, IpLITR 1.1b WT_{CYT} does not. These observations informed a shift in my perspective that only certain receptor CYTs can co-opt the cellular machinery of AD293 cells to evoke phagocytosis, but perhaps the intracellular signaling networks can be altered to allow the CYT of IpLITR 1.1b to do the same. In other words, can I ‘knock-in’ IpLITR 1.1b WT_{CYT}-mediated phagocytic signaling in IpLITR 1.1b WT_{CYT}-expressing AD293 cells?

4.2.5 Co-expressing IpLITR 1.1b WT_{CYT} with vSrc does not evoke phagocytic signaling

IpLITR 1.1b WT_{CYT} activates phagocytic signaling in the mammalian myeloid cell line RBL-2H3 (5, 7), but data presented in section 4.2.4 of this chapter show that IpLITR 1.1b WT_{CYT} is not phagocytic in AD293 cells. To determine if receptor phosphorylation is insufficient to evoke IpLITR 1.1b WT_{CYT}-mediated phagocytosis, I co-expressed a promiscuous viral Src kinase (vSrc) in stable IpLITR-expressing AD293 cells. vSrc constitutively phosphorylates a broad range of tyrosine-based motifs (330) and has been used elsewhere to maximize receptor phosphorylation (216).

IpLITR 1.1b WT_{CYT} stable cells transiently co-expressing a FLAG-tagged vSrc (vSrc-FLAG) kinase showed 46.3% bead association with 5.4% and 40.9% of cells in the phagocytic and surface-bound phenotype, respectively (Figure 4.9A). This result was similar to IpLITR 1.1b WT_{CYT} stables transfected with empty p3XFLAG-CMV14 vector (EV) control at 6.6% phagocytic and 41.5% surface-bound phenotype. When EV and vSrc-FLAG were transfected into IpFcR γ -L WT_{CYT}-expressing AD293 cells, a marginal increase in overall bead association from 38.6% to 48.7% accompanied an increased phagocytic phenotype from 33.6% to 41.4%, respectively (Figure 4.9A), although indexed data shows no differences between their phenotypes (Figure 4.9B). Indeed, indexed data also shows no increase in IpLITR 1.1b WT_{CYT}-mediated phagocytic phenotype at 17.5% and 11.6% for EV and vSrc-FLAG co-expressing cells, respectively (Figure 4.9B). To control for successful expression of vSrc-FLAG, I performed transfections prior to the phagocytosis assays in duplicate. Duplicate wells were lysed and probed with HRP-conjugated mouse α FLAG M2 antibody. Both stable IpFcR γ -L WT_{CYT}- and IpLITR 1.1b WT_{CYT}-expressing AD293 cell lysates demonstrated FLAG-reactive bands at the expected 60 kDa weight for vSrc-FLAG, but EV transfected cells did not (Figure 4.9C, top blot).

To ensure equivalent amounts of lysate were loaded into each lane, an anti- β -actin loading control blot was included (Figure 4.9C, bottom blot). Overall, these data indicate that co-expressing vSrc in stable IpLITR 1.1b WT_{CYT}-expressing cells does not activate phagocytic signaling.

4.2.6 Over-expressing Syk or SAP in IpLITR 1.1b WT_{CYT}-expressing cells does not activate phagocytic signaling

Next I sought to determine if differences in signaling molecule expression levels between cell-types might account for the lack of IpLITR 1.1b WT_{CYT}-mediated phagocytosis in AD293 cells by over-expressing Syk or SAP signaling molecules in stable IpLITR-expressing AD293 cells.

IpLITR 1.1b WT_{CYT}-expressing cells transiently transfected with FLAG-tagged Syk (Syk-FLAG) showed 49.3% bead association with 4.3% and 45.0% of cells in the phagocytic and surface-bound phenotype, respectively (Figure 4.10A). When transfected with FLAG-tagged SAP, these cells showed 47.0% bead association with 4.8% and 42.2% of cells in the phagocytic and surface-bound phenotype, respectively (Figure 4.10A). These results are similar to empty p3XFLAG-CMV14 vector (EV) transfected IpLITR 1.1b WT_{CYT} stable cells that show 43.7% bead association with 5.6% and 38.1% of cells in the phagocytic and surface-bound phenotype, respectively (Figure 4.10A). For comparison, cells expressing IpFcR γ -L WT_{CYT} were transfected with EV or Syk-FLAG. While the data show a 38.6% bead association with 33.3% phagocytic and 5.3% surface-bound cells for EV-transfected IpFcR γ -L WT_{CYT} stable cells, these same cells show an increased bead association of 55.8% with 53.0% phagocytic (statistically significant increase compared to EV) and 2.8% surface-bound cells when transfected with Syk-FLAG (Figure 4.10A). When data is indexed, Syk-FLAG transfected IpFcR γ -L WT_{CYT}-expressing cells

show a trend towards increased phagocytosis compared to IpFcR γ -L WT_{CYT} only cells, while IpLITR 1.1b WT_{CYT}-expressing cells remain non-phagocytic (Figure 4.10B). To control for successful expression of Syk- and SAP-FLAG signaling molecules, I performed transfections prior to the phagocytosis assays in duplicate. Duplicate wells were lysed and probed with HRP-conjugated mouse α FLAG M2 antibody. Both stable IpFcR γ -L WT_{CYT}- and IpLITR 1.1b WT_{CYT}-expressing AD293 cell lysates demonstrated FLAG-reactive bands at expected weights: 72 kDa for Syk-FLAG (Figure 4.10C, top blot) and 15 kDa for SAP-FLAG (Figure 4.10C, middle blot), but EV transfected cells did not. Multiple bands in Syk-FLAG transfected lanes indicate FLAG-reactive degradation or partially synthesized products. To ensure equivalent amounts of lysate were loaded into each lane, an anti- β -actin loading control blot was included (Figure 4.10C, bottom blot). Collectively, the over-expression of Syk or SAP did not result in the activation of phagocytic signaling by IpLITR 1.1b WT_{CYT}. These data strongly suggested that IpLITR 1.1b WT_{CYT} was not stimulatory under the tested conditions.

4.2.7 Pervanadate stimulation followed by co-immunoprecipitation show that IpLITR 1.1b WT_{CYT} recruits Csk and SHP2 to the proximal CYT motif Y⁴⁵³ and distal CYT motif ITIM Y⁴⁷⁷, respectively

I developed a system to assess biochemical recruitment potential by stimulating cells using pervanadate (outlined in Figure 4.11). Pervanadate is a cellular phosphatase inhibitor that allows endogenous cellular kinases (e.g. membrane-bound initiators of receptor activation, the Src family kinases) to phosphorylate and activate transmembrane receptors (331). In contrast with GST-CYT pulldowns, this simulates physiological recruitment potential in intact cells as opposed to recruitment from a cellular lysate. I generated three additional motif-specific IpLITR 1.1b CYT YF mutant constructs by site-directed mutagenesis (Figure 4.12A) including IpLITR

1.1b Y⁴⁵³F_{CYT} (previously shown to recruit Csk (6)) and two ITIM YF mutants: IpLITR 1.1b Y⁴⁷⁷F_{CYT} and IpLITR 1.1b Y⁴⁹⁹F_{CYT} (both previously implicated in recruiting SHP2 (6, 188)). Stable IpLITR 1.1b CYT YF mutant construct expression levels were confirmed by flow cytometric staining. Relatively similar expression levels were indicated by α HA mAb staining. Notably, parental AD293 cells show very little α HA staining, similar to IgG3 isotype control antibody staining (Figure 4.12B).

In all, co-immunoprecipitations (co-IPs) of three target FLAG-tagged signaling molecules are shown in Figure 4.13 including (A) SHP2, (B) Csk and (C) Syk. Initially, I conducted three control blots. First, co-IP samples were probed with an HRP-conjugated α HA antibody to ensure that IpLITR CYT constructs precipitated. The top blot of each panel is the IP sample displaying α HA reactive bands at the expected weights for IpFcR γ -L WT_{CYT} at ~51 kDa and all IpLITR 1.1b CYT constructs at ~70 kDa (Figure 4.13). Next, I blotted co-IP samples with an α -phosphotyrosine mAb (PY20) to confirm receptor phosphorylation after pervanadate treatment. The upper middle blot in each panel of Figure 4.13 shows bands at the expected receptor weights. An additional band at ~55 kDa is present in all lanes, likely representing the heavy chain of the mouse α HA antibody used for IP cross-reacting with the HRP-conjugated goat α -rabbit secondary antibody used to detect PY20. Finally, transfected whole cell lysates before IP were probed with an HRP-conjugated mouse α FLAG M2 antibody to confirm successful expression of target FLAG-tagged signaling molecules. Importantly, the unexpected technical coincidence that the HRP-conjugated mouse α FLAG M2 blotting antibody cross-reacts with IpLITR 1.1b WT_{CYT} necessitated the design of truncated SHP2 and Syk constructs (denoted by Δ in Figure 4.13). Truncated molecules contain SH2 domains only (i.e. they exclude the catalytic domains of each molecule), shifting their detection in the blots from their native ~70

kDa weight (same as the IpLITR 1.1b CYT constructs) to ~30 kDa so they are not obscured by IpLITR 1.1b CYT constructs. The bottom blot of each panel in Figure 4.13 is the lysate displaying α FLAG reactive bands at the expected weights for: (A) SHP2 at 28 kDa, (B) Csk at 51 kDa and (C) Syk at 32 kDa. After controls, target molecule co-IP was detected in the lower middle blot of each panel. SHP2 was not detected with IpFcR γ -L WT_{CYT} but did co-IP with IpLITR 1.1b WT_{CYT}. When proximal and distal CYT segment mutants were tested, SHP2 was only detected with IpLITR 1.1b Y^{prox}F_{CYT}, indicating that the distal CYT segment is responsible for the observed recruitment. When the distal CYT segment ITIM mutant constructs IpLITR 1.1b Y⁴⁷⁷F_{CYT} and IpLITR 1.1b Y⁴⁹⁹F_{CYT} were tested, IpLITR 1.1b Y⁴⁷⁷F_{CYT} lost the ability to recruit SHP2 while IpLITR 1.1b Y⁴⁹⁹F_{CYT} did not (Figure 4.13A). Next I looked at the recruitment of Csk which was not detected with IpFcR γ -L WT_{CYT} but did co-IP with IpLITR 1.1b WT_{CYT}. When proximal and distal CYT segment mutants were tested, Csk was only detected with IpLITR 1.1b Y^{dist}F_{CYT}, indicating that the proximal CYT segment is responsible for recruitment. When the proximal segment mutant motif construct IpLITR 1.1b Y⁴⁵³F_{CYT} was tested, the ability to recruit Csk was lost (Figure 4.13B). Additional bands above 62 kDa in the IpLITR 1.1b Y^{dist}F_{CYT} and IpLITR 1.1b Y⁴⁵³F_{CYT} lanes are likely the α FLAG cross-reactive IpLITR CYT constructs while smaller bands elsewhere are partial FLAG-tagged Csk products. These smaller products are also prevalent in the lysate blot (Figure 4.13B, bottom blot). Next I tested the recruitment potential of the stimulatory signaling molecule Syk, which is known to bind CYT ITAMs (332) and was recruited by IpLITR 1.1b WT_{CYT} in GST pulldowns presented in section 4.2.3 above. The IpFcR γ -L WT_{CYT} was the only construct capable of recruiting Syk (Figure 4.13C, lower middle blot).

Altogether, this co-IP data shows that IpLITR 1.1b WT_{CYT} associates with inhibitory signaling molecules Csk at proximal CYT motif Y⁴⁵³ and SHP2 at the distal CYT segment ITIM Y⁴⁷⁷, but not the stimulatory signaling molecule Syk.

4.3 DISCUSSION

Immunoregulatory receptor functional plasticity results from signaling versatility. In other words, receptors can activate functions via signaling that cannot always be predicted based on the presence of canonical CYT motifs. Recently, our lab reported a phagocytic function for an ITIM-containing receptor, IpLITR 1.1b. In this chapter, I established a new AD293 cell system to study the molecular signal transduction events that underlie IpLITR 1.1b WT_{CYT} functional plasticity. My results demonstrate that although IpLITR 1.1b WT_{CYT} is capable of recruiting phagocytic signaling molecules in GST pulldowns, a phagocytic function and a stimulatory recruitment profile are not demonstrated under physiological conditions. This raises interesting questions regarding the nature of cell context-dependent functional plasticity and the events that allow receptors to engage signaling pathways.

My functional and biochemical characterizations of IpLITR 1.1b WT_{CYT} phagocytic signaling were conducted in the non-immune, human epithelioid AD293 cell line. Derived from HEK293, these cells lack classical phagocytic receptors and are not endogenously phagocytic, however, they can perform this function when transfected with a ‘bona fide’ phagocytic receptor that engages phagocytic signaling pathways. For example, heterologous expression of the ITAM-containing FcγRIIA mediates phagocytosis in AD293 cells (329). While the development of stable IpLITR-expressing AD293 cell systems was successful, the biochemical recruitment profile obtained by GST pulldown was not re-capitulated by the physiologically-directed inhibitory molecule recruitment profile obtained after cellular activation by pervanadate. In line

with the latter profile, IpLITR 1.1b WT_{CYT} was incapable of activating phagocytic signaling upon receptor cross-linking by target beads during functional assessments, thus not supporting previous notions of IpLITR 1.1b WT_{CYT} as a ‘bona fide’ phagocytic receptor in AD293 cells.

The activation of specific immunoregulatory receptor functions is dependent on limited repertoires of recruited signaling molecules, known as a receptor interactome (333, 334). For phagocytosis, SH2 domains within signaling molecules recognize specifically phosphorylated linear CYT motifs and initiate signaling cascades that converge upon F-actin polymerization and target engulfment (21, 157, 158, 160). Therefore, underlying CYT-dependent phagocytic mechanisms can be predicted by comparing linear motif-SH2 domain interactomes generated by SH2 domain binding specificity libraries (135–137, 335, 336). Collectively, these binding studies highlight six critical residues that strongly influence SH2 domain binding specificity including: the phosphorylated tyrosine (pY; designated position 0), the two upstream residues (i.e. Y – 2, X-X-pY) and the three downstream residues (i.e. Y + 3, pY-X-X-X). This sequence makes up a consensus binding motif (X-X-pY-X-X-X) for an SH2 domain from a given signaling molecule. Previously, we showed that IpLITR 1.1b WT_{CYT} activated a unique ‘short-circuited’ ITAM-independent mode of phagocytosis in RBL-2H3 cells (7), using a pathway similar to Nck-dependent CEACAM3-mediated phagocytosis (216). The Nck1 SH2 domain consensus binding motif is H/P/V-I/L-pY-D/E-T/E-V/P (135, 337) and IpLITR 1.1b WT_{CYT} contains this consensus binding motif at H-I-Y⁴³³-D-T-V within the proximal CYT segment. Subsequently, I showed proximal CYT segment-specific Nck1 binding by GST pulldown. By applying consensus binding motif hypotheses, several potential phagocytic signaling participants, including Syk, were shown to bind IpLITR 1.1b WT_{CYT}. However, the accuracy in translating GST pulldown recruitment data (i.e. an interactome) to a mechanism underlying a cellular response (i.e. a

signalosome) is limited. This is due in large part to the complex dynamics that underlie physiological receptor activation which are not present during GST-CYT pulldowns from cellular lysates.

Functional assessments of phagocytosis presented in this chapter have demonstrated that IpLITR 1.1b WT_{CYT} is not phagocytic in human AD293 cells, despite binding several stimulatory signaling molecules in GST pulldowns. The initial events that underlie phagocytic signaling occur as three distinct phases including target capture, synapse formation and internalization (338), but due to technical aspects, data presented in this chapter highlights the synapse formation and internalization phases only. For example, the use of stable IpLITR-expressing cell lines enhances reproducibility of results by mitigating variability due to receptor expression level which would otherwise affect target binding avidity, receptor clustering and signal strength (339–341). Centrifuging cells immediately after adding bead targets induces target-cell interactions and drastically reduces reliance of subsequent phases on capturing targets. Furthermore, by performing these steps at 4°C, the initial target-cell interactions remain static while synapse formation and internalization begin while re-warming cells to 37°C. The synapse formation and internalization phases require receptor clustering, activation of phosphotyrosine-dependent signaling by cellular SFKs and the recruitment of SH2 domain-containing signaling molecules. In the case of IpLITR 1.1b WT_{CYT}, these events were not sufficient to evoke target internalization.

Src family kinases (SFKs) are inner membrane-associated enzymes involved in signal transduction. Upon receptor cross-linking and clustering, SFKs initiate signaling cascades by phosphorylating receptor CYTs. This family includes nine primary proteins in humans, including Src, Fyn, Yes, Lyn, Hck, Fgr, Blk, Lck and Frk, that exhibit tissue-specific expression. Lyn, Hck,

Fgr, Blk and Lck are expressed in the brain and hematopoietic cells. Frk is primarily expressed in epithelial cells, while Src, Fyn and Yes are broadly expressed (342). The recognition and phosphorylation of receptor CYT substrates is also selective and differs between members. For example, each SFK member contains an SH2 domain which influences sub-cellular localization and substrate recognition. In addition, the catalytic kinase domains of each member show a preference in phosphorylating specific tyrosine-based motifs (252, 343–345). This facilitated my hypothesis that co-expressing a viral Src kinase (vSrc), that exhibits constitutive activity towards a broad repertoire of tyrosine-based motifs (216, 330), with IpLITR 1.1b WT_{CYT} may evoke phagocytic signaling (Figure 4.14, i.). However, vSrc co-expression did not activate IpLITR 1.1b WT_{CYT}-mediated phagocytic signaling (Figure 4.9).

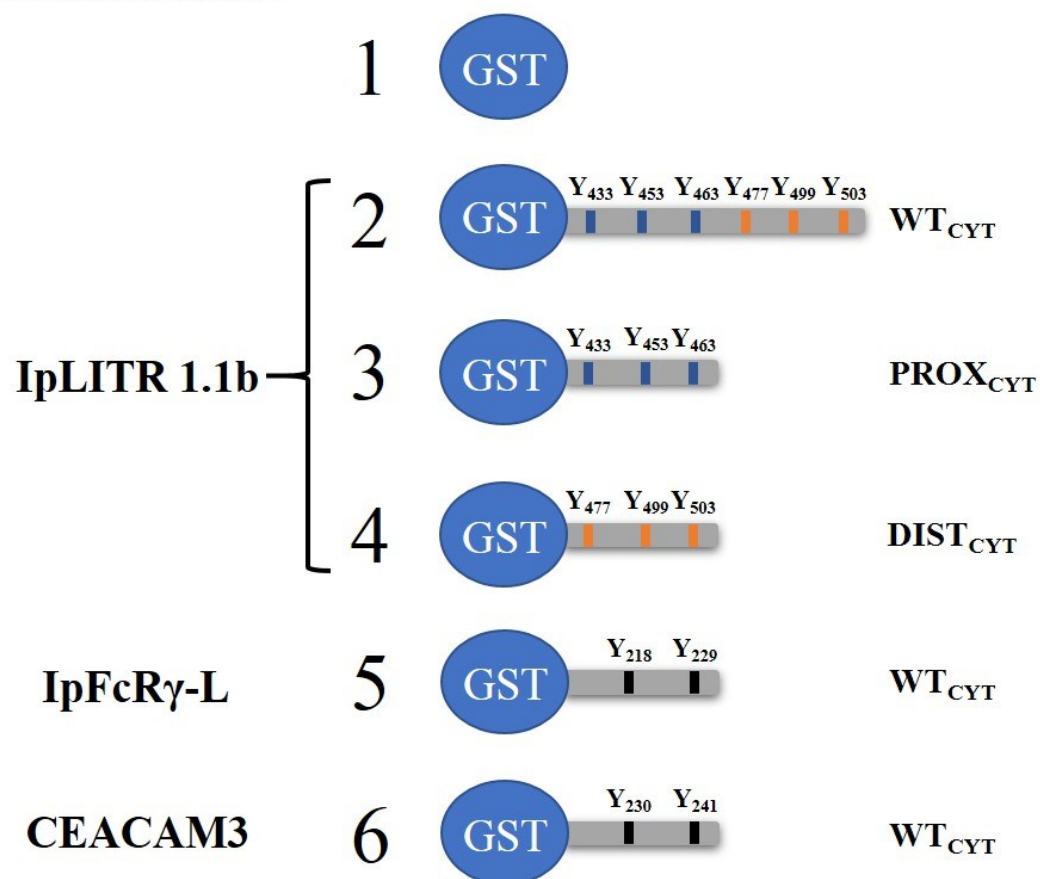
Previous observations of IpLITR 1.1b WT_{CYT}-mediated phagocytosis were reported in RBL-2H3 cells (5, 7). These myeloid cells display a marked difference in the pattern of signaling molecule expression compared to epithelioid AD293 cells. This may render IpLITR 1.1b WT_{CYT} incapable of phagocytic signaling in two ways: (1) relatively higher signaling molecule expression levels in immune compared to epithelioid cells (e.g Syk (346); Figure 4.14, ii) or (2) the lack of expression of a critical signaling molecule in AD293 cells, like the SLAM-associated protein (SAP; Figure 4.14, iii), which is expressed in immune cells where it activates responses downstream of the SLAM family of IgSF receptors (347, 348). Interestingly, SLAM family receptors bind to SAP at CYT ITSMs which switches their function and signaling from inhibitory to stimulatory (236, 243, 349, 350). IpLITR 1.1b WT_{CYT} contains an ITSM at Y⁵⁰³ and a SAP-dependent mechanism was proposed previously (5), however SAP over-expression did not evoke IpLITR 1.1b WT_{CYT}-mediated phagocytosis in my experiments (Figure 4.10).

The phosphotyrosine-dependent signaling events that drive phagocytosis are preceded by receptor-membrane dynamics which dictate signaling outcomes. During phagocytosis for example, these sub-membrane dynamics control target capture and receptor clustering within lipid raft microdomains. These events are pre-requisites for triggering intimate target-cell binding (i.e. phagocytic synapse formation) and signaling for target internalization (295, 351, 352). Studies of sub-membrane dynamics have demonstrated central roles for the actin cytoskeleton and actin-binding adaptor molecules. For example, the mobility of receptors to sites of target-cell engagement, known as the phagocytic synapse, is controlled, to a large extent, by transmembrane receptor ‘pickets’ anchored to sub-membrane cytoplasmic actin ‘fences’. Once a target is bound, receptors are released from the confines of this ‘picket fence’ and shuttled to the forming synapse. This is explained, in part, by receptor-actin linkages mediated by actin-binding adaptor molecules like the protein 4.1 family, which are expressed in immune cells and bind the Fc γ RI CYT (290). Indeed, constitutive 4.1 protein association with Fc γ RI was critical for targeting the receptor to lipid raft microdomains (293). Another well-studied example is the CD44 CYT which binds actin adaptor ezrin-radixin-moesin (ERM) proteins (287, 353). While this receptor has diverse biological roles, a phagocytic function was reported in mouse macrophages (354). It is important to note however, that these cells express additional phagocytic receptors and subsequent reports showed that CD44 tethered targets to the cell surface while inducing inside-out activation of $\alpha_M\beta_2$ integrin which co-ordinated the internalization of bound targets (355). Importantly, these examples illustrate the importance of receptor-actin dynamics that directly influence the outcome of receptor signaling in the initiation of phagocytosis. Although untested, actin-mediated IpLITR 1.1b WT_{CYT} trafficking may render

this receptor incapable of phagocytic signaling in AD293 cells by preventing phagocytic synapse formation.

When IpLITR 1.1b WT_{CYT} was activated by pervanadate treatment and precipitated, only the inhibitory signaling molecules Csk and SHP2 were detected by Western blot. This indicates that although IpLITR 1.1b WT_{CYT} contains binding motifs for several signaling molecules, the context within which recruitment occurs drastically influences its interactome. Specifically, while GST pulldowns effectively combine large amounts of both receptor CYT and signaling molecule that freely interact within a lysate, pervanadate stimulation relies upon physiological factors including available cellular SFKs for receptor activation, signaling molecule expression repertoire and sub-membrane dynamics to co-ordinate recruitment, but not receptor cross-linking. Since pervanadate irreversibly inhibits global phosphatase activity (331) and full activation of SFKs requires dephosphorylation at C-terminal Y⁵²⁷ and phosphorylation at catalytic domain Y⁴¹⁶ (356), pervanadate may only partially activate certain SFKs leading to phosphorylation of a restricted repertoire of receptor CYT motifs. This may introduce bias in subsequent phosphorylation-dependent recruitment profiles of receptor CYTs. However, the second tyrosine residue within the catalytic domain of SFKs (i.e. Y⁴¹⁶) is phosphorylated after pervanadate treatment (357), suggesting that SFKs may be fully activated. Furthermore, this approach has been successfully applied for assessing receptor recruitment in intact cells in numerous studies. Consequently, pervanadate recruitment better reflects a physiological recruitment profile or receptor signalosome, which is more predictive of stimulatory or inhibitory signaling outcomes and helps explain why IpLITR 1.1b WT_{CYT} is not phagocytic in AD293 cells.

Altogether, data presented in this chapter established the ‘bona fide’ phagocytic function of the IpFcR γ -L WT_{CYT} but biochemical data suggest an inhibitory function for IpLITR 1.1b WT_{CYT}. These data facilitated a shift in my objectives from characterizing the ‘bona fide’ phagocytic signaling potential of IpLITR 1.1b WT_{CYT} to applying the AD293 cell system for exploring other aspects of IpLITR signaling biology. IpLITRs and their isoforms contain highly similar extracellular domains (e.g. $\geq 77\%$, 86%, 92% and 94% identity for D1, D2, D3 and D4, respectively) indicating they may bind common ligands and IpLITRs are co-expressed by fish immune cells (2). Since multiple immunoregulatory receptor inputs to immune cells are integrated to modulate signaling outcomes and AD293 cells are highly suited to transfection, my research will now focus on establishing an assay to measure the potential cross-talk regulation of IpFcR γ -L WT_{CYT}-driven phagocytosis by IpLITR 1.1b WT_{CYT}.

A. Derived from:

B.

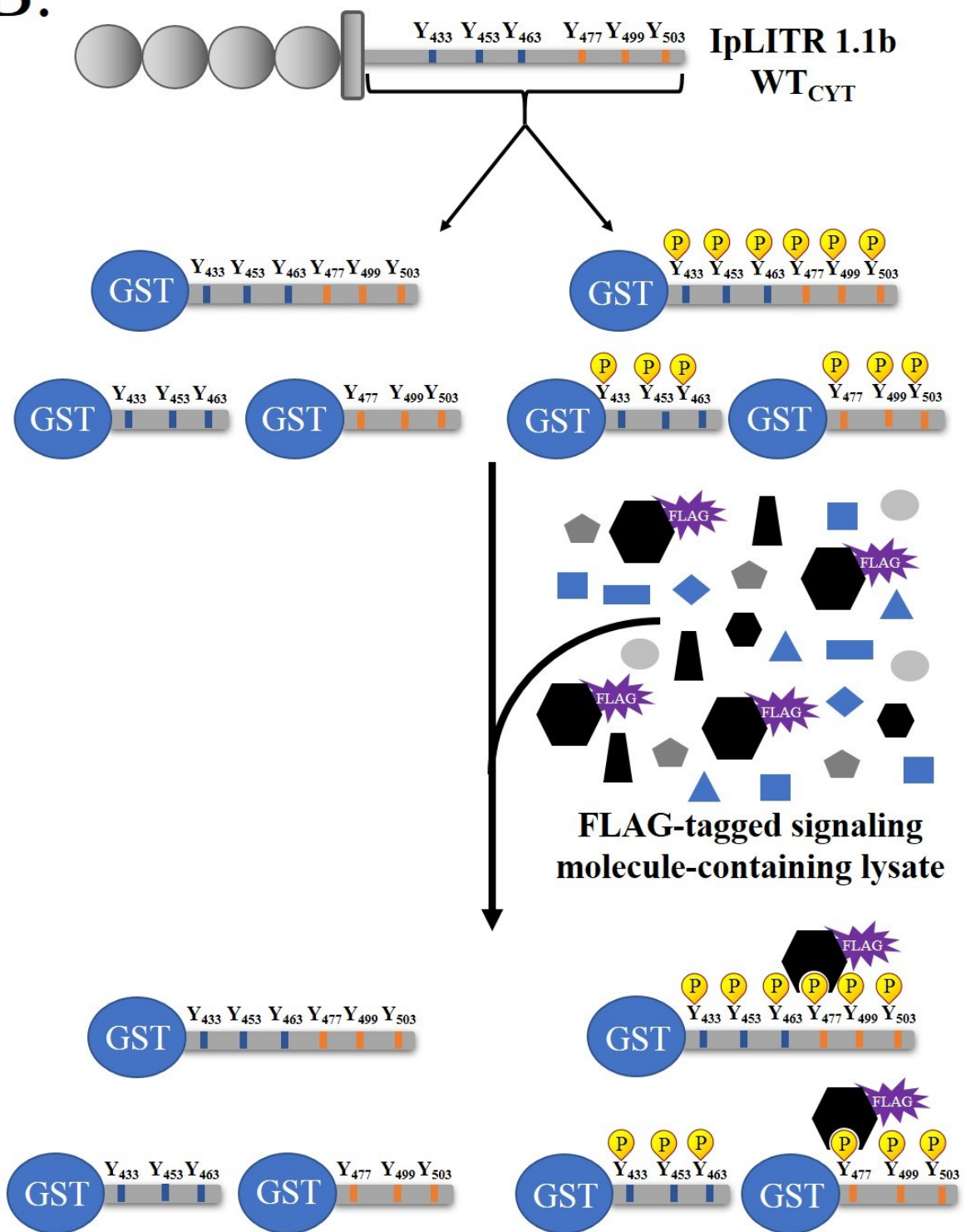
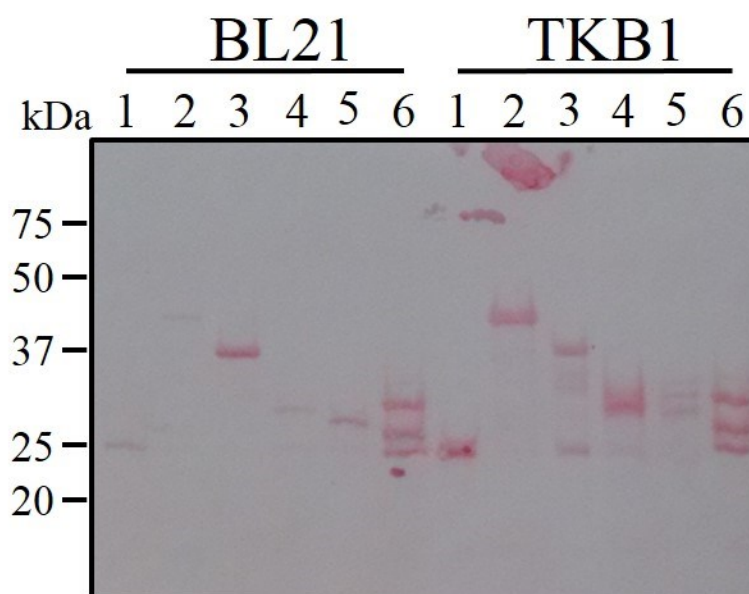


Figure 4.1. Schematic representations of the N-terminal tagged GST-CYT fusion proteins and overview of the GST pulldown assay. (A) Six GST-CYT fusion proteins derived from three immunoregulatory receptor proteins (i.e. IpLITR 1.1b, IpFcR γ -L and human CEACAM3) were generated as ‘bait’ for GST pulldown assays. They include a GST-wild-type (WT)_{CYT} fusion protein for each parent receptor protein. In addition to the GST-WT_{CYT} fusion protein derived from IpLITR 1.1b, proximal CYT segment (PROX_{CYT}; blue colour-coded motifs) and distal CYT segment (DIST_{CYT}; orange colour-coded motifs) fusion proteins were generated to identify segment-specific recruitment to the IpLITR 1.1b WT_{CYT} region. A GST epitope tag only protein was generated as a negative control for signaling molecule recruitment. (B) GST pulldowns were performed using two sets of GST-CYT fusion proteins: phosphorylated and unphosphorylated. Each set of fusion proteins was incubated with C-terminal FLAG-tagged signaling molecule (i.e. ‘prey’)-containing AD293 cell lysates and purified. Phosphotyrosine-dependent signaling molecule recruitment to a particular CYT region is demonstrated if phosphorylated ‘bait’ co-precipitates FLAG-tagged ‘prey’, while GST only negative controls and unphosphorylated ‘bait’ do not.

- A.**
- | | |
|---|---|
| 1 | GST |
| 2 | GST-IpLITR 1.1b WT _{CYT} |
| 3 | GST-IpLITR 1.1b PROX _{CYT} |
| 4 | GST-IpLITR 1.1b DIST _{CYT} |
| 5 | GST-IpFcR γ -L WT _{CYT} |
| 6 | GST-CEACAM3 WT _{CYT} |



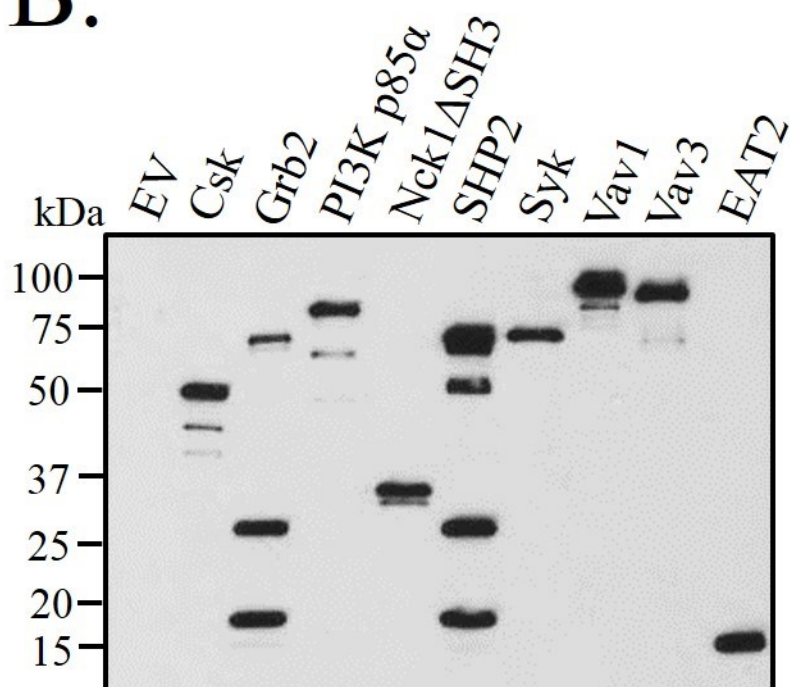
B.blot α FLAG

Figure 4.2. Generation of N-terminal tagged GST-CYT fusion protein ‘bait’ and C-terminal FLAG-tagged signaling molecule ‘prey’-containing cellular lysates.

(A) Each immunoregulatory protein CYT sequence was sub-cloned into the 1- β -D-thiogalactopyranoside (IPTG)-inducible GST expression vector, pFN2A, and transformed into BL21 or TKB1 *E. coli*. Bacterial cultures were induced with IPTG at 37°C for 2 h. BL21 *E. coli* were pelleted and frozen at -80°C overnight. TKB1 *E. coli* contain an inducible tyrosine kinase (TK), Elk1, that was activated after pelleting and re-suspending cells in TK induction media and incubating at 37°C for 1 h, after which, cells were pelleted again and frozen at -80°C overnight. Affinity purification of all GST-CYT fusion protein ‘bait’ was visualized by eluting beads in reducing buffer and separating by 12% SDS-PAGE gel electrophoresis. After transfer, nitrocellulose membranes were stained with Ponceau, a non-specific protein dye. (B) Nine human SH2 domain-containing signaling molecules were cloned from an AD293 cell cDNA library. PCR fragments were sub-cloned into pJET1.2/blunt, digested using restriction enzymes and sub-cloned into the p3XFLAG-CMV14 eukaryotic expression vector which were confirmed by sequencing. To generate lysates, 2 μ g sequenced vector was transfected into AD293 cultures using TurboFECT® transfection reagent and cells were grown at 37°C for 24-48 h. Cells were lysed in 1% triton-X TBS lysis buffer and clarified supernatants were collected after centrifugation. Samples were separated by SDS-PAGE and FLAG-tagged signaling molecule ‘prey’ expression was confirmed by Western blotting using the mouse HRP-conjugated M2 α FLAG antibody.

- A.**
- | | |
|---|---|
| 1 | GST |
| 2 | GST-IpLITR 1.1b WT _{CYT} |
| 3 | GST-IpLITR 1.1b PROX _{CYT} |
| 4 | GST-IpLITR 1.1b DIST _{CYT} |
| 5 | GST-IpFcR γ -L WT _{CYT} |

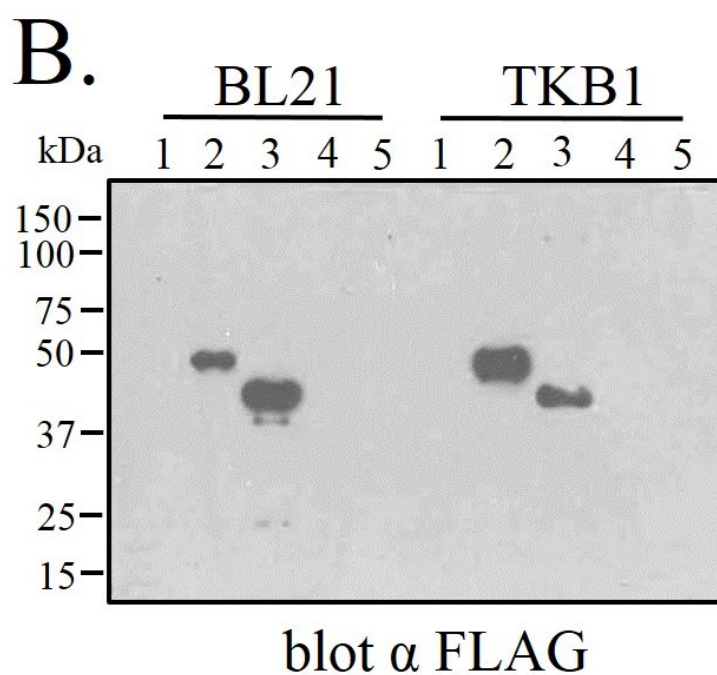
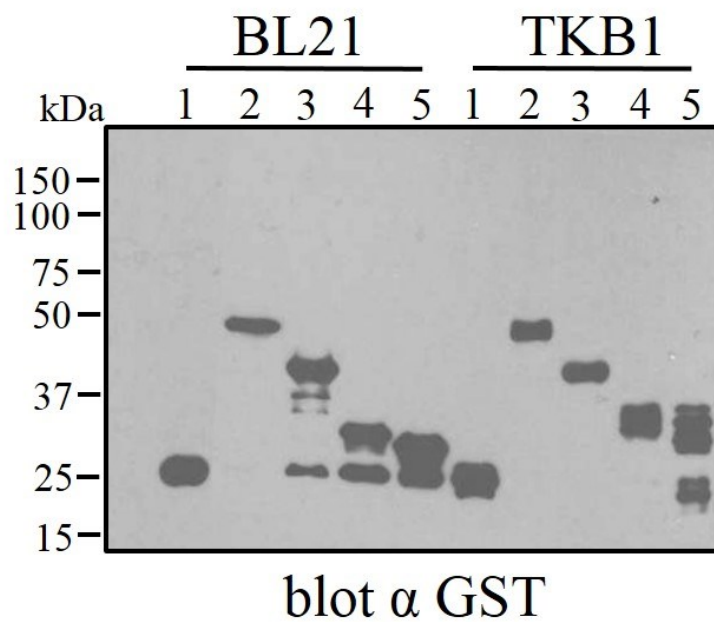
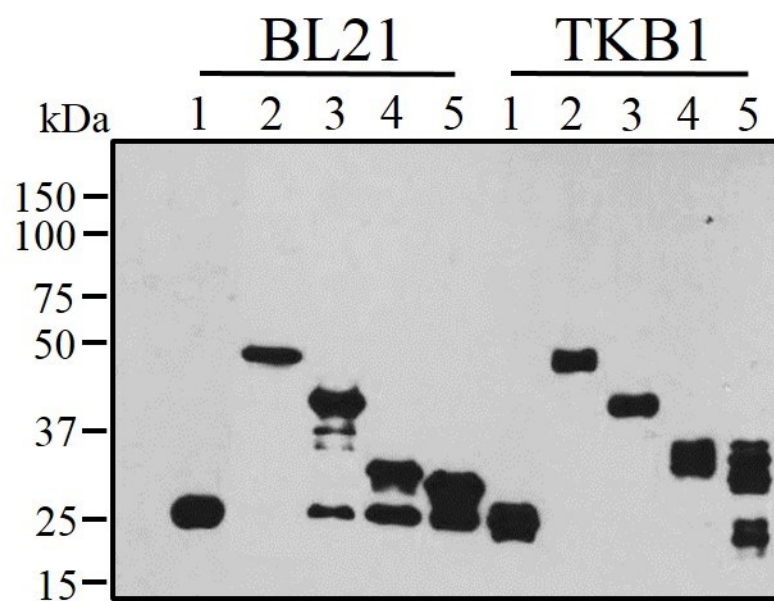


Figure 4.3. GST-IpLITR 1.1b WT_{CYT} and GST-IpLITR 1.1b PROX_{CYT} fusion proteins cross-react with α FLAG M2 monoclonal blotting antibody.

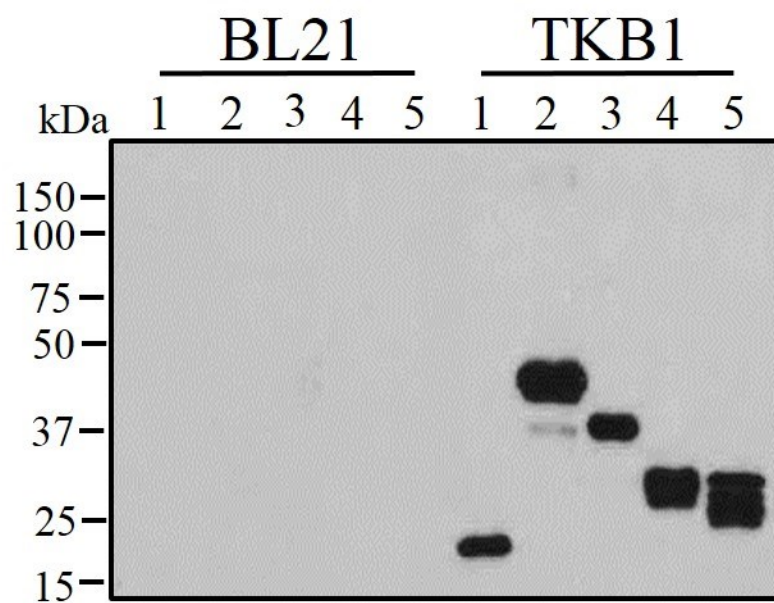
Unphosphorylated (BL21) and phosphorylated (TKB1) N-terminal GST-CYT fusion protein ‘bait’ was affinity purified on glutathione-conjugated sepharose beads. After eluting samples in reducing buffer, proteins were separated by 12% SDS-PAGE, transferred to nitrocellulose membranes and probed with (A) an α GST monoclonal antibody to detect unphosphorylated and phosphorylated ‘bait’ proteins or (B) a mouse HRP-conjugated α FLAG M2 monoclonal antibody. Each lane corresponds to a single ‘bait’ protein purification; see legend for ‘bait’ protein identity. Blots shown are representative of 3 independent experiments.

- A.**
- | | |
|---|---|
| 1 | GST |
| 2 | GST-IpLITR 1.1b WT _{CYT} |
| 3 | GST-IpLITR 1.1b PROX _{CYT} |
| 4 | GST-IpLITR 1.1b DIST _{CYT} |
| 5 | GST-IpFcR γ -L WT _{CYT} |



blot α GST

- B.**
- | | |
|---|---|
| 1 | GST |
| 2 | GST-IpLITR 1.1b WT _{CYT} |
| 3 | GST-IpLITR 1.1b PROX _{CYT} |
| 4 | GST-IpLITR 1.1b DIST _{CYT} |
| 5 | GST-IpFcR γ -L WT _{CYT} |



blot α phospho-tyrosine

C.

- | | |
|---|---|
| 1 | GST |
| 2 | GST-IpLITR 1.1b WT _{CYT} |
| 3 | GST-IpLITR 1.1b PROX _{CYT} |
| 4 | GST-IpLITR 1.1b DIST _{CYT} |
| 5 | GST-IpFcR γ -L WT _{CYT} |

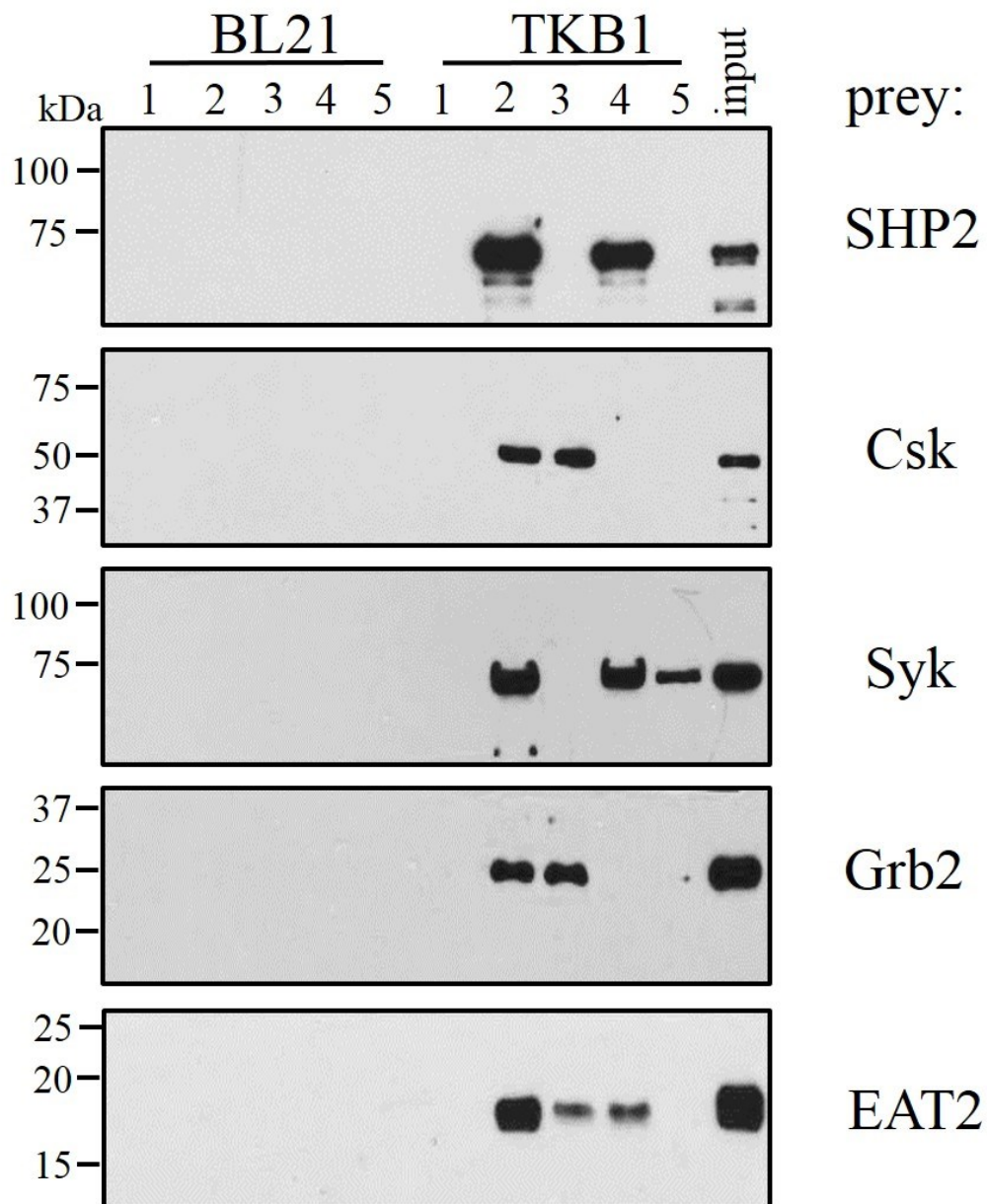
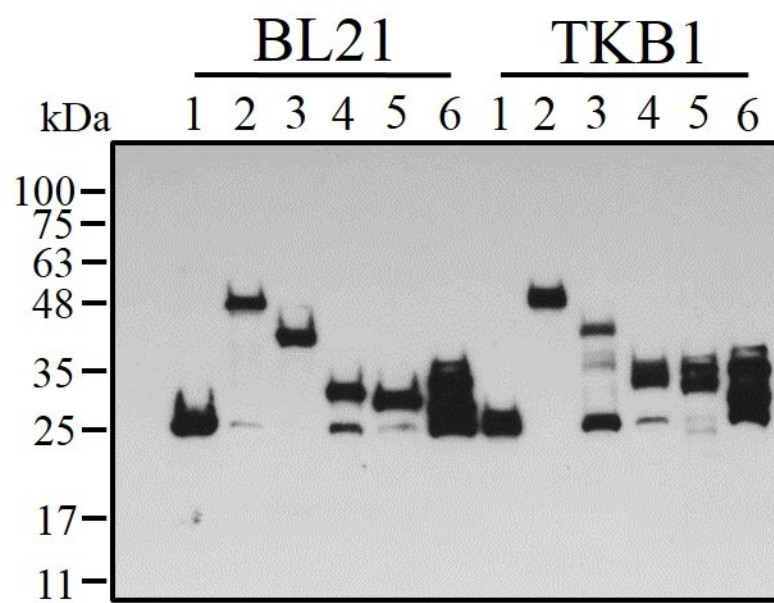
blot α FLAG

Figure 4.4. Differential phosphotyrosine-dependent recruitment of C-terminal FLAG-tagged signaling molecules to the proximal and distal CYT segments of IpLITR 1.1b WT_{CYT} by GST pulldown. Unphosphorylated (BL21) and phosphorylated (TKB1) N-terminal GST-CYT fusion protein ‘bait’ was affinity purified on glutathione-conjugated sepharose beads and incubated with C-terminal FLAG-tagged signaling molecule ‘prey’-containing AD293 cell lysates. Samples were separated by 12% SDS-PAGE under reducing conditions, transferred to nitrocellulose membranes and probed with (A) an α GST mAb to detect unphosphorylated and phosphorylated ‘bait’ proteins or (B) an α -phosphotyrosine mAb to detect phosphorylation of TKB1-derived ‘bait’ proteins. (C) Samples from (A) and (B) above were probed with the mouse HRP-conjugated α FLAG M2 mAb to detect co-precipitating signaling molecule ‘prey’. Each lane corresponds to a single ‘bait’ protein tested; see legend for ‘bait’ protein identity. Input lane represents the ‘prey’-containing AD293 whole cell lysate before the pulldowns were performed. Target signaling molecule ‘prey’ shown here include SHP2, Csk, Syk, Grb2 and EAT2. Blots shown are representative of 3 independent experiments.

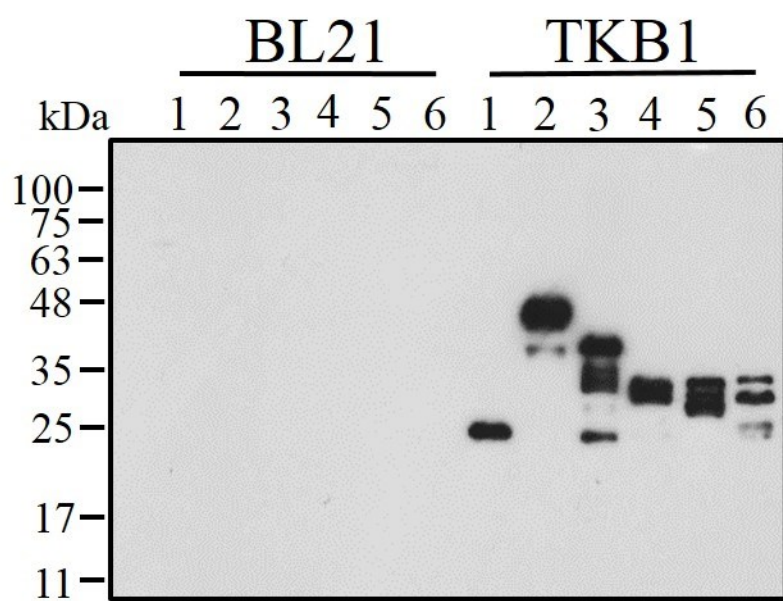
- A.**
- | | |
|---|---|
| 1 | GST |
| 2 | GST-IpLITR 1.1b WT _{CYT} |
| 3 | GST-IpLITR 1.1b PROX _{CYT} |
| 4 | GST-IpLITR 1.1b DIST _{CYT} |
| 5 | GST-IpFcR γ -L WT _{CYT} |
| 6 | GST-CEACAM3 WT _{CYT} |



blot α GST

B.

- 1 GST
- 2 GST-IpLITR 1.1b WT_{CYT}
- 3 GST-IpLITR 1.1b PROX_{CYT}
- 4 GST-IpLITR 1.1b DIST_{CYT}
- 5 GST-IpFcR γ -L WT_{CYT}
- 6 GST-CEACAM3 WT_{CYT}



blot α phospho-tyrosine

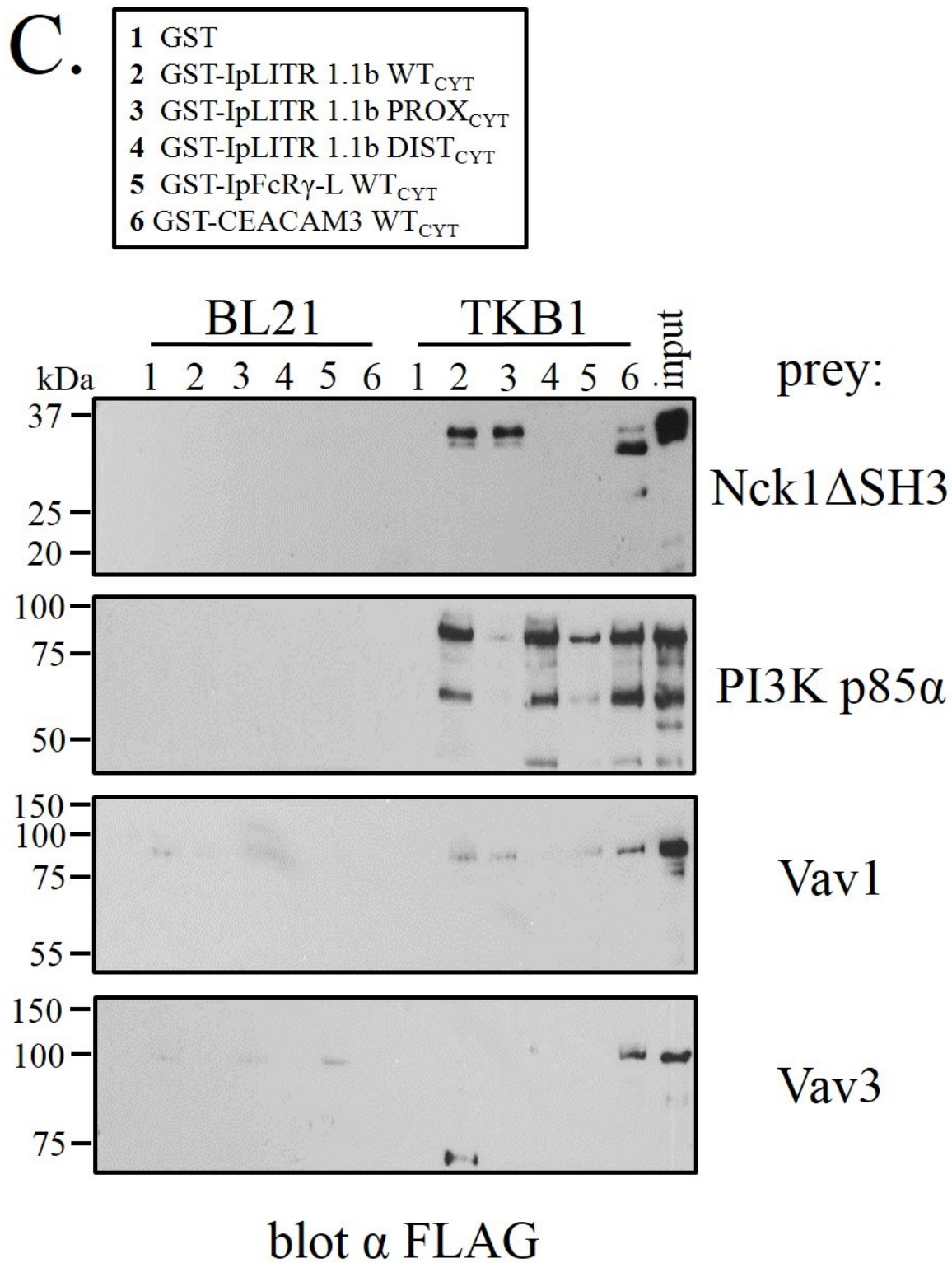


Figure 4.5. Differential phosphotyrosine-dependent recruitment of C-terminal FLAG-tagged signaling molecules to the proximal and distal CYT segments of IpLITR 1.1b WT_{CYT} by GST pulldown. Unphosphorylated (BL21) and phosphorylated (TKB1) N-terminal GST-CYT fusion protein ‘bait’ was affinity purified on glutathione-conjugated sepharose beads and incubated with C-terminal FLAG-tagged signaling molecule ‘prey’-containing AD293 cell lysates. Samples were separated by 12% SDS-PAGE under reducing conditions, transferred to nitrocellulose membranes and probed with (A) an α GST mAb to detect unphosphorylated and phosphorylated ‘bait’ proteins or (B) an α -phosphotyrosine mAb to detect phosphorylation of TKB1-derived ‘bait’ proteins. (C) Samples from (A) and (B) above were probed with the mouse HRP-conjugated α FLAG M2 mAb to detect co-precipitating signaling molecule ‘prey’. Each lane corresponds to a single ‘bait’ protein tested; see legend for ‘bait’ protein identity. Input lane represents the ‘prey’-containing AD293 whole cell lysate before the pulldowns were performed. Target signaling molecule ‘prey’ shown here include Nck1, PI3K p85 α , Vav1, and Vav3. Blots shown are representative of 3 independent experiments.

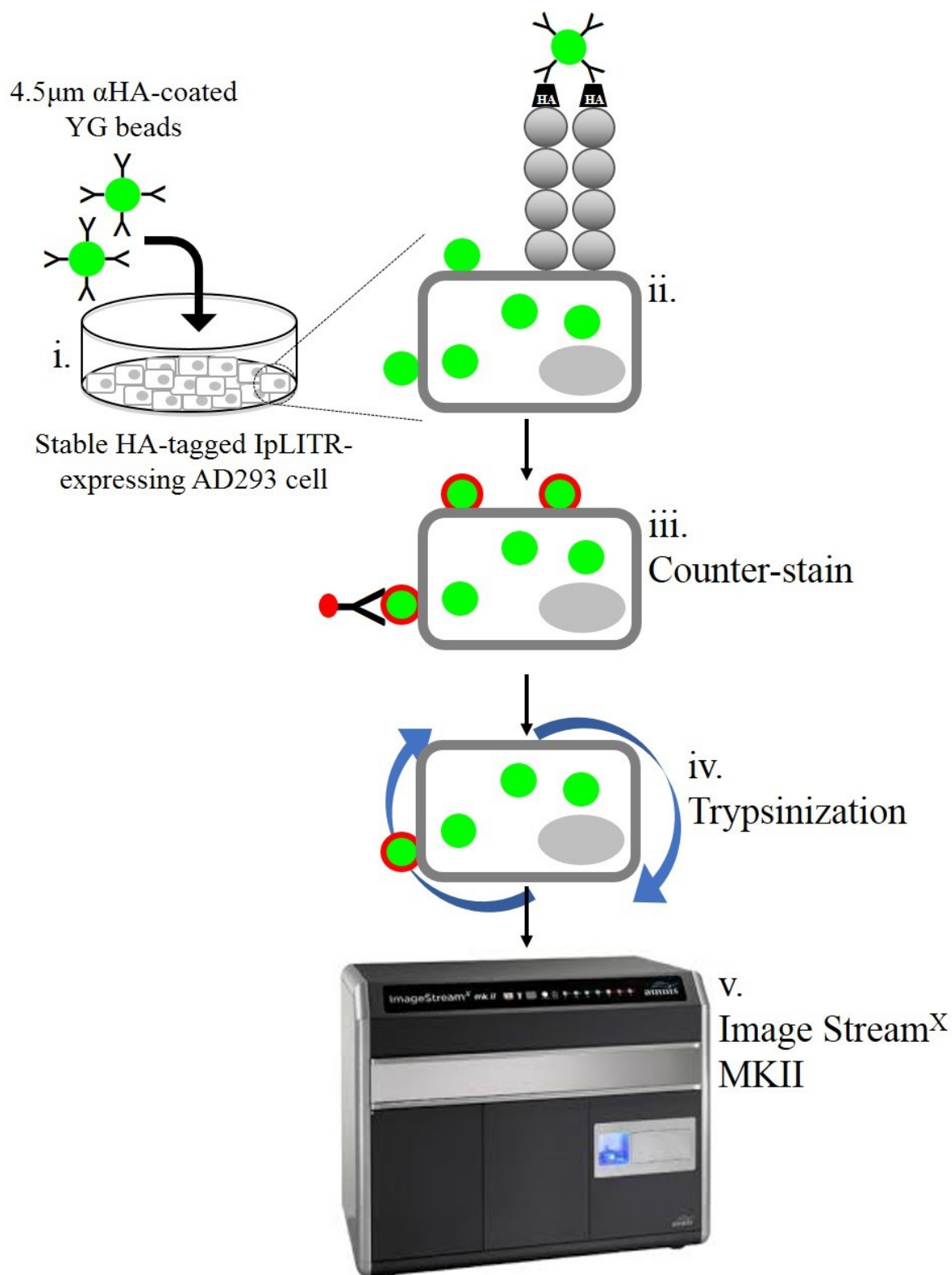
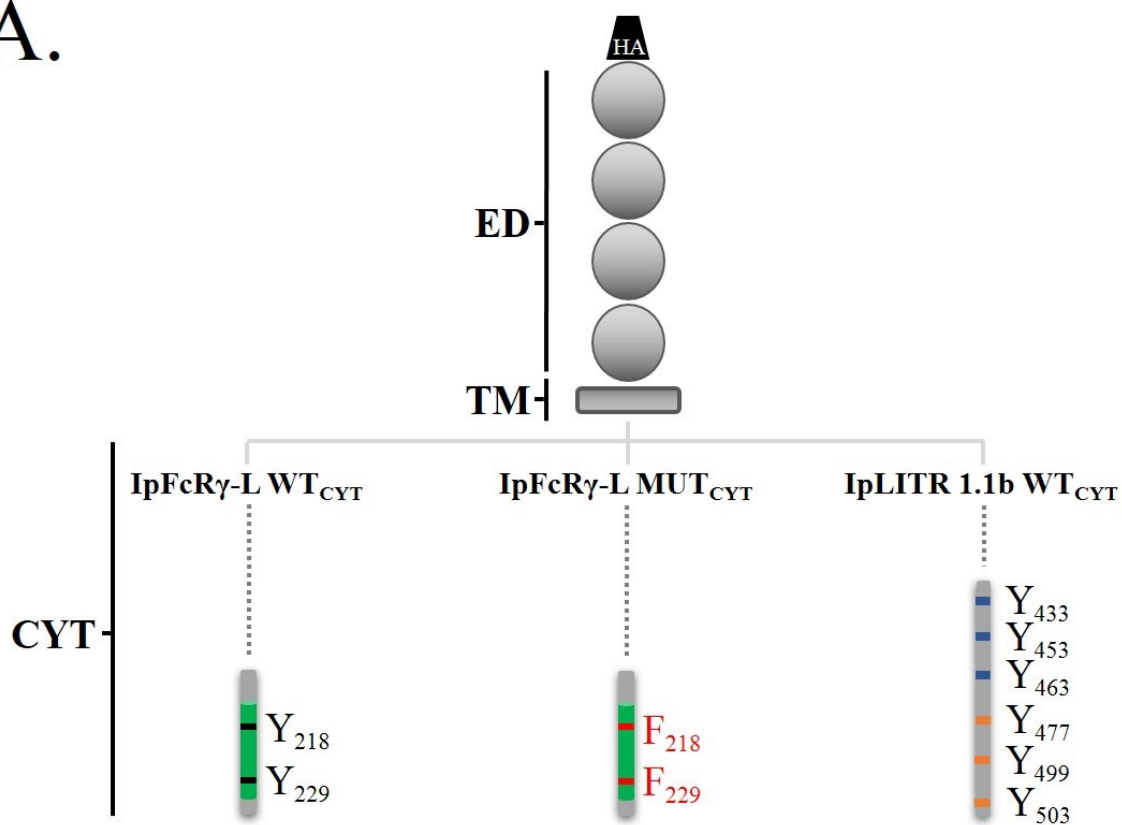


Figure 4.6. Schematic representation of the Image Stream-based phagocytosis assay. (i) 4.5 μm mouse αHA antibody-coated green fluorescent (YG) beads are added to stable HA epitope-tagged IpLITR-expressing AD293 cells. (ii) After centrifugation to synchronize bead-cell engagement, cells were incubated at 37°C for 30 min to activate phagocytic signaling. (iii) Then, cells were incubated at 4°C for 30 min with AlexaFluor647-conjugated rabbit α -mouse secondary to label surface-exposed YG beads, followed by (iv) trypsinization, consisting of a 37°C incubation for 5 min in harvest buffer containing 0.05% trypsin and 1.2 mM EDTA. This incubation also removed non-specifically cell-adsorbed YG beads. (v) Cells were centrifuged and pellets re-suspended in 1% paraformaldehyde fixative before data collection on the Image Stream^X MKII imaging flow cytometer.

A.



B.

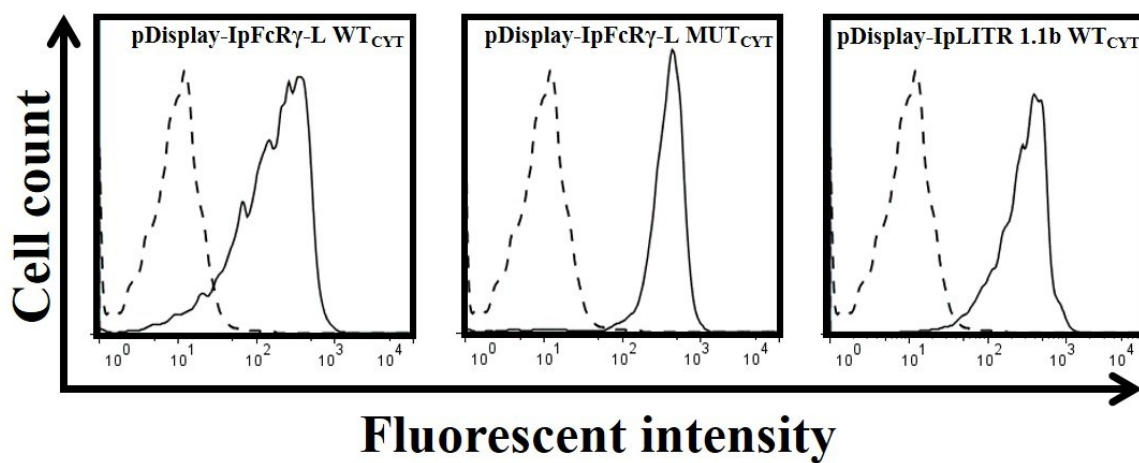
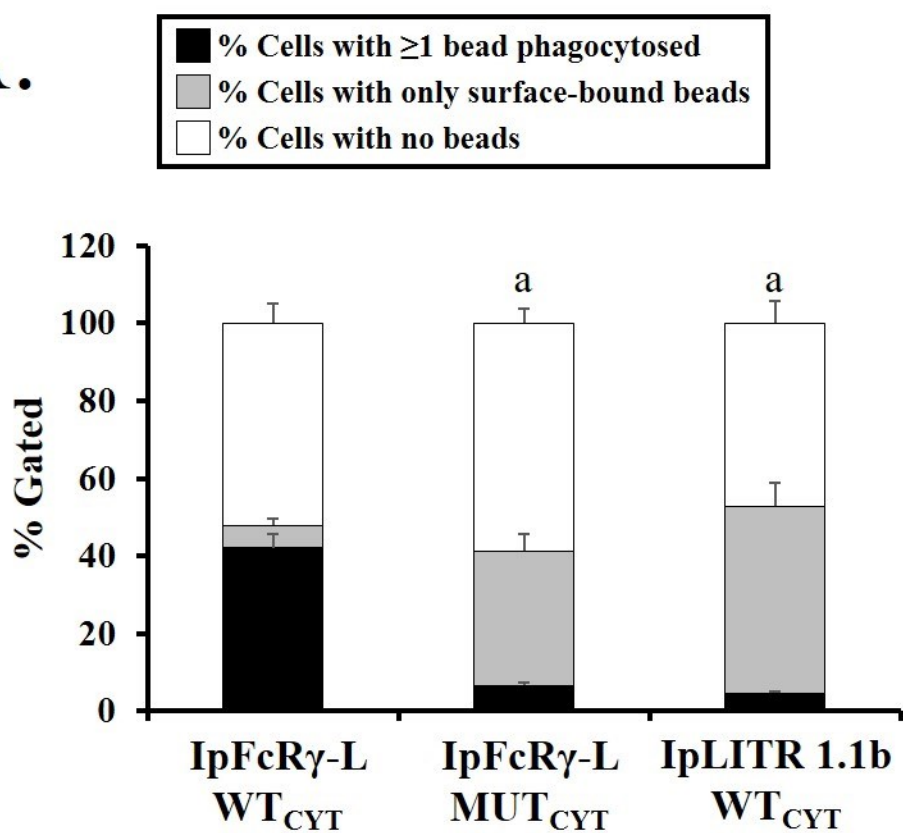


Figure 4.7. Generation and stable expression of N-terminal HA epitope-tagged IpLITR 1.1b CYT constructs in AD293 cells. (A) Schematic representations of the three IpLITR 1.1b CYT constructs tested. Each construct contains an N-terminal HA epitope tag and the four extracellular Ig-like domains (ED) and transmembrane (TM) segment of wild-type IpLITR 1.1b fused to a different CYT region. In the first construct, the IpLITR 1.1b ED-TM is fused to the ITAM-containing CYT region of wild-type IpFcR γ -L (IpFcR γ -L WT_{CYT}). The second construct is fused to a Y \rightarrow F mutant (i.e. both ITAM tyrosine residues are phenylalanine) IpFcR γ -L CYT (IpFcR γ -L MUT_{CYT}) and the third construct is the wild-type IpLITR 1.1b (IpLITR 1.1b WT_{CYT}). Locations of the tyrosine residues within each CYT region are indicated by the corresponding tyrosine positions within the native protein sequences of the wild-type molecules, as previously published (4, 6). (B) Parental AD293 cells were transfected with pDisplay-encoded IpLITR 1.1b CYT constructs and incubated at 37°C for 48 h, at which point cells were cultured in selective media containing G418 antibiotic for two weeks and cloned by serial dilution into 96-well plates. Confluent wells containing an individual clone were transferred to a 24-well plate, grown to confluence and stained for cell surface IpLITR expression with the α HA mAb HA.C5 (solid line) or the mouse IgG3 isotype control antibody (dotted line), followed by PE-conjugated goat α -mouse IgG polyclonal antibody counter-staining. After 5-10 passages, stable IpLITR 1.1b CYT construct expression levels were confirmed by flow cytometry. A representative stain of at least 3 independent experiments for each cell line is shown.

A.



B.

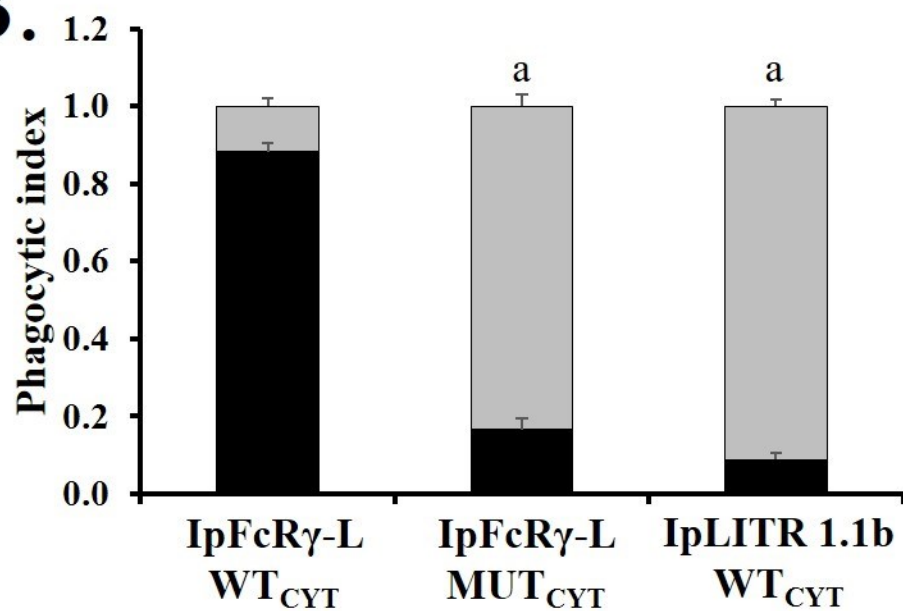
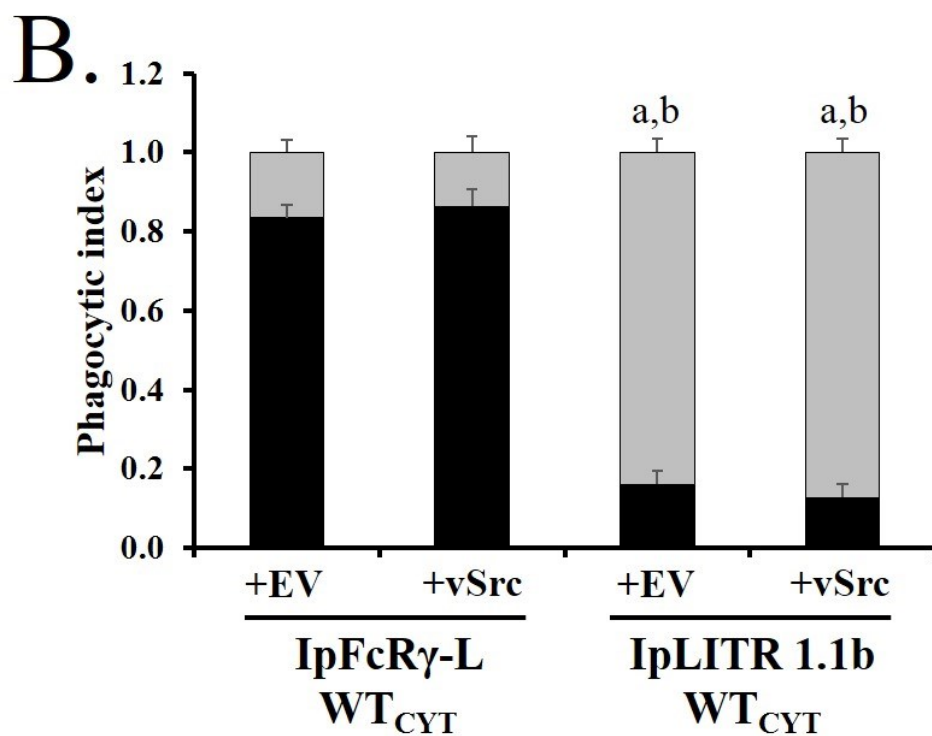
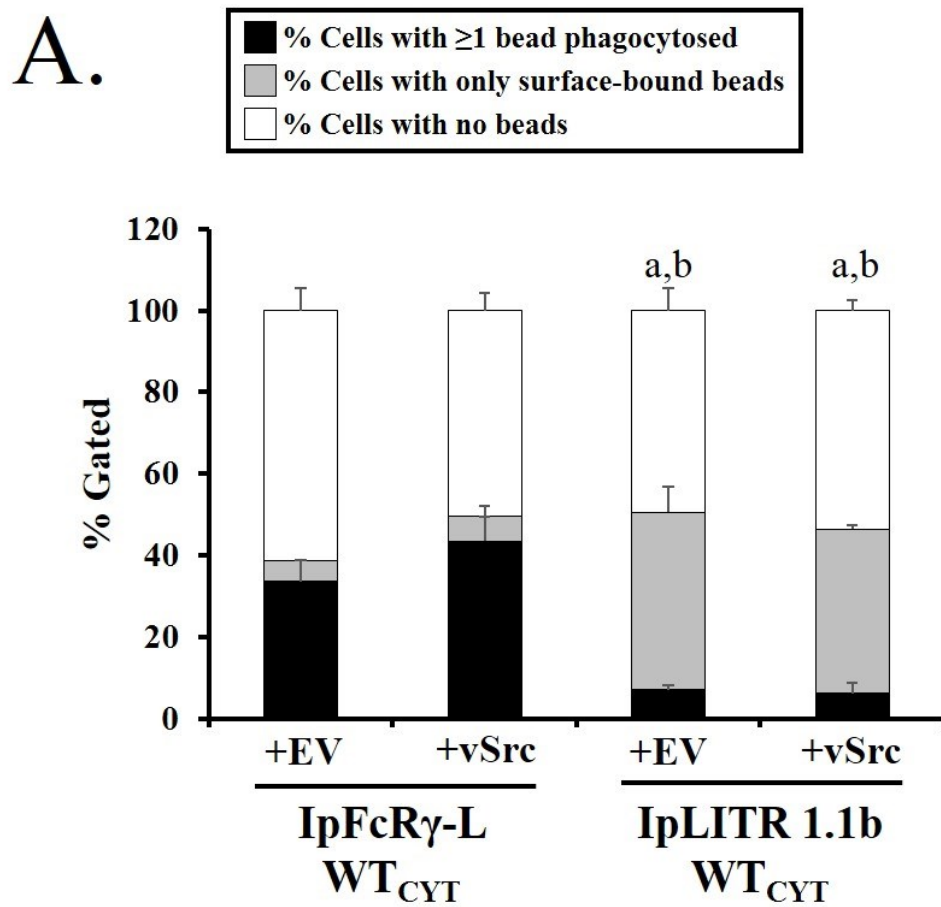


Figure 4.8. α HA-coated bead-induced cross-linking of IpFcR γ -L WT_{CYT}, but not IpLITR 1.1b WT_{CYT}, mediates CYT-dependent phagocytic signaling.

Mouse α HA antibody-coated green fluorescent (YG) 4.5 μ m beads were added to HA epitope-tagged stable IpLITR 1.1b CYT construct-expressing AD293 cells for 30 min at 37°C. Surface-bound YG beads were counter-stained with AlexaFluor647-conjugated rabbit α -mouse secondary antibody. Cells were harvested by trypsinization and fixed in 1% paraformaldehyde prior to data collection on the Image Stream^X MKII flow cytometer. Raw image files were subjected to component masking analysis by template-assisted batching using IDEAS v6.2 software as previously described (327). Each black bar represents the percentage of phagocytic cells (i.e. a cell with ≥ 1 bead fully internalized), grey bars represent the percentage of cells with only surface-bound beads (no beads internalized) and the white bars represent the percentage of cells with no associated beads (e.g. none bound or internalized). Results are representative of the mean \pm SEM of three independent experiments as (A) raw or (B) indexed data. Phagocytic index was calculated as: % phagocytic or surface-bound cells / % total bead-associated cells. Lower case 'a' represents a statistically significant difference ($p < 0.05$) compared to IpFcR γ -L WT_{CYT} % phagocytic cells, respectively.



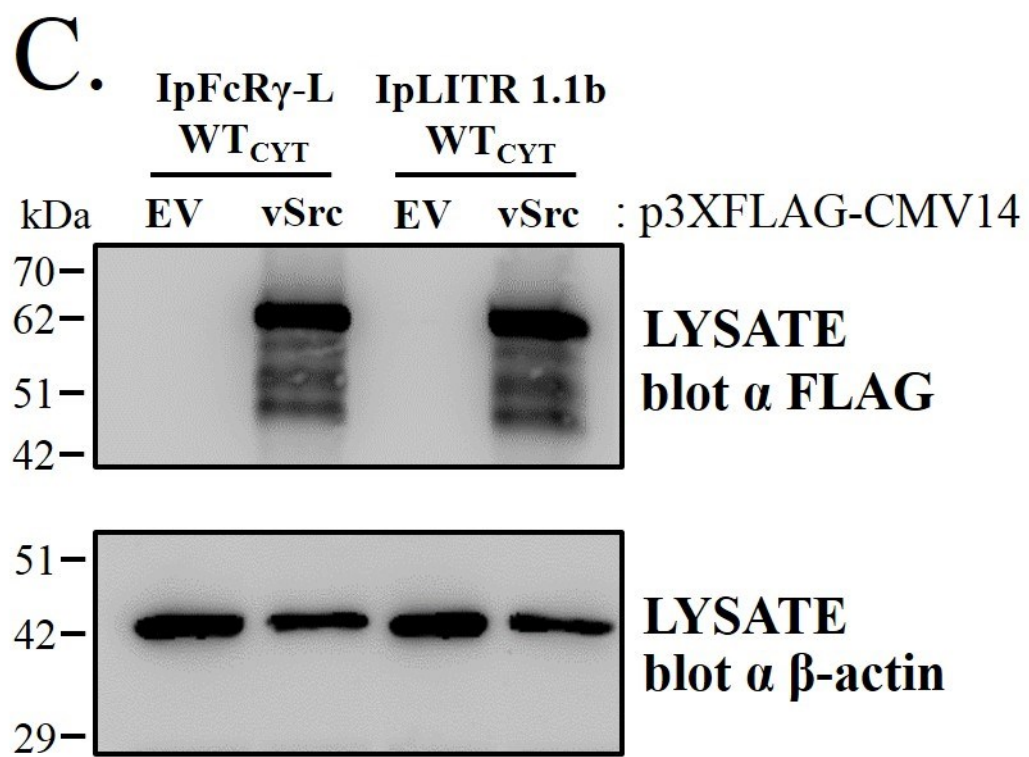
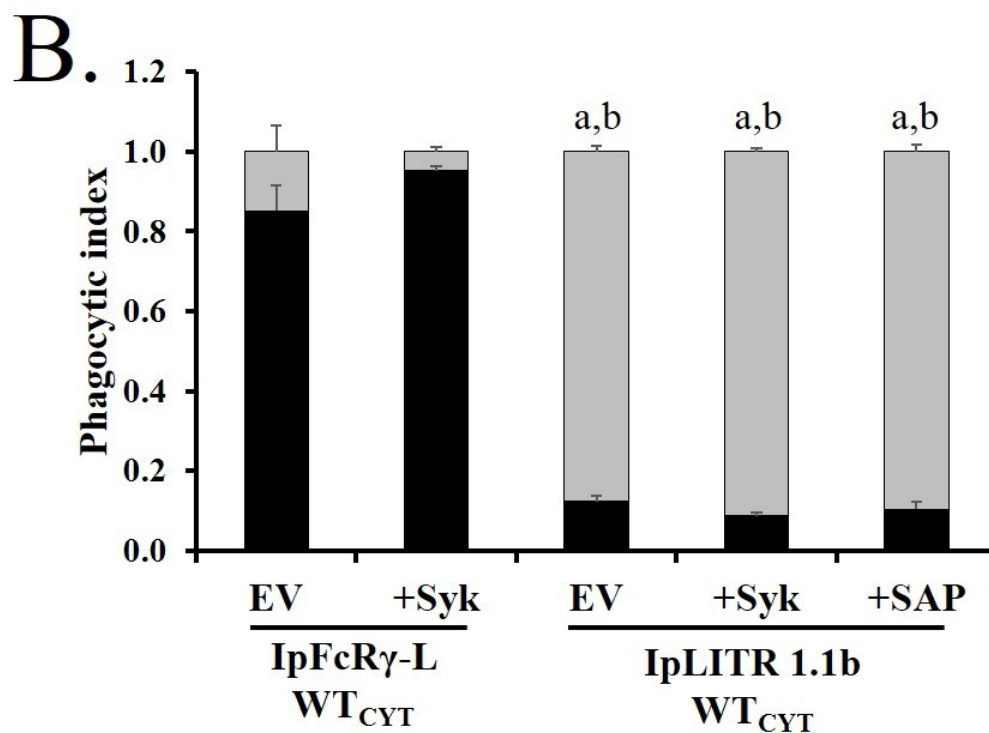
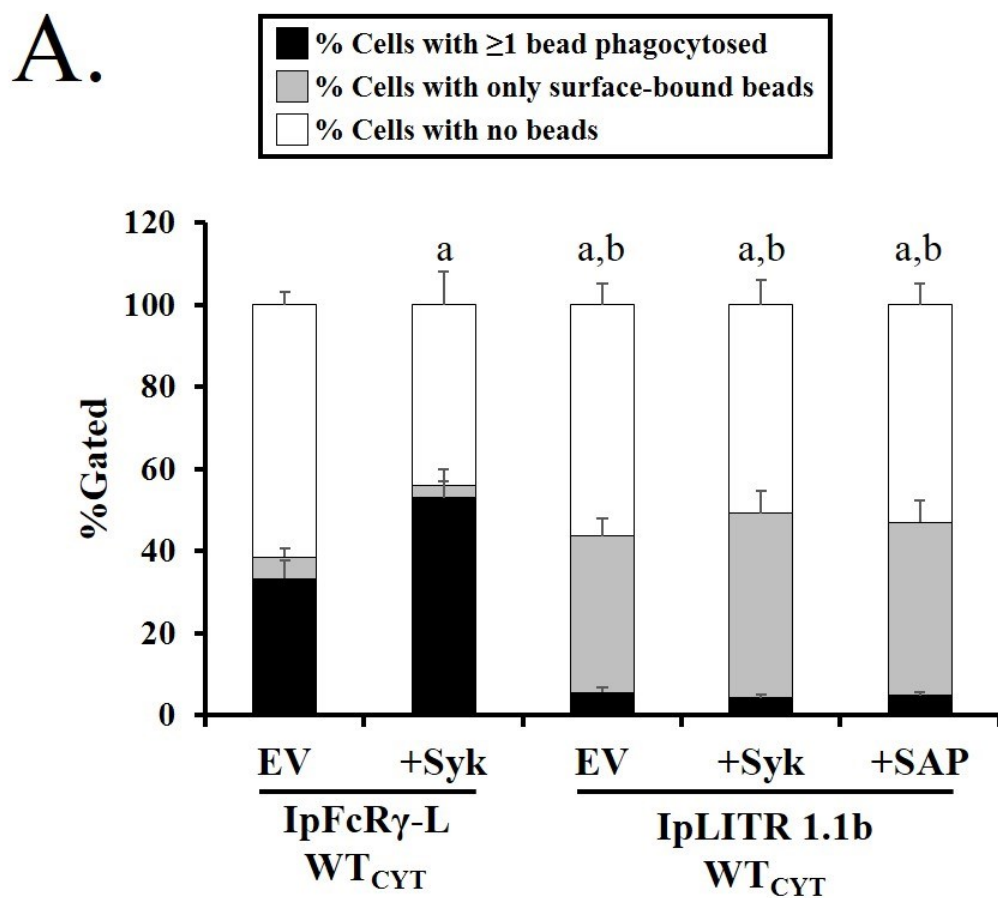


Figure 4.9. Co-expressing IpLITR 1.1b WT_{CYT} with a promiscuous Src kinase, vSrc, does not activate phagocytic signaling. AD293 cells stably expressing IpLITR 1.1b CYT constructs were transiently transfected with empty p3XFLAG-CMV14 (EV) or a FLAG-tagged vSrc kinase for 48 h. Mouse α HA antibody-coated green fluorescent (YG) 4.5 μ m beads were added to HA epitope-tagged stable IpLITR 1.1b CYT construct-expressing AD293 cells for 30 min at 37°C. Surface-bound YG beads were counter-stained with AlexaFluor647-conjugated rabbit α -mouse secondary antibody. Cells were harvested by trypsinization and fixed in 1% paraformaldehyde prior to data collection on the Image Stream^X MKII flow cytometer. Raw image files were subjected to component masking analysis by template-assisted batching using IDEAS v6.2 software as previously described (327). Each black bar represents the percentage of phagocytic cells (i.e. a cell with ≥ 1 bead fully internalized), grey bars represent the percentage of cells with only surface-bound beads (i.e. no beads internalized) and the white bars represent the percentage of cells with no associated beads (i.e. none bound or internalized). Results are representative of the mean \pm SEM of at least three independent experiments as (A) raw or (B) indexed data. Phagocytic index was calculated as: % phagocytic or surface-bound cells / % total bead-associated cells. Lower case ‘a’ and ‘b’ represent statistically significant differences ($p < 0.05$) compared to IpFcR γ -L WT_{CYT} +EV and +vSrc % phagocytic cells, respectively. (C) After 48 h transfection, a duplicate well from (A and B) was lysed and clarified by centrifugation before boiling in reducing buffer. Samples were separated by 10% SDS-PAGE gel electrophoresis and transferred to nitrocellulose for probing with an HRP-conjugated mouse α FLAG M2 mAb (top blot) or goat anti- β -actin pAb (bottom blot) to confirm successful transfection and expression of the promiscuous FLAG-tagged vSrc kinase and as a loading control, respectively. Blots shown are representative of 2 independent experiments.



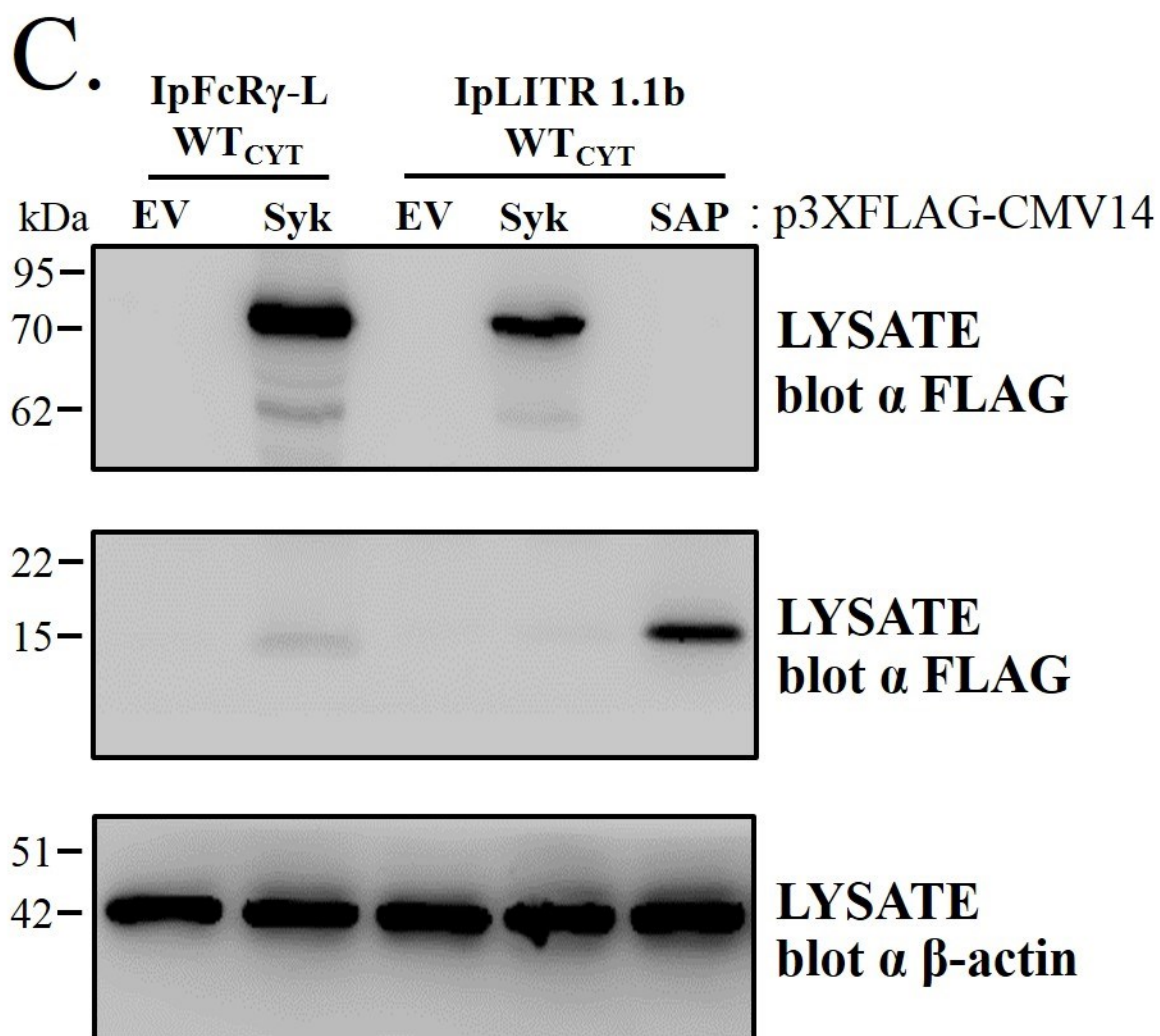


Figure 4.10. Over-expressing Syk or SAP in IpLITR 1.1b WT_{CYT}-expressing cells does not activate phagocytic signaling. AD293 cells stably expressing IpLITR 1.1b CYT constructs were transiently transfected with empty p3XFLAG-CMV14 (EV) or FLAG-tagged Syk or SAP for 48 h. Mouse α HA antibody-coated green fluorescent (YG) 4.5 μ m beads were added to HA epitope-tagged stable IpLITR 1.1b CYT construct-expressing AD293 cells for 30 min at 37°C. Surface-bound YG beads were counter-stained with AlexaFluor647-conjugated rabbit α -mouse secondary antibody. Cells were harvested by trypsinization and fixed in 1% paraformaldehyde prior to data collection on the Image Stream^X MKII flow cytometer. Raw image files were subjected to component masking analysis by template-assisted batching using IDEAS v6.2 software as previously described (327). Each black bar represents the percentage of phagocytic cells (i.e. a cell with ≥ 1 bead fully internalized), grey bars represent the percentage of cells with only surface-bound beads (i.e. no beads internalized) and the white bars represent the percentage of cells with no associated beads (i.e. none bound or internalized). Results are representative of the mean \pm SEM of at least 3 independent experiments as (A) raw or (B) indexed data. Phagocytic index was calculated as: % phagocytic or surface-bound cells / % total bead-associated cells. Lower case ‘a’ and ‘b’ represent statistically significant differences ($p < 0.05$) compared to IpFcR γ -L WT_{CYT} +EV and +vSrc % phagocytic cells, respectively. (C) After 48 h transfection, a duplicate well from (A)/(B) was lysed and clarified by centrifugation before boiling in reducing buffer. Samples were separated by 10% SDS-PAGE gel electrophoresis and transferred to nitrocellulose for probing with an HRP-conjugated mouse α FLAG M2 mAb (top two blots) and goat anti- β -actin pAb (bottom blot) to confirm transfection and expression of FLAG-tagged Syk or SAP and as a loading control, respectively. Blots shown are representative of 2 independent experiments.

FLAG-tagged SH2 domain-containing signaling molecule

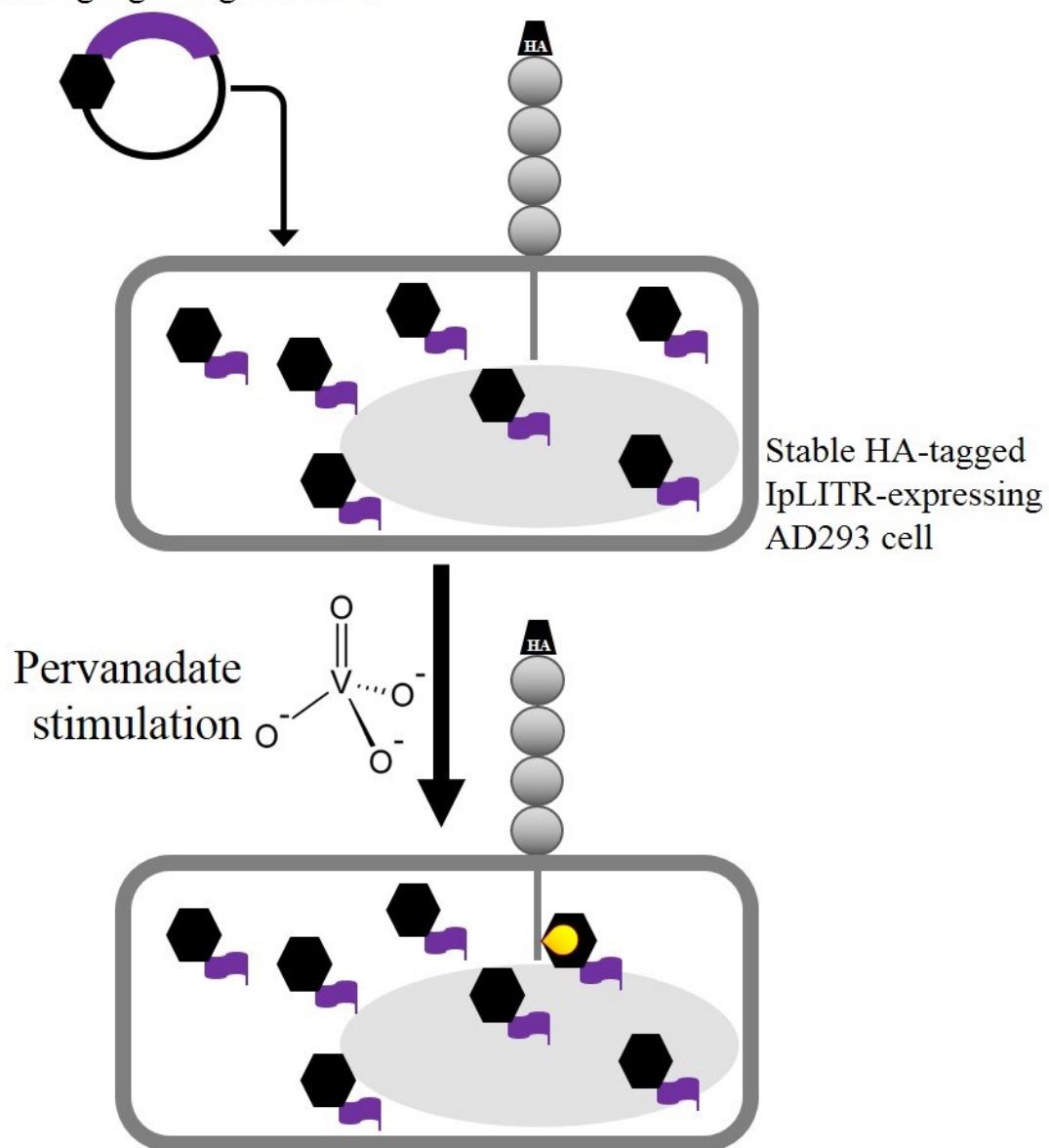
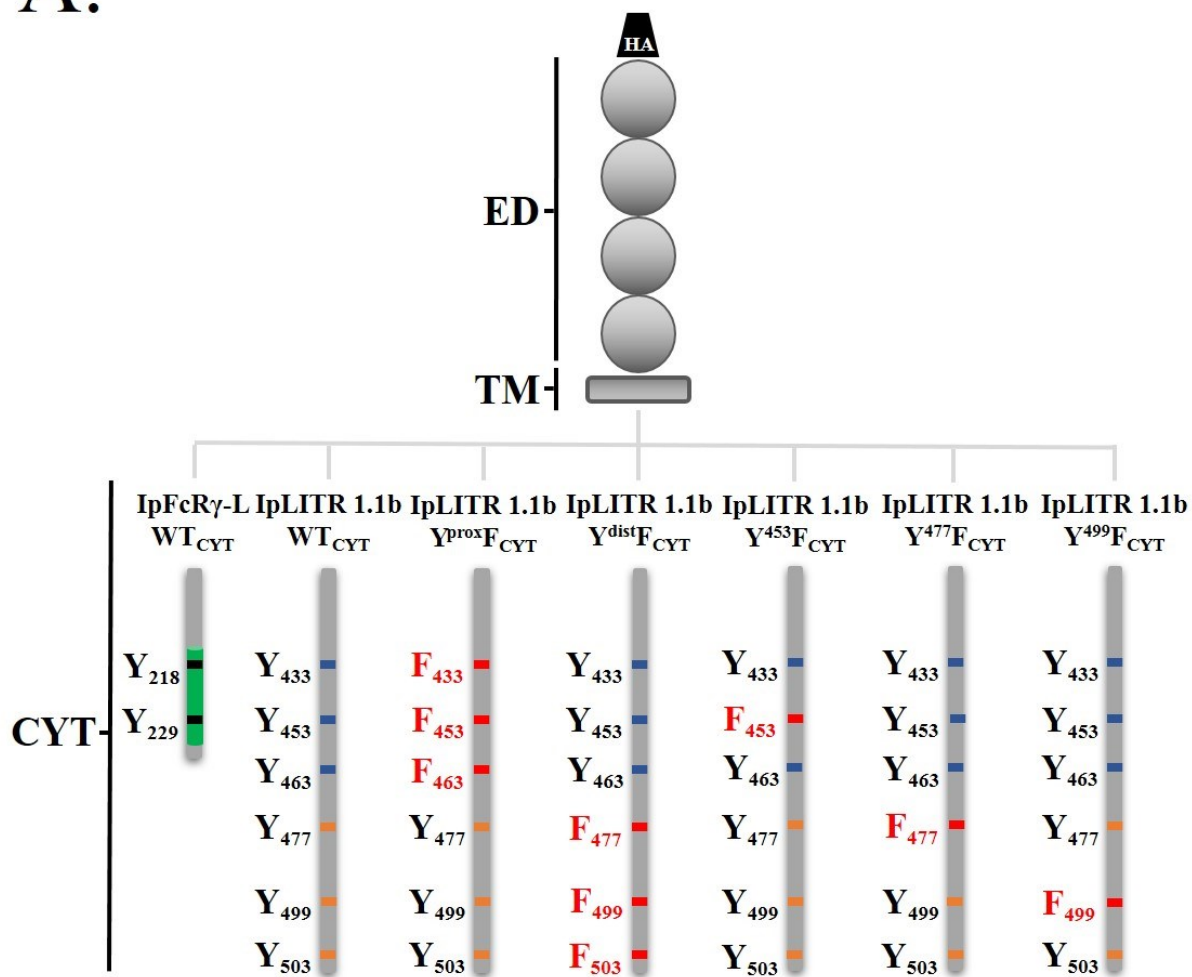


Figure 4.11. Schematic representation of pervanadate-mediated cellular activation and signaling molecule recruitment. p3XFLAG-CMV14-encoded signaling molecules were transiently transfected into stable IpLITR-expressing AD293 cells for 48 h prior to cellular activation with pervanadate at 37°C for 10 min. Cells were harvested immediately after activation and centrifuged at 4°C for 2 min at 500xg. Pellets were re-suspended in 1% triton-X TBS lysis buffer and incubated on ice for 30 min. After high-speed centrifugation, clarified lysates were diluted to 1 mL and combined with washed mouse α HA antibody-coated magnetic sepharose beads prior to an overnight 4°C incubation on a rotating mixer. Beads were washed 3x with lysis buffer and eluted in reducing buffer by boiling. Samples were separated by electrophoresis on 11% SDS-PAGE gels and transferred to nitrocellulose membranes for Western blotting.

A.



B.

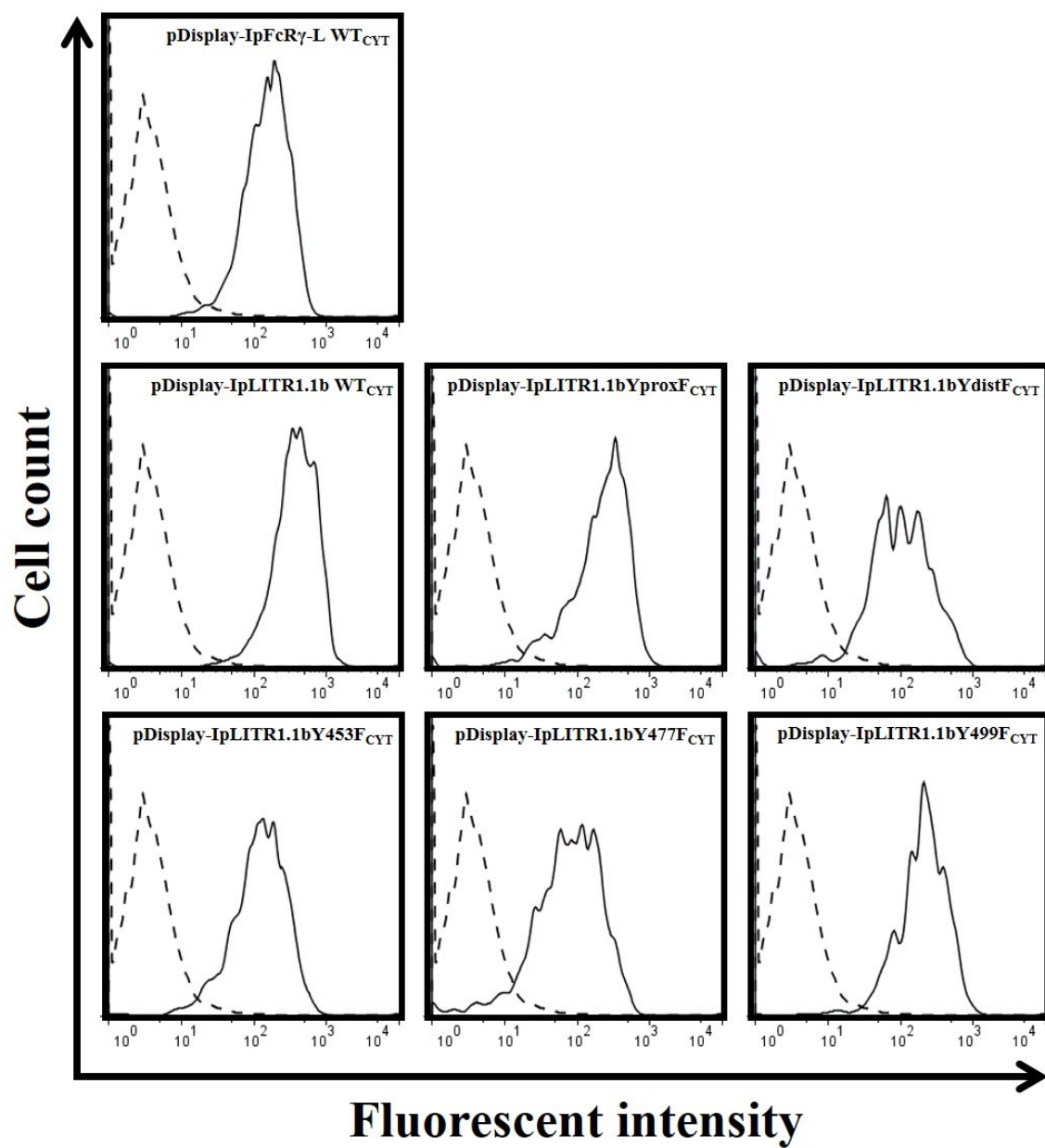
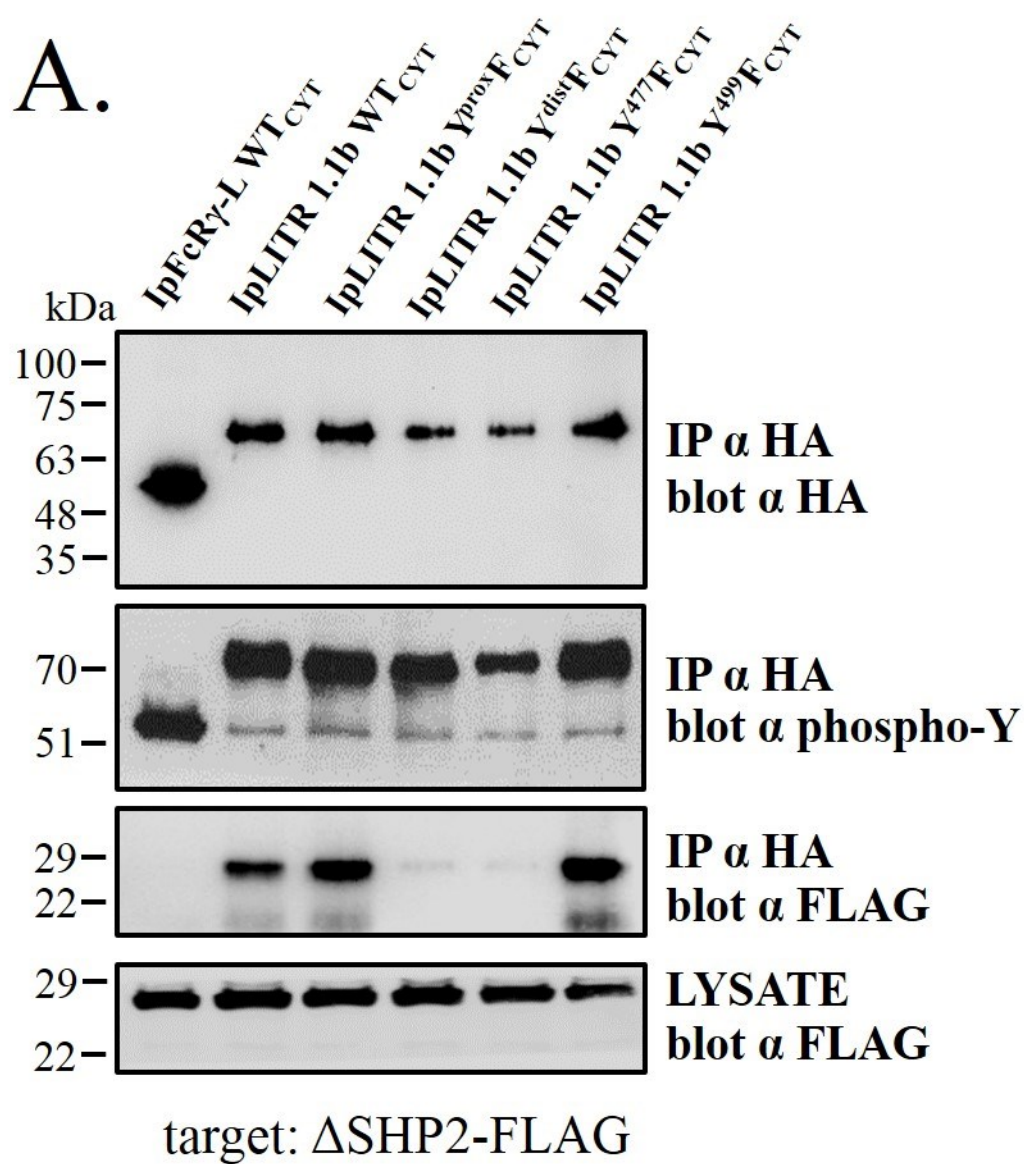
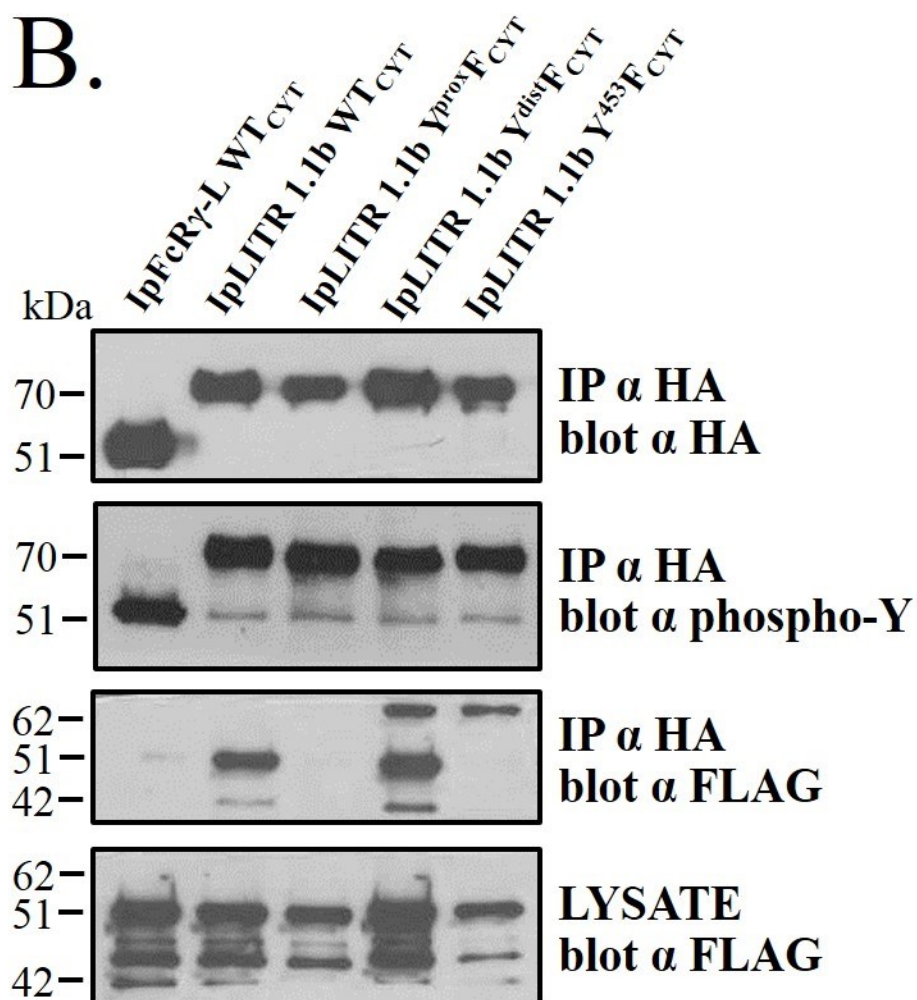


Figure 4.12. Generation and stable expression of N-terminal HA epitope-tagged IpLITR 1.1b CYT YF mutant constructs in AD293 cells for co-immunoprecipitation assays.

(A) Schematic representations of the seven IpLITR 1.1b CYT constructs tested. To characterize motif-specific signaling molecule recruitment potential, five IpLITR 1.1b YF mutant receptor constructs were generated by site-directed mutagenesis. Two constructs contain proximal and distal CYT segment-specific mutations: IpLITR 1.1b Y^{prox}F (i.e. Y^{433,453,463}F) and IpLITR 1.1b Y^{dist}F (i.e. Y^{477,499,503}F). Three constructs contain motif-specific mutations: IpLITR 1.1b Y⁴⁵³F (previously reported to recruit Csk; Montgomery et al., 2012), IpLITR 1.1b Y⁴⁷⁷F and IpLITR 1.1b Y⁴⁹⁹F (both of which are implicated in SHP2 recruitment previously; Montgomery et al., 2012). Wild-type constructs containing the CYT regions of IpFcR γ -L and IpLITR 1.1b were also tested. Locations of the tyrosine residues within each CYT region are indicated by the corresponding tyrosine positions within the native protein sequences of the wild-type molecules, as previously published (5, 6). (B) Parental AD293 cells were transfected with pDisplay-encoded IpLITR 1.1b CYT constructs and incubated at 37°C for 48 h, at which point cells were cultured in selective media containing G418 antibiotic for two weeks and cloned by serial dilution into 96-well plates. Confluent wells containing an individual clone were transferred to a 24-well plate, grown to confluence and stained for cell surface IpLITR expression with the α HA mAb HA.C5 (solid line) or a mouse IgG3 isotype control antibody (dotted line), followed by PE-conjugated goat α -mouse IgG pAb counter-staining. After 5-10 passages, stable IpLITR 1.1b CYT construct expression levels were confirmed by flow cytometry. Representative stains for each cell line are shown.



B.



target: Csk-FLAG

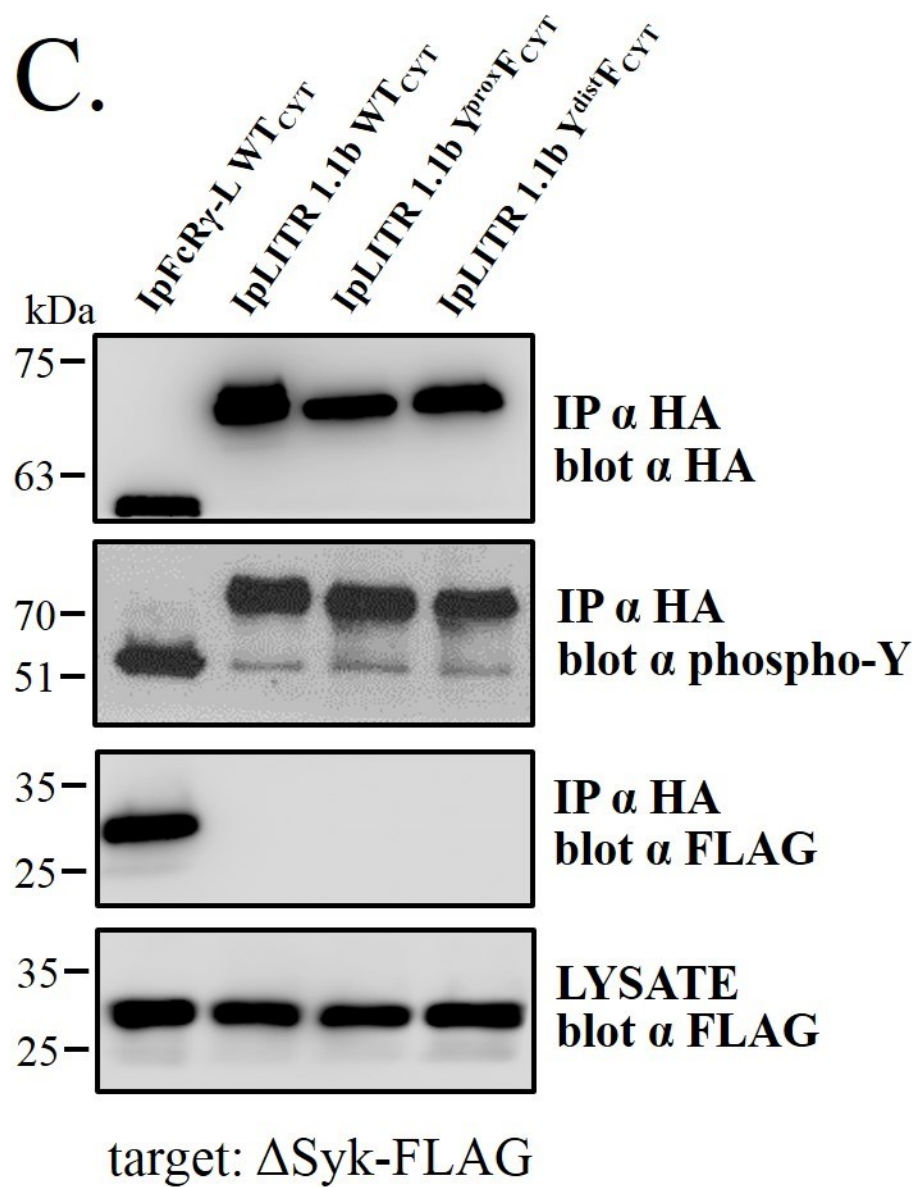


Figure 4.13. Wild-type IpLITR 1.1b recruits the inhibitory signaling molecules Csk and SHP2 to the proximal CYT segment Y⁴⁵³ and distal CYT segment ITIM Y⁴⁷⁷, respectively. Stable IpLITR-expressing cells were transiently transfected with FLAG-tagged signaling molecules for 48 h. Cells were then stimulated with pervanadate, lysed and receptors were immunoprecipitated with α HA antibody-coated magnetic beads. After elution in reducing buffer by boiling, samples were separated on 11% SDS-PAGE gels, transferred to nitrocellulose membranes and probed with HRP-conjugated mouse α HA, α -phosphotyrosine (phospho-Y) PY20 or HRP-conjugated α FLAG M2 mAbs. The top blot in each panel is a control blot to confirm that IpLITRs precipitated. The upper middle blot in each panel is a control to show receptor phosphorylation. The lower middle blot in each panel shows a co-immunoprecipitating target FLAG-tagged signaling molecule. The bottom blot in each panel is a whole cell lysate control blot to confirm FLAG-tagged signaling molecule expression prior to co-immunoprecipitation. The target signaling molecules are (A) SHP2, (B) Csk and (C) Syk. Lanes are labeled with the IpLITR construct tested. Blots are representative of 3 independent experiments.

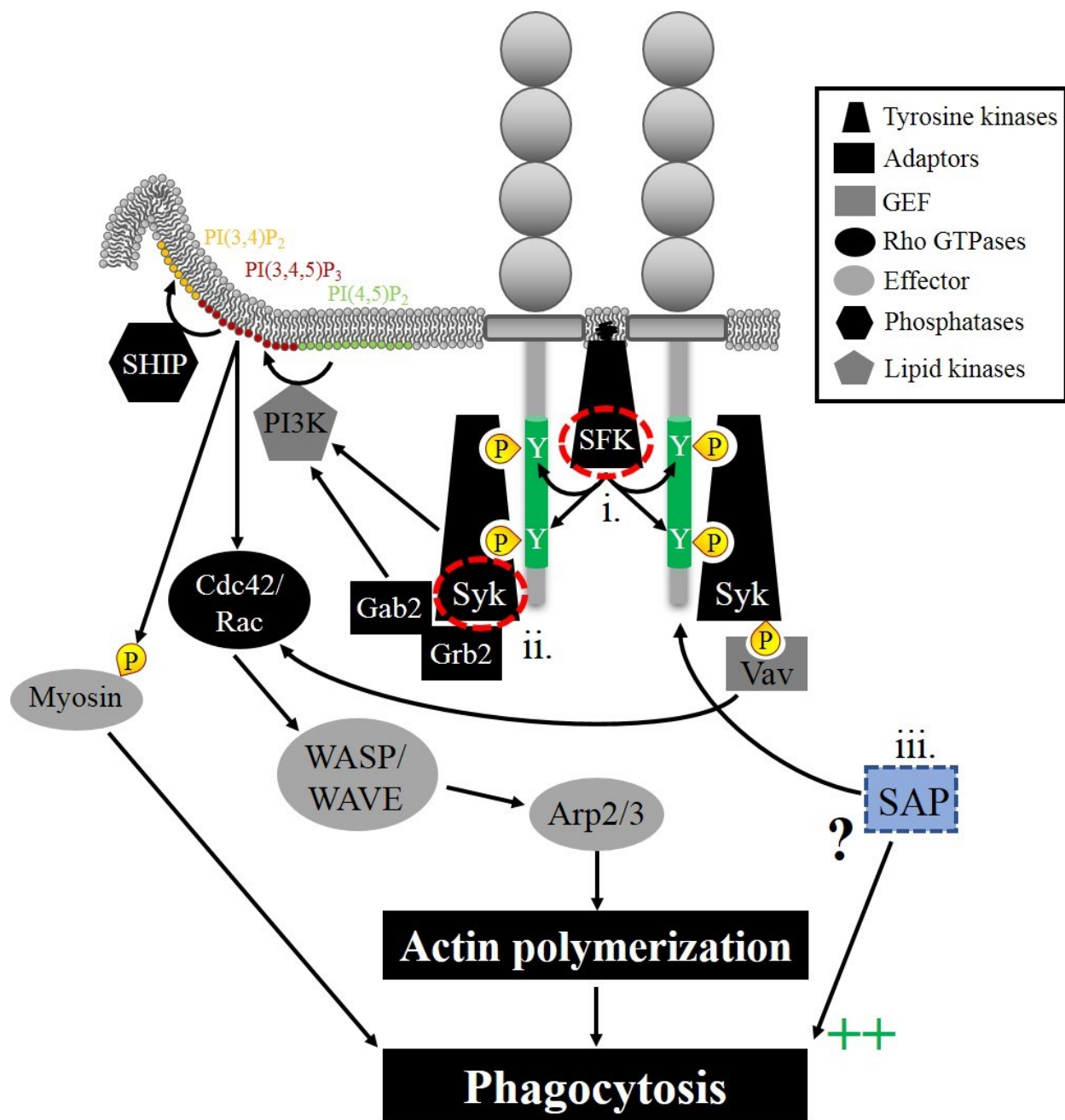


Figure 4.14. Schematic representation of the ITAM-dependent phagocytic signaling networks of IpFcR γ -L WT_{CYT}, highlighting hypothetical sites for molecular alteration of signaling. Upon receptor clustering by an extracellular target/ligand, CYT region tyrosine-based motifs (i.e. ITAMs; drawn here as green CYTs) are phosphorylated by membrane-associated Src family kinases (SFKs) leading to the recruitment of spleen tyrosine kinase (Syk). Syk acts as a hub for the recruitment/activation of several downstream molecules, including adaptor molecules (e.g. Grb2 and Gab2), lipid kinases (e.g. phosphoinositide 3-kinase (PI3K)), guanine nucleotide exchange factors (e.g. Vav), small GTPases (e.g. cdc42 and Rac) and ultimately, the actin nucleation machinery (e.g. WAVE and Arp2/3) which results in target engulfment. Sites of molecular alterations tested to enhance/activate phagocytic signaling are: (i) enhanced receptor CYT phosphorylation by an SFK, (ii) over-expression of key signaling intermediates (e.g. Syk) or (iii) the supplementation of a non-endogenously AD293-expressed signaling molecule, SAP.

CHAPTER V

**DEVELOPING NOVEL IMAGING FLOW CYTOMETRY-BASED
PHAGOCYTOSIS ASSAYS TO CHARACTERIZE I_pLITR 1.1b
WT_{CYT}-MEDIATED CROSS-TALK INHIBITION OF ITAM-DRIVEN
PHAGOCYTTIC SIGNALING**

Parts of this chapter are published:

Zwozdesky et al., 2019. An imaging flow cytometry protocol for studying immunoregulatory receptor-mediated regulation of phagocytosis. *Methods in Molecular Biology*, accepted.

5.1 INTRODUCTION

Innate immune cellular responses like phagocytosis and cellular cytotoxicity are controlled by the integration of signals from cell surface-expressed immunoregulatory receptors. Signal transduction involves sensing extracellular stimuli/ligands which cross-links transmembrane receptors to form signaling complexes or signalosomes that transmit intracellular signals. Importantly, the formation of signalosomes results from the clustering, or oligomerization, of receptors at the site of receptor-ligand interaction. Oligomerization is, therefore, a key early signal transduction event that brings receptors into close proximity, allowing them to modulate or cross-talk with one another and set the context for downstream stimulatory or inhibitory outcomes (155, 358–361).

Several innate immune receptors are known to oligomerize (e.g. TLRs, KIRs, FcγRs; 322–324) which directly impacts the formation of stable signalosomes (i.e. a sustained signaling complex which typically leads to the stimulation of downstream responses) or dissociates signalosomes (i.e. inhibits downstream responses). For example, multiple related inhibitory KIR-types are known to bind MHC class I molecules on target cells (365) and co-cluster with stimulatory receptors within forming signalosomes (366). As a result, NK cell-mediated cytotoxicity is attenuated because stimulatory signals are counter-acted by inhibitory KIR2DL3

signaling (125). In the context of phagocytosis, oligomerization is critical for organizing phagocytic synapse formation. A phagocytic synapse contains receptor-target complexes as well as additional co-receptors. Co-receptors may facilitate synapse formation in several ways. These include segregating the forming synapse away from membrane-bound inhibitory phosphatases (294, 367, 368), securing captured targets (329, 369–371) and activating signals for internalization (153, 158, 372, 373). However, co-receptors may also attenuate signaling. For example, SIRP α and Fc γ RIIB are known to down-regulate phagocytic signaling through ITAM-containing Fc γ Rs. Engaging CD47 with SIRP α on phagocytes results in ITIM phosphorylation and inhibition of Fc γ R-mediated phagocytosis (374, 375). Similarly, phosphorylated Fc γ RIIB ITIMs inhibit Fc γ R-mediated phagocytosis via CYT-mediated mechanisms (376–378). In this scenario, the binding of common ligands (i.e. IgG antibodies) by Fc γ Rs leads to co-cross-linking-induced cross-talk inhibition of phagocytic signals. Altogether, these Fc γ R studies highlight how oligomerization induced by co-cross-linking allows receptors to regulate phagocytic signaling. While well-studied in mammals, the cross-talk regulation of phagocytosis in earlier vertebrate models like fish has not been investigated.

Various channel catfish immune cell-types co-express stimulatory and inhibitory IpLITR-types (2). All known IpLITR-types contain both D1 and D2 extracellular domains which contain a putative MHC class I binding site (94). This suggests that IpLITRs may bind common ligands. Furthermore, these receptors are known to control several innate immune cell responses, including phagocytosis (5, 7), and IpLITR-types are known to oligomerize (3). Altogether, these observations strongly support the hypothesis that receptor cross-talk may play a role during IpLITR-mediated control of cellular responses.

In the previous chapter, I demonstrated that the ITAM-containing IpFcR γ -L WT_{CYT} receptor stimulates phagocytosis of antibody-coated bead targets in AD293 cells. In contrast, the ITIM-containing IpLITR 1.1b WT_{CYT} was not phagocytic. However, physiological recruitment data showed that the phosphorylated membrane distal CYT ITIM Y⁴⁷⁷ binds SHP2. In addition, the phosphorylated membrane proximal CYT Y⁴⁵³ binds the inhibitory kinase Csk. This biochemical data strongly supports a prediction that IpLITR 1.1b WT_{CYT} may transmit motif-specific inhibitory signals as previously observed in our NK cell studies (6). Combining these observations with previous reports of ITIM-dependent cross-talk inhibition of Fc γ R-mediated phagocytosis, the main research question addressed in this chapter is: Are IpLITRs capable of mediating CYT-dependent cross-talk regulation of phagocytosis (outlined in Figure 5.1)?

In this chapter, I use three transfection strategies and adapt the phagocytosis assay from chapter IV to examine IpLITR CYT-mediated cross-talk regulation of phagocytosis of light yellow (LY) bead targets. The first two transfection strategies involve co-transfecting HA epitope-tagged IpLITRs into parental AD293 cells. To control co-expression, I generated eGFP-tagged IpLITR 1.1b WT_{CYT} constructs that were transfected into stable IpFcR γ -L WT_{CYT}-expressing AD293 cells. This allowed me to separate eGFP negative (i.e. IpFcR γ -L WT_{CYT} only expressing) and eGFP positive (e.g. IpLITR 1.1b WT_{CYT}-eGFP and IpFcR γ -L WT_{CYT} co-expressing) cell populations during data analysis. Since previous studies demonstrated that the ITIM-dependent recruitment of phosphatases (e.g. SHPs) effectively inhibits ITAM-driven phagocytosis and IpLITR 1.1b WT_{CYT} recruits SHP2 to the distal CYT segment (188), I predict that IpLITR 1.1b WT_{CYT} will demonstrate CYT-dependent cross-talk inhibition of ITAM-driven IpFcR γ -L WT_{CYT} phagocytosis. In establishing a novel imaging flow cytometry-based

phagocytosis assay, I specifically assess IpLITR 1.1b WT_{CYT}-mediated cross-talk inhibition of phagocytosis and establish a system to study the underlying molecular cross-talk mechanism.

My results show that co-transfecting a phagocytic ITAM-containing IpLITR construct with an ITIM-containing IpLITR construct into parental AD293 cells appears to attenuate phagocytic signaling upon engaging YG bead targets. Similar results are observed when the phagocytic IpLITR construct is co-transfected with an eGFP-tagged ITIM-containing IpLITR construct. Furthermore, observations using YF mutant constructs indicate that the membrane proximal and distal CYT segments of this ITIM-containing IpLITR-type may not be equally effective at inhibiting phagocytosis. Finally, transiently transfecting an eGFP-tagged ITIM-containing IpLITR construct into stable phagocytic ITAM-containing IpLITR construct-expressing cells allows for better control of IpLITR construct co-expression to optimize quantification of CYT motif-dependent cross-talk inhibition of phagocytosis. Altogether, these data demonstrate the cross-talk signaling potential of IpLITR-types during the regulation of innate immune cell responses.

5.2 RESULTS

5.2.1 IpLITR 1.1b WT_{CYT} mediates cross-talk inhibition of IpFcR γ -L WT_{CYT}-driven phagocytosis in transiently co-transfected AD293 cells

To assess potential IpLITR 1.1b WT_{CYT}-mediated cross-talk regulation of phagocytosis, I co-transfected IpLITR 1.1b WT_{CYT} and IpFcR γ -L WT_{CYT} into parental AD293 cells (schematically outlined in Figure 5.2). At 48 h post-transfection, cells were tested in a flow cytometry-based phagocytosis assay using YG beads. For data analysis, cells were gated as three major functional phenotypes: phagocytic cells (i.e. cells that fully internalized at least 1 bead),

non-phagocytic cells (i.e. cells that associated with, but did not fully internalize any beads), and cells that did not associate with any beads.

When IpFcR γ -L WT_{CYT} was co-transfected with IpLITR 1.1b WT_{CYT}, 56.2% of cells associated with at least one bead with 19.9% and 36.3% displaying phagocytic and non-phagocytic (e.g. surface bound) phenotypes, respectively (Figure 5.3A). Mock transfected cells were transfected with the IpFcR γ -L WT_{CYT} construct only and an equivalent volume of TurboFECT® transfection reagent instead of a second construct. These cells showed a 44.8% bead association with 38.7% phagocytic and 6.1% surface-bound cells. The second control group involved co-transfecting parental cells with a second construct that was not predicted to down-regulate phagocytic signaling but contained an equivalent amount of total plasmid. As shown in Figure 5.3A, 54.4% of double IpFcR γ -L WT_{CYT} co-transfected cells associated with at least one bead with 38.8% and 15.6% displaying phagocytic and surface-bound phenotypes, respectively. Since cell-bead association is required to initiate phagocytic signaling, data was normalized to help visualize inter-group differences of bead-associated cells only. To normalize the phagocytic vs. non-phagocytic (i.e. surface-bound) phenotype data, the bead-associated cell population data was indexed by dividing % phagocytic or non-phagocytic cells by % bead associated cells. As shown in Figure 5.3B, IpFcR γ -L WT_{CYT} + IpLITR 1.1b WT_{CYT} co-transfected cells display a significant reduction in phagocytosis at 38.3% compared to 86.2% and 72.7% for each control group. For all groups, the transfection efficiency (determined by % bead association) was between 40-60%, however, controlling for IpLITR co-expressing cells and single IpLITR-expressing cells during analysis was not possible using this transfection approach. Altogether, these observations indicate that cross-talk is observed between IpLITR 1.1b WT_{CYT} and IpFcR γ -L WT_{CYT}.

5.2.2 eGFP-tagged IpLITR 1.1b WT_{CYT} (IpLITR 1.1b WT_{CYT}-eGFP) mediates inhibition of IpFcR γ -L WT_{CYT}-driven phagocytosis through its proximal and distal CYT segment motifs

To separate IpLITR co-expressing cells from single IpLITR-expressing cells during analysis of phagocytosis data, I assessed the inhibitory function of IpLITR 1.1b WT_{CYT} after adding an eGFP tag to its C-terminus (see Figure 5.4 schematic) and by using the same co-transfection strategy as described in the previous section. Tagging with eGFP allowed me to separate green fluorescent (i.e. eGFP positive) and non-fluorescent (i.e. eGFP negative) cells during data analysis but required the use of light yellow fluorescent beads instead of YG beads (327). In addition, I included two important controls: (1) eGFP only, to ensure the tag was not interfering with ITAM-driven phagocytic signaling, and (2) an IpLITR 1.1b mutant CYT construct (called IpLITR 1.1b MUT_{CYT}), where all six CYT tyrosines are mutated to phenylalanines. This construct is a control for tyrosine-based inhibitory signaling. Furthermore, I tested two IpLITR 1.1b CYT segment mutants: IpLITR 1.1b Y^{prox}_{CYT} and IpLITR 1.1b Y^{dist}_{CYT} in which the first three (i.e. proximal Y⁴³³, Y⁴⁵³ and Y⁴⁶³) and last three (i.e. distal Y⁴⁷⁷, Y⁴⁹⁹ and Y⁵⁰³) CYT motifs are converted to phenylalanine, respectively (see Figure 4.12 schematic).

When the eGFP positive cell populations were examined, they displayed bead associations between 37-74% (Figure 5.5A). When co-transfected with IpLITR 1.1b WT_{CYT}-eGFP, 63.1% of cells associated with at least one bead with 7.8% and 55.3% displaying a phagocytic and surface-bound phenotype, respectively. Negative control cells co-transfected with eGFP and IpLITR 1.1b MUT_{CYT}-eGFP showed 37.3% and 66.5% associations, respectively. While 33.4% and 3.9% were phagocytic and surface-bound for eGFP, 25.7% and

40.8% were phagocytic and surface-bound for IpLITR 1.1b MUT_{CYT}-eGFP, respectively (Figure 5.5A). IpLITR 1.1b Y^{prox}F_{CYT}-eGFP showed 73.8% association with 10.7% phagocytic cells and 63.1% surface-bound cells. IpLITR 1.1b Y^{dist}F_{CYT}-eGFP showed 64.4% association with 17.6% of cells phagocytic and 46.8% of cells surface-bound. When indexed, IpLITR 1.1b WT_{CYT}-eGFP co-transfected cells show 12.4% phagocytic phenotype, compared to 88.7% and 41.2% for eGFP and IpLITR 1.1b MUT_{CYT}-eGFP co-transfectants, respectively (Figure 5.5B). For segment mutants, IpLITR 1.1b Y^{prox}F_{CYT}-eGFP showed 15.1% phagocytic phenotype while IpLITR 1.1b Y^{dist}F_{CYT}-eGFP showed 28.6% phagocytic phenotype (Figure 5.5B).

As shown in Figure 5.5C, eGFP negative cell populations show bead associations between 16-24%. When co-transfected with IpLITR 1.1b WT_{CYT}-eGFP, 24.0% of cells associated with at least one bead with 12.0% and 12.0% displaying phagocytic and surface-bound phenotypes, respectively. For comparison, the first negative control eGFP co-transfected cells showed 17.1% of cells associated with at least one bead with 15.0% and 2.1% displaying phagocytic and surface-bound phenotypes, respectively. An additional control for inhibition was cells co-transfected with IpLITR 1.1b MUT_{CYT}-eGFP. These cells showed 20.9% association with 13.8% and 7.1% displaying a phagocytic and surface-bound phenotype, respectively. Finally, the two segment-specific mutants IpLITR 1.1b Y^{prox}F_{CYT}-eGFP and IpLITR 1.1b Y^{dist}F_{CYT}-eGFP displayed associations of 16.7% and 18.6%, respectively. While IpLITR 1.1b Y^{prox}F_{CYT}-eGFP co-transfectants displayed 3.9% phagocytic and 12.8% surface-bound phenotypes, IpLITR 1.1b Y^{dist}F_{CYT}-eGFP cells displayed 10.7% phagocytic and 7.9% surface-bound phenotypes (Figure 5.5C). To simplify visualization of the phagocytic vs. surface-bound phenotypes, the bead-associated cell population data was indexed by normalizing % phagocytic or surface-bound cells to % bead associated cells (Figure 5.5D). IpLITR 1.1b WT_{CYT}-eGFP co-

transfected cells show 42.6% phagocytic phenotype, compared to 78.1% and 55.4% for eGFP and IpLITR 1.1b MUT_{CYT}-eGFP co-transfectants, respectively. For segment mutants, IpLITR 1.1b Y^{prox}_{F_{CYT}}-eGFP showed 21.9% phagocytic phenotype while IpLITR 1.1b Y^{dist}_{F_{CYT}}-eGFP showed 49.3% phagocytic phenotype (Figure 5.5D).

In summary, these data clearly demonstrate that eGFP-tagged IpLITR 1.1b WT_{CYT} construct expression defines a selectable cell population during analysis and that these constructs mediate cross-talk signaling events. In addition, while each segment of IpLITR 1.1b WT_{CYT} appears to inhibit phagocytosis, the degree of inhibition is not equivalent. However, eGFP negative cell populations showed low bead association % and reductions in phagocytosis which were not expected since these cells only express IpFcR γ -L WT_{CYT} and should be phagocytic. To ensure eGFP negative cells expressed IpFcR γ -L WT_{CYT}, I tested whether eGFP-tagged constructs could be transfected into stable IpFcR γ -L WT_{CYT}-expressing cells.

5.2.3 eGFP-tagged IpLITR 1.1b WT_{CYT} (IpLITR 1.1b WT_{CYT}-eGFP) mediates CYT motif-dependent cross-talk inhibition of ITAM-driven phagocytosis in IpFcR γ -L-expressing AD293 stable cells

The random expression profile (i.e. some cells express one plasmid while others express both or neither) that results from co-transfecting plasmid-encoded receptors is exemplified by the eGFP negative cell population data from the previous section. Specifically, low bead association percentages and the apparent inhibition of phagocytosis in all groups but eGFP, indicate that IpFcR γ -L WT_{CYT} was not expressed by more than approximately 25% of cells. To better control receptor expression in eGFP negative and positive cell populations, eGFP-tagged IpLITR 1.1b CYT constructs were transiently transfected into stable IpFcR γ -L WT_{CYT}-expressing AD293 cells (outlined in Figure 5.6). Theoretically, this strategy controls for receptor expression since

all cells stably express IpFcR γ -L WT_{CYT} and co-expressing cells gain green fluorescence (i.e. eGFP-tagged IpLITR 1.1b CYT construct expression).

All eGFP negative cells express only IpFcR γ -L WT_{CYT} (i.e. no inhibition of phagocytosis is expected) while eGFP positive cells co-express both IpFcR γ -L WT_{CYT} and an eGFP-tagged IpLITR 1.1b CYT constructs (gating strategy outlined in Figure 5.7A). Examples of the eGFP negative and positive cellular phenotypes and the corresponding fluorescent images captured by the Image Stream^X flow cytometer are presented in Figure 5.7B.

In eGFP positive, IpFcR γ -L WT_{CYT} and IpLITR 1.1b CYT-eGFP construct co-expressing cells, the bead association ranges between 62-71% (Figure 5.8A). When co-expressing IpLITR 1.1b WT_{CYT}-eGFP, 62.5% of cells associated with at least one bead with 14.4% and 48.1% displaying a phagocytic and surface-bound phenotype, respectively. Negative control cells co-expressing eGFP and IpLITR 1.1b MUT_{CYT}-eGFP showed 68.4% and 71.0% bead associations, respectively. Within these two groups, 64.3% and 4.1% were phagocytic and surface-bound for eGFP, while 49.6% and 21.4% were phagocytic and surface-bound for IpLITR 1.1b MUT_{CYT}-eGFP, respectively (Figure 5.8A). Upon indexing the data, IpLITR 1.1b WT_{CYT}-eGFP co-expressing cells show 23.9% phagocytic phenotype, compared to 94.2% and 72.3% for eGFP and IpLITR 1.1b MUT_{CYT}-eGFP groups, respectively (Figure 5.8B).

The IpFcR γ -L WT_{CYT} only-expressing cell populations (i.e. eGFP negative) show a range of bead associations between 56-61%. Approximately 60% of IpLITR 1.1b WT_{CYT}-eGFP transfected cells associated with at least one bead with 51.6% and 8.4% displaying phagocytic and surface-bound phenotypes, respectively (Figure 5.8C). In comparison, eGFP transfected cells showed 60.2% of cells associated with at least one bead with 56.8% and 3.4% displaying phagocytic and surface-bound phenotypes, respectively. IpLITR 1.1b MUT_{CYT}-eGFP transfected

cells showed 56.4% association with 50.7% and 5.7% displaying a phagocytic and surface-bound phenotype, respectively. To simplify visualization of the phagocytic vs. surface-bound phenotypes, the bead-associated cell population data was indexed by normalizing % phagocytic or surface-bound cells to % bead associated cells (Figure 5.8D). IpLITR 1.1b WT_{CYT}-eGFP transfected cells show 85.6% phagocytic phenotype, compared to 94.5% and 89.2% for eGFP and IpLITR 1.1b MUT_{CYT}-eGFP transfectants, respectively (Figure 5.8D).

Overall, these data clearly demonstrate that while all IpFcR γ -L WT_{CYT} only- (i.e. eGFP negative) and IpFcR γ -L WT_{CYT} cells co-expressing eGFP or IpLITR 1.1b MUT_{CYT}-eGFP are phagocytic, IpFcR γ -L WT_{CYT} and IpLITR 1.1b WT_{CYT}-eGFP co-expressing cells are non-phagocytic.

5.2.4 Effect of receptor expression levels on eGFP-tagged IpLITR 1.1b WT_{CYT} (IpLITR 1.1b WT_{CYT}-eGFP)-mediated cross-talk inhibition of IpFcR γ -L WT_{CYT}-driven phagocytosis

Using stable IpFcR γ -L WT_{CYT}-expressing cells that transiently co-express eGFP-tagged IpLITR 1.1b CYT constructs is an effective system for measuring IpLITR-mediated cross-talk regulation of phagocytosis. However, receptor expression level directly impacts signaling dynamics in part, by increasing cell avidity for a target at higher compared to lower expression levels (379–384). Since eGFP fluorescence is directly proportional to eGFP-tagged receptor expression level (385–387), my gating strategy offers an additional level of control for optimizing this system. Specifically, eGFP positive cell populations were separated into low, middle and high eGFP-gated populations before performing phenotypic analysis (outlined in Figure 5.9). Importantly, this allows for the analysis of cross-talk in cells where inhibitory receptor expression level optimally inhibits phagocytic signaling.

Figure 5.10 shows the same data that was presented in Figure 5.8 under the label ‘avg’ (i.e. the average eGFP fluorescence for all cells) in addition to the gated data for low (lo), middle (mid) and high (hi)-level eGFP-expressing cell populations. In general, eGFP only co-expressing cells demonstrate similar phagocytic phenotypes with 64.3%, 64.6%, 63.3% and 64.3% phagocytic cells for average, low, middle and high-level fluorescent cells, respectively (Figure 5.10A). For both IpLITR 1.1b WT_{CYT}-eGFP and IpLITR 1.1b MUT_{CYT}-eGFP co-expressing cells, the % phagocytic cells show an eGFP fluorescence-dependent response as increasing fluorescence correlates with decreasing % phagocytic phenotype. Specifically, 14.4% and 49.6% of cells are phagocytic for IpLITR 1.1b WT_{CYT}-eGFP and IpLITR 1.1b MUT_{CYT}-eGFP at average fluorescence, respectively. However, as fluorescence increases from low to high, IpLITR 1.1b WT_{CYT}-eGFP cells display 19.4%, 10.7% and 9.4% phagocytic phenotype. In comparison, IpLITR 1.1b MUT_{CYT}-eGFP cells display 58.7%, 52.0% and 34.4% phagocytic phenotype as fluorescence increases from low to high (Figure 5.10A). Indexed data shows 94.2%, 94.3%, 92.4% and 94.0% phagocytic cells for average-, low-, middle- and high-level eGFP-expressing cells, respectively. IpLITR 1.1b WT_{CYT}-eGFP expressing cells display 23.9% phagocytic cells at average-level eGFP while 31.2%, 17.6% and 15.2% are phagocytic as fluorescence increases. For IpLITR 1.1b MUT_{CYT}-eGFP expressing cells, 72.3% are phagocytic at average-level eGFP while 82.6%, 73.1% and 47.2% are phagocytic as fluorescence increases.

The optimal eGFP expression level corresponds with the greatest difference between IpLITR 1.1b WT_{CYT}-eGFP and IpLITR 1.1b MUT_{CYT}-eGFP % phagocytic cells. The difference in % phagocytic cells at average-, low-, middle- and high-level eGFP expression for raw data is 35.2%, 39.3%, 41.3% and 25.0%, respectively (Figure 5.10A). The difference in % phagocytic cells at average-, low-, middle- and high-level eGFP expression for indexed data is 48.5%,

51.4%, 55.6% and 32.0%, respectively (Figure 5.10B). Altogether, this data indicates that mid-level eGFP expression is optimal for measuring cross-talk in this system.

5.3 DISCUSSION

IpLITR signaling controls several innate immune cell responses. While unique CYT compositions have consequences for signaling, upstream events set the stage for signaling such as dimerization which has been demonstrated for IpLITRs (3). Dimerization may profoundly influence IpLITR-mediated ligand recognition and signal transduction. For example, the potential for IpLITR-mediated cross-talk would allow IpLITRs to modulate signaling through one another, but this has not been investigated. In this chapter, I explored the potential for IpLITR-mediated cross-talk regulation of ITAM-driven phagocytosis using the AD293 cell system. I developed and optimized a novel light yellow (LY) bead imaging cytometry-based phagocytosis assay to quantify IpLITR 1.1b WT_{CYT}-mediated cross-talk inhibition of IpFcR γ -L WT_{CYT}-driven phagocytosis. Overall, my results show that IpLITR 1.1b WT_{CYT} is capable of cross-talk down-regulation of phagocytic signaling through IpFcR γ -L WT_{CYT}, adding another capability to IpLITR signaling versatility.

IpLITR signaling versatility may depend on the nature of receptor activation (i.e. the type of stimulus used to cross-link receptors), the type of cell being assessed (i.e. immune vs. non-immune) and the ability of receptor CYTs to network into signaling pathways. Importantly, previous work has relied on heterologous expression of IpLITRs in mammalian cell lines. Due to the unknown nature of IpLITR ligands, these receptors are activated by antibody-mediated cross-linking of HA epitope-tagged constructs. Using this approach, previous work has demonstrated that following antibody cross-linking, the ITAM-containing IpFcR γ -L WT_{CYT} activates degranulation and cytokine secretion (4). When cross-linked by antibody-coated beads, IpFcR γ -

L WT_{CYT} also activates the phagocytic process (5). On the other hand, the heterologous expression approach has demonstrated predictable as well as unexpected signaling versatility of the ITIM-containing IpLITR 1.1b WT_{CYT}.

Not only does this receptor exhibit intra-CYT inhibitory signaling versatility, it can also stimulate ITIM-independent cellular responses. Original characterizations showed intra-CYT versatility as IpLITR 1.1b WT_{CYT} inhibits NK cell-mediated cytotoxicity through a predictable membrane distal CYT ITIM-dependent SHP-mediated pathway. Unexpectedly, a membrane proximal Y⁴⁵³-dependent Csk-mediated pathway also completely inhibited cytotoxicity (6). The emerging concept of functional plasticity is defined by signaling versatility of ITIM-containing receptors that results in the activation of cellular functions. Subsequently, IpLITR 1.1b WT_{CYT} evoked phagocytic signaling in myeloid RBL-2H3 cells (5). This prompted detailed mechanistic studies that revealed the formation of actin-rich filopodial protrusions that contacted and secured targets to the cell surface where they could be internalized. Interestingly, these protrusions were not inhibited at reduced temperatures, supporting a minimal signaling molecule recruitment model that is not heavily dependent on kinase activity (7, 8). Furthermore, recent biochemical evidence supports a putative mechanism involving the membrane proximal Y⁴³³-dependent recruitment of the Nck adaptor molecule (326). In an effort to further study mechanisms of IpLITR 1.1b WT_{CYT}-mediated phagocytosis, I developed a non-immune cell system using epithelioid AD293 cells. In chapter IV, I showed that IpLITR 1.1b WT_{CYT} does not activate phagocytic signaling in the epithelioid AD293 cell line (Figure 4.8). In addition, IpLITR 1.1b WT_{CYT}-mediated phagocytic signaling was not re-constituted in AD293 cells co-expressing a viral SFK, vSrc (Figure 4.9), nor was it re-constituted by over-expressing phagocytic signaling molecules (Figure 4.10). However, my observations in this chapter have added a novel signaling

capability to the repertoire of IpLITR 1.1b WT_{CYT}: cross-talk regulation of phagocytosis (Figure 5.8). This is the first time two teleost immunoregulatory receptors have been studied simultaneously, as previous studies focus on the inhibitory or stimulatory signaling capabilities of a single receptor. Since teleost immunoregulatory receptor gene families are highly expanded, diversified and co-expressed, studying the cross-talk control of cellular responses *in vitro* represents their co-operative regulatory potential of immunity in fish. In fact, co-operativity of immunoregulatory receptor cross-talk in immune regulation is common in vertebrates.

Cross-talk regulation is a critical feature of immune regulatory networks, not only because innate immune cells co-express multiple receptors that may be co-activated, but because the localization of signaling within microdomains that form at sites of target contact relies on the activation of co-receptors. In general, co-receptor activation is important for fine-tuning cellular responses to tailor immune responses, avoid excessive cellular activation and mitigate deleterious pro-inflammatory downstream effects. In fact, recently characterized mammalian FcRLs have evolved highly specialized roles in fine-tuning B cell responses and considering three of particular interest highlights their signaling versatility and cross-talk potential. The FcRL family includes 6 members in humans (*FCRL1-6*) and 3 members in mice (e.g. *Fcrl1*, *Fcrl5* and *Fcrl6*). Human FcRL1-5 modulate BCR signaling and B cell functions. For example, while FcRL3 and FcRL4 down-regulate BCR signaling by SHP1/2 ITIM-dependent mechanisms, they simultaneously enhance TLR9-induced responses by unresolved mechanisms (301, 302). FcRL family members are evolutionary relatives (i.e. homologs) of IpLITRs according to bioinformatic-based analyses (95) and contain similarly diverse CYT motif compositions. Specifically, IpLITR 1.1b WT_{CYT} contains an ITAM-like motif (Y⁴³³ to Y⁴⁵³), two ITIMs (Y⁴⁷⁷ and Y⁴⁹⁹) and an ITSM (Y⁵⁰³) while both FcRL3 and FcRL4 CYTs contain an

ITAM-like motif and an ITIM. Another example of FcRL signaling versatility is mouse FcRL5 which contains an ITAM-like motif and an ITIM and switches between stimulatory and inhibitory signaling depending on SHP1 expression levels in innate-like B1 cells. When SHP1 expression is high, FcRL5 inhibits cellular activation downstream of BCR activation. However, when SHP1 expression is lower, the ITAM-like dependent recruitment of the Lyn SFK modulates calcium mobilization downstream of BCR activation (305).

With respect to phagocytosis, co-receptor activation plays major roles in target capture, internalization and sub-cellular trafficking. In particular, signaling events during the capture and internalization stages occur at sites of cell-target engagement, known as the phagocytic synapse. Studies of mammalian Fc γ Rs and dectin1 have defined key molecular events that orchestrate phagocytic synapse formation. Specifically, to limit synapse microdomain formation and facilitate internalization, Fc γ Rs induce the ‘inside-out’ activation of integrins. This results in an outwardly diffusing integrin barrier that removes CD45 and CD148 phosphatases from the forming synapse (367, 388). Dectin1-mediated internalization of a fungal PAMP β -glucan also results in the exclusion of CD45 and CD148 from the forming phagocytic synapse (153, 368). However, while these examples demonstrate that certain phagocytic receptors are capable of triggering efficient internalization, other examples highlight the role of cross-talk in target capture and sub-cellular degradation of targets. For example, CD14 stimulates ‘inside-out’ activation of $\alpha_M\beta_2$ via TLR2-dependent PI3K signaling, resulting in efficient internalization of *Mycobacterium bovis* (389). In fact, the intra- to extra-cellular or ‘inside-out’ activation of integrins is a well-known priming mechanism for enhancing phagocytosis. The adhesion receptor CD44 induces the ‘inside-out’ activation of $\alpha_M\beta_2$ to phagocytose red blood cells (355). In addition, TIM4 binds apoptotic cells but relies on integrin-mediated signals to internalize these

targets (329). Furthermore, several TLRs are known to enhance Fc γ R-mediated phagocytosis and direct phagosome maturation which affects antigen presentation and inflammation (390–392). The fine-tuning of phagocytic signaling by cross-talk as described in these examples is critical for efficiently clearing microbes and in the case of apoptotic cell clearance, for mitigating auto-immunity. My observations have demonstrated that IpLITR 1.1b WT_{CYT} down-regulates the formation of a phagocytic synapse driven by an ITAM-containing receptor (Figure 5.8). In addition, it appears that the proximal and distal CYT segments of IpLITR 1.1b WT_{CYT} do not equally down-regulate phagocytosis. As shown in Figure 5.5B, the membrane proximal and distal CYT segments down-regulate phagocytosis by 12.6% and 26.0%, respectively, compared to IpLITR 1.1b MUT_{CYT}. Molecular details of IpLITR 1.1b WT_{CYT}-mediated cross-talk down-regulation of phagocytosis are explored further in chapter VI. The remainder of this discussion will focus on validating aspects of the transient transfection approach that I used in my study.

To assess the cross-talk potential of IpLITRs, I transiently transfected the eGFP-tagged IpLITR 1.1b WT_{CYT} into stable IpFcR γ -L WT_{CYT}-expressing cells and co-cross-linked these HA-epitope tagged receptors with α HA antibody-coated beads. Subsequent IpFcR γ -L WT_{CYT} phagocytic signaling competes with inhibitory signals from IpLITR 1.1b WT_{CYT} resulting in bead targets left secured on the cell surface instead of internalized. Importantly, to examine a CYT-mediated cross-talk mechanism, I designed these two receptors to differ only in CYT composition and also tested an IpLITR 1.1b mutant CYT construct (i.e. IpLITR 1.1b MUT_{CYT}). This construct controls for phosphotyrosine-dependent cross-talk mechanisms because all CYT tyrosine-based motifs are converted to phenylalanine.

Despite widespread use in studying molecular mechanisms, transient transfection approaches have technical caveats including alterations to cellular biology that may affect

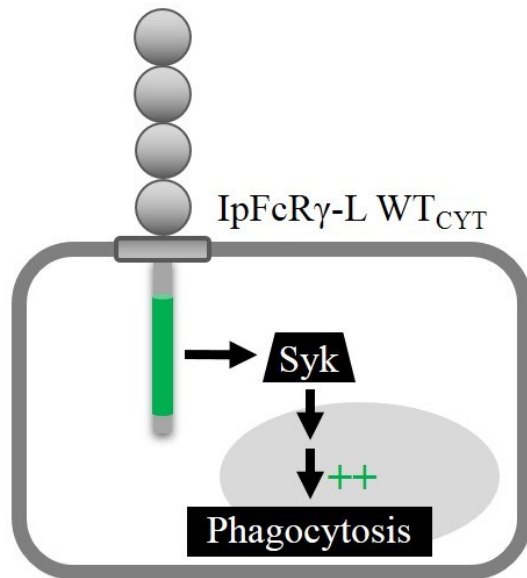
signaling and consistency of transfection efficiency. While transfections are a simple and rapid method for expressing proteins and assessing specific functions, there may be differences in how transiently versus stably transfected cells adapt to transfection (393, 394). When using a transient transfection approach, several conditions must be empirically determined for optimal transfection efficiency including the type of reagent and plasmid, the ratio of plasmid to reagent used in the transfection protocol and the amount of time given to cells to take-up and express the plasmid (395). After optimizing these conditions, protein expression level can vary by as much as 100-fold (based on eGFP fluorescence intensity) which directly impacts signaling outcomes (339–341). Since eGFP fluorescence is proportional to eGFP-tagged receptor expression level (385–387), I limited analysis to a specific eGFP positive cell population which revealed optimal cross-talk signaling at mid-level eGFP expression (Figure 5.10).

Another important consideration is the nature of receptor activation. In general, endogenous ligands are preferred as they represent receptor-ligand interactions where affinity, avidity and conformation match a physiological context. For example, IgG opsonized red blood cells are common in Fc γ R studies (284, 378, 396–398). Due to the unknown nature of IpLITR ligands, this system employs HA epitope-tagged receptors ligated by α HA antibody-coated bead targets. To mitigate artefacts caused by high affinity antibody-induced receptor cross-linking, receptor constructs contain matching extracellular domains and TM segments (366). This balances receptor dynamics at the synapse by preventing receptor exclusion due to differences in the number of extracellular domains (399, 400). Indeed, the effects of high affinity cross-linking are a likely explanation for the reduced phagocytic signaling observed for IpLITR 1.1b MUT_{CYT} compared to eGFP alone (Figure 5.10).

In stable IpFcR γ -L WT_{CYT}-expressing cells transiently transfected with eGFP-tagged constructs, my results show that eGFP and IpLITR 1.1b MUT_{CYT}-eGFP showed 63.3% and 53.0% phagocytic cell phenotypes, respectively. Two possible explanations for the difference are: (1) tyrosine-independent pathways signal cross-talk inhibition or (2) IpLITR 1.1b MUT_{CYT} receptors are trapped within forming signalosomes and physically obstruct synapse formation. In support of the first explanation, several receptors are linked to the actin cytoskeleton via actin adaptors such as the 4.1 family proteins. These adaptors bind alternative CYT motifs and directly influence receptor trafficking and synapse formation. IpLITR 1.1b WT_{CYT} contains basic residue-rich motifs that may be able to recruit adaptor molecules like 4.1 family proteins (290). In addition, this receptor contains 19 threonine/serine residues that may activate distinct signaling pathways, like protein kinase C (283). Signaling through alternative pathways may result in down-regulation of IpFcR γ -L WT_{CYT} clustering. On the other hand, IpLITR 1.1b MUT_{CYT} receptor dynamics that would normally displace this receptor from the forming synapse may not be sufficient due to high affinity α HA-coated bead-receptor cross-linking.

The next chapter focuses on characterizing the tyrosine-based molecular cross-talk signaling events that underlie IpLITR 1.1b WT_{CYT}-mediated regulation of phagocytosis.

A.



B.

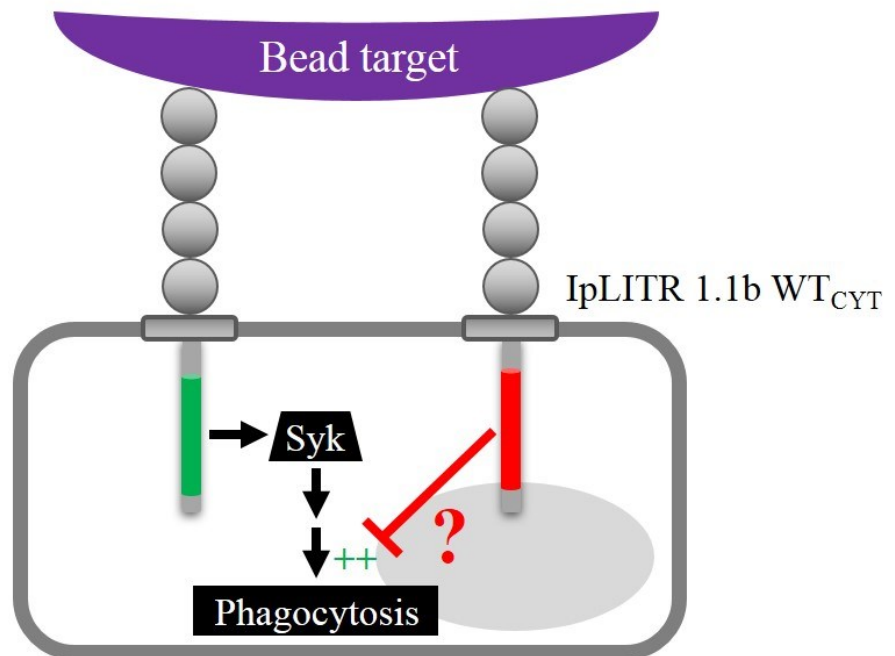


Figure 5.1. Schematic representations of IpLITR CYT-mediated signaling potential in AD293 cells. (A) IpFcR γ -L WT_{CYT} activates phagocytosis by recruiting spleen tyrosine kinase (Syk) to the CYT ITAM (drawn in green). (B) Hypothetical IpLITR CYT-mediated cross-talk regulation of phagocytic signaling explored in chapter V. Specifically, does the phosphotyrosine-dependent recruitment of signaling molecules (e.g. CYT ITIM, drawn in red) allow IpLITR 1.1b WT_{CYT} to inhibit phagocytosis driven by the ITAM-containing IpFcR γ -L WT_{CYT}?

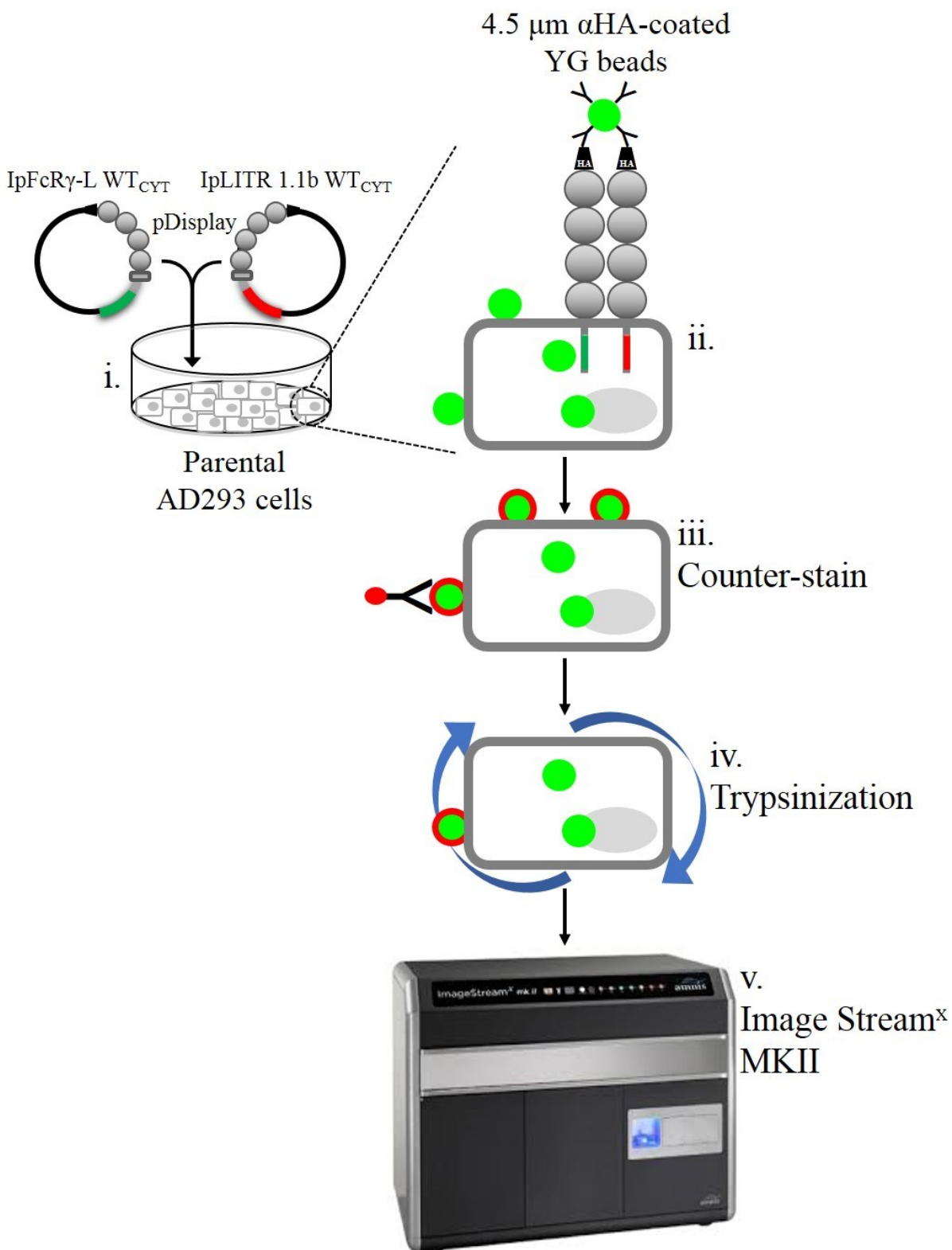
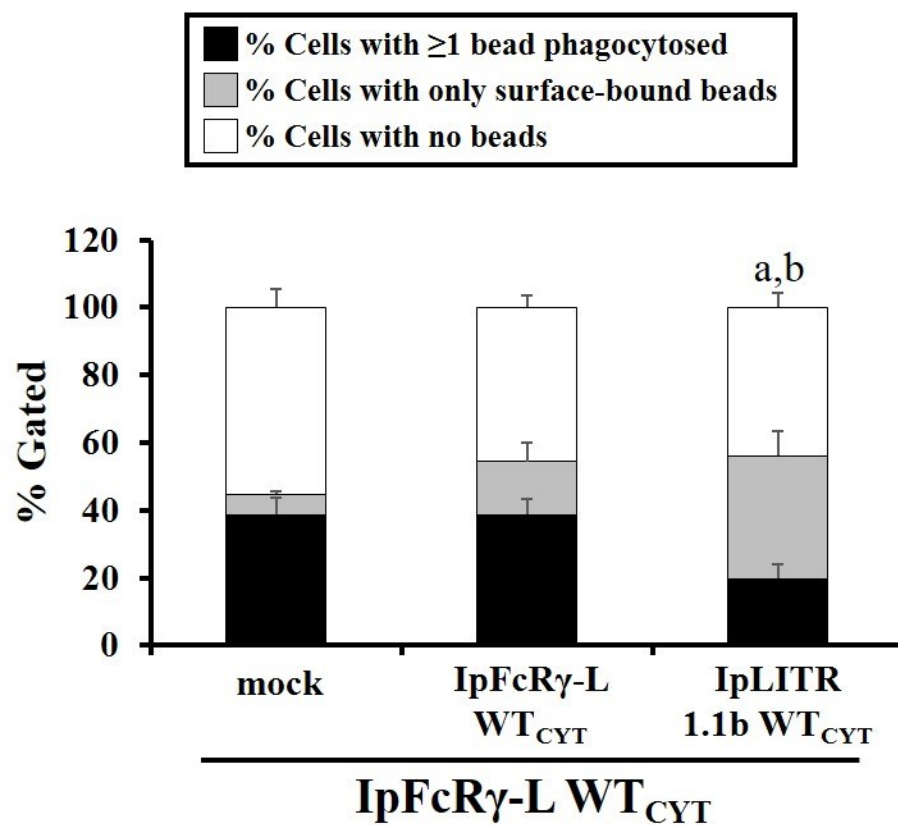


Figure 5.2. Schematic representation of IpLITR 1.1b WT_{CYT}-mediated cross-talk regulation of IpFcR γ -L WT_{CYT}-driven phagocytosis by an Image Stream-based yellow green (YG) bead assay in transiently co-transfected parental AD293 cells. (i) pDisplay-encoded IpFcR γ -L WT_{CYT} and IpLITR 1.1b WT_{CYT} receptors were co-transfected into parental AD293 cells using TurboFECT® transfection reagent for 48 h. (ii) 4.5 μ m mouse α HA antibody-coated YG beads were added to IpLITR co-transfected cells and incubated at 37°C for 40 min to co-cross-link receptors. (iii) Cells were incubated at 4°C for 30 min with rabbit α -mouse AlexaFluor647-conjugated secondary antibody to label surface-exposed YG beads, followed by (iv) trypsinization, consisting of a 37°C incubation for 5 min in harvest buffer containing 0.05% trypsin and 1.2 mM EDTA. This incubation also removed non-specifically cell-adsorbed YG beads. (v) Cells were centrifuged and pellets re-suspended in 1% paraformaldehyde fixative before data collection on the Image Stream^X MKII imaging flow cytometer.

A.



B.

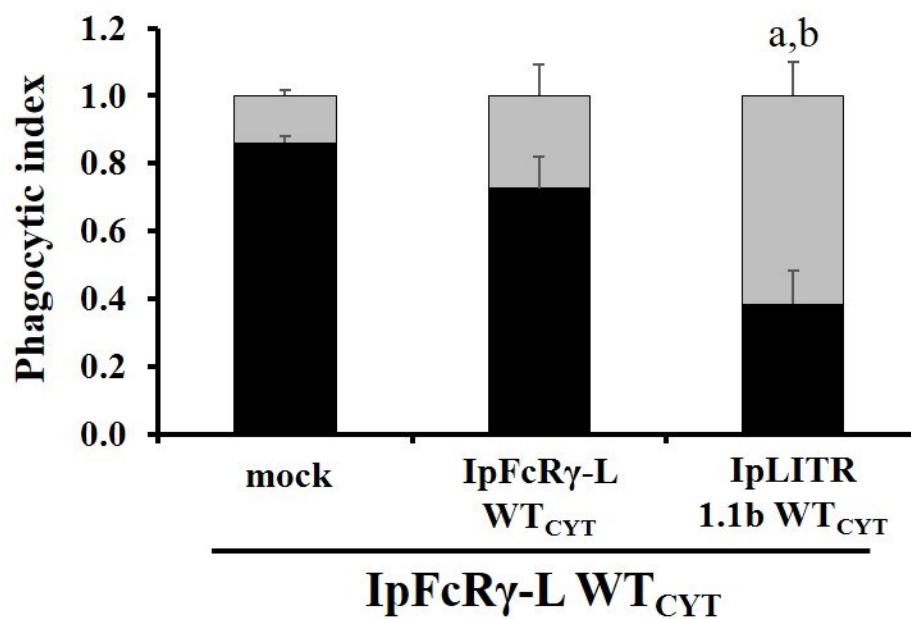


Figure 5.3. IpLITR 1.1b WT_{CYT} appears to mediate cross-talk inhibition of IpFcR γ -L WT_{CYT}-driven phagocytosis in transiently co-transfected AD293 cells. pDisplay-encoded IpFcR γ -L WT_{CYT} and IpLITR 1.1b WT_{CYT} receptors were co-transfected into parental AD293 cells using TurboFECT® transfection reagent for 48 h. Mouse α HA antibody-coated 4.5 μ m yellow green fluorescent (YG) beads were added to cells for 30 min at 37°C. Surface-bound YG beads were counter-stained with rabbit α -mouse AlexaFluor647-conjugated secondary antibody. Cells were harvested by trypsinization and fixed in 1% paraformaldehyde prior to data collection on the Image Stream^X MKII flow cytometer. Raw image files were subjected to component masking analysis by template-assisted batching using IDEAS v6.2 software as previously described (327). Each black bar represents the percentage of phagocytic cells (i.e. a cell with ≥ 1 bead fully internalized), grey bars represent the percentage of cells with only surface-bound beads (i.e. no beads internalized) and the white bars represent the percentage of cells with no associated beads (i.e. none bound or internalized). Results are representative of the mean \pm SEM of at least three independent experiments as (A) raw or (B) indexed data. Phagocytic index was calculated as: % phagocytic or surface-bound cells / % total bead-associated cells. Lower case ‘a’ and ‘b’ represent statistically significant differences ($p < 0.05$) compared to +mock and +IpFcR γ -L WT_{CYT} % phagocytic cells, respectively.

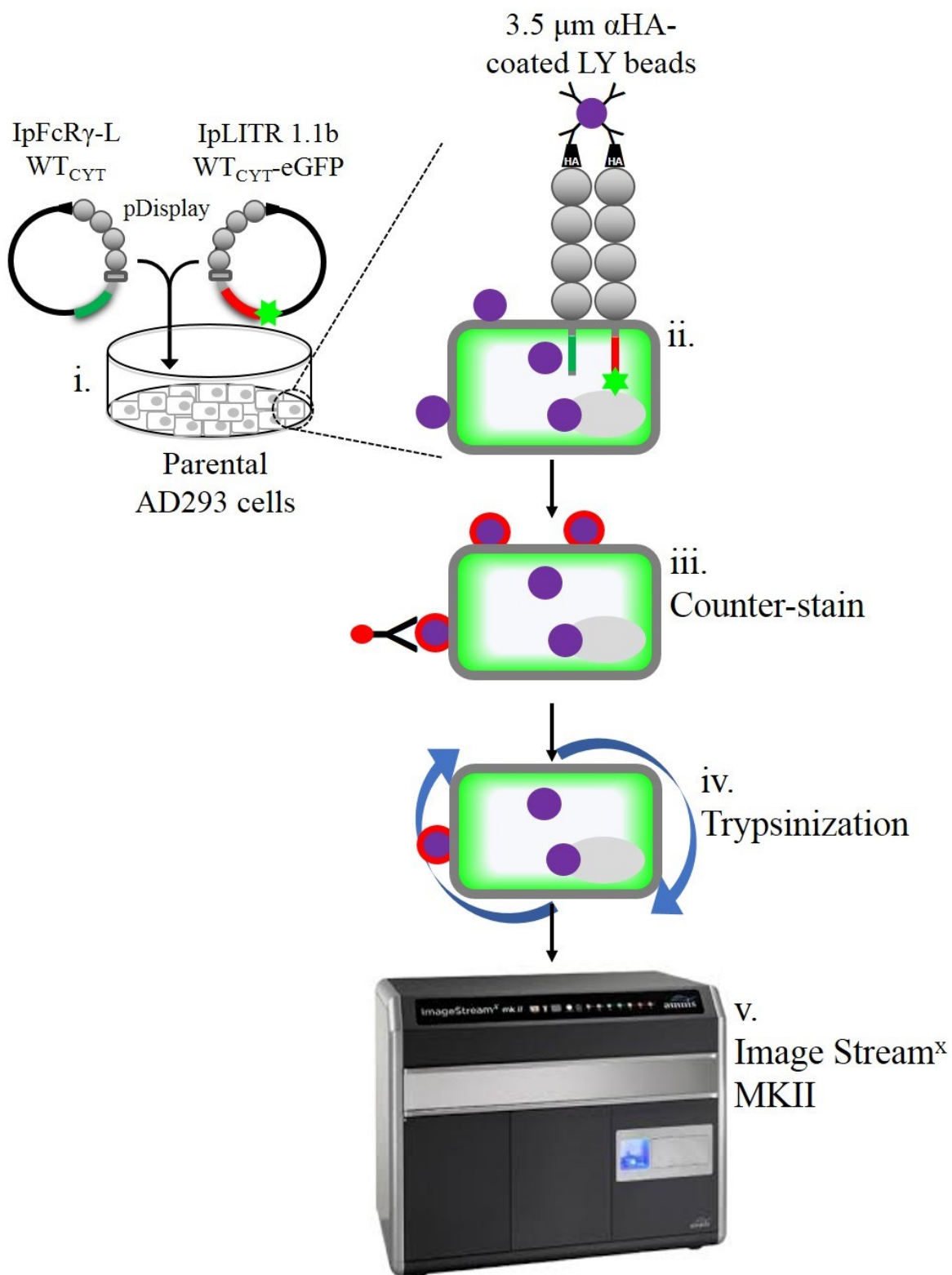
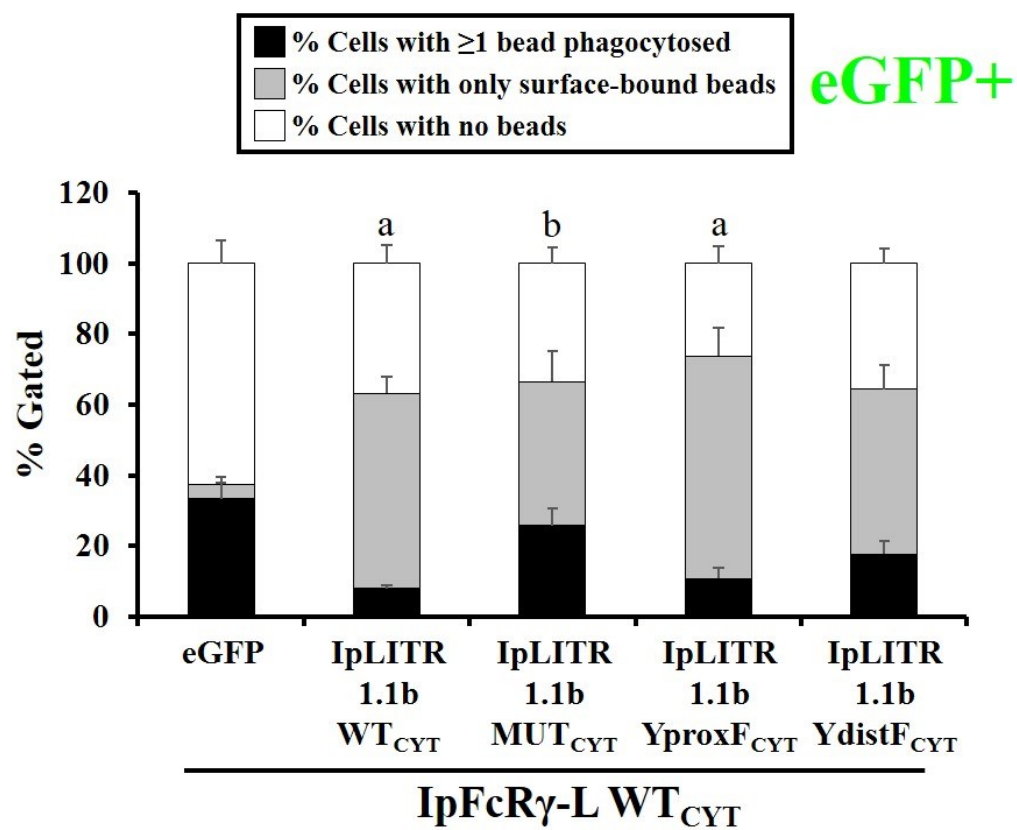
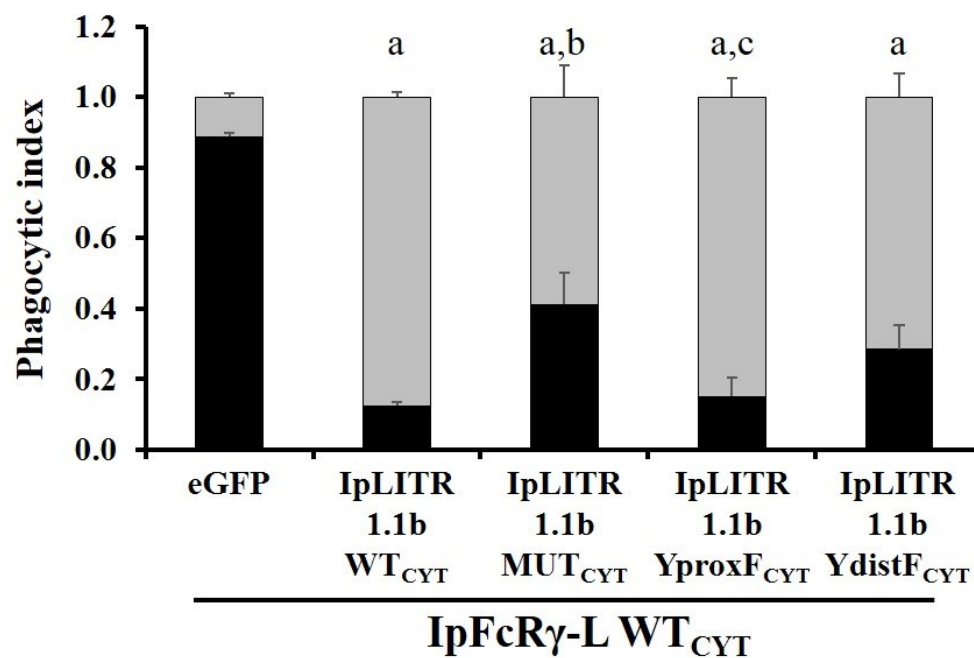


Figure 5.4. Schematic representation of IpLITR 1.1b WT_{CYT}-mediated cross-talk regulation of IpFcR γ -L WT_{CYT}-driven phagocytosis by an Image Stream-based light yellow (LY) bead assay in transiently co-transfected parental AD293 cells. (i) pDisplay-encoded IpFcR γ -L WT_{CYT} and eGFP-tagged IpLITR 1.1b WT_{CYT} receptors were co-transfected into parental AD293 cells using TurboFECT® transfection reagent for 48 h. (ii) 3.5 μ m mouse α HA antibody-coated LY beads were added to IpLITR co-transfected cells and incubated at 37°C for 40 min to co-cross-link receptors. (iii) Cells were incubated at 4°C for 30 min with rabbit α -mouse AlexaFluor647-conjugated secondary to label surface-exposed LY beads, followed by (iv) trypsinization, consisting of a 37°C incubation for 5 min in harvest buffer containing 0.05% trypsin and 1.2 mM EDTA. Trypsinization also removed non-specifically cell-adsorbed LY beads. (v) Cells were centrifuged and pellets re-suspended in 1% paraformaldehyde fixative before data collection on the Image Stream^X MKII imaging flow cytometer.

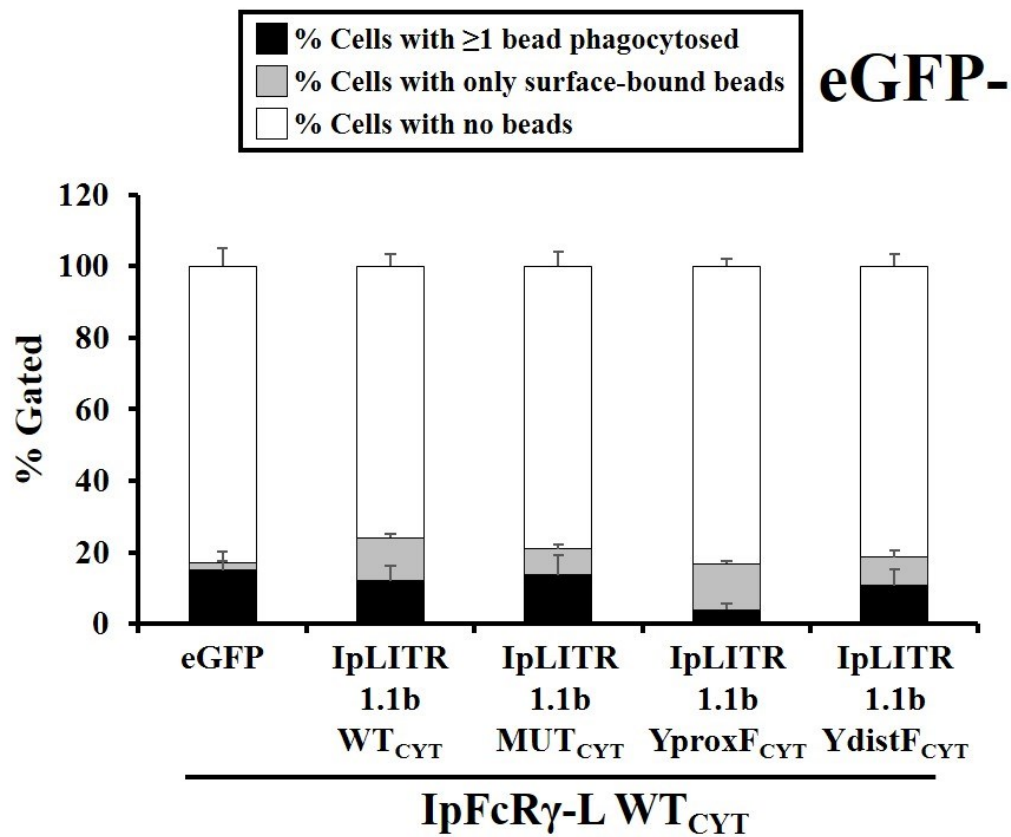
A.



B.



C.



D.

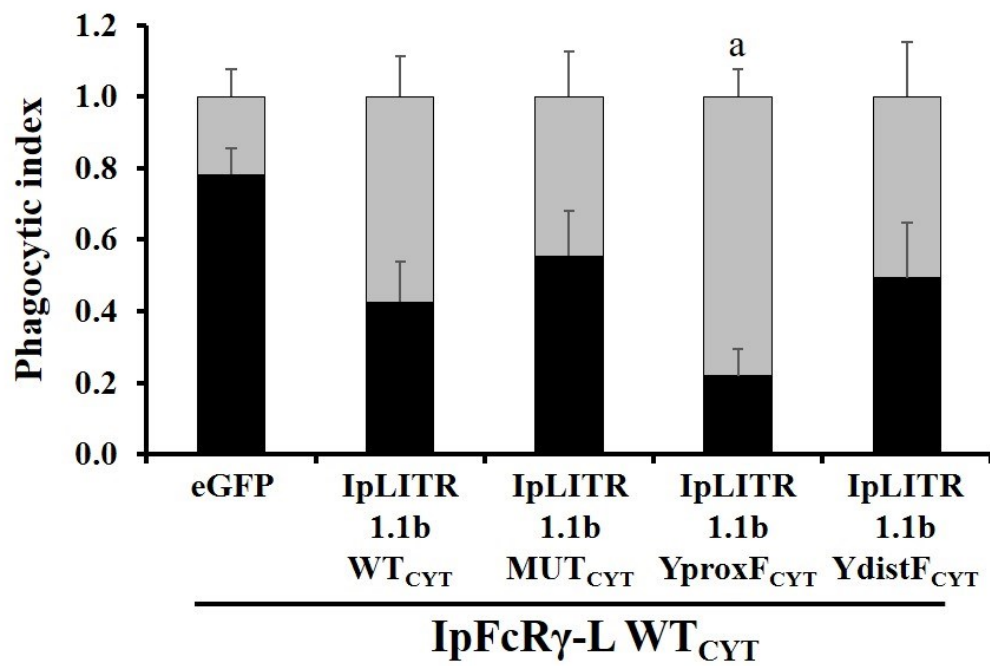


Figure 5.5. eGFP-tagged IpLITR 1.1b WT_{CYT} appears to mediate inhibition of IpFcR γ -L WT_{CYT}-driven phagocytosis through both proximal and distal CYT segment tyrosine-based motifs. pDisplay-encoded IpFcR γ -L WT_{CYT} and eGFP-tagged IpLITR 1.1b CYT receptors were co-transfected into parental AD293 cells using TurboFECT® transfection reagent for 48 h. Mouse α HA antibody-coated 3.5 μ m light yellow (LY) beads were added to cells for 40 min at 37°C. Surface-bound LY beads were counter-stained with rabbit α -mouse AlexaFluor647-conjugated secondary antibody. Cells were harvested by trypsinization and fixed in 1% paraformaldehyde prior to data collection on the Image Stream^X MKII flow cytometer. Raw image files were subjected to a component masking analysis modified from Fei et al. (2017) that separates eGFP positive (eGFP⁺) and negative (eGFP⁻) cell populations. Each black bar represents the percentage of phagocytic cells (i.e. a cell with ≥ 1 bead fully internalized), grey bars represent the percentage of cells with only surface-bound beads (i.e. no beads internalized) and the white bars represent the percentage of cells with no associated beads (i.e. none bound or internalized). Results for eGFP⁺ cells (A and B) and eGFP⁻ cells (C and D) are representative of the mean \pm SEM of at least three independent experiments as (A and C) raw or (B and D) indexed data. Phagocytic index was calculated as: % phagocytic or surface-bound cells / % total bead-associated cells. Lower case a, b and c represent statistically significant differences ($p < 0.05$) compared to +eGFP, +IpLITR 1.1b WT_{CYT} and +IpLITR 1.1b MUT_{CYT} % phagocytic cells, respectively.

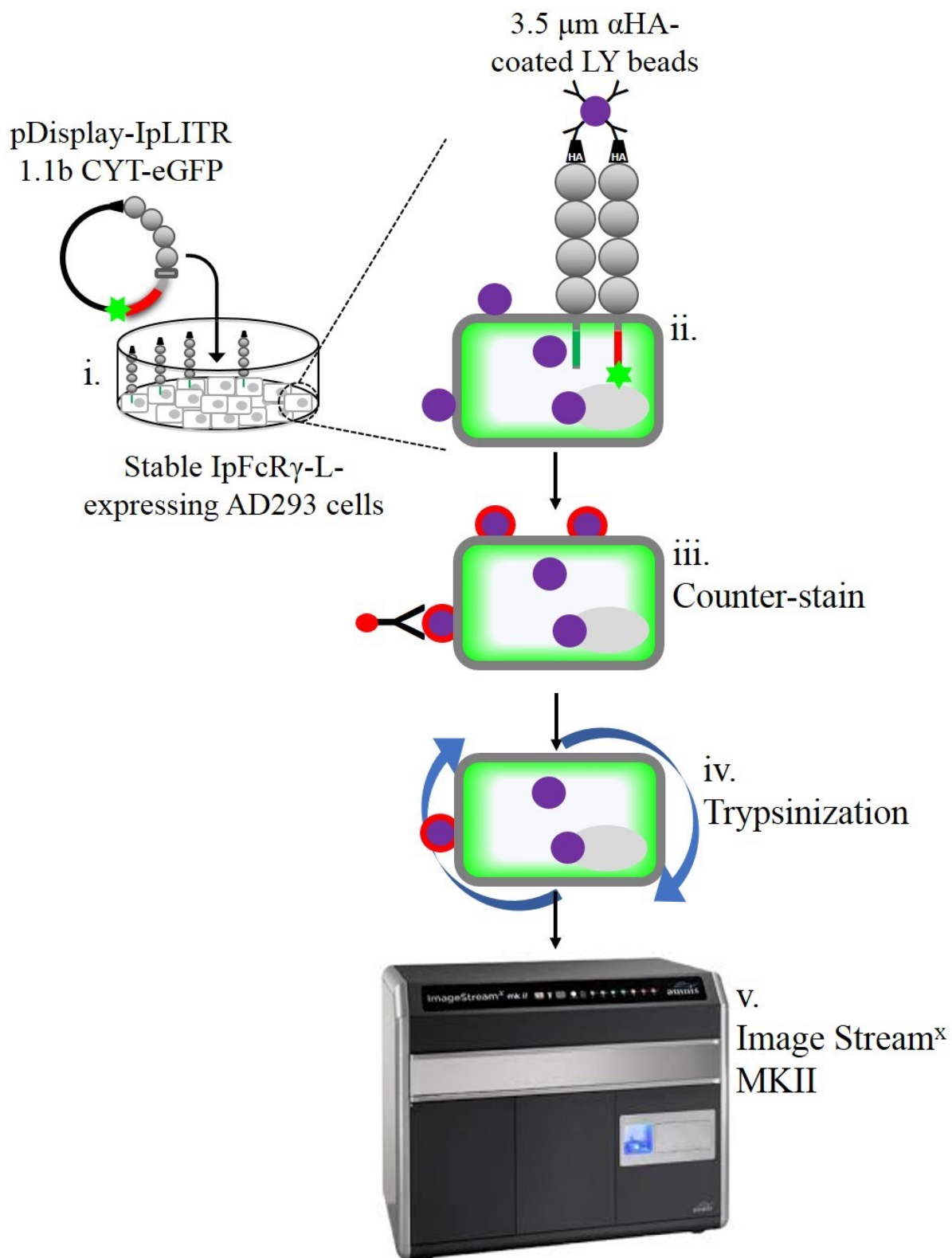
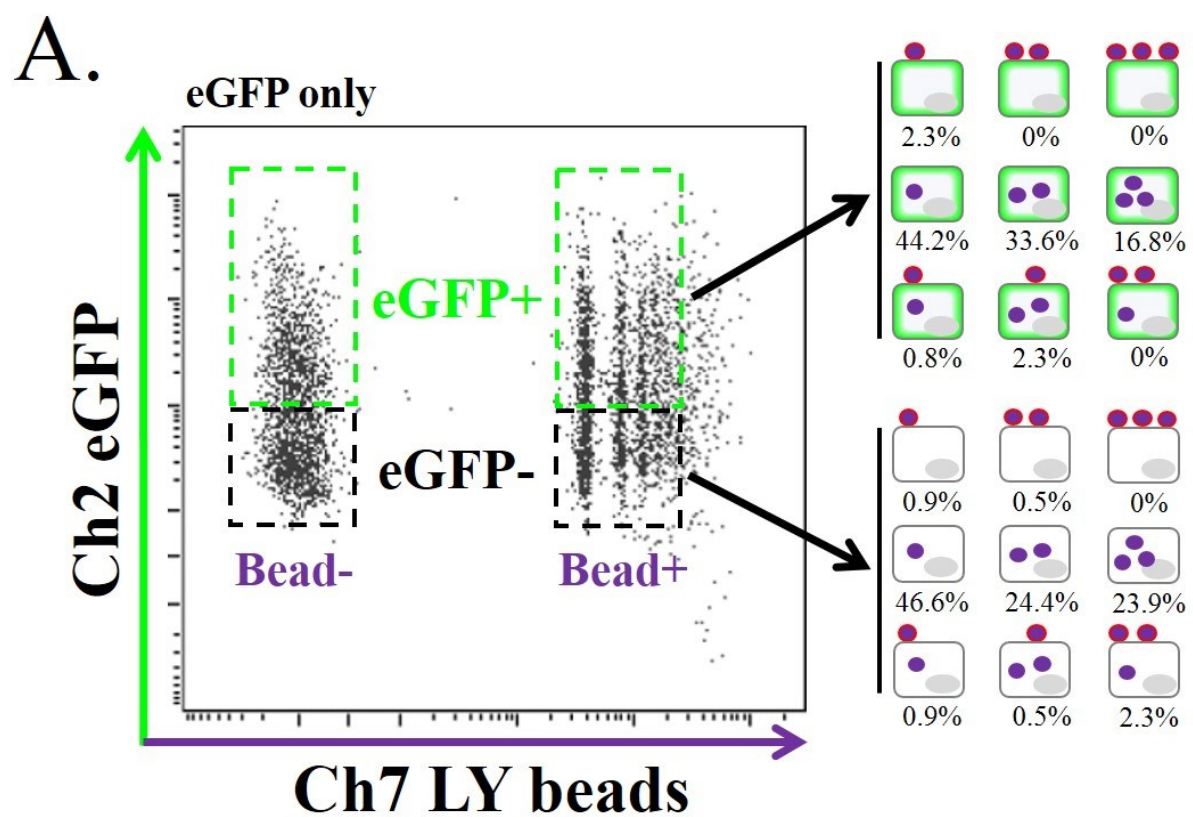
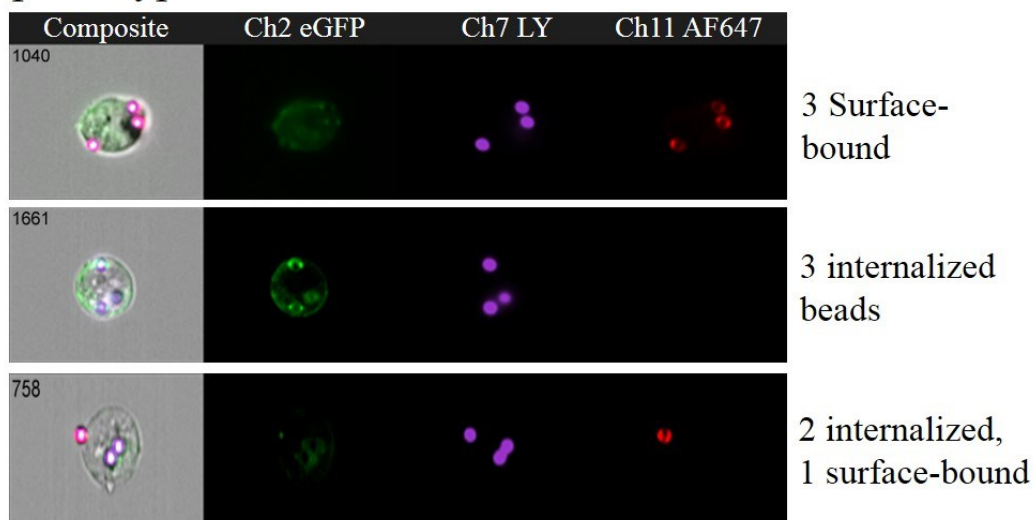


Figure 5.6. Schematic representation of eGFP-tagged IpLITR 1.1b WT_{CYT}-mediated cross-talk regulation of ITAM-driven phagocytosis in stable IpFcR γ -L WT_{CYT}-expressing AD293 cells via imaging cytometry-based light yellow (LY) bead phagocytosis assay. (i) pDisplay-encoded eGFP-tagged IpLITR 1.1b CYT constructs were transfected into stable IpFcR γ -L WT_{CYT}-expressing AD293 cells using TurboFECT® transfection reagent for 48 h. (ii) 3.5 μ m mouse α HA antibody-coated LY beads were added and cells were incubated at 37°C for 40 min to co-cross-link receptors. (iii) Cells were incubated at 4°C for 30 min with rabbit α -mouse AlexaFluor647-conjugated secondary antibody to label surface-exposed LY beads, followed by (iv) trypsinization, consisting of a 37°C incubation for 5 min in harvest buffer containing 0.05% trypsin and 1.2 mM EDTA. Trypsinization also removed non-specifically cell-adsorbed LY beads. (v) Cells were centrifuged and pellets re-suspended in 1% paraformaldehyde fixative before data collection on the Image Stream^X MKII imaging flow cytometer.



B. Stable IpFcR γ -L WT_{CYT}-expressing, eGFP-tagged IpLITR 1.1b CYT construct co-expressing AD293 cell phagocytic phenotypes:



Stable IpFcR γ -L WT_{CYT}-expressing AD293 cell phagocytic phenotypes:

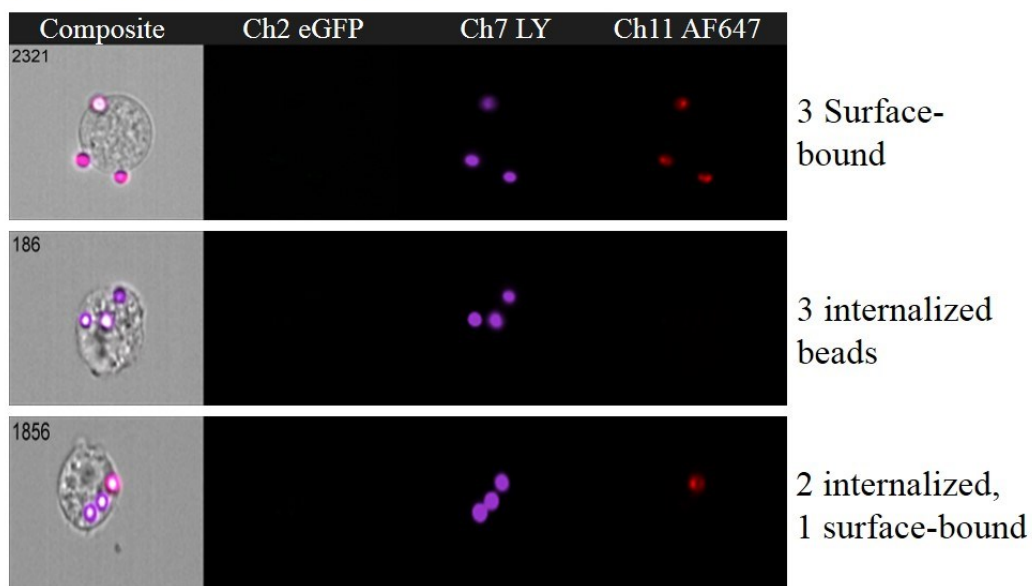
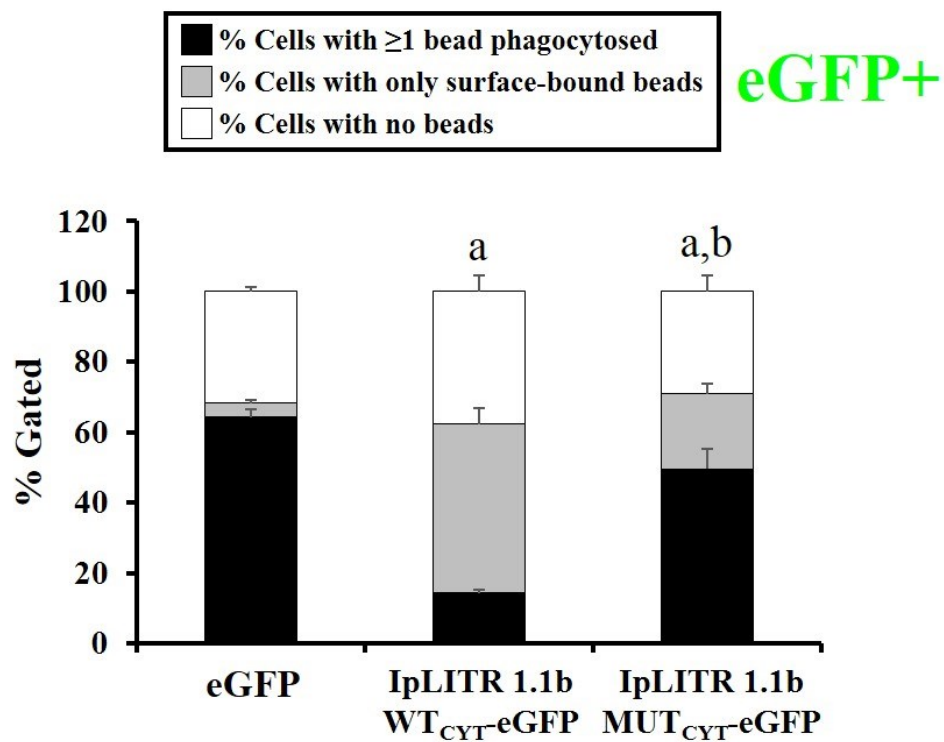
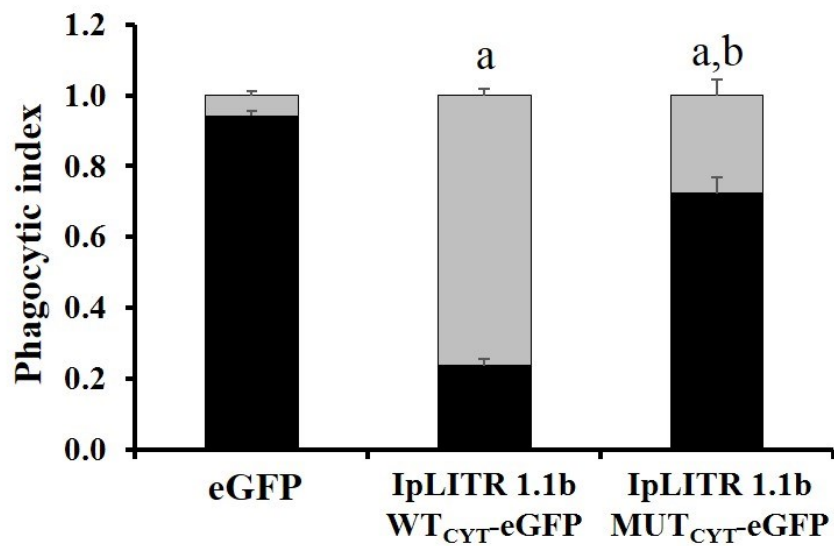


Figure 5.7. Gating strategy for Image Stream-based analysis of cells with phagocytosed and/or surface-bound light yellow (LY) beads. (A) Cells are gated into four populations based on LY bead association (Ch 7; bead- or bead+) and eGFP fluorescence (Ch 2; eGFP- or eGFP+). Bead+eGFP- and bead+eGFP+ populations were subjected to component masking analysis (modified from Fei et al., 2017) to determine phagocytic phenotypes of cells with up to 3 associated beads. Schematic representations of the nine phagocytic phenotypes within the bead+eGFP+ (top) and bead+eGFP- (bottom) cell populations are illustrated to the right of the gates along with the proportion of bead-associated cells within each individual phenotype for eGFP only transfected cells. (B) Examples of images from channel 2 (eGFP), channel 7 (LY beads) and channel 11 (AF647 counter-stain) are shown for eGFP+ (top panels) and eGFP- (bottom panels) cell phagocytic phenotypes. Individual channels are merged and superimposed onto a brightfield image and displayed as a composite (far left).

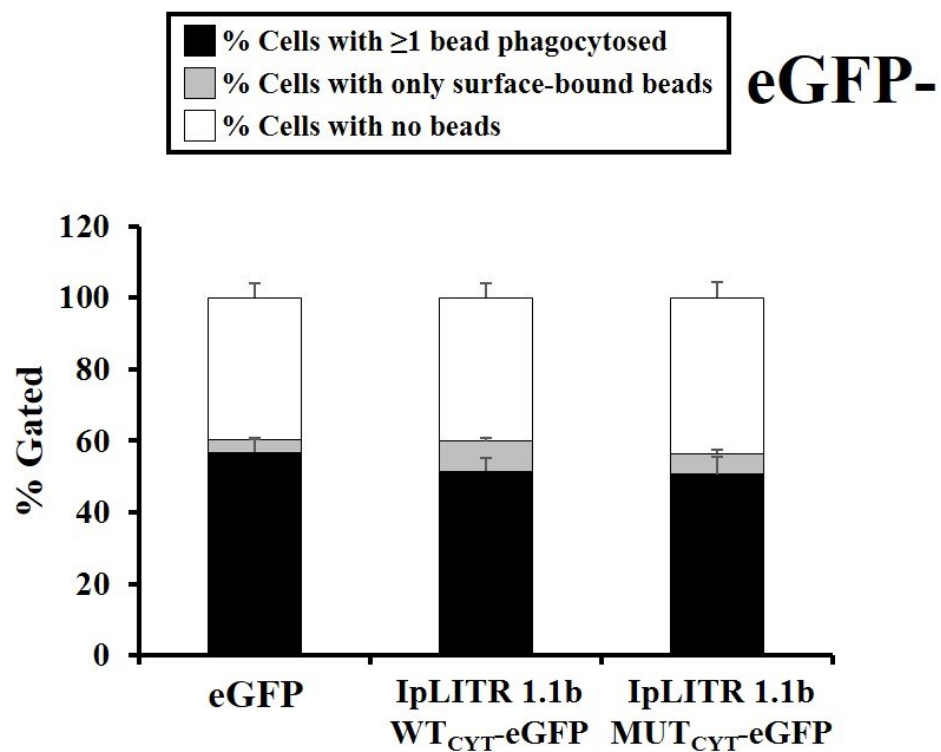
A.



B.



C.



D.

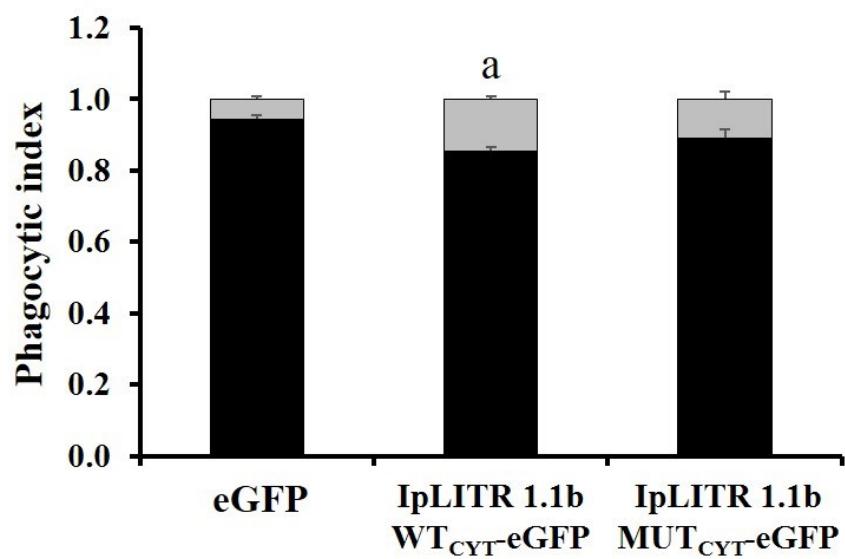


Figure 5.8. eGFP-tagged IpLITR 1.1b WT_{CYT} mediates CYT motif-dependent cross-talk inhibition of ITAM-driven phagocytosis in stable IpFcR γ -L-expressing AD293 cells. pDisplay-encoded eGFP-tagged IpLITR 1.1b WT_{CYT} and MUT_{CYT} receptors were transfected into stable IpFcR γ -L WT_{CYT}-expressing AD293 cells using TurboFECT® transfection reagent for 48 h. Mouse α HA antibody-coated 3.5 μ m light yellow (LY) fluorescent beads were added to cells for 40 min at 37°C. Surface-bound LY beads were counter-stained with AlexaFluor 647-conjugated rabbit α -mouse secondary antibody. Cells were harvested by trypsinization and fixed in 1% paraformaldehyde prior to data collection on the Image Stream^X MKII flow cytometer. Raw image files were subjected to a component masking analysis modified from Fei et al. (2017) that separates eGFP positive (eGFP⁺) and negative (eGFP⁻) cell populations. Each black bar represents the percentage of phagocytic cells (i.e. a cell with ≥ 1 bead fully internalized), grey bars represent the percentage of cells with only surface-bound beads (i.e. no beads internalized) and the white bars represent the percentage of cells with no associated beads (i.e. none bound or internalized). Results for eGFP⁺ (A and B) and eGFP⁻ (C and D) cells are representative of the mean \pm SEM of at least three independent experiments as (A and C) raw or (B and D) indexed data. Phagocytic index was calculated as: % phagocytic or surface-bound cells / % total bead-associated cells. Lower case a and b represent statistically significant differences ($p < 0.05$) compared to eGFP and IpLITR 1.1b WT_{CYT} % phagocytic cells, respectively.

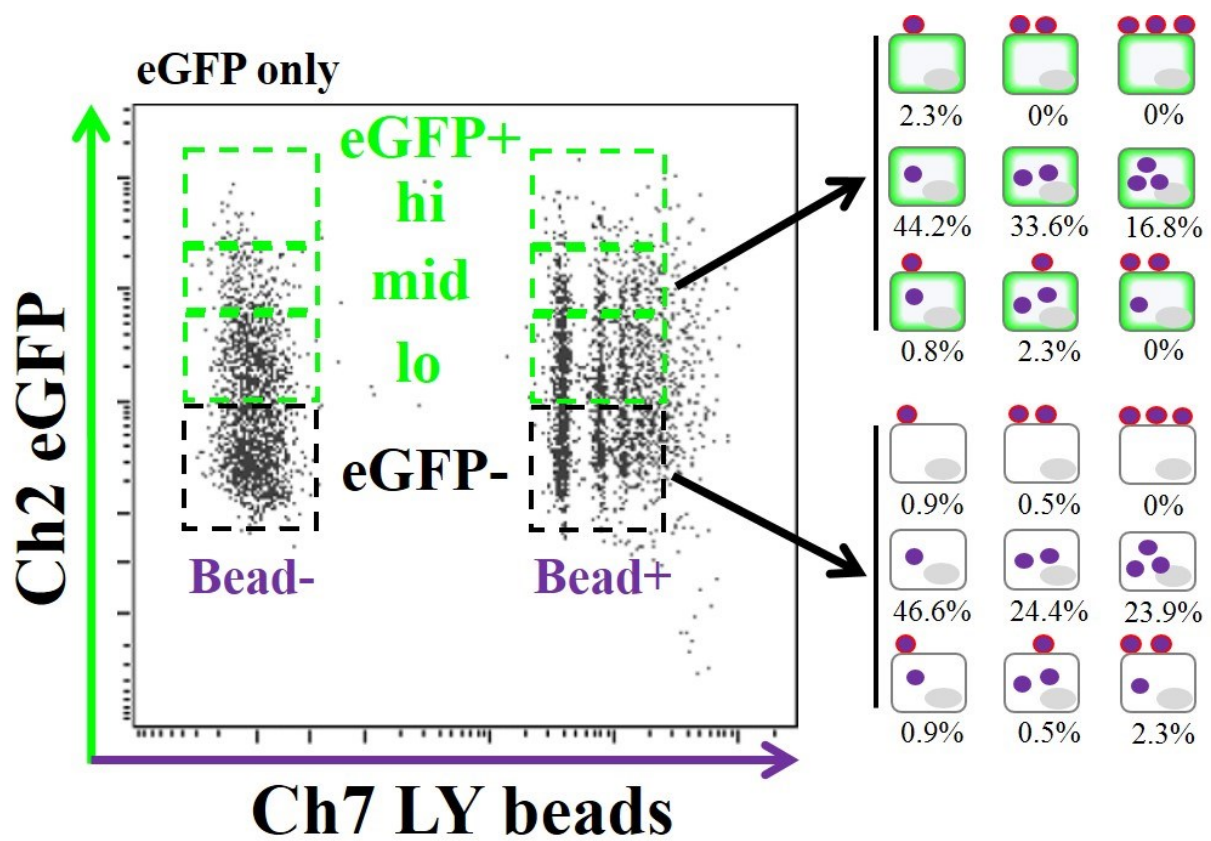
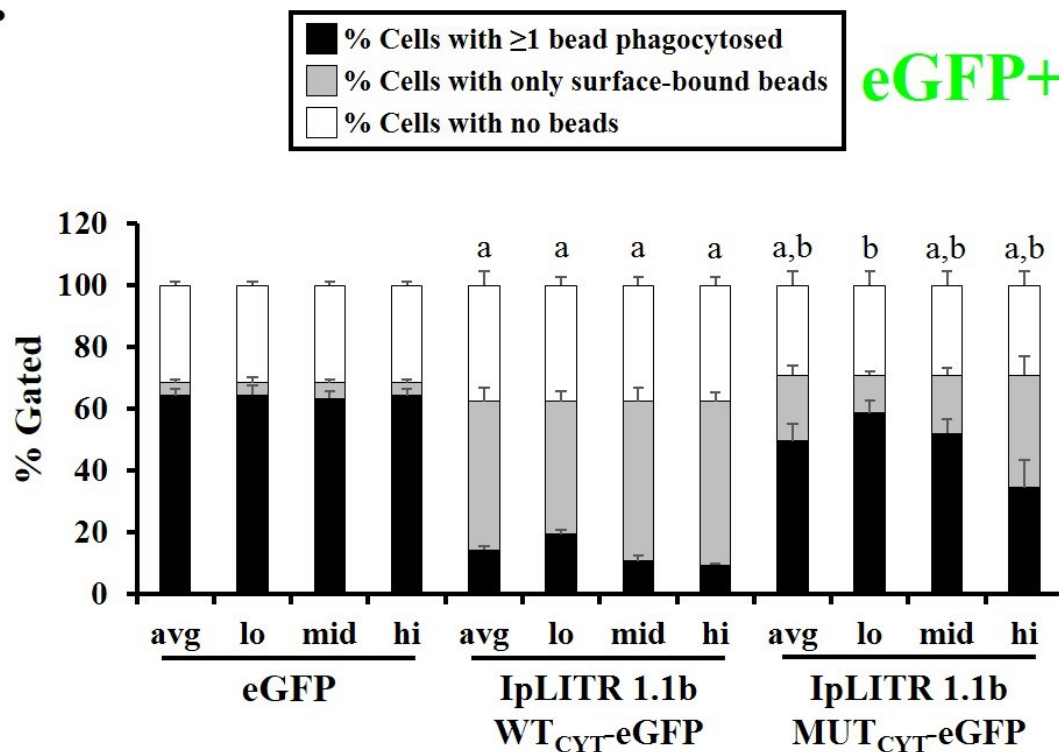


Figure 5.9. Gating strategy for eGFP-tagged IpLITR 1.1b CYT construct expression level during Image Stream-based analysis of cells with phagocytosed and/or surface-bound light yellow (LY) beads. Cells are gated into four primary populations based on LY bead association (Ch 7; bead- or bead+) and eGFP fluorescence (Ch 2; eGFP- or eGFP+). eGFP+ cells are further gated into three populations based on the level of eGFP expression including low (lo), middle (mid) and high (hi). Bead+eGFP- and bead+eGFP lo, mid or hi+ populations were separately subjected to component masking analysis (modified from Fei et al., 2017) to determine phagocytic phenotypes of cells with up to 3 associated beads. Schematic representations of the nine phagocytic phenotypes within the bead+eGFP+ (top) and bead+eGFP- (bottom) cell populations are illustrated to the right of the gates along with the proportion of bead-associated cells within each individual phenotype for eGFP only transfected cells.

A.



B.

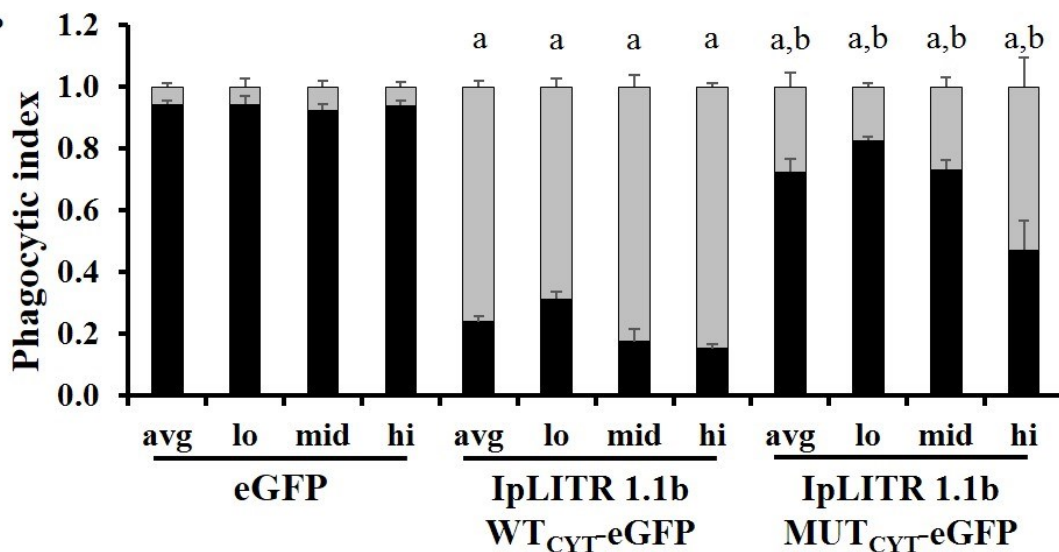


Figure 5.10. Effect of receptor expression levels on eGFP-tagged IpLITR 1.1b WT_{CYT}-mediated cross-talk inhibition of IpFcR γ -L WT_{CYT}-driven phagocytosis. Data from Figure 5.8 was re-analyzed using separate gates for average (avg; i.e. all eGFP+ cells), low (lo), middle (mid) and high (hi) eGFP expression (see Figure 5.7A for gates). Each black bar represents the percentage of phagocytic cells (i.e. a cell with ≥ 1 bead fully internalized), grey bars represent the percentage of cells with only surface-bound beads (i.e. no beads internalized) and the white bars represent the percentage of cells with no associated beads (i.e. none bound or internalized). Results are representative of the mean \pm SEM of at least three independent experiments as (A) raw or (B) indexed data. Phagocytic index was calculated as: % phagocytic or surface-bound cells / % total bead-associated cells. Lower case ‘a’ and ‘b’ represent statistically significant differences ($p < 0.05$) compared to eGFP and IpLITR 1.1b WT_{CYT} % phagocytic cells at the corresponding eGFP expression level, respectively.

CHAPTER VI
**MOLECULAR CHARACTERIZATION OF IpLITR 1.1b WT_{CYT}-
MEDIATED CROSS-TALK INHIBITION OF ITAM-DRIVEN
PHAGOCYTIC SIGNALING**

6.1 INTRODUCTION

The results of the last chapter showed that IpLITR 1.1b WT_{CYT} down-regulates ITAM-driven phagocytic signaling of IpFcR γ -L WT_{CYT}. In addition, I established a novel imaging flow cytometry-based system for characterizing IpLITR-mediated cross-talk regulation of phagocytosis. Immunoregulatory receptor cross-talk allows cells to integrate multiple incident signals and fine-tune signal transduction pathways to regulate effector responses. More specifically, cross-talk is the modulation of a signal transduction pathway downstream of an activated receptor by another co-activated receptor. In the case of phagocytosis, a phagocytic receptor activates synapse formation, internalization, sub-cellular trafficking, and degradation of a target within the cell. Cross-talk from co-activated receptors fine-tunes various stages of this process. For example, receptor co-cross-linking at the cell membrane may block target capture, phagocytic synapse formation and all downstream signaling events.

Several human diseases have links to dysregulated phagocytosis including cancer, neurodegeneration and bacterial/viral infection (397, 401, 410, 411, 402–409). Importantly, a critical step in the initiation of phagocytic signaling relies on immunoregulatory receptor-mediated cross-talk at the cell surface. Many mammalian immunoregulatory receptors have been identified and molecular details of negative regulatory mechanisms have been characterized. In human monocytes, antibody-mediated co-ligation of LILRB1/2 with Fc γ RI results in decreased phosphorylation of the ITAM-containing FcR γ chain, reduced Syk activation and decreased Ca²⁺ mobilization, presumably through ITIM-dependent SHP recruitment (412). In a second example,

engaging CD47 with SIRP α on phagocytes results in the recruitment of SHPs to phosphorylated SIRP α and the inhibition of Fc γ R-mediated phagocytosis (374, 375). Similarly, Fc γ RIIB inhibits Fc γ R-mediated phagocytosis via phosphorylated CYT ITIMs which recruit the lipid phosphatase SHIP and/or the cytoplasmic phosphatases SHP1/2 (376–378). In this case, the binding of common ligands (i.e. IgG antibodies) by Fc γ Rs leads to co-cross-linking of receptors and CYT-mediated cross-talk inhibition of phagocytic signals. Collectively, these mammalian examples highlight the importance of phosphorylated CYT ITIM-mediated recruitment of cytoplasmic phosphatases for the down-regulation of phagocytosis.

Using the phagocytosis assay that I developed in chapter V, the objective of this chapter was the molecular characterization of IpLITR 1.1b WT_{CYT}-mediated down-regulation of IpFcR γ -L WT_{CYT}-driven phagocytosis. In particular, I aimed to identify motif-dependent pathways using eGFP-tagged IpLITR 1.1b WT_{CYT} tyrosine (Y) to phenylalanine (F; i.e. YF) mutant constructs (schematics in Figure 6.1). In addition, I used dominant negative signaling molecules and shRNA-mediated protein knockdown approaches to identify signaling molecule participants. Finally, to determine if extracellular and transmembrane segment domain composition of the ITAM-containing phagocytic receptor affects cross-talk regulation, I tested IpLITR 1.1b WT_{CYT}-mediated down-regulation against IpLITR 2.6b/IpFcR γ -L WT_{CYT}, a stimulatory chimeric receptor construct used previously (4, 5, 7). In contrast to the ITAM-containing IpFcR γ -L WT_{CYT} phagocytic receptor used thus far, the IpLITR 2.6b/IpFcR γ -L WT_{CYT} phagocytic receptor construct contains the two extracellular domains (i.e. D1 and D2) of IpLITR 2.6b fused to the ITAM-containing adaptor molecule IpFcR γ -L.

Four key past observations led to the formulation of the molecular hypotheses tested in this chapter. First, data from chapter IV showed that Csk and SHP2 were recruited to the membrane

proximal CYT Y⁴⁵³ and distal CYT ITIM Y⁴⁷⁷ of IpLITR 1.1b WT_{CYT}, respectively. Second, data from chapter V showed that IpLITR 1.1b WT_{CYT}-mediated down-regulation of phagocytosis occurs via independent membrane proximal and distal CYT segment-mediated mechanisms. Third, ITIMs mediate SHP-dependent negative cross-talk mechanisms in mammals. Lastly, IpLITR 1.1b WT_{CYT} is known to completely inhibit NK cell-mediated cytotoxicity using distinct membrane proximal and distal CYT-dependent mechanisms via Csk and SHP1/2 pathways, respectively. Therefore, I predicted that IpLITR 1.1b WT_{CYT} uses a membrane proximal Y⁴⁵³ Csk-dependent mechanism and a membrane distal CYT ITIM Y⁴⁷⁷ SHP2-dependent mechanism that may both contribute to the down-regulation of IpFcR γ -L WT_{CYT}-driven phagocytosis (outlined in Figure 6.2). Results presented in this chapter extended previous functional and biochemical characterizations of IpLITR 1.1b WT_{CYT} immunoregulatory biology. Here I demonstrate a novel inhibitory function that relies on co-operative CYT segment-dependent signaling capabilities to down-regulate phagocytosis. Specifically, I show that IpLITR 1.1b WT_{CYT} requires co-operativity between the proximal CYT Y⁴⁵³ and distal CYT ITIM Y⁴⁷⁷ motifs to optimally inhibit phagocytosis. While the distal CYT ITIM Y⁴⁷⁷-dependent mechanism partially operates through SHP2, the proximal CYT Y⁴⁵³-dependent mechanism is Csk-independent. Furthermore, at relatively “high” expression levels, IpLITR 1.1b WT_{CYT} synergistically inhibits IpLITR 2.6b/IpFcR γ -L WT_{CYT}-driven phagocytosis using Y⁴⁵³- and Y⁴⁷⁷-dependent co-operative pathways. Overall, these data demonstrate a novel down-regulatory signaling capability of IpLITR 1.1b WT_{CYT} that requires co-operating CYT segment-dependent signaling pathways. This has expanded our understanding of evolutionarily conserved immunoregulatory receptor signaling potential across vertebrate lineages to include receptor cross-talk capabilities in teleost fish.

6.2 RESULTS

6.2.1 eGFP-tagged IpLITR 1.1b WT_{CYT} segments differentially modulate cross-talk inhibition of IpFcR γ -L WT_{CYT}-driven phagocytosis via proximal CYT Y⁴⁵³ and distal CYT ITIM Y⁴⁷⁷

To examine the specific CYT motifs of IpLITR 1.1b WT_{CYT} required for down-regulating phagocytosis, I transfected stable IpFcR γ -L WT_{CYT}-expressing cells with eGFP-tagged IpLITR 1.1b CYT YF mutant constructs. As shown in Figure 6.3A (eGFP positive cells), four IpLITR 1.1b CYT constructs show significantly reduced phagocytosis including IpLITR 1.1b WT_{CYT}-eGFP, Y^{prox}FCYT-eGFP, Y⁴⁵³FCYT-eGFP and Y⁴⁹⁹FCYT-eGFP with 17.5%, 24.7%, 15.3% and 23.5% phagocytic cells, respectively, compared to eGFP and IpLITR 1.1b MUT_{CYT}-eGFP. In addition, IpLITR 1.1b Y^{dist}FCYT-eGFP and Y⁴⁷⁷FCYT-eGFP constructs show reduced phagocytosis with 58.3% and 61.2%, respectively, compared to IpLITR 1.1b MUT_{CYT}-eGFP (73.1% phagocytic cells). Indexed data shows the same trends despite varying bead associations ranging from 45.3-71.0% (Figure 6.3B). Indexed data for eGFP negative cells (i.e. cells only expressing IpFcR γ -L WT_{CYT}) showed 91.1% phagocytic phenotype on average, with 85.6% phagocytic phenotype being the lowest (Figure 6.3C). The indexed data shows the same trends despite varying bead associations ranging from 46.5-59.9% (Figure 6.3D). Collectively, this data reveals that the IpLITR 1.1b proximal and distal CYT segments independently down-regulate phagocytic signaling, and that the distal CYT segment is as effective at abrogating phagocytosis as the WT_{CYT}.

6.2.2 Co-expressing IpLITR 1.1b Y^{dist}F_{CYT}-eGFP with dominant-negative Csk does not restore IpFcR γ -L WT_{CYT}-driven phagocytosis

To specifically test the Y⁴⁵³ Csk-dependent mechanism for IpLITR 1.1b WT_{CYT}-mediated down-regulation of phagocytosis, I co-expressed a truncated, dominant-negative FLAG-tagged Csk (Δ Csk) molecule with eGFP-tagged IpLITR 1.1b WT_{CYT} and IpLITR 1.1b Y^{dist}F_{CYT}. Each eGFP-tagged construct was co-transfected with empty p3XFLAG-CMV14 vector (EV) or Δ Csk. In eGFP positive cells, IpLITR 1.1b WT_{CYT}-eGFP showed 22.0% or 29.6% phagocytosis when co-transfected with EV or Δ Csk compared to 73.1% or 76.2% for IpLITR 1.1b MUT_{CYT}-eGFP, respectively (Figure 6.4A). To control for potential co-operating (i.e. ITIM-dependent) signaling through the distal CYT segment of IpLITR 1.1b WT_{CYT}, I tested a distal CYT mutant construct in which all distal segment motifs are mutated to phenylalanine (named IpLITR 1.1b Y^{dist}F_{CYT}-eGFP). When IpLITR Y^{dist}F_{CYT}-eGFP was co-transfected with EV or Δ Csk, cells showed 62.4% or 59.4% phagocytic phenotype, respectively. For comparison, eGFP only co-transfected with EV or Δ Csk showed 92.4% or 91.0% phagocytic phenotype, while IpLITR 1.1b MUT_{CYT}-eGFP cells displayed 73.1% or 76.2% phagocytosis, respectively (Figure 6.4A). The raw data used to calculate the indexed data is presented in Figure 6.4B. The range of bead association is 53.5-71.0%. Indexed data for eGFP negative (i.e. only IpFcR γ -L WT_{CYT} expressing) cells showed 90.4% phagocytic phenotype on average, with the lowest group at 86.2% phagocytic phenotype (Figure 6.4C). The raw data used to calculate the indexed data shows the same trends and varying bead associations ranging from 47.9-60.8% (Figure 6.4D). Altogether, no statistically significant increases between EV and Δ Csk were observed for any group. Overall, these results indicate that co-expressing IpLITR 1.1b WT_{CYT} or IpLITR 1.1b Y^{dist}F_{CYT} with a dominant-negative Csk does not restore phagocytosis.

To confirm the expression of Δ Csk used in the functional experiments described above, co-transfections were performed in duplicate and one well was lysed and probed with an α FLAG M2 mouse mAb to detect FLAG-tagged Δ Csk. While wild-type Csk contains an SH2 domain, an SH3 domain and a catalytic kinase domain for a total size of 50 kDa, Δ Csk is truncated after the SH3 domain (i.e. it does not contain a kinase domain). In each Δ Csk co-transfected lane, a band for Δ Csk is present at ~24 kDa (Figure 6.4E, top blot). To ensure the same amount of lysate was loaded in each lane, an anti- β -actin loading control is also shown (Figure 6.4E, bottom blot).

6.2.3 Co-expressing IpLITR 1.1b Y^{prox}F_{CYT} with dominant-negative SHP2 partially restores phagocytic signaling through IpFcR γ -L WT_{CYT}

To specifically test the Y⁴⁷⁷ SHP2-dependent mechanism for IpLITR 1.1b WT_{CYT}-mediated down-regulation of phagocytosis, I co-expressed a truncated, dominant-negative FLAG-tagged SHP2 (Δ SHP2) molecule with eGFP-tagged IpLITR 1.1b WT_{CYT} and IpLITR 1.1b Y^{prox}F_{CYT}. Each eGFP-tagged construct was co-transfected with empty p3XFLAG-CMV14 vector (EV) or Δ SHP2. In eGFP positive cells, IpLITR 1.1b WT_{CYT}-eGFP showed 22.0% or 29.0% phagocytic phenotype when co-transfected with EV or Δ SHP2 compared to 73.1% or 77.3% for IpLITR 1.1b MUT_{CYT}-eGFP, respectively (Figure 6.5A). To control for potential co-operating (i.e. Y⁴⁵³-dependent) signaling via the proximal CYT segment of IpLITR 1.1b WT_{CYT}, I tested a proximal CYT segment mutant construct (i.e. all proximal segment tyrosines mutated to phenylalanine; IpLITR 1.1b Y^{prox}F_{CYT}-eGFP). When IpLITR 1.1b Y^{prox}F_{CYT}-eGFP was co-transfected with EV or Δ SHP2, cells displayed 30.0% or 52.2% phagocytic phenotype, respectively (Figure 6.5A). For comparison, eGFP only co-transfected with EV or Δ SHP2 displayed 92.4% or 93.0% phagocytic phenotype, while IpLITR 1.1b MUT_{CYT}-eGFP cells showed 73.1% and 77.3% phagocytosis, respectively (Figure 6.5A). The indexed data was

calculated from the raw data presented in Figure 6.5B. The range of bead association is 51.7-71.0%. Indexed data for eGFP negative (i.e. only IpFcR γ -L WT_{CYT} expressing) cells showed 91.7% phagocytic phenotype on average, with 88.1% phagocytosis in the lowest group (Figure 6.5C). Raw data that was used to calculate indexed data displayed bead associations ranging from 45.5-60.8% (Figure 6.5D). Taken together, when co-inhibitory signals through the proximal CYT segment are absent (i.e. in IpLITR 1.1b Y^{prox}F_{CYT}-eGFP co-expressing cells), Δ SHP2 partially restores phagocytic signaling through IpFcR γ -L WT_{CYT}. A statistically significant difference (indicated by 'g') was observed in Figure 6.5A, where IpLITR 1.1b Y^{prox}F_{CYT} cells co-expressing EV or Δ SHP2 show 30.0% or 52.2% phagocytosis, respectively. Overall, these results indicate that co-expressing IpLITR 1.1b Y^{prox}F_{CYT} with a dominant-negative SHP2 partially restores phagocytosis.

To confirm the expression of Δ SHP2, duplicate co-transfections provided an additional well that was lysed and probed with an α FLAG M2 mouse mAb to detect FLAG-tagged Δ SHP2. Wild-type SHP2 contains two SH2 domains linked to a catalytic phosphatase domain for a total size of 50 kDa. Δ SHP2 is truncated after the second SH2 domain (i.e. it does not contain the phosphatase domain). In each Δ SHP2 co-transfected lane, a band for Δ SHP2 is present at ~28 kDa (Figure 6.5E, top blot). To ensure the same amount of lysate was loaded in each lane, an anti- β -actin loading control is also shown (Figure 6.5E, bottom blot).

6.2.4 Csk knockdown does not reverse IpLITR 1.1b WT_{CYT}-mediated cross-talk inhibition of IpFcR γ -L WT_{CYT}-driven phagocytosis

To specifically test the role of Csk in IpLITR 1.1b WT_{CYT}-mediated down-regulation of phagocytosis, I transfected eGFP-tagged IpLITR 1.1b WT_{CYT} and IpLITR 1.1b Y^{dist}F_{CYT} into Csk deficient IpFcR γ -L WT_{CYT}-expressing cell lines. Each eGFP-tagged construct was

transfected into scramble (i.e. non-targeted) or Csk-targeted knockdown (KD) cell lines. IpLITR 1.1b WT_{CYT}-eGFP positive cells displayed 26.5% and 29.3% phagocytosis in scramble and KD cells, respectively (Figure 6.6A). To control for potential co-operating (i.e. ITIM-dependent) signaling through the distal CYT segment of IpLITR 1.1b WT_{CYT}, I also transfected cells with a distal CYT segment mutant construct in which all distal segment motifs are mutated to phenylalanine (IpLITR 1.1b Y^{dist}_{FCYT}-eGFP). IpLITR 1.1b Y^{dist}_{FCYT}-eGFP transfected scramble or KD cells showed 67.2% and 57.1% phagocytic phenotype, respectively. EGFP only transfected scramble and KD cells showed 88.3% and 87.7% phagocytic phenotype, while IpLITR 1.1b MUT_{CYT}-eGFP cells displayed 73.1% and 76.2% phagocytosis, respectively (Figure 6.6A). The raw data used to calculate indexed data is presented in Figure 6.6B, which also shows bead associations between 59.7-68.4%. Indexed data for eGFP negative (i.e. only express IpFcR γ -L WT_{CYT}) cells showed 93.2% phagocytic phenotype on average, with the lowest group at 89.4% phagocytic phenotype (Figure 6.6C). Raw data used to calculate indexed data shows the trends and varying bead associations ranging from 47.9-60.8% (Figure 6.6D). Collectively, no statistically significant increases in phagocytosis when comparing KD vs. scramble control cells were observed for any group. Altogether, reduced expression of Csk does not reverse IpLITR 1.1b WT_{CYT}-mediated cross-talk inhibition of IpFcR γ -L WT_{CYT}-driven phagocytosis.

To determine the relative knockdown levels (i.e. loss of expression) of Csk protein, stable knockdown cell lines were lysed and probed with a rabbit α Csk polyclonal antibody. Expected bands for Csk were observed at 50 kDa and are significantly dimmer in KD lanes (Figure 6.6E, top blot). Densitometric values normalized to an anti- β -actin loading control (Figure 6.6E, bottom blot) show 9% of scramble control Csk in KD lanes, indicating a Csk protein expression reduction of >90% (Figure 6.6F).

6.2.5 SHP2 knockdown partially reverses IpLITR 1.1b WT_{CYT}-mediated cross-talk inhibition of IpFcR γ -L WT_{CYT}-driven phagocytosis

To examine the role of SHP2 in IpLITR 1.1b WT_{CYT}-mediated down-regulation of phagocytosis, I transfected eGFP-tagged IpLITR 1.1b WT_{CYT} and IpLITR 1.1b Y^{prox}FCYT into stable SHP2 deficient IpFcR γ -L WT_{CYT}-expressing cell lines. Each eGFP-tagged construct was transfected into scramble (i.e. non-targeted) or SHP2-targeted knockdown (KD) cell lines. IpLITR 1.1b WT_{CYT}-eGFP positive cells showed 26.5% and 42.2% phagocytosis in scramble and KD cells, respectively (Figure 6.7A). To control for potential co-operating (i.e. Y⁴⁵³-dependent) signaling through the proximal CYT segment of IpLITR 1.1b WT_{CYT}, I transfected cells with a proximal CYT segment mutant construct in which all proximal segment motifs are converted to phenylalanine (IpLITR 1.1b Y^{prox}FCYT-eGFP). When IpLITR 1.1b Y^{prox}FCYT-eGFP was transfected into scramble or KD cells, 31.6% and 44.7% of cells displayed a phagocytic phenotype, respectively. EGFP only-transfected scramble and KD cells showed 88.3% and 91.2% phagocytic phenotype, while IpLITR 1.1b MUT_{CYT}-eGFP cells showed 87.7% and 82.7% phagocytosis, respectively (Figure 6.7A). The raw data used to calculate indexed data is presented in Figure 6.7B and also shows bead associations ranging from 52.2%-70.9%. Indexed data for eGFP negative (i.e. only express IpFcR γ -L WT_{CYT}) cells showed 92.6% phagocytic phenotype on average with 89.4% in the lowest group (Figure 6.7C). The raw data used to calculate indexed data shows the same trends within receptor groups while bead associations varied from 43.5-65.1% (Figure 6.7D). Collectively, although no statistically significant increases were calculated when comparing KD vs. scramble control cells for any receptor group, SHP2 KD cells clearly display similarly increased % phagocytic cell trends. Specifically, IpLITR 1.1b WT_{CYT}-eGFP expressing scramble and KD cells display increased phagocytosis at 26.5%

and 42.2%, respectively (Figure 6.7A). Similarly, IpLITR Y^{prox}FCYT-eGFP expressing scramble and KD cells also display increased phagocytosis at 31.6% and 44.7%, respectively (Figure 6.7A). Altogether, this may indicate that SHP2 knockdown partially reverses IpLITR 1.1b WT_{CYT}-mediated cross-talk inhibition of IpFcR γ -L WT_{CYT}-driven phagocytosis.

To confirm the knockdown (i.e. loss of expression) of SHP2 protein, stable knockdown cell lines were lysed and probed with a rabbit α SHP2 mAb. Expected bands for SHP2 were observed at 70 kDa and are much dimmer in KD lanes (Figure 6.7E, top blot). Densitometric values normalized to an anti- β -actin loading control (Figure 6.7E, bottom blot) show 9% of scramble control SHP2 in KD lanes, indicating a >90% reduction in SHP2 protein expression (Figure 6.7F).

6.2.6 Effect of receptor expression levels on eGFP-tagged IpLITR 1.1b WT_{CYT}-mediated cross-talk inhibition of IpLITR 2.6b/IpFcR γ -L WT_{CYT}-driven phagocytosis

To determine the potential effect of receptor expression levels on IpLITR 1.1b WT_{CYT}-mediated down-regulation of IpLITR 2.6b/IpFcR γ -L WT_{CYT}-driven phagocytosis (outlined in Figure 6.8), I transiently transfected eGFP-tagged IpLITR 1.1b CYT constructs into stable IpLITR 2.6b/IpFcR γ -L WT_{CYT}-expressing cells. Figure 6.9 shows data for average (avg; i.e. all eGFP positive gated cells), low (lo), middle (mid) and high (hi)-level eGFP expressing cell populations. Both IpLITR 1.1b WT_{CYT}-eGFP and IpLITR 1.1b MUT_{CYT}-eGFP co-expressing cells show an eGFP fluorescence-dependent response as increasing fluorescence correlates with decreasing % phagocytic phenotype. Indexed data shows 93.5%, 92.3%, 94.6% and 93.4% phagocytic cells for average-, low-, middle- and high-level eGFP only-expressing cells, respectively (Figure 6.9A). IpLITR 1.1b WT_{CYT}-eGFP-expressing cells display 57.3% phagocytic cells at average-level eGFP expression while 73.0%, 53.7% and 29.4% are

phagocytic as fluorescence increases. For IpLITR 1.1b MUT_{CYT}-eGFP-expressing cells, 73.8% are phagocytic at average-level eGFP while 81.5%, 74.9% and 67.0% are phagocytic as fluorescence increases (Figure 6.9A). Raw data used to calculate indexed data displays similar trends as 34.7% and 50.5% of cells are phagocytic for IpLITR 1.1b WT_{CYT}-eGFP and IpLITR 1.1b MUT_{CYT}-eGFP at average fluorescence, respectively, with decreasing % phagocytic phenotypes as fluorescence increases (Figure 6.9B).

The optimal eGFP expression level corresponds with the greatest difference between IpLITR 1.1b WT_{CYT}-eGFP and IpLITR 1.1b MUT_{CYT}-eGFP % phagocytic cells. The difference in % phagocytic cells at average-, low-, middle- and high-level eGFP expression for indexed data is 16.5%, 8.5%, 21.2% and 37.6%, respectively (Figure 6.9A). The difference in % phagocytic cells at average-, low-, middle- and high-level eGFP expression for raw data is 15.8%, 11.3%, 18.3% and 28.6%, respectively (Figure 6.9B). Taken together, this data indicates that high-level eGFP expression is optimal for measuring IpLITR 1.1b WT_{CYT}-mediated cross-talk inhibition of IpLITR 2.6b/IpFcR γ -L WT_{CYT}-driven phagocytosis.

6.2.7 eGFP-tagged IpLITR 1.1b WT_{CYT} segments synergistically down-regulate IpLITR 2.6b/IpFcR γ -L WT_{CYT}-driven phagocytosis through distinct CYT motif Y⁴⁵³- and Y⁴⁷⁷-dependent pathways

To examine the specific IpLITR 1.1b WT_{CYT} motifs involved in down-regulating IpLITR 2.6b/IpFcR γ -L WT_{CYT}-driven phagocytosis, I transfected eGFP-tagged IpLITR 1.1b CYT YF mutant constructs into stable IpLITR 2.6b/IpFcR γ -L WT_{CYT}-expressing cells. Figure 6.10A shows that for eGFP positive cells, IpLITR 1.1b WT_{CYT}-eGFP shows greatly reduced phagocytosis at 29.4%. Three constructs displaying the next greatest reductions in phagocytosis are IpLITR 1.1b Y^{prox}F_{CYT}-eGFP, Y⁴⁵³F_{CYT}-eGFP and Y⁴⁹⁹F_{CYT}-eGFP at 44.4%, 47.8% and

38.2%, respectively. Next, IpLITR 1.1b Y^{dist}FCYT-eGFP and Y⁴⁷⁷FCYT-eGFP constructs show slightly reduced phagocytic signaling at 56.3% and 59.6%, respectively, compared to IpLITR 1.1b MUT_{CYT}-eGFP at 67.0% phagocytic cells (Figure 6.10A). Importantly, a close inspection of these data reveal that relative to IpLITR 1.1b MUT_{CYT}-eGFP, IpLITR 1.1b Y^{prox}FCYT-eGFP and Y⁴⁵³FCYT-eGFP reduce phagocytosis by 22.6% and 19.2% and IpLITR 1.1b Y^{dist}FCYT-eGFP and Y⁴⁷⁷FCYT-eGFP reduce phagocytosis by 10.7% and 7.4%, respectively. Taken together, the predicted reduction in phagocytosis for IpLITR 1.1b WT_{CYT}-eGFP by the additive effects of the membrane proximal CYT Y⁴⁵³ and membrane distal CYT ITIM Y⁴⁷⁷ should be 26.6% (i.e. 19.2% + 7.4%). However, IpLITR 1.1b WT_{CYT}-eGFP reduced phagocytosis by 37.6% relative to IpLITR 1.1b MUT_{CYT}-eGFP, showing a more than additive (i.e. synergistic) inhibitory effect. Similar trends in the raw data used to calculate indexed data are evident along with varying bead associations ranging from 50.1-68.4% (Figure 6.10B). In comparison, indexed data for cells that were eGFP negative (i.e. only express IpLITR 2.6b/IpFcR γ -L WT_{CYT}) are on average 93.2% phagocytic, with a low of 91.6% phagocytic phenotype (Figure 6.10C). Raw data used to calculate indexed data shows the same trends despite varying bead associations ranging from 50.5-56.5% (Figure 6.10D). Altogether, these data show that IpLITR 1.1b WT_{CYT} segments synergistically down-regulate ITAM-driven phagocytosis through IpLITR 2.6b/IpFcR γ -L WT_{CYT}.

6.3 DISCUSSION

In this chapter, I characterized the molecular requirements of IpLITR 1.1b WT_{CYT}-mediated down-regulation of IpFcR γ -L WT_{CYT}-driven phagocytosis. My results demonstrate that IpLITR 1.1b WT_{CYT} mediates down-regulation using a co-operative membrane proximal CYT Y⁴⁵³- and distal CYT ITIM Y⁴⁷⁷-dependent mechanism(s). In addition, dominant negative and

signaling molecule knockdown approaches demonstrated that SHP2 plays a partial role via the membrane distal CYT ITIM Y⁴⁷⁷. Furthermore, “high” expression of IpLITR 1.1b WT_{CYT} is capable of optimally inhibiting IpLITR 2.6b/IpFcR γ -L WT_{CYT}-driven phagocytic signaling when both CYT segments are intact. Overall, I have revealed a novel signaling capability of IpLITR 1.1b WT_{CYT} involving the co-operative proximal and distal CYT-dependent cross-talk down-regulation of ITAM-driven phagocytosis.

Mammalian studies have provided molecular details of CYT ITIM-dependent down-regulation of ITAM-driven phagocytosis through the dephosphorylation of downstream targets by cytoplasmic phosphatases. For example, phosphorylated SIRP α recruits SHP1 and down-regulates macrophage-mediated phagocytosis of red blood cells and platelets. In total, SIRP α contains 3 CYT ITIMs, but the specific CYT ITIM responsible for down-regulating phagocytosis is not known (374, 375, 413). Despite this lack of molecular detail, downstream targets for inhibitory signaling have been revealed. Active SHP1 targets phagocytic effector molecules myosin IIA in macrophages (414) and paxillin and cofilin in microglia (415) for dephosphorylation resulting in the inhibition of phagocytosis. In another well-studied example, Fc γ RIIB contains a single CYT ITIM that recruits SHP1. When co-cross-linked with the phagocytic Fc γ RIIA, activated SHP1 recruited to Fc γ RIIB dephosphorylates both the Fc γ RIIA ITAM and Syk, resulting in the inhibition of phagocytosis (376–378). While both of these studies focus on CYT ITIM SHP1-dependent mechanisms, my data demonstrate a specific CYT ITIM Y⁴⁷⁷ SHP2-dependent down-regulation of ITAM-driven phagocytosis. However this mechanism does not mediate IpLITR 1.1b WT_{CYT} down-regulation alone, because complete recovery of phagocytic signaling was not observed in IpLITR 1.1b Y⁴⁷⁷F_{CYT} mutant construct,

Δ SHP2 nor SHP2 knockdown experiments (Figure 6.3, Figure 6.5 and Figure 6.7). Taken together, this indicates that co-inhibitory proximal CYT-dependent signals are involved.

A co-inhibitory signaling mechanism is suspected to play a role in IpLITR 1.1b WT_{CYT}-mediated inhibition of phagocytosis through membrane proximal CYT Y⁴⁵³-dependent Csk recruitment. While the mammalian IgSF immunoregulatory receptors LILRB1 (416) and LAIR1 (417) are known to recruit Csk, a direct role for Csk downstream of immunoregulatory receptor-mediated regulation of phagocytosis has never been shown. A closely related study reported that Csk differentially down-regulates phagocytosis in mouse macrophages exposed to non-opsonized zymosan (i.e. a fungal PAMP), complement-opsonized zymosan and *E. coli* targets via pathways downstream of mannose-fucose/ β -glucan receptors, complement receptor 3 receptor and CD14, respectively (251). Csk partially down-regulates phagocytosis of non-opsonized zymosan, with only marginal effects on complement-opsonized zymosan and *E. coli* targets. Since non-opsonized zymosan binds mannose-fucose/ β -glucan receptors and several of these receptors are co-expressed on mouse macrophages, receptor CYT requirements of a more specific pathway cannot be compared to IpLITR 1.1b WT_{CYT}. Interestingly, Csk-dependent mechanisms for immune evasion by bacteria involve the EPIYA/G motif-containing family of effector proteins (404). Two particular effectors, LspA from *Haemophilus ducreyi* and CagA from *Helicobacter pylori*, are phosphorylated within mammalian cells allowing them to bind and activate Csk. This leads to inactivation of SFKs and inhibition of Fc γ R-mediated phagocytosis (418). In fact, the prevalence of bacterial effectors that are phosphorylated within mammalian cells lead to the discovery of endogenous EPIYA/G motif-containing proteins in mammals. For example, phosphorylated pragmin activates an EPIYA/G motif, Csk-dependent pathway that regulates SFKs (419) and plays a role in oncogenesis and metastasis (420). In agreement with

these examples, an IpLITR 1.1b Y^{dist}_{FCYT} mutant that can bind Csk partially down-regulates phagocytosis. Notably though, dominant-negative (DN) Δ Csk and Csk knockdown did not restore phagocytosis, indicating that alternative Y⁴⁵³-dependent mechanisms must be operating. Before discussing IpLITR 1.1b WT_{CYT}-mediated down-regulatory mechanisms, a number of important caveats regarding the molecular techniques used here must be considered.

Two designs for DN molecules include truncated (Δ) and catalytically inactive constructs. Since regions of the signaling molecule outside of the catalytic domain may be important for propagating signaling or stabilizing a signaling complex, Δ molecules may not be able to restore signaling not because the enzyme plays a role, but because they are prematurely displaced from the signaling complex (421). Since AD293 cells do not express SHP1 (which can bind IpLITR 1.1b WT_{CYT}; 6, 188), this may explain why Δ SHP2 in my experiments was less effective at restoring phagocytosis than the SHP2 KDs. In particular, IpLITR 1.1b WT_{CYT}-eGFP expressing cells show a 7% and 16% increase in phagocytosis compared to control in dominant-negative and knockdown experiments, respectively (Figure 6.5A and Figure 6.7A). Furthermore, IpLITR 1.1b Y^{dist}_{FCYT} and Y⁴⁷⁷_{FCYT} constructs (i.e. only contain one functional inhibitory motif, Y⁴⁵³) show slight inhibitory function (Figure 6.3). Since Y⁴⁵³ is known to bind Csk (Figure 4.13B; 6), this indicates that Csk may play a role in IpLITR 1.1b WT_{CYT} down-regulation of phagocytosis, however the DN Δ Csk used here did not restore phagocytosis in support of this hypothesis. To help mitigate these caveats, catalytically inactive DN constructs should be tested because full-length molecules better preserve binding affinity and kinetics of wild-type molecules, but in their absence, I used a complementary shRNA-mediated knockdown approach to assess specific signaling molecule involvement.

The removal of protein expression is a convincing method for assessing their critical signaling roles because the absence of a critical signaling molecule stalls signaling and halts all major pathways (i.e. catalytic and scaffolding) operating via said signaling protein. In my experiments, this would cause frustrated or incomplete internalization which results in partially engulfed, surface-exposed target beads. Csk knockdown data do not support any role for Csk operation during IpLITR 1.1b WT_{CYT}-mediated down-regulation of phagocytosis (Figure 6.6). SHP2 knockdown data on the other hand, did show trends towards restoration of phagocytosis compared to scramble controls for both IpLITR 1.1b WT_{CYT} and Y^{prox}F_{CYT} constructs (Figure 6.7). This indicates Csk does not operate downstream of a membrane proximal CYT-dependent mechanism. In addition, SHP2 plays a partial role in IpLITR 1.1b WT_{CYT}-mediated down-regulation of phagocytosis through a membrane distal CYT segment-dependent mechanism.

To summarize, my data support independent IpLITR 1.1b WT_{CYT}-mediated membrane proximal and distal CYT segment mechanisms that may differentially down-regulate ITAM-driven phagocytosis but are most effective when co-operating. Specifically, the membrane distal CYT ITIM Y⁴⁷⁷ is predominantly responsible for inhibiting phagocytosis but, SHP2 only plays a partial role. In addition, the proximal CYT segment contributes signals through Y⁴⁵³ that inhibit phagocytosis, but these signals are independent of Csk. This differs from previous characterizations of IpLITR 1.1b WT_{CYT} that showed both segments completely inhibit NK cell-mediated cytotoxicity using Csk or SHP1/2 pathways. Instead, my data indicate that IpLITR 1.1b WT_{CYT} Y⁴⁵³ and Y⁴⁷⁷ co-operate for maximum inhibition of ITAM-driven phagocytosis. However, a proximal CYT Y⁴⁵³-dependent, Csk-independent mechanism can reduce phagocytosis only slightly while a distal CYT ITIM Y⁴⁷⁷-dependent mechanism drastically

reduces phagocytosis using SHP2 and (an)other molecule(s). An examination of IpLITR 1.1b WT_{CYT} motifs reveals a consensus SHIP binding motif at Y⁴⁷⁷ (422).

My molecular assessments so far have focused on CYT-mediated cross-talk mechanisms, because standardized receptor constructs used thus far contain four identical extracellular domains and a common TM segment but varied CYT compositions. However, since phagocytic receptors typically possess one or two extracellular domains, I characterized the molecular effect(s) of extracellular domain number and TM segment compositions on the cross-talk down-regulation of phagocytosis. Specifically, I tested IpLITR 1.1b WT_{CYT}-mediated cross-talk inhibition of IpLITR 2.6b/IpFcR γ -L WT_{CYT}-driven phagocytic signaling. Importantly, IpLITR 2.6b/IpFcR γ -L WT_{CYT} contains two extracellular domains fused to a TM-neutral endogenous IpFcR γ -L adaptor molecule as opposed to the four extracellular domains and TM segment of wild-type IpLITR 1.1b (outlined in Figure 6.8). This strategy better represents receptor co-cross-linking in a physiological phagocytic synapse because phagocytic receptors like Fc γ RIIA, CEACAM3 and dectin1 contain one or two extracellular domains. IpLITR 1.1b WT_{CYT} displayed identical motif requirements, although inhibition was not as great in general, against IpLITR 2.6b/IpFcR γ -L WT_{CYT} as seen previously (compare Figure 6.3 and Figure 6.10). Interestingly, a higher IpLITR 1.1b WT_{CYT} expression level was required to optimize inhibitory signaling against IpLITR 2.6b/IpFcR γ -L WT_{CYT}. This indicates that greater inhibitory signaling is required to shut off IpLITR 2.6b/IpFcR γ -L WT_{CYT}-driven phagocytosis. While IpLITR 1.1b WT_{CYT} does not dimerize (3), an ability for IpLITR 2.6b/IpFcR γ -L WT_{CYT} to dimerize has not been tested but this receptor must bring targets closer to the cell membrane. If the IpLITR 2.6b/IpFcR γ -L WT_{CYT} can form dimers, increased inhibitory signaling may be required to shut down phagocytic signaling because dimers display relatively lower dissociation constants (423).

Simultaneously, two extracellular domain-containing phagocytic receptors hold targets closer to the cell membrane. This proximity physically excludes large extracellular domain-containing proteins from the synapse (399, 400). In this case, the four Ig-like domain-containing IpLITR 1.1b WT_{CYT} may be excluded from the phagocytic synapse formed by the two Ig-like domain-containing IpLITR 2.6b/IpFcR γ -L WT_{CYT}. It is also important to note that phagocytic signaling proceeded for 30 min (for IpLITR 2.6b/IpFcR γ -L WT_{CYT}) or 40 min (for IpFcR γ -L WT_{CYT}) in my experiments. This approach measures a functional endpoint because at these timepoints signaling dynamics have likely reached completion. As such, my experiments do not assess signaling through SHP2 and Csk during earlier stages of phagocytosis. If their inhibitory signaling has been de-activated, cells may complete the internalization process resulting in the partial phagocytic phenotypes I observed. As such, a time course including 10, 20 and 30 min may show dynamic inhibitory signaling profiles.

Finally, before extending the implications of my data to account for temporal signaling dynamics of phagocytosis, an important question regarding receptor dynamics in my system must be re-visited. Are co-cross-linked IpLITRs able to re-organize during phagocytic signaling? Although antibody-mediated co-cross-linking likely prevents receptor re-organization, an accurate answer to this question is not available. Therefore, I am proposing two conclusions regarding the temporal mechanisms of IpLITR 1.1b WT_{CYT}-mediated down-regulation of ITAM-driven phagocytosis implied by my data. One conclusion assumes receptor re-organization during phagocytic signaling and the other assumes the opposite. If IpLITR 1.1b WT_{CYT} is able to re-organize, then the proximal and distal CYT segments of IpLITR 1.1b co-operate to sustain inhibitory signaling, in part, by maintaining IpLITR 1.1b WT_{CYT} within the phagocytic synapse while all mutant constructs are eventually displaced. This explains why IpLITR 1.1b WT_{CYT}

displays complete inhibition against IpLITR 2.6b/IpFcR γ -L WT_{CYT} at the endpoint while no mutant constructs maintain complete inhibition. On the other hand, if receptors are not able to re-organize and therefore remain within the synapse, then the signaling complex formed by IpLITR 1.1b WT_{CYT} maintains active inhibitory signaling, while all mutant constructs eventually switch to permit phagocytic signaling. Further imaging and biochemical studies will be required to answer these hypotheses.

Overall, results of this chapter comprehensively demonstrate that IpLITR 1.1b WT_{CYT} activates a co-operative membrane proximal and distal CYT segment-dependent cross-talk signaling mechanism to down-regulate ITAM-driven phagocytosis. This represents the most detailed study of IpLITR signaling mechanisms and the first report of cross-talk signaling capabilities for any fish immunoregulatory receptors to date.

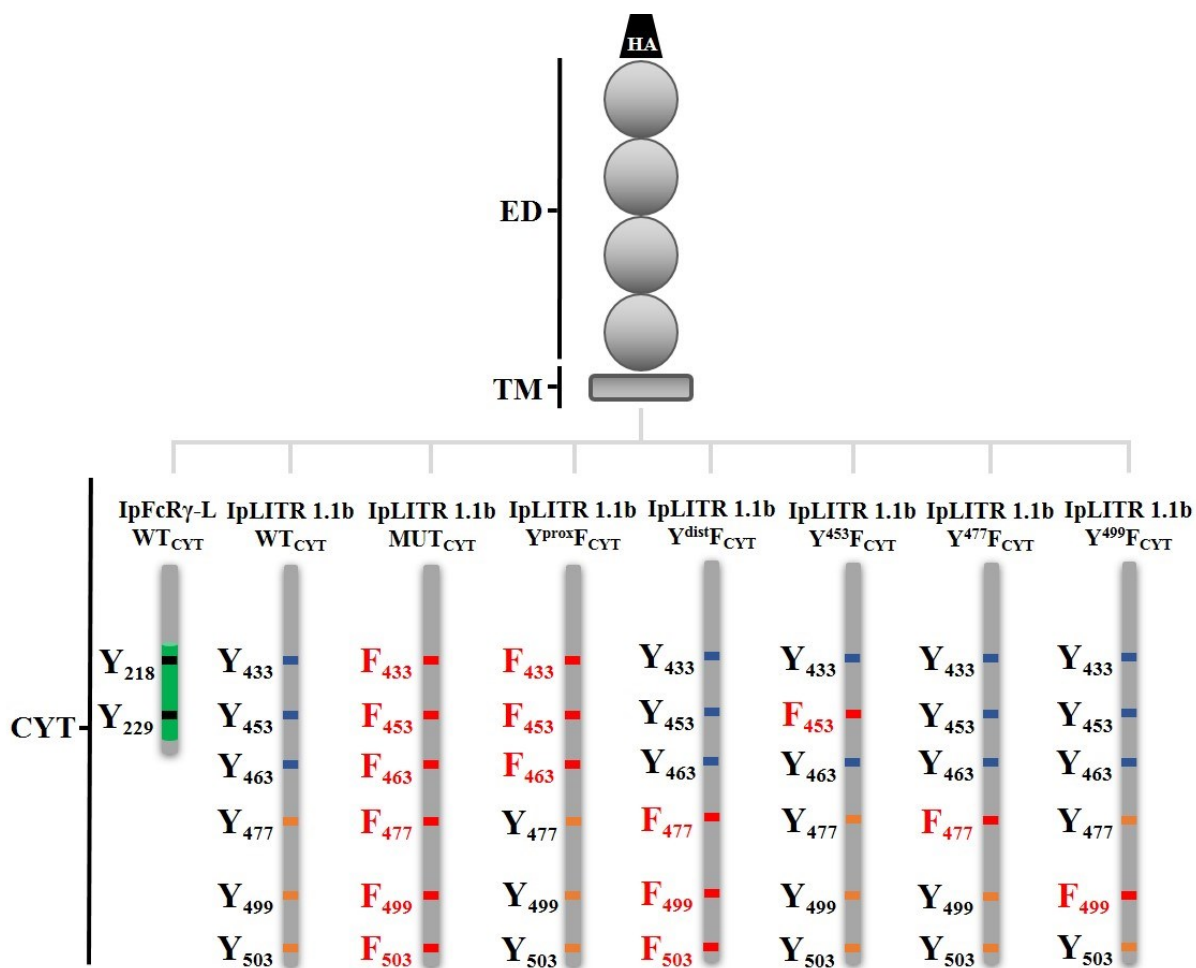


Figure 6.1. Schematic representations of 8 IpLITR cytoplasmic tail (CYT) constructs used in chapter VI. Standardized constructs contain an N-terminal hemagglutinin (HA) epitope tag; extracellular domains (ED) and transmembrane (TM) segments are derived from wild-type (WT) IpLITR 1.1b. Two WT constructs include an ITAM-containing IpFcR γ -L WT_{CYT} (green) and IpLITR 1.1b WT_{CYT}. Tyrosine (Y) to phenylalanine (F) mutant (red) constructs include IpLITR 1.1b MUT_{CYT}, IpLITR 1.1b Y^{prox}F_{CYT}, IpLITR 1.1b Y^{dist}F_{CYT}, IpLITR 1.1b Y⁴⁵³F_{CYT}, IpLITR 1.1b Y⁴⁷⁷F_{CYT} and IpLITR 1.1b Y⁴⁹⁹F_{CYT}.

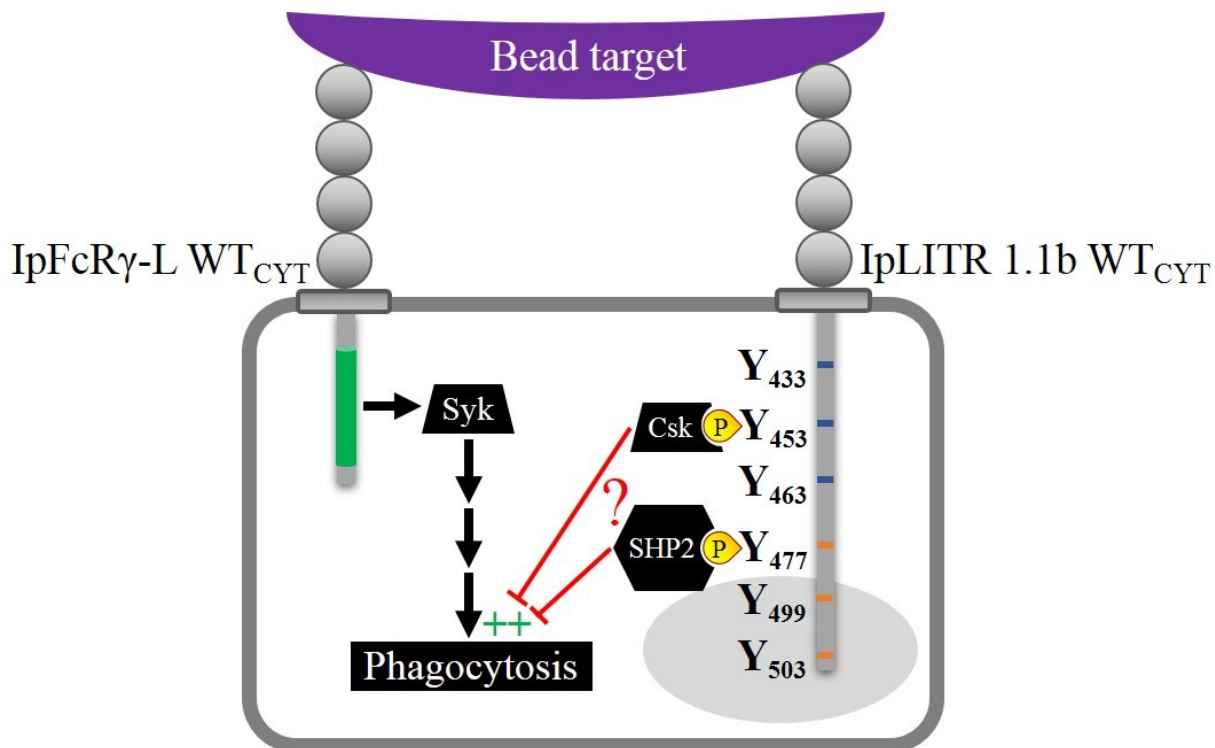
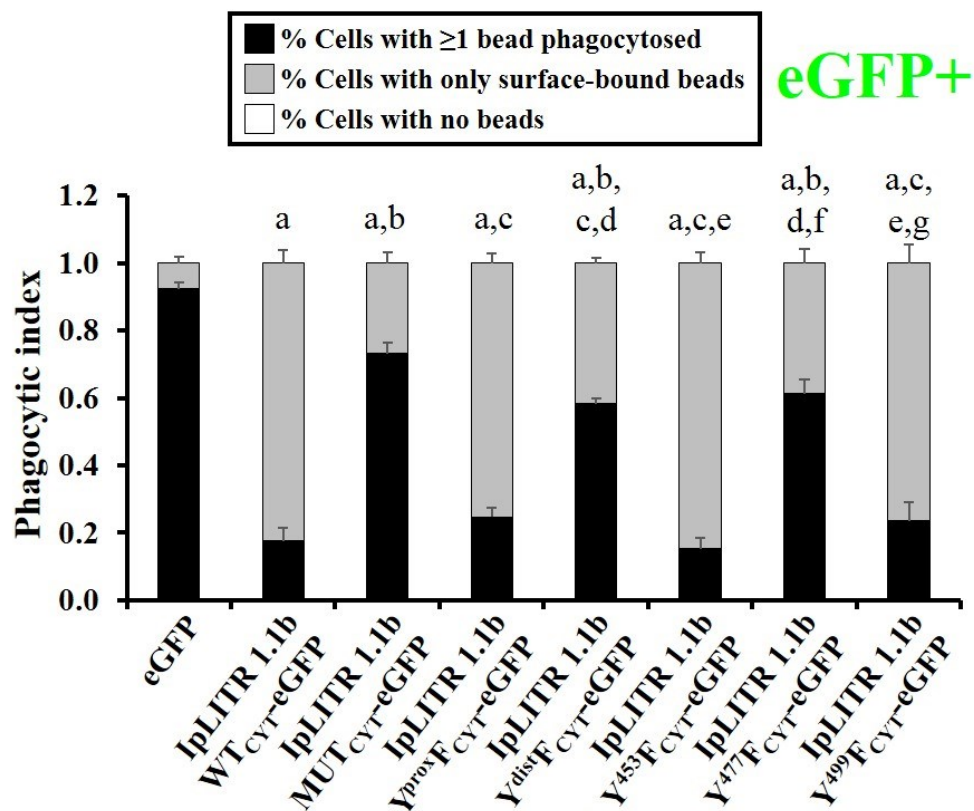
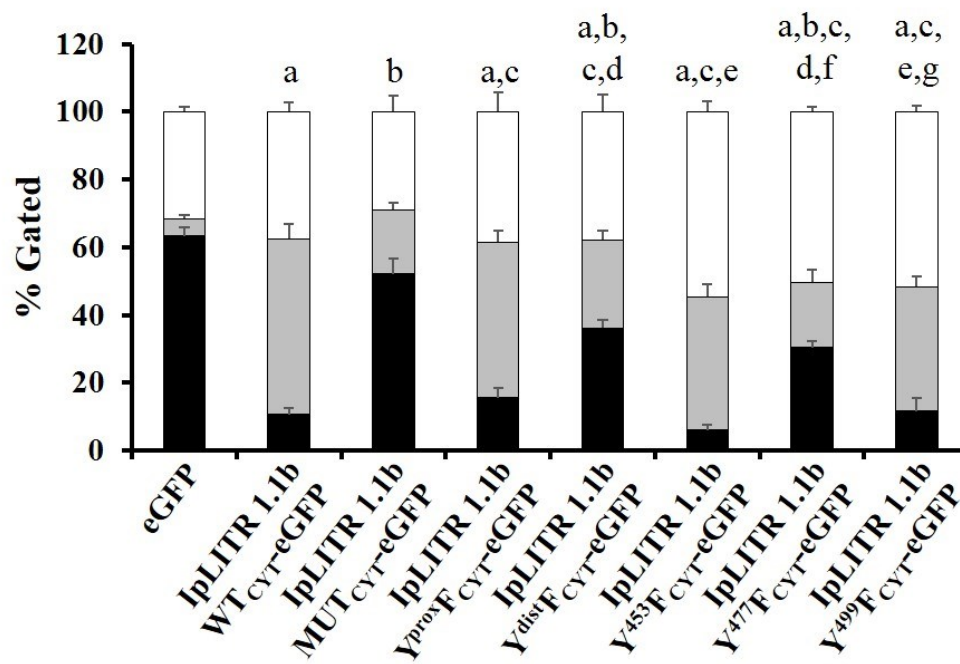


Figure 6.2. Schematic representation of IpLITR 1.1b WT_{CYT}-mediated mechanisms of cross-talk inhibition of IpFcR γ -L WT_{CYT}-driven phagocytic signaling explored in chapter VI.

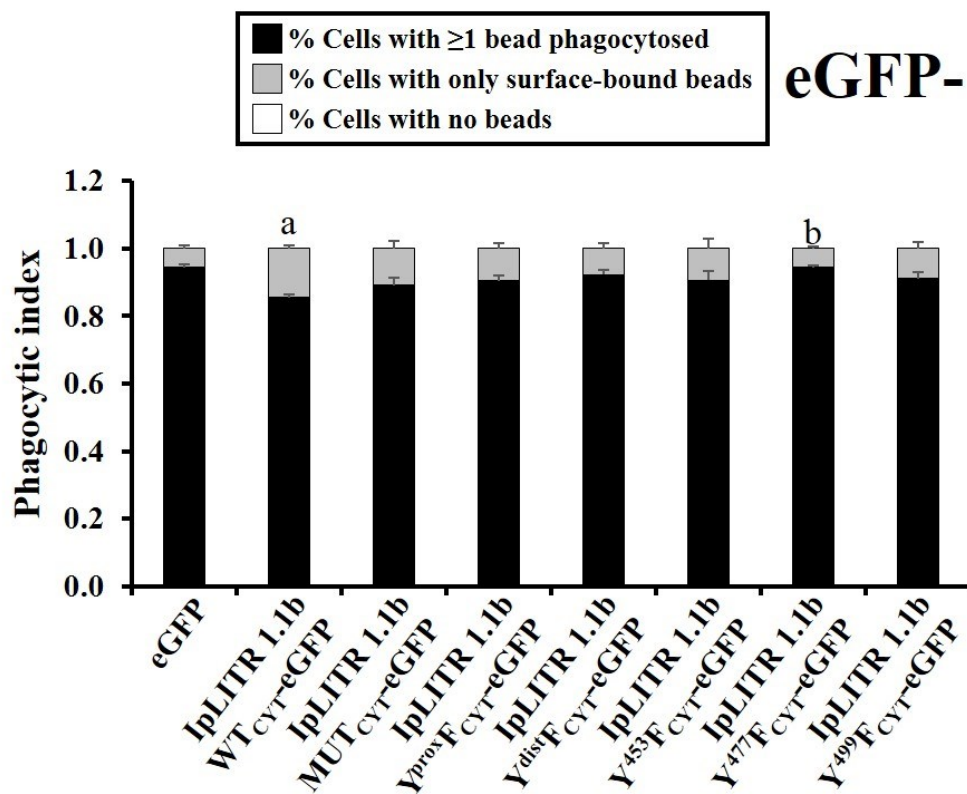
A.



B.



C.



D.

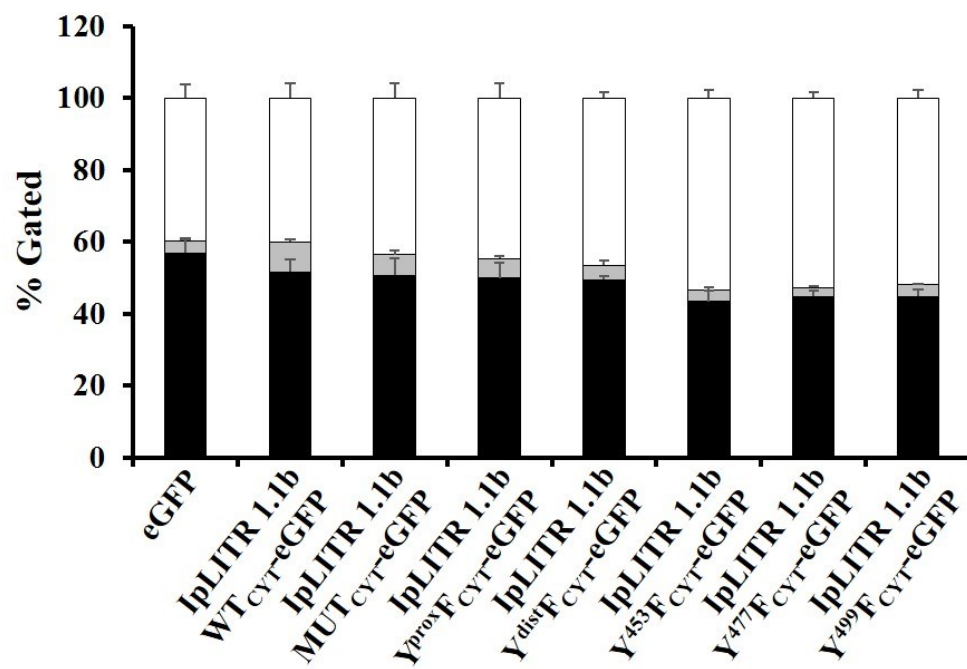
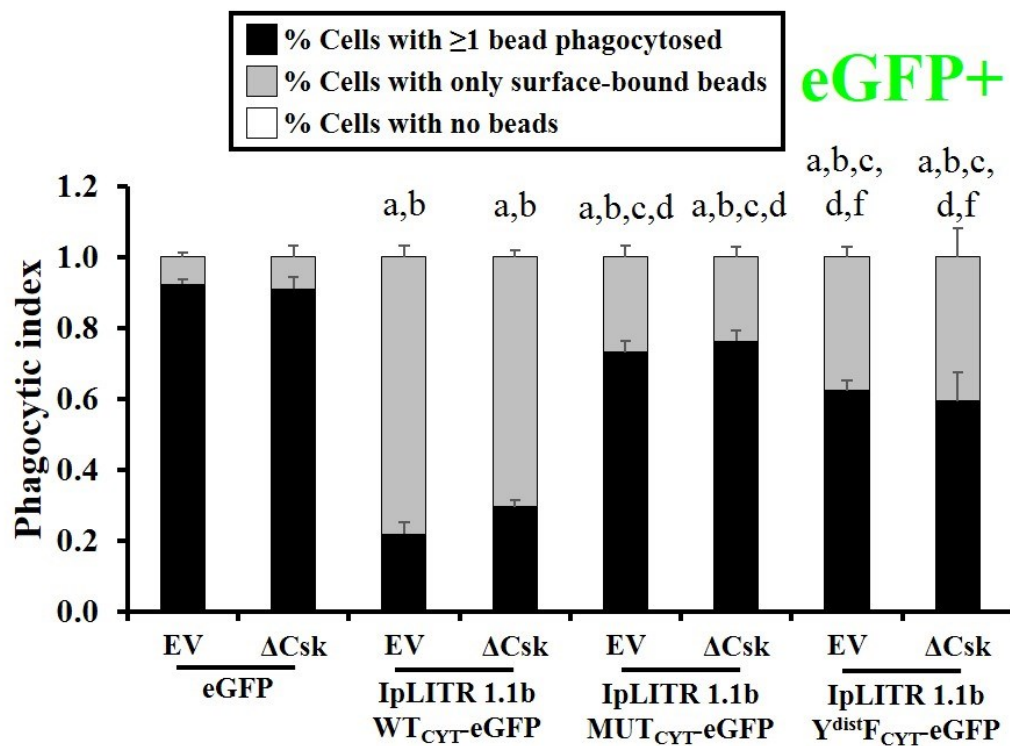
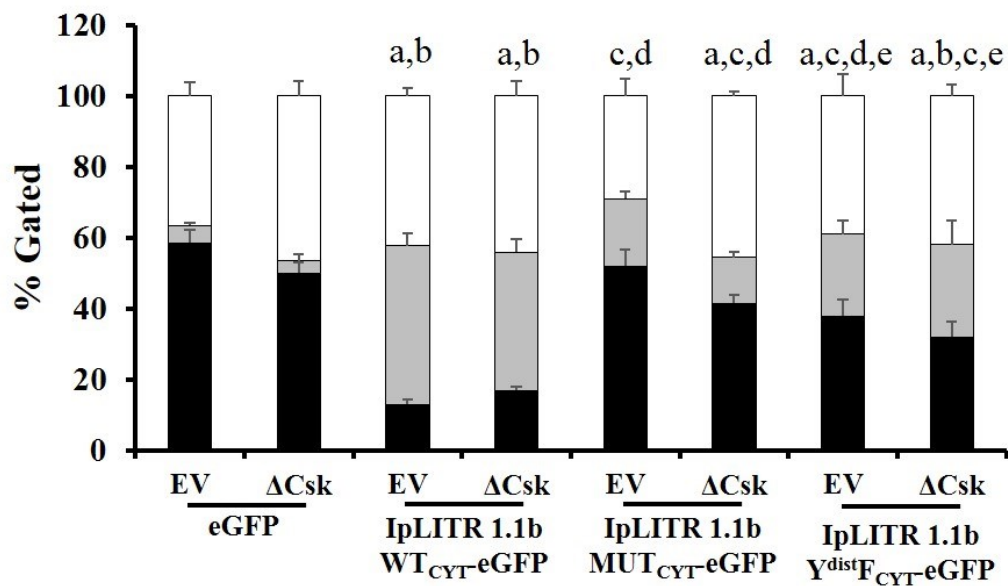


Figure 6.3. eGFP-tagged IpLITR 1.1b WT_{CYT} segments differentially modulate cross-talk inhibition of IpFcR γ -L WT_{CYT}-driven phagocytosis via proximal CYT Y⁴⁵³ and distal CYT ITIM Y⁴⁷⁷. pDisplay-encoded eGFP-tagged IpLITR 1.1b CYT YF mutant receptors were transfected into stable IpFcR γ -L WT_{CYT}-expressing AD293 cells for 48 h. Mouse α HA antibody-coated 3.5 μ m light yellow (LY) fluorescent beads were added to cells for 40 min at 37°C. Surface-bound LY beads were counter-stained with rabbit α -mouse AlexaFluor647-conjugated secondary antibody. Cells were harvested by trypsinization and fixed in 1% paraformaldehyde prior to data collection on the Image Stream^X MKII flow cytometer. Raw image files were subjected to a component masking analysis modified from Fei et al., (2017) that separates eGFP positive (eGFP+) and negative (eGFP-) cell populations. Each black bar represents the percentage of phagocytic cells (i.e. a cell with ≥ 1 bead fully internalized), grey bars represent the percentage of cells with only surface-bound beads (i.e. no beads internalized) and the white bars represent the percentage of cells with no associated beads (i.e. none bound or internalized). Results for (A and B) eGFP+ and (C and D) eGFP- cells are representative of the mean \pm SEM of at least three independent experiments as (A and C) indexed or (B and D) raw data. Phagocytic index was calculated as: % phagocytic or surface-bound cells / % total bead-associated cells. Lower case ‘a’, ‘b’, ‘c’, ‘d’, ‘e’, ‘f’ and ‘g’ represent statistically significant differences ($p < 0.05$) compared to eGFP, IpLITR 1.1b WT_{CYT}-eGFP, IpLITR 1.1b MUT_{CYT}-eGFP, IpLITR 1.1b Y^{prox}_{F_{CYT}}-eGFP, IpLITR 1.1b Y^{dist}_{F_{CYT}}-eGFP, IpLITR 1.1b Y⁴⁵³_{F_{CYT}}-eGFP and IpLITR 1.1b Y⁴⁷⁷_{F_{CYT}}-eGFP % phagocytic cells, respectively.

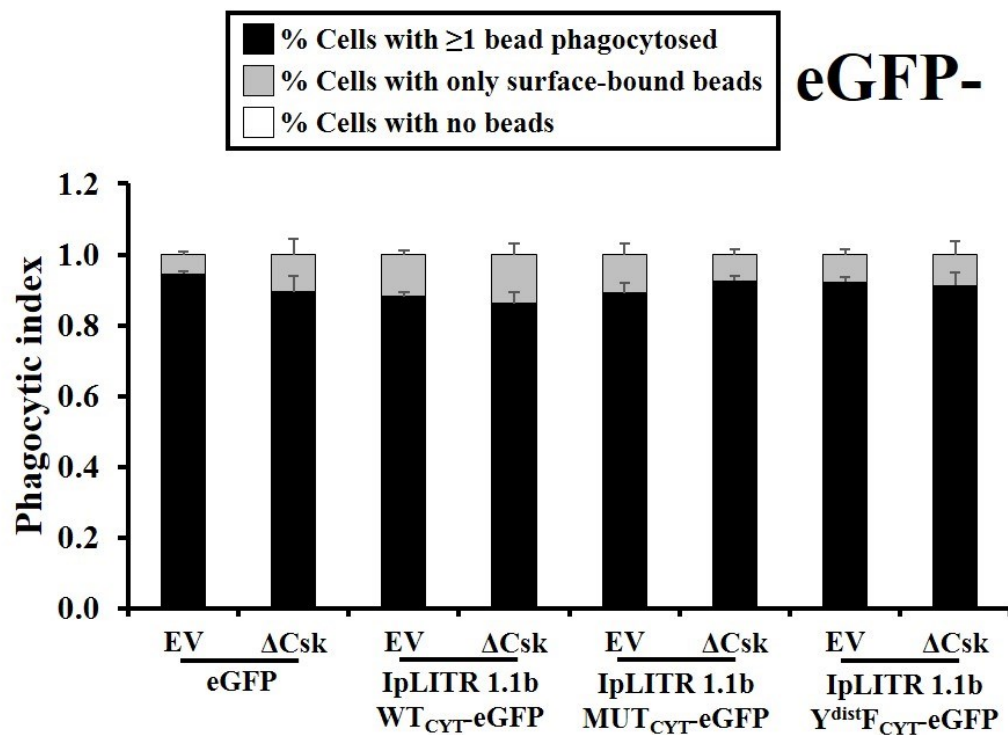
A.



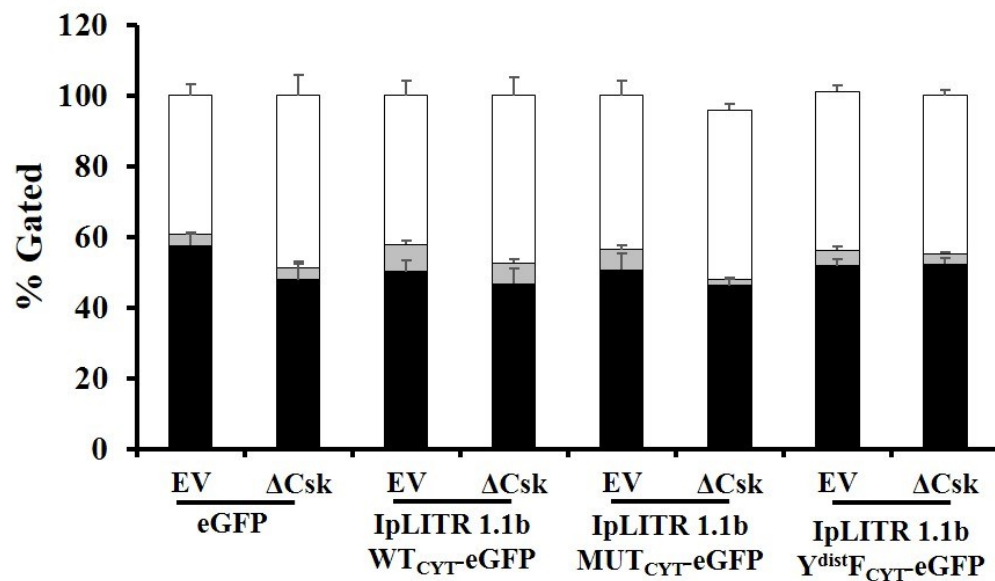
B.



C.



D.



E.

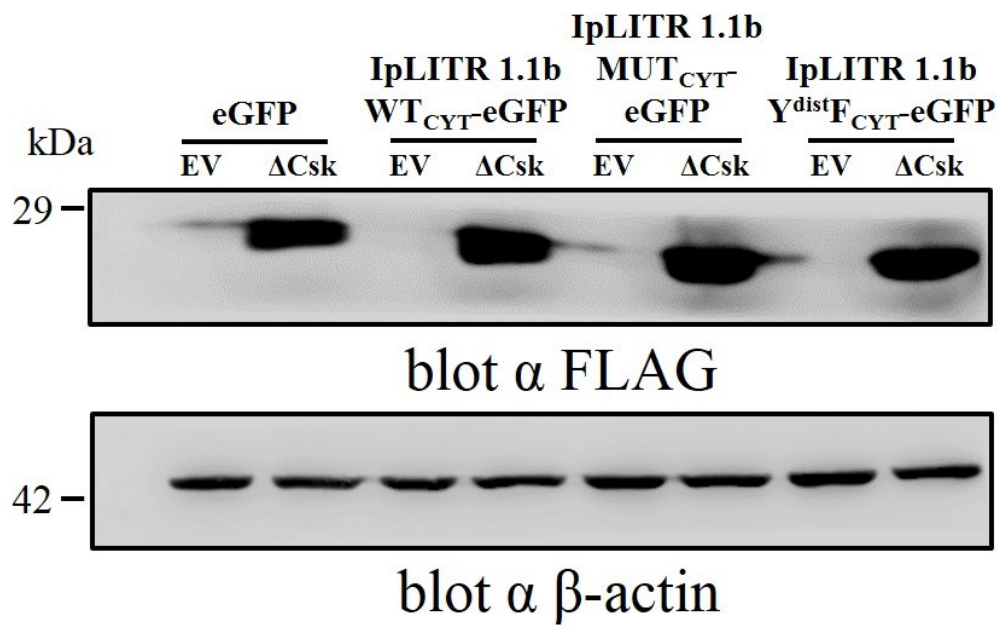
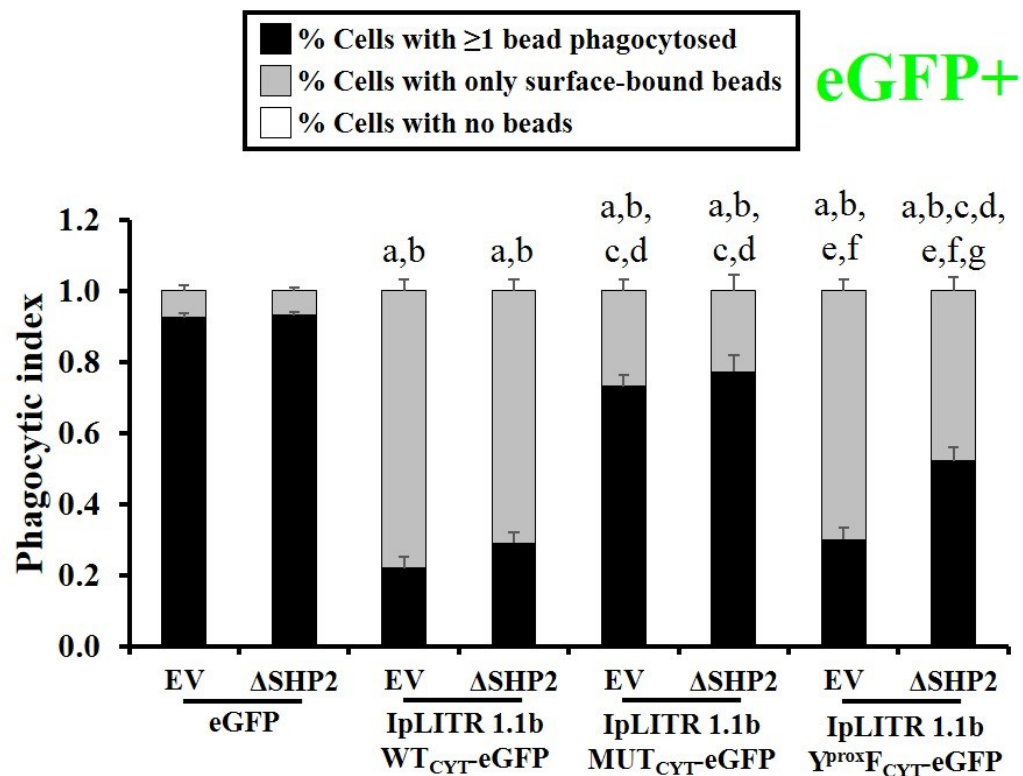


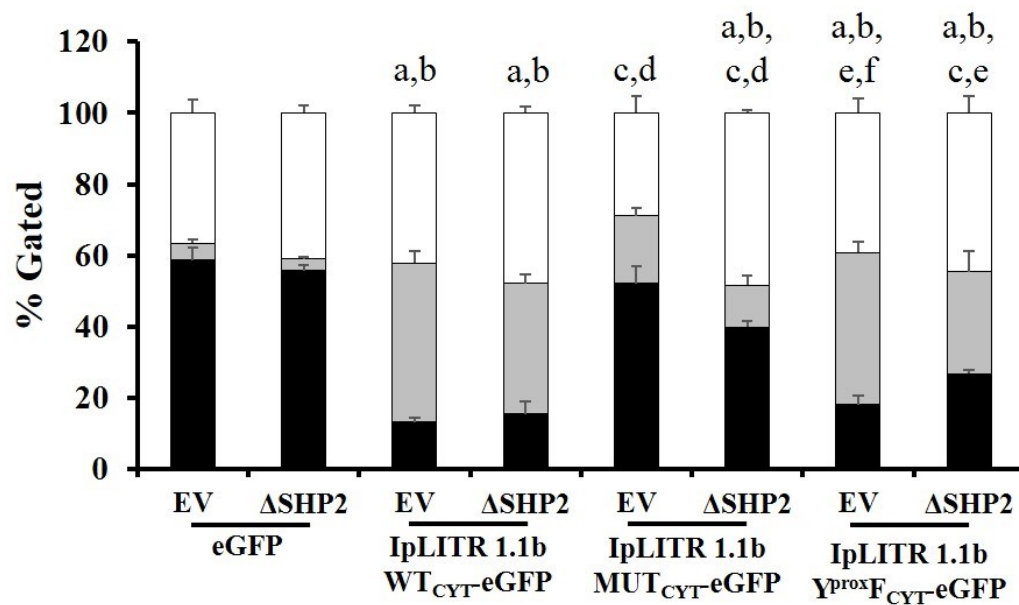
Figure 6.4. Co-expressing IpLITR 1.1b WT_{CYT} with dominant-negative Csk does not restore IpFcR γ -L WT_{CYT}-driven phagocytosis. eGFP-tagged IpLITR 1.1b WT_{CYT}, MUT_{CYT} and Y^{dist}F_{CYT} mutant constructs were each co-transfected with dominant-negative FLAG-tagged Csk into stable IpFcR γ -L WT_{CYT}-expressing AD293 cells for 48 h. Mouse α HA antibody-coated light yellow (LY) fluorescent beads were added to cells for 40 min at 37°C. Surface-bound LY beads were counter-stained with AlexaFluor647-conjugated rabbit α -mouse secondary antibody. Cells were harvested by trypsinization and fixed in 1% paraformaldehyde prior to data collection on the Image Stream^X MKII flow cytometer. Raw image files were subjected to a component masking analysis modified from Fei et al., (2017) that separates eGFP positive (eGFP+) and negative (eGFP-) cell populations. Each black bar represents the percentage of phagocytic cells (i.e. a cell with ≥ 1 bead fully internalized), grey bars represent the percentage of cells with only surface-bound beads (i.e. no beads internalized) and the white bars represent the percentage of cells with no associated beads (i.e. none bound or internalized). Results for (A and B) eGFP+ and (C and D) eGFP- cells are representative of the mean \pm SEM of at least three independent experiments as (A and C) indexed or (B and D) raw data. Phagocytic index was calculated as: % phagocytic or surface-bound cells / % total bead-associated cells. Lower case ‘a’, ‘b’, ‘c’, ‘d’, ‘e’ and ‘f’ represent statistically significant differences ($p < 0.05$) compared to eGFP EV, eGFP Δ Csk, IpLITR 1.1b WT_{CYT}-eGFP EV, IpLITR 1.1b WT_{CYT}-eGFP Δ Csk, and IpLITR 1.1b MUT_{CYT}-eGFP EV and IpLITR 1.1b MUT_{CYT}-eGFP Δ Csk % phagocytic cells, respectively. (E) After 48 h transfection, a duplicate well from (A-D) was lysed and clarified by centrifugation before boiling in reducing buffer. Samples were separated by 10% SDS-PAGE gel electrophoresis and transferred to nitrocellulose for probing with an HRP-conjugated mouse α FLAG M2 mAb (top blot) or goat anti- β -actin pAb (bottom

blot) to confirm successful transfection and expression of Δ Csk-FLAG and as a loading control, respectively. Blots shown are representative of 2 independent experiments.

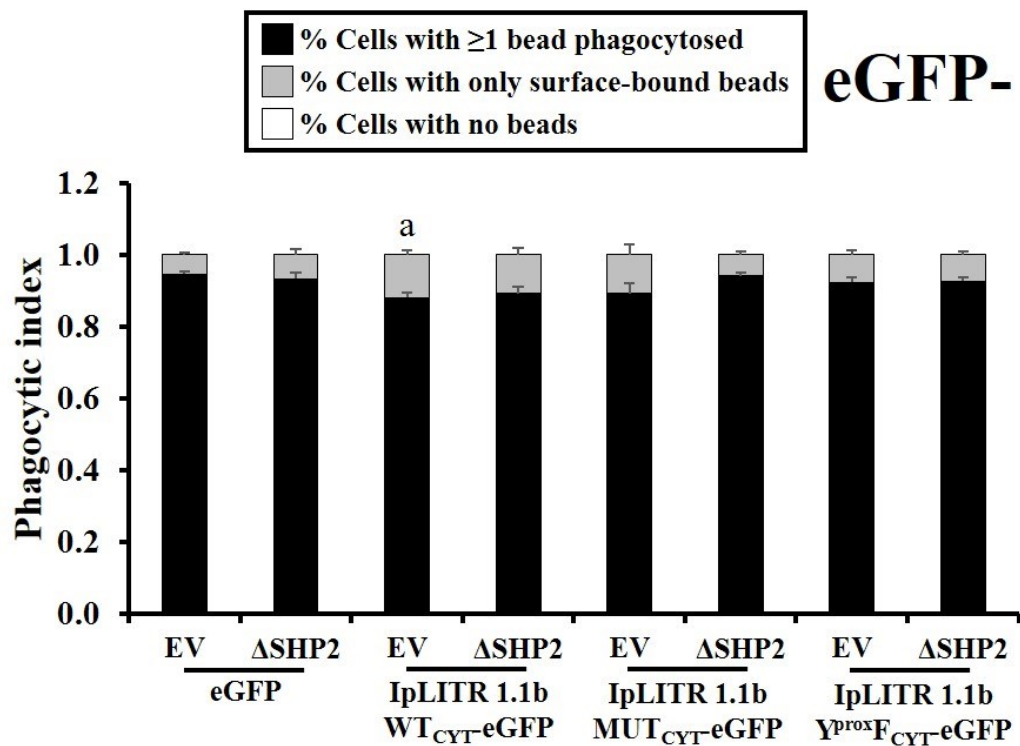
A.



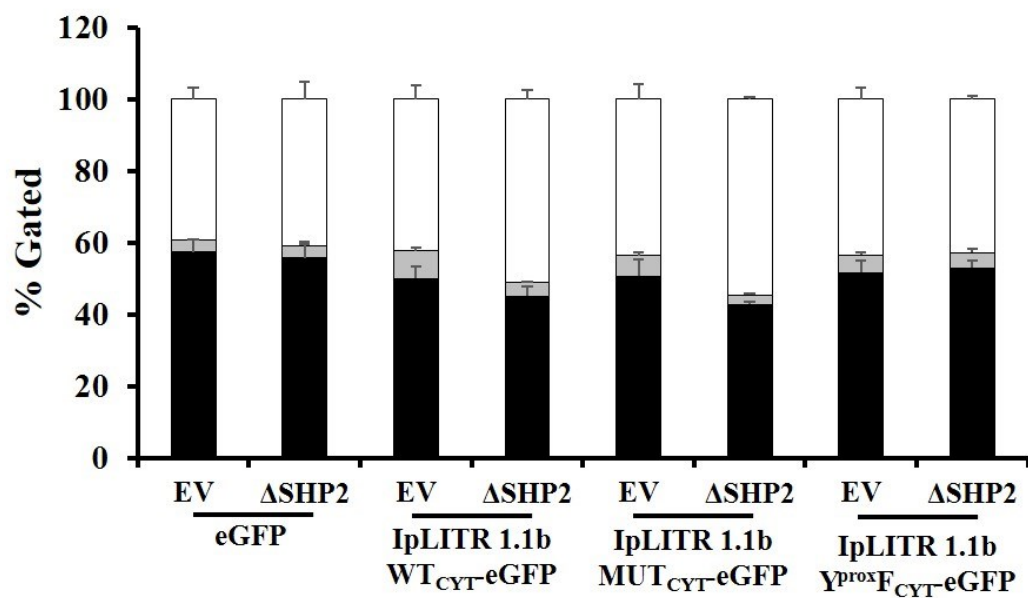
B.



C.



D.



E.

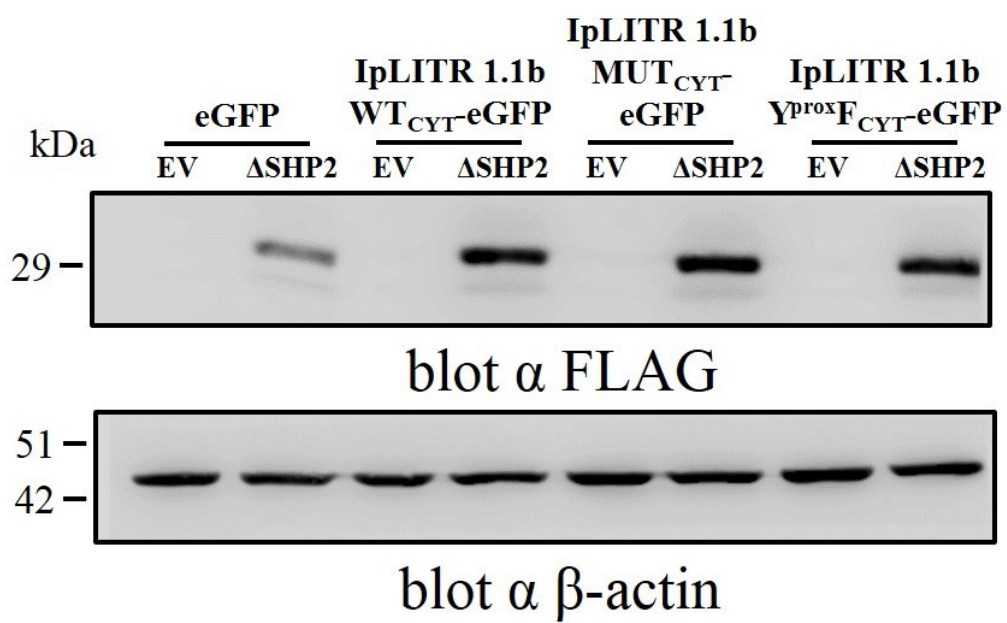
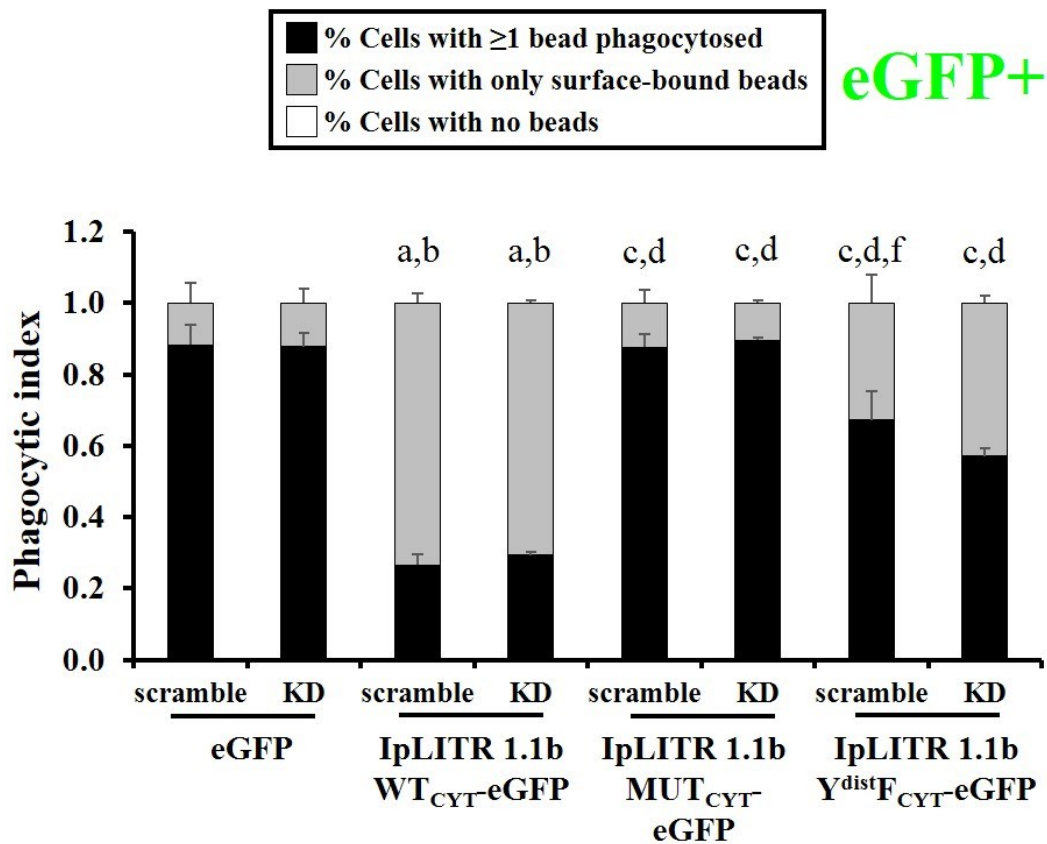


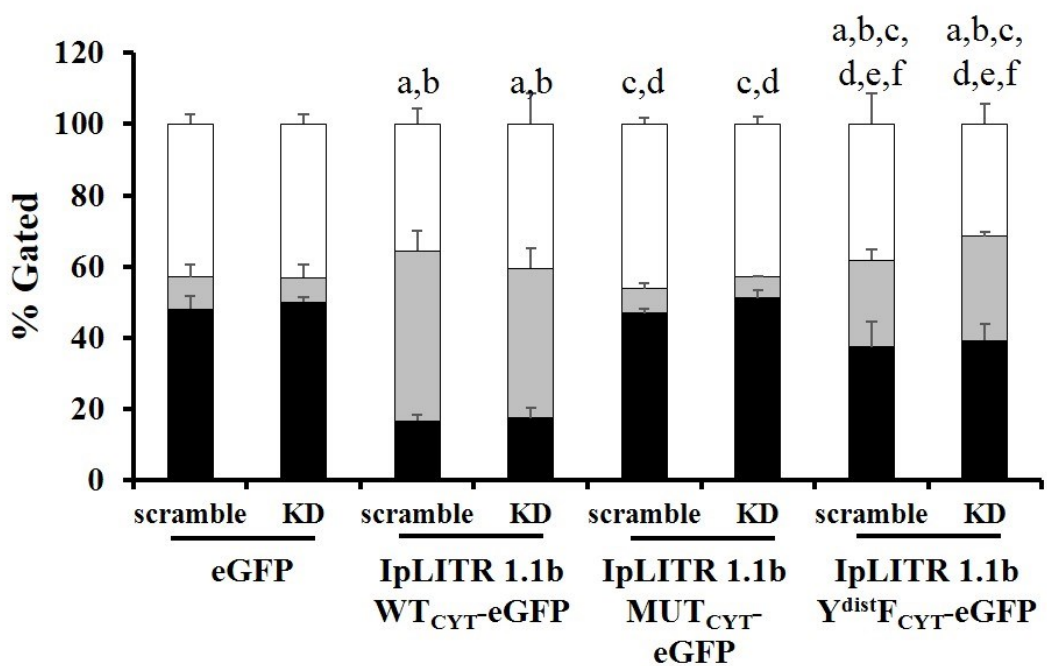
Figure 6.5. Co-expressing IpLITR 1.1b WT_{CYT} with dominant-negative SHP2 partially restores phagocytic signaling through IpFcR γ -L WT_{CYT}. eGFP-tagged IpLITR 1.1b WT_{CYT}, MUT_{CYT} and Y^{prox}F_{CYT} mutant constructs were each co-transfected with dominant-negative FLAG-tagged SHP2 in to stable IpFcR γ -L WT_{CYT}-expressing AD293 cells for 48 h. Mouse α HA antibody-coated light yellow (LY) fluorescent beads were added to cells for 40 min at 37°C. Surface-bound LY beads were counter-stained with AlexaFluor647-conjugated rabbit α -mouse secondary antibody. Cells were harvested by trypsinization and fixed in 1% paraformaldehyde prior to data collection on the Image Stream^X MKII flow cytometer. Raw image files were subjected to a component masking analysis modified from Fei et al., (2017) that separates eGFP positive (eGFP+) and negative (eGFP-) cell populations. Each black bar represents the percentage of phagocytic cells (i.e. a cell with ≥ 1 bead fully internalized), grey bars represent the percentage of cells with only surface-bound beads (i.e. no beads internalized) and the white bars represent the percentage of cells with no associated beads (i.e. none bound or internalized). Results for (A and B) eGFP+ and (C and D) eGFP- cells are representative of the mean \pm SEM of at least three independent experiments as (A and C) indexed or (B and D) raw data. Phagocytic index was calculated as: % phagocytic or surface-bound cells / % total bead-associated cells. Lower case ‘a’, ‘b’, ‘c’, ‘d’, ‘e’, ‘f’ and ‘g’ represent statistically significant differences ($p < 0.05$) compared to eGFP EV, eGFP Δ SHP2, IpLITR 1.1b WT_{CYT}-eGFP EV, IpLITR 1.1b WT_{CYT}-eGFP Δ SHP2, and IpLITR 1.1b MUT_{CYT}-eGFP EV, IpLITR 1.1b MUT_{CYT}-eGFP Δ SHP2 and IpLITR 1.1b Y^{prox}F_{CYT} EV % phagocytic cells, respectively. (E) After 48 h transfection, a duplicate well from (A-D) was lysed and clarified by centrifugation before boiling in reducing buffer. Samples were separated by 10% SDS-PAGE gel electrophoresis and transferred to nitrocellulose for probing with an HRP-conjugated mouse α FLAG M2 mAb (top blot) or goat

anti- β -actin pAb (bottom blot) to confirm successful transfection and expression of Δ SHP2-FLAG and as a loading control, respectively. Blots shown are representative of 2 independent experiments.

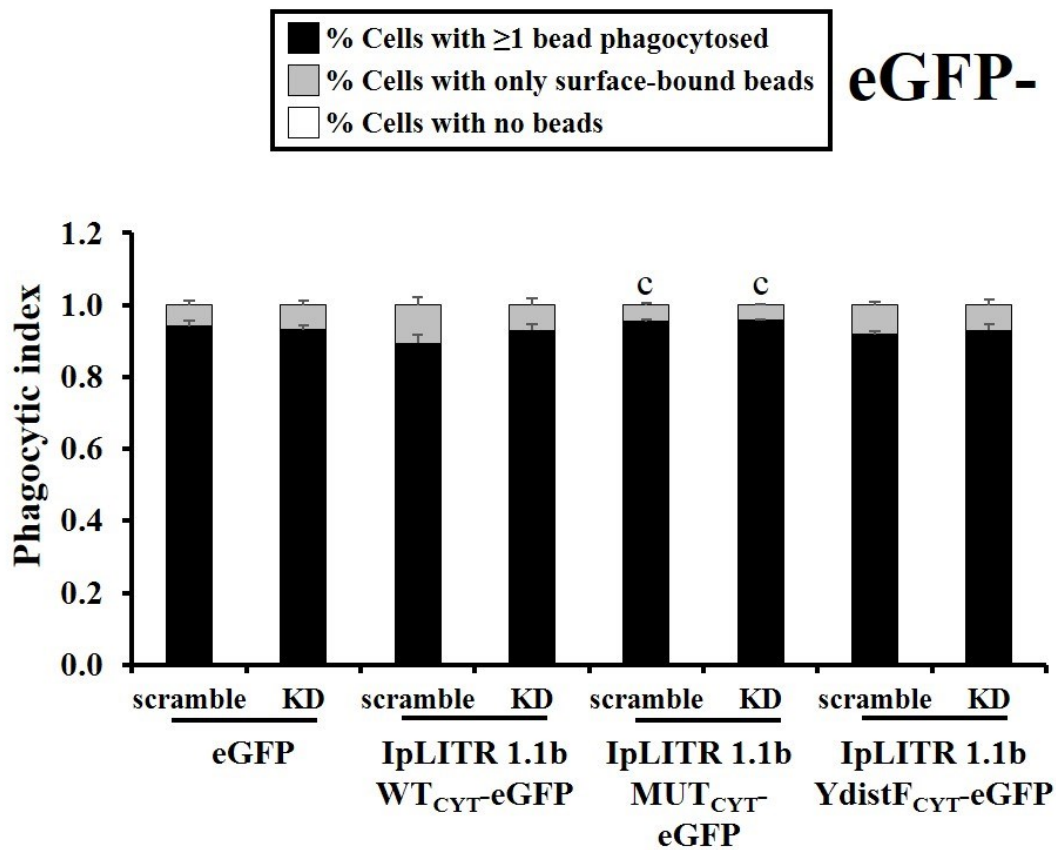
A.



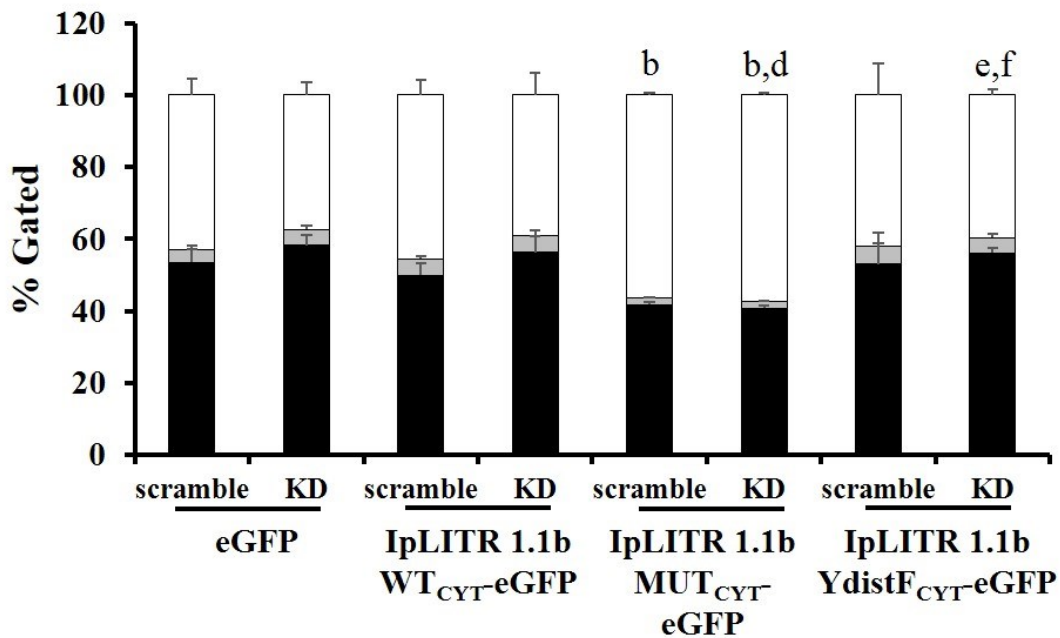
B.



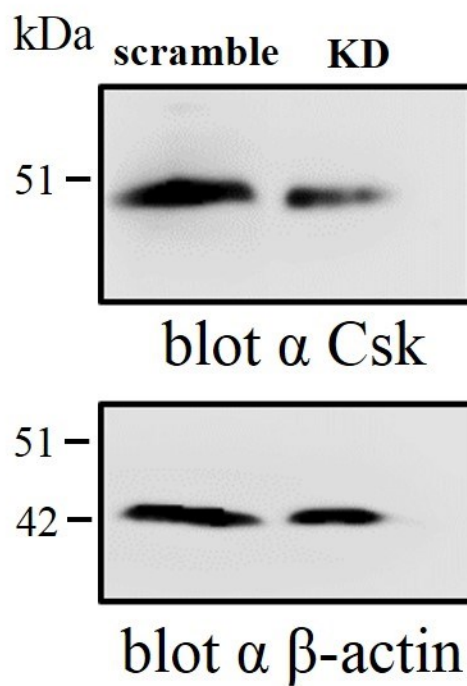
C.



D.



E.



F.

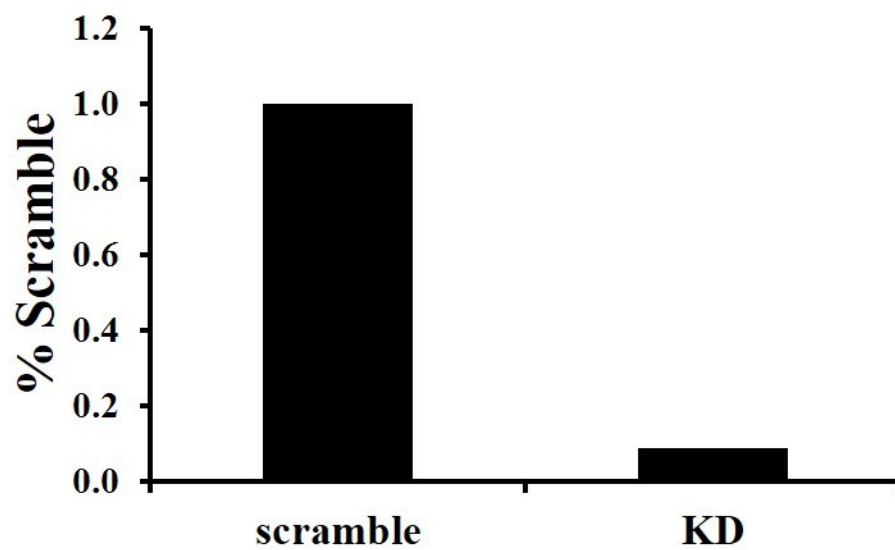
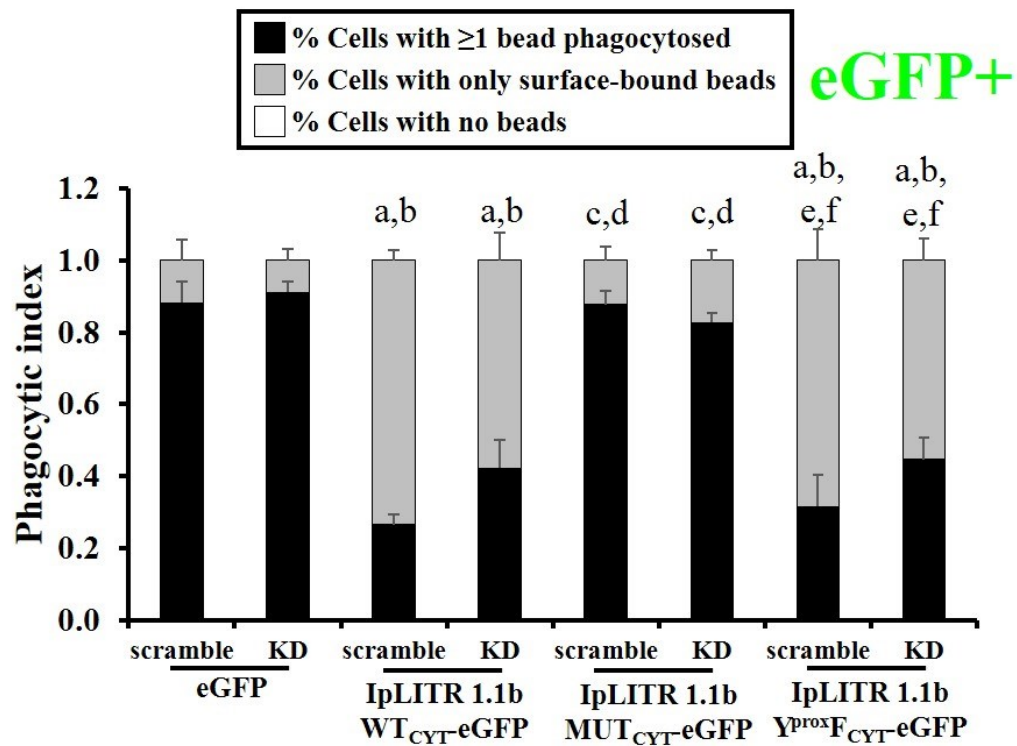


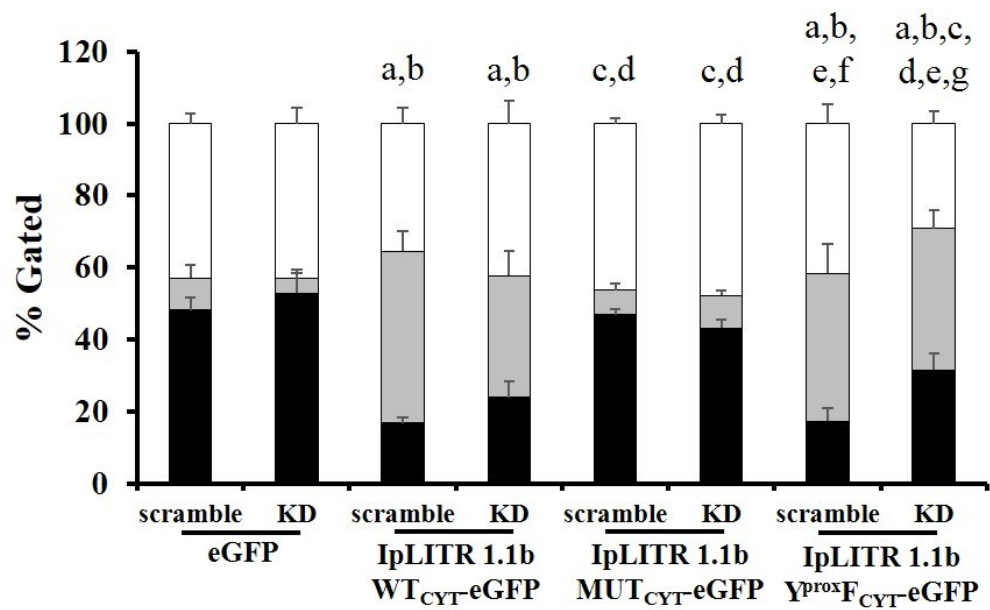
Figure 6.6. Csk knockdown does not reverse IpLITR 1.1b WT_{CYT}-mediated cross-talk inhibition of IpFcR γ -L WT_{CYT}-driven phagocytosis. eGFP-tagged IpLITR 1.1b WT_{CYT}, MUT_{CYT} and Y^{dist}F_{CYT} constructs were each co-transfected in to stable IpFcR γ -L WT_{CYT}-expressing Csk knockdown (KD) AD293 cells for 48 h. Mouse α HA antibody-coated light yellow (LY) fluorescent beads were added to cells for 40 min at 37°C. Surface-bound LY beads were counter-stained with AlexaFluor647-conjugated rabbit α -mouse secondary antibody. Cells were harvested by trypsinization and fixed in 1% paraformaldehyde prior to data collection on the Image Stream^X MKII flow cytometer. Raw image files were subjected to a component masking analysis modified from Fei et al., (2017) that separates eGFP positive (eGFP+) and negative (eGFP-) cell populations. Each black bar represents the percentage of phagocytic cells (i.e. a cell with ≥ 1 bead fully internalized), grey bars represent the percentage of cells with only surface-bound beads (i.e. no beads internalized) and the white bars represent the percentage of cells with no associated beads (i.e. none bound or internalized). Results for (A and B) eGFP+ and (C and D) eGFP- cells are representative of the mean \pm SEM of at least three independent experiments as (A and C) indexed or (B and D) raw data. Phagocytic index was calculated as: % phagocytic or surface-bound cells / % total bead-associated cells. Lower case ‘a’, ‘b’, ‘c’, ‘d’, ‘e’ and ‘f’ represent statistically significant differences ($p < 0.05$) compared to eGFP scramble, eGFP KD, IpLITR 1.1b WT_{CYT}-eGFP scramble, IpLITR 1.1b WT_{CYT}-eGFP KD, and IpLITR 1.1b MUT_{CYT}-eGFP scramble and IpLITR 1.1b MUT_{CYT}-eGFP KD % phagocytic cells, respectively. (E) Stable IpFcR γ -L WT_{CYT}-expressing Csk knockdown cells were lysed and clarified by centrifugation before boiling in reducing buffer. Samples were separated by 10% SDS-PAGE gel electrophoresis and transferred to nitrocellulose for probing with a rabbit α Csk polyclonal antibody (top blot) or goat anti- β -actin polyclonal antibody (bottom

blot) to confirm knockdowns relative to a scramble control. (F) Knockdown was quantified by densitometry. Blots shown are representative of at least 3 independent experiments.

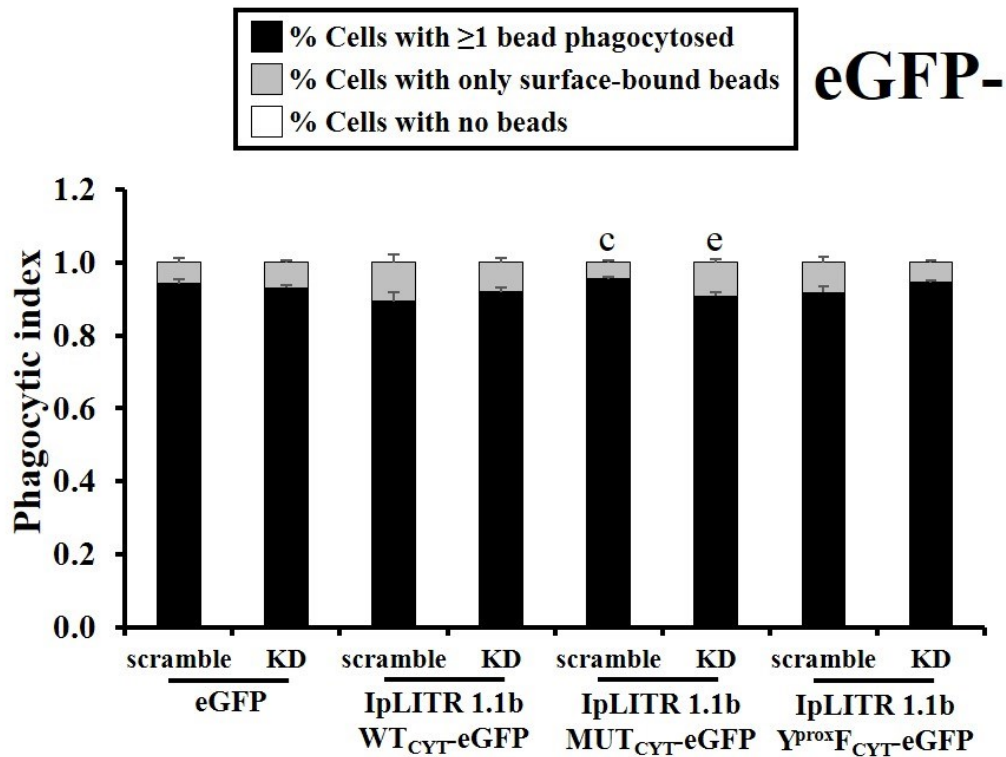
A.



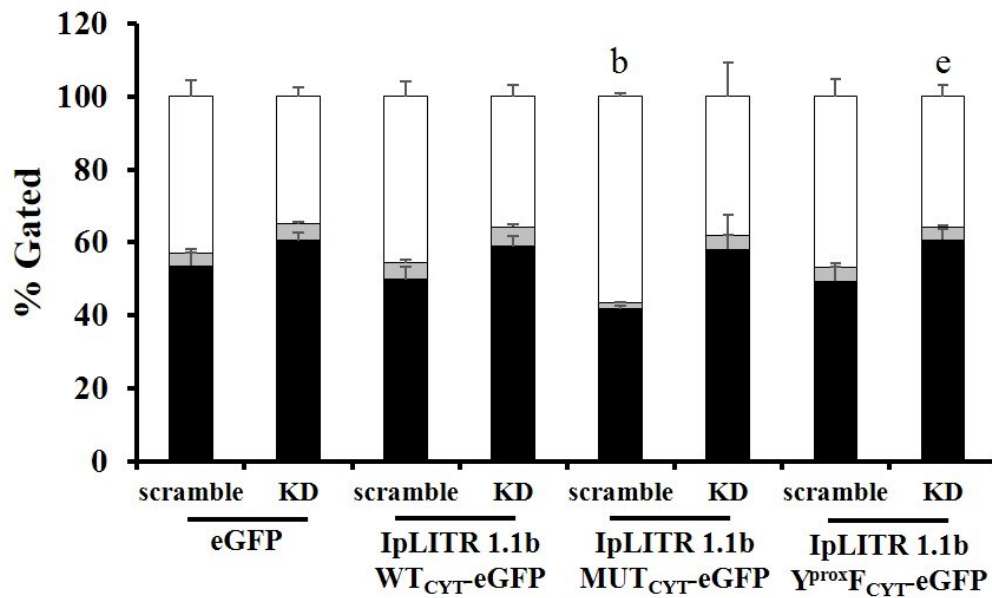
B.



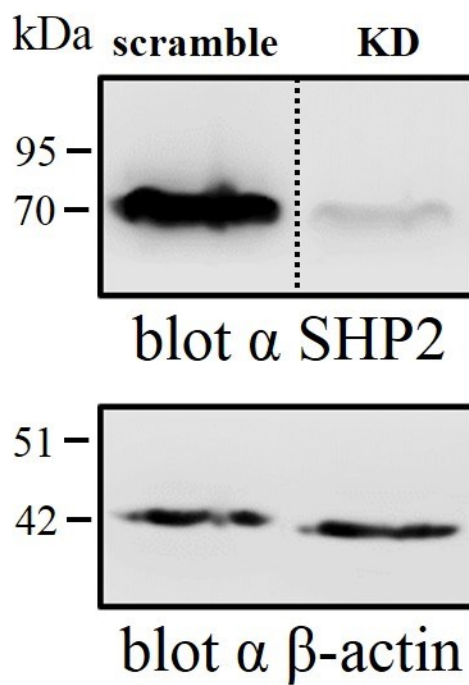
C.



D.



E.



F.

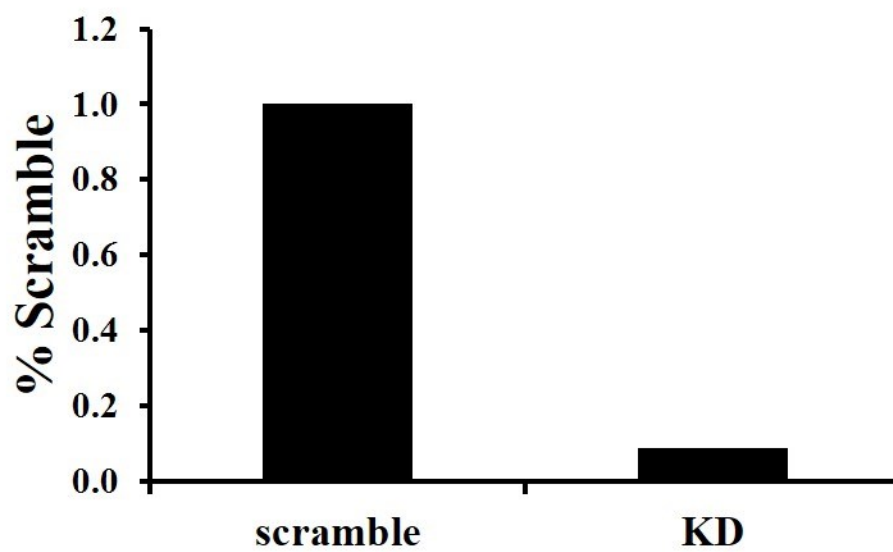


Figure 6.7. SHP2 knockdown partially reverses IpLITR 1.1b WT_{CYT}-mediated cross-talk inhibition of IpFcR γ -L WT_{CYT}-driven phagocytosis. eGFP-tagged IpLITR 1.1b WT_{CYT}, MUT_{CYT} and Y^{prox}F_{CYT} constructs were each co-transfected in to stable IpFcR γ -L WT_{CYT}-expressing SHP2 knockdown (KD) AD293 cells for 48 h. Mouse α HA antibody-coated light yellow (LY) fluorescent beads were added to cells for 40 min at 37°C. Surface-bound LY beads were counter-stained with AlexaFluor647-conjugated rabbit α -mouse secondary antibody. Cells were harvested by trypsinization and fixed in 1% paraformaldehyde prior to data collection on the Image Stream^X MKII flow cytometer. Raw image files were subjected to a component masking analysis modified from Fei et al., (2017) that separates eGFP positive (eGFP+) and negative (eGFP-) cell populations. Each black bar represents the percentage of phagocytic cells (i.e. a cell with ≥ 1 bead fully internalized), grey bars represent the percentage of cells with only surface-bound beads (i.e. no beads internalized) and the white bars represent the percentage of cells with no associated beads (i.e. none bound or internalized). Results for (A and B) eGFP+ and (C and D) eGFP- cells are representative of the mean \pm SEM of at least three independent experiments as (A and C) indexed or (B and D) raw data. Phagocytic index was calculated as: % phagocytic or surface-bound cells / % total bead-associated cells. Lower case ‘a’, ‘b’, ‘c’, ‘d’, ‘e’, ‘f’ and ‘g’ represent statistically significant differences ($p < 0.05$) compared to eGFP scramble, eGFP KD, IpLITR 1.1b WT_{CYT}-eGFP scramble, IpLITR 1.1b WT_{CYT}-eGFP KD, IpLITR 1.1b MUT_{CYT}-eGFP scramble, IpLITR 1.1b MUT_{CYT}-eGFP KD and IpLITR 1.1b Y^{prox}F_{CYT}-eGFP scramble % phagocytic cells, respectively. (E) Stable IpFcR γ -L WT_{CYT}-expressing SHP2 knockdown cells were lysed and clarified by centrifugation before boiling in reducing buffer. Samples were separated by 10% SDS-PAGE gel electrophoresis and transferred to nitrocellulose for probing with a rabbit α SHP2 mAb (top blot; dotted line indicates splice to bring

distant lanes side-by-side) or goat anti- β -actin pAb (bottom blot) to confirm knockdowns relative to a scramble control. (F) Knockdowns were quantified by densitometry. Blots shown are representative of at least 3 independent experiments.

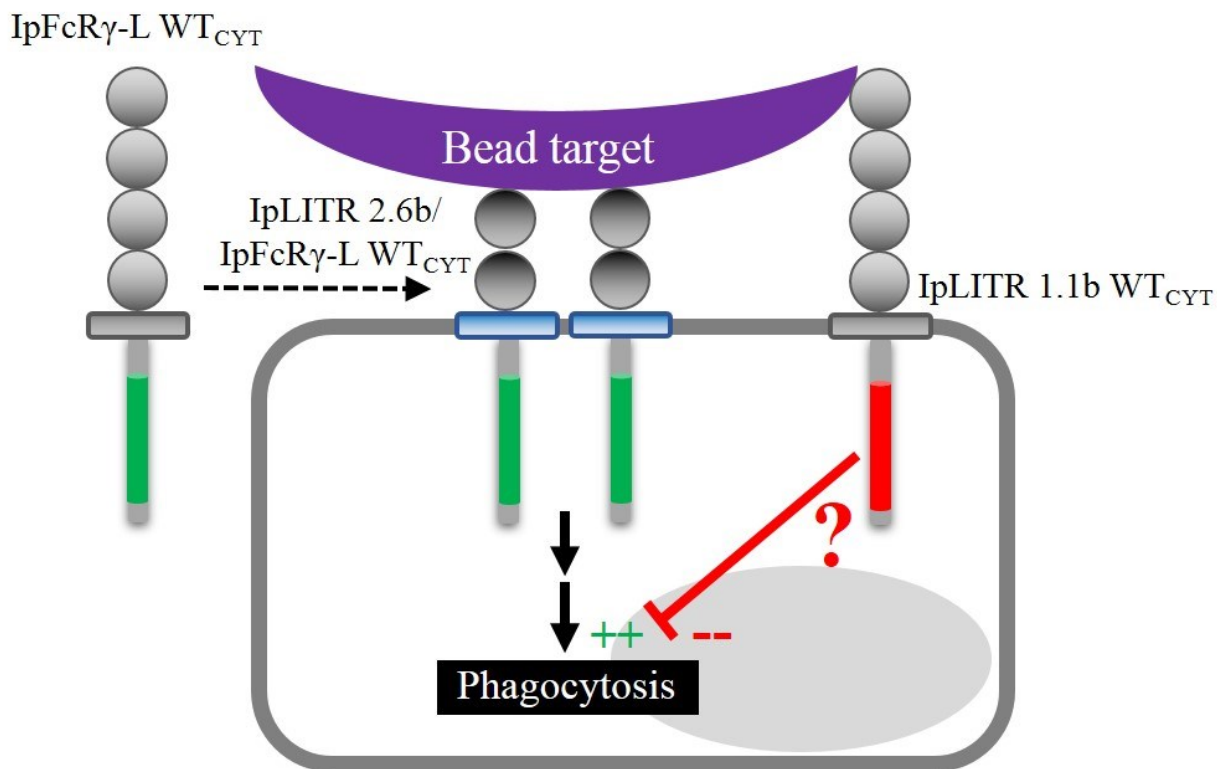
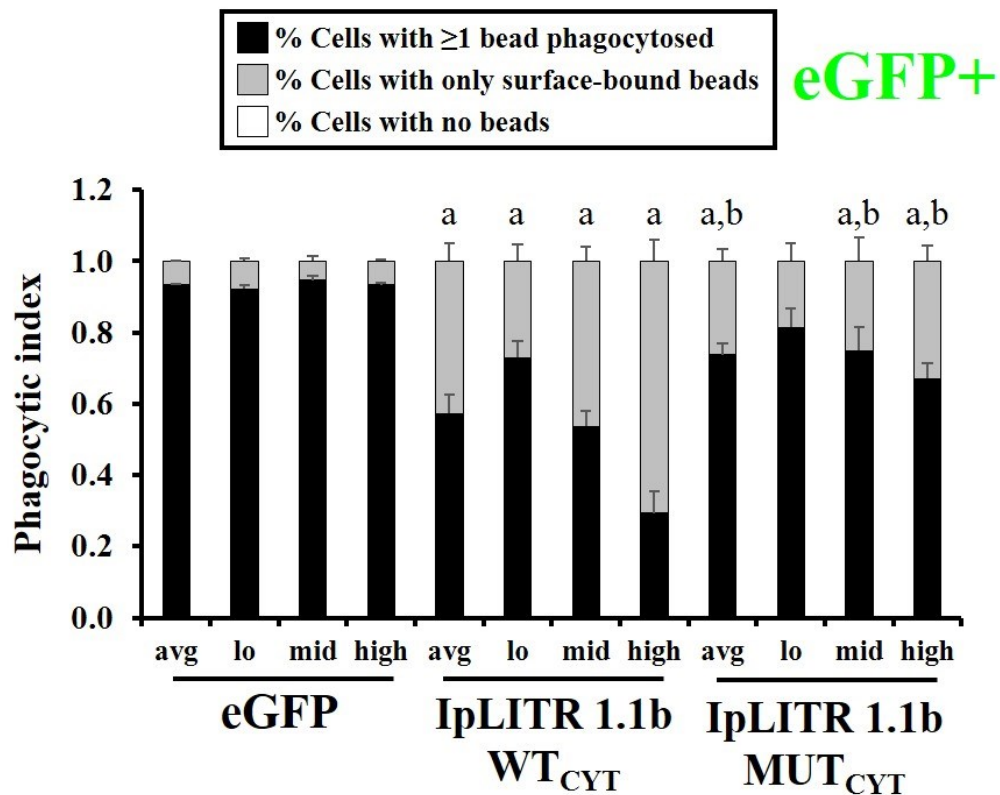


Figure 6.8. Schematic representation of IpLITR 1.1b WT_{CYT}-mediated cross-talk inhibition of IpLITR 2.6b/IpFcR γ -L WT_{CYT}-driven phagocytic signaling.

A.



B.

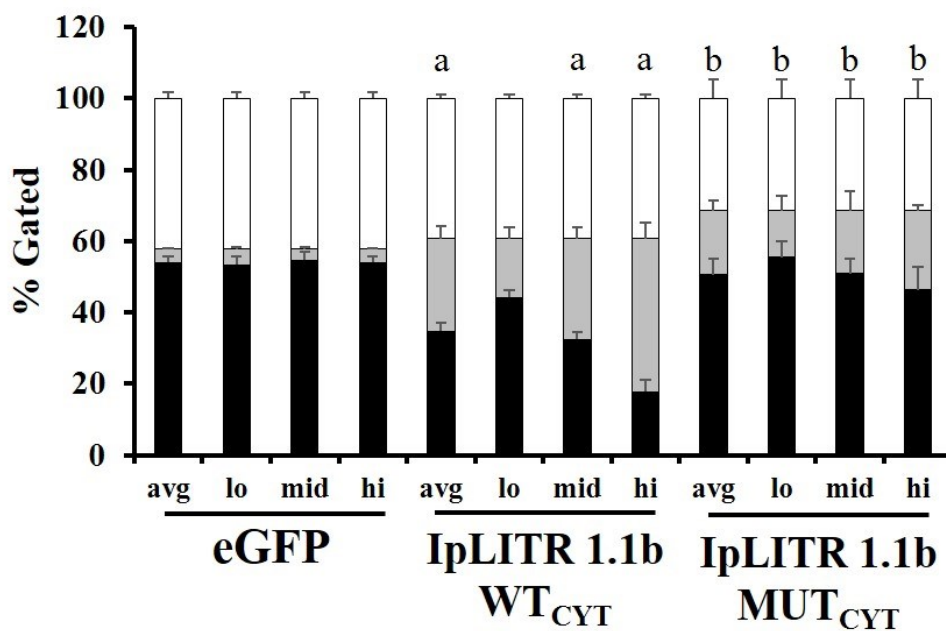
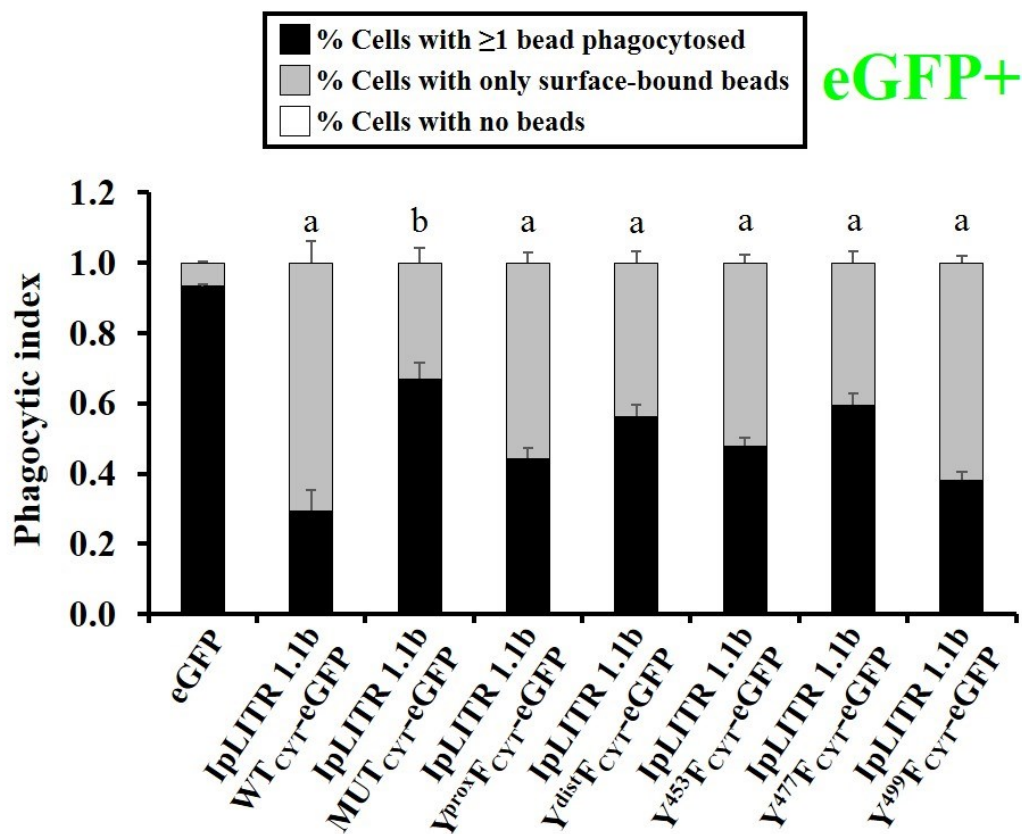


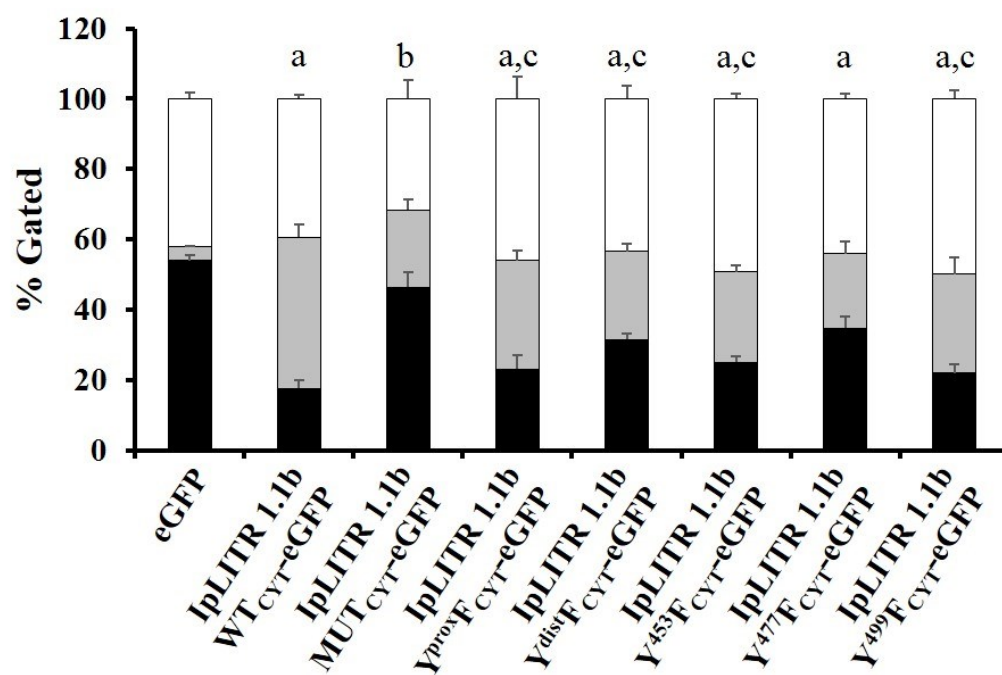
Figure 6.9. Effect of receptor expression levels on eGFP-tagged IpLITR 1.1b WT_{CYT}-mediated cross-talk inhibition of IpFcR γ -L WT_{CYT}-driven

phagocytosis. Stable IpLITR 2.6b/IpFcR γ -L WT_{CYT}-expressing AD293 cells were transfected with eGFP-tagged IpLITR 1.1b CYT constructs for 48 h. Mouse α HA antibody-coated light yellow (LY) fluorescent beads were added to cells for 30 min at 37°C. Surface-bound LY beads were counter-stained with AlexaFluor647-conjugated rabbit α -mouse secondary antibody. Cells were harvested by trypsinization and fixed in 1% paraformaldehyde prior to data collection on the Image Stream^X MKII flow cytometer. Raw image files were subjected to component masking analysis modified from Fei et al., (2017) using separate gates for average (avg; i.e. all eGFP+ cells), low (lo), middle (mid) and high (hi) eGFP expression (see Figure 5.7A for gates). Each black bar represents the percentage of phagocytic cells (i.e. a cell with ≥ 1 bead fully internalized), grey bars represent the percentage of cells with only surface-bound beads (i.e. no beads internalized) and the white bars represent the percentage of cells with no associated beads (i.e. none bound or internalized). Results are representative of the mean \pm SEM of at least three independent experiments as (A) indexed or (B) raw data. Phagocytic index was calculated as: % phagocytic or surface-bound cells / % total bead-associated cells. Lower case ‘a’ and ‘b’ represent statistically significant differences ($p < 0.05$) compared to eGFP and IpLITR 1.1b WT_{CYT}-eGFP % phagocytic cells at corresponding eGFP expression level, respectively.

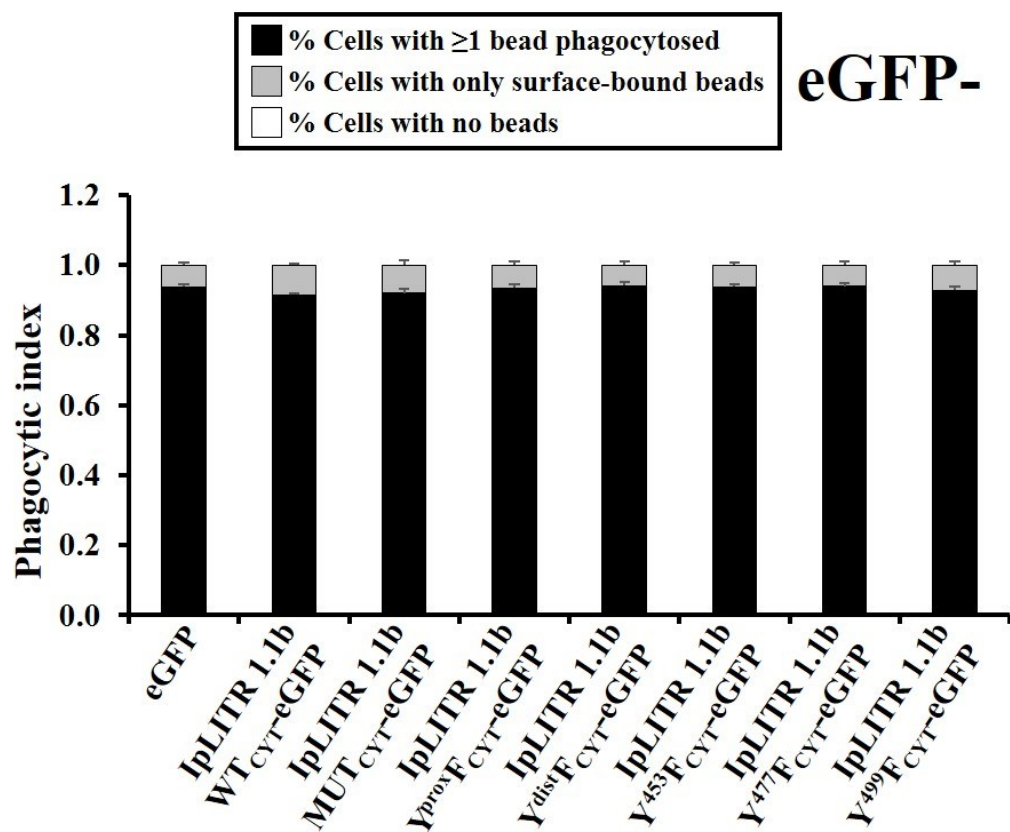
A.



B.



C.



D.

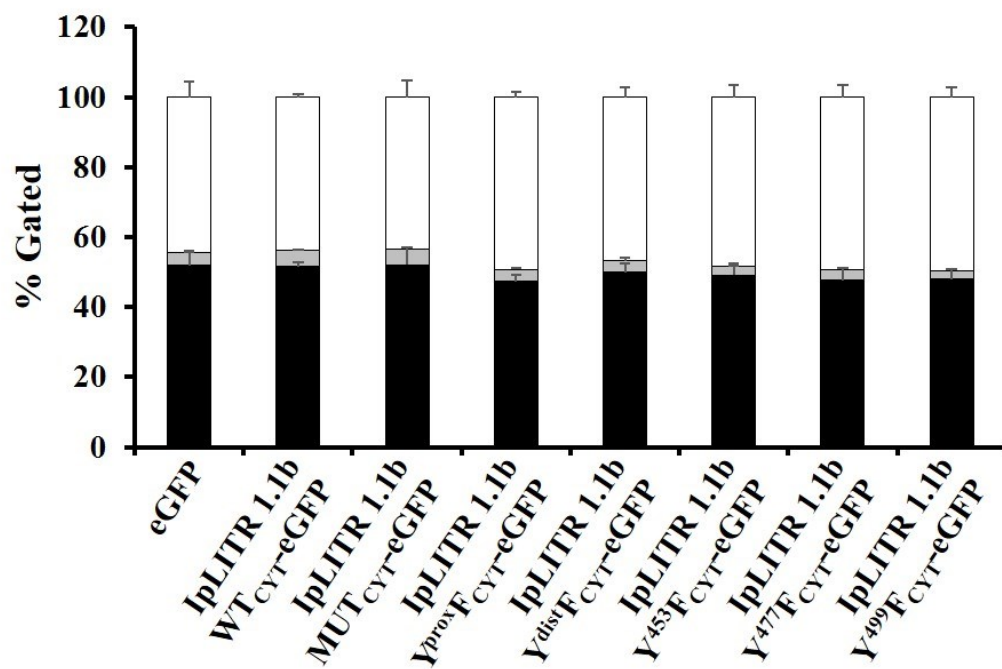


Figure 6.10. eGFP-tagged IpLITR 1.1b WT_{CYT} segments synergistically down-regulate IpLITR 2.6b/IpFcR γ -L WT_{CYT}-driven phagocytosis through distinct CYT motif Y⁴⁵³- and Y⁴⁷⁷-dependent pathways. pDisplay-encoded eGFP-tagged IpLITR 1.1b CYT YF mutant receptors were transfected into stable IpLITR 2.6b/IpFcR γ -L WT_{CYT}-expressing AD293 cells for 48 h. Mouse α HA antibody-coated light yellow (LY) fluorescent beads were added to cells for 30 min at 37°C. Surface-bound LY beads were counter-stained with AlexaFluor647-conjugated rabbit α -mouse secondary antibody. Cells were harvested by trypsinization and fixed in 1% paraformaldehyde prior to data collection on the Image Stream^X MKII flow cytometer. Raw image files were subjected to a component masking analysis modified from Fei et al., (2017) that separates eGFP positive (eGFP+) and negative (eGFP-) cell populations. Each black bar represents the percentage of phagocytic cells (i.e. a cell with ≥ 1 bead fully internalized), grey bars represent the percentage of cells with only surface-bound beads (i.e. no beads internalized) and the white bars represent the percentage of cells with no associated beads (i.e. none bound or internalized). Results for (A and B) eGFP+ and (C and D) eGFP- cells are representative of the mean \pm SEM of at least three independent experiments as (A and C) indexed or (B and D) raw data. Phagocytic index was calculated as: % phagocytic or surface-bound cells / % total bead-associated cells. Lower case ‘a’, ‘b’, and ‘c’ represent statistically significant differences ($p < 0.05$) compared to eGFP, IpLITR 1.1b WT_{CYT}-eGFP and IpLITR 1.1b MUT_{CYT}-eGFP % phagocytic cells, respectively.

CHAPTER VII

GENERAL DISCUSSION AND FUTURE DIRECTIONS

7.1 Summary of thesis findings

Several diversified immunoregulatory receptor gene families have been discovered across teleost lineages, however, functional and biochemical characterizations of their potential roles in innate immunity are very limited. The findings in this thesis have expanded the current understanding of immunoregulatory receptor CYT-mediated signaling events during the control of cellular responses. In particular, immunoregulatory receptors contain diverse CYT region motif compositions capable of differential and selective signaling molecule recruitment potential. However, the regulation of signaling and functional outcomes is highly dependent on the cellular context of receptor expression.

IpLITR 1.1b WT_{CYT} was originally shown to inhibit NK cell-mediated cytotoxicity when expressed in mouse NK cells (6) and was later shown to activate a unique phagocytic phenotype in rat myeloid RBL-2H3 cells (5, 7, 8). While IpLITR 1.1b WT_{CYT} segments recruited several stimulatory molecules from a non-immune cell AD293 lysate (Figure 4.4 and Figure 4.5), receptor cross-linking via antibody-coated bead targets did not activate phagocytosis (Figure 4.8) and IpLITR 1.1b WT_{CYT} demonstrated an inhibitory signaling molecule recruitment profile in AD293 cells (Figure 4.13). In addition, supplementing AD293 cells with over-expressed stimulatory signaling pathway molecules did not re-constitute IpLITR 1.1b WT_{CYT}-mediated phagocytic signaling, suggesting that vSrc (Figure 4.9), Syk or SAP co-expression (Figure 4.10) on their own cannot re-wire IpLITR 1.1b WT_{CYT} inhibitory signaling potential in these cells to re-constitute phagocytosis. Conversely, the ITAM-containing IpFcR γ -L WT_{CYT} receptor activated phagocytosis in AD293 cells (Figure 4.8). By demonstrating phagocytic gain-of-

function downstream of IpFcR γ -L WT_{CYT} activation, this provided a system to test immunoregulatory receptor cross-talk.

The findings in my thesis appear to be the first direct observations of cross-talk for any teleost immunoregulatory receptor family. In particular, ITIM-containing receptors can use independent but co-operating CYT segment-dependent mechanisms to inhibit ITAM-driven phagocytosis (Figure 6.3 and Figure 6.10). My results further support LITRs as useful tools to study immunoregulatory receptor-mediated signal transduction events, especially emerging concepts of CYT-dependent signaling versatility. Overall, my thesis research offers new insights into the regulatory capabilities of teleost immunoregulatory receptors by providing novel information showing that an ITIM-containing inhibitory receptor, IpLITR 1.1b, down-regulates ITAM-driven phagocytosis using a co-operative mechanism via two separate CYT region segment motifs.

Based on previous observations of IpLITR 1.1b WT_{CYT}-mediated phagocytosis in RBL-2H3 cells, I developed molecular hypotheses for IpLITR 1.1b WT_{CYT}-dependent phagocytic signaling and established a non-immune AD293 cell expression system to test them. To isolate CYT-mediated signaling capabilities in my studies, I standardized the design of the IpLITR constructs used in most of my experiments so that they differ only in CYT composition. In other words, the phagocytic receptor construct IpFcR γ -L WT_{CYT} is composed of the four extracellular domains and TM segment of wild-type IpLITR 1.1b coupled to the ITAM-containing IpFcR γ -L WT_{CYT}.

Chapter IV results showed that despite recruiting stimulatory and inhibitory signaling molecules in GST-CYT fusion protein pulldowns from cellular lysates, IpLITR 1.1b WT_{CYT} recruited the inhibitory signaling molecules Csk and SHP2 after pervanadate stimulation. IpLITR

1.1b WT_{CYT} failed to stimulate phagocytosis of target beads, leading to the formulation of molecular gain-of-function re-constitution hypotheses to restore phagocytic signaling (outlined in Figure 4.14). Since Fc γ R ITAM-dependent phagocytic signaling involves selective SFK-mediated CYT motif phosphorylation, I transfected stable IpLITR 1.1b WT_{CYT}-expressing cells with a promiscuous SFK (i.e. vSrc, phosphorylates a wide range of motifs). Since Syk is critical for Fc γ R-mediated phagocytosis and it is expressed at relatively low endogenous levels in AD293 cells, I over-expressed Syk in IpLITR 1.1b WT_{CYT}-expressing cells. In addition, the IpLITR 1.1b WT_{CYT} contains an ITSM, which is known to facilitate stimulatory signaling downstream of other immunoregulatory receptors in the presence of a hematopoietic cell-restricted signaling molecule adaptor SAP. To test whether SAP-dependent pathways could activate phagocytosis downstream of IpLITR 1.1b WT_{CYT} activation, I over-expressed SAP in IpLITR 1.1b WT_{CYT}-expressing cells. Altogether, the vSrc (Figure 4.9) and signaling molecule (Figure 4.10) hypotheses failed to re-constitute IpLITR 1.1b WT_{CYT}-mediated phagocytic signaling. These results indicate that IpLITR 1.1b WT_{CYT} is not a 'bona fide' phagocytic receptor and that this receptor may facilitate inhibitory signaling pathways within AD293 cells instead.

The ability to engage phagocytic signaling pathways depends on the organization of a phagocytic synapse after receptor cross-linking. The events leading to this outcome involve SFK-mediated CYT motif phosphorylation and recruitment of molecules that result in actin polymerization (i.e. WAVE/WASp-Arp2/3 complexes; 158, 273, 352). Therefore, enhancing receptor CYT phosphorylation or supplementing cells with a critical signaling molecule intermediate would allow phagocytic synapse formation. The CEACAM3 phagocytic receptor was co-expressed with vSrc to enhance CYT phosphorylation in cells and subsequent Western blot detection of an Nck1-WAVE2 complex (216), which facilitates phagocytic signaling. Since

AD293 cells express four of the nine known SFK members and SFK-mediated phosphorylation is substrate specific, an inability to target IpLITR 1.1b WT_{CYT} motifs involved in phagocytic signaling is a possibility. For example, Nck facilitates CEACAM3-mediated phagocytosis (216) and GST pulldown data from chapter IV show that Nck is recruited to the proximal CYT segment of IpLITR 1.1b WT_{CYT} (Figure 4.5). An Nck consensus binding motif is present at Y⁴³³ within the proximal CYT segment of IpLITR 1.1b WT_{CYT}. However, physiological recruitment profiles show that Csk and SHP2 are recruited to IpLITR 1.1b WT_{CYT} at Y⁴⁵³ and Y⁴⁷⁷, respectively (Figure 4.13). These observations indicate that Y⁴⁵³ and Y⁴⁷⁷, but not Y⁴³³ are the main targets for SFK-mediated phosphorylation in AD293 cells. Phagocytosis assays showed that IpLITR 1.1b WT_{CYT} co-expression with vSrc did not result in phagocytic signaling (Figure 4.9). Alternatively, the expression levels of available signaling molecules may prevent formation of a phagocytic synapse. For example, Syk is a critical signaling molecule downstream of ITAM-dependent pathways (424, 425) and is recruited to the IpLITR 1.1b WT_{CYT} in my GST pulldown assays (Figure 4.4). However, Syk is expressed at much higher levels in myeloid cells compared to epithelioid cells (346, 426), which may prevent physiological recruitment to/activation by IpLITR 1.1b WT_{CYT}. Conversely, the lack of expression of a particular signaling molecule may prevent stimulatory signaling. This is best exemplified by the SLAM family (SLAMF) receptors, which activate NK cell-mediated cytotoxicity in the presence of the ITSM-binding adaptor molecule SAP. In the absence of SAP, SLAMF receptors inhibit NK cell activation by recruiting SHP (238, 243). Although IpLITR 1.1b WT_{CYT} contains a C-terminal ITSM, it does not activate phagocytosis when co-expressed with SAP in AD293 cells (Figure 4.10).

IpLITR 1.1b WT_{CYT} contains several potential alternative CYT motifs that may facilitate tyrosine-independent recruitment of signaling molecules. Specifically, serine/threonine

phosphorylation and/or actin-binding adaptors play major roles in segregating membrane components and organizing signalosome formation (283–285, 293, 351, 427–429). The IpLITR 1.1b CYT region contains nineteen serine/threonine residues but whether they are substrates of serine/threonine kinases has not been tested. With respect to actin-mediated roles, perhaps the trafficking of either IpLITR 1.1b WT_{CYT} or other complexes prevents stable formation of a phagocytic synapse. The family of 4.1 proteins are known to link receptors to the actin cytoskeleton and may enhance trafficking during phagocytosis (430–433). The 4.1G adaptor binds basic residue-rich motifs like QKKKL (289) or Φ xxBxxxBB (where Φ is a hydrophobic residue and B is a basic residue; 290). These sequences bear similarities to MKKKE or LEIKPQKKAK sequences within IpLITR 1.1b WT_{CYT} and it would be interesting to know if 4.1G (or other actin-binding adaptors) bind the IpLITR 1.1b WT_{CYT}. Overall, while IpFcR γ -L WT_{CYT} stimulated phagocytosis, the physiological recruitment of Csk and SHP2 to IpLITR 1.1b WT_{CYT} indicated an inhibitory signaling potential and these two observations lead to the formulation of alternative hypotheses that I explored further using the AD293 cell system.

In chapter V, I tested new hypotheses to explore novel cross-talk signaling potential between IpLITRs during the regulation of phagocytosis. Specifically, to explore IpLITR 1.1b WT_{CYT}-mediated cross-talk regulation of ITAM-driven phagocytosis, I performed several proof-of-principle experiments and established a novel imaging flow cytometry-based phagocytosis assay. Initially, I co-transfected IpLITR 1.1b WT_{CYT} and IpFcR γ -L WT_{CYT} constructs into parental AD293 cells, incubated them with yellow green (YG) target beads and then performed an imaging flow cytometer-based phagocytosis assay (outlined in Figure 5.2; 292). My results indicated that co-cross-linking IpLITR 1.1b WT_{CYT} with IpFcR γ -L WT_{CYT} reduced phagocytosis of YG beads (Figure 5.3). Based on these observations, I tested additional IpLITR 1.1b WT_{CYT}

constructs and tagged these constructs with eGFP to control detection of expression within cell populations. To that end, I generated eGFP-tagged IpLITR 1.1b WT_{CYT} constructs (IpLITR 1.1b WT_{CYT}-eGFP) and switched to light yellow (LY) bead targets, allowing me to separate an eGFP⁺ (i.e. IpFcR γ -L WT_{CYT} and IpLITR 1.1b WT_{CYT}-eGFP co-expressing) cell population from the eGFP⁻ (i.e. IpFcR γ -L WT_{CYT} only-expressing) cell population (outlined in Figure 5.4). My results showed similar trends to the previous experiment but also that differential inhibitory potential appeared to be regulated by the proximal and distal IpLITR 1.1b WT_{CYT} segments (Figure 5.5AB). However, the eGFP⁻ control cell population was not phagocytic as expected (Figure 5.5CD). This indicated that IpLITR 1.1b WT_{CYT}-eGFP constructs were functional but IpFcR γ -L WT_{CYT} was not uniformly nor efficiently transfected into eGFP⁻ cells. Finally, I transiently transfected two IpLITR 1.1b CYT-eGFP constructs into stable IpFcR γ -L WT_{CYT}-expressing cells and repeated the LY bead-based phagocytosis assay (outlined in Figure 5.6 and Figure 5.7). Since eGFP⁻ cells were phagocytic and phagocytosis was not inhibited in eGFP⁺ cells co-expressing the tyrosine motif null mutant IpLITR 1.1b MUT_{CYT}-eGFP, my results demonstrated that IpLITR 1.1b WT_{CYT} mediates phosphotyrosine-dependent signals to down-regulate ITAM-driven phagocytosis (Figure 5.8). I now had a system to test the IpLITR 1.1b WT_{CYT} motif requirements for down-regulating ITAM-driven phagocytosis in the next chapter.

In chapter VI, I employed three molecular techniques to test hypothetical models of IpLITR 1.1b WT_{CYT} requirements for down-regulating ITAM-driven phagocytosis including site-directed mutant IpLITR 1.1b WT_{CYT} constructs (i.e. tyrosine to phenylalanine knock-out), dominant-negative signaling molecule constructs and shRNA-mediated signaling protein knockdown (outlined in Figure 6.2). When testing IpLITR 1.1b CYT YF mutants, the proximal CYT Y⁴⁵³ and distal CYT Y⁴⁷⁷ ITIM residues were critical for inhibitory signaling (Figure 6.3).

These signals were not affected by co-expression of a dominant-negative Csk construct (Figure 6.4) but were partially blocked by dominant-negative SHP2 (Figure 6.5), indicating that a distal CYT Y⁴⁷⁷ ITIM-dependent SHP2 inhibitory signaling pathway is partly involved in down-regulating phagocytosis. Furthermore, SHP2 knockdown partially blocked inhibitory signaling (Figure 6.7) while Csk knockdown had no effect (Figure 6.6), indicating that a SHP2 inhibitory signaling pathway is involved but not critical, while Csk is not involved in IpLITR 1.1b WT_{CYT}-mediated down-regulation of ITAM-driven phagocytosis. Lastly, I tested IpLITR 1.1b WT_{CYT}-mediated inhibitory cross-talk against the chimeric IpLITR 2.6b/IpFcR γ -L WT_{CYT} construct. Co-cross-linking IpLITR 1.1b WT_{CYT} and IpLITR 2.6b/IpFcR γ -L WT_{CYT} resembles a physiological synapse where the phagocytic receptor contains two extracellular domains (e.g. like Fc γ RIIA). My results showed that IpLITR 1.1b WT_{CYT} required both proximal and distal CYT segment motifs Y⁴⁵³ and Y⁴⁷⁷, respectively, to maximally inhibit phagocytosis (Figure 6.10).

Several mammalian receptors are known to inhibit phagocytic signaling including Fc γ RIIB, SIRP α and LILRB4. Fc γ RIIB inhibits Fc γ RIIA ITAM-dependent phagocytosis via CYT ITIM-dependent SHIP1 and SHP1 pathways, indicating inhibitory signaling versatility (376–378). SIRP α recruits SHP1, presumably to a CYT ITIM, and dephosphorylates phagocytic signaling intermediates myosin IIA, paxillin and cofilin which shuts off Fc γ R-mediated phagocytosis (414, 415). Lastly, LILRB4 is capable of regulating phosphotyrosine signaling in myeloid cells. Co-cross-linking LILRB4 with Fc γ RI reduced phosphorylation of several signaling molecules including Syk and reduces phagocytosis. Interestingly, dephosphorylation still occurs in the presence of a SHP1-specific inhibitor, indicating SHP1-independent inhibitory pathways are involved downstream of LILRB4 (434, 435). The mechanisms presented in these examples generally involve a single CYT motif recruiting an inhibitory signaling molecule that

dephosphorylates stimulatory pathway intermediates to block phagocytosis. Interestingly, while SHIP is recruited to Fc γ RIIB at CYT ITIM Y²⁹², the C-terminal 16 residue, non-tyrosine-containing segment of Fc γ RIIB is required to fully activate SHIP likely because it contains the Y+3 leucine of the ITIM (263). In contrast, IpLITR 1.1b WT_{CYT}-mediated down-regulation of ITAM-dependent phagocytic signaling depends on two distinct CYT motifs (i.e. Y⁴⁵³ and Y⁴⁷⁷) that activate SHP/SHIP/Csk-independent inhibitory pathways. The detailed molecular mechanism may involve either recruitment of two different molecules to each of these motifs or the recruitment of a single molecule by one motif and activation of that molecule by the other motif. This signaling pathway adds to the versatility of previously described IpLITR 1.1b WT_{CYT} region-mediated inhibitory signaling that involves differential pathways via Y⁴⁵³-dependent Csk and Y⁴⁷⁷/Y⁴⁹⁹-dependent SHP1/2 to inhibit NK cell-mediated cytotoxicity. Future work will be required to identify the signaling molecule participants needed for IpLITR 1.1b WT_{CYT}-mediated cross-talk down-regulation of phagocytosis.

7.2 Future directions

IpLITR research has so far relied on the evolutionary conservation of phosphotyrosine-dependent signaling networks to allow examinations of the functional and biochemical signaling potential of two representative channel catfish receptors. The findings presented in this thesis have added cross-talk signaling potential to their list of capabilities but a ‘true’ mechanism, including the signaling molecules involved during cell-mediated immune responses in fish, remains uncharacterized. In addition, the zebrafish and goldfish models offer great opportunities to expand LITR research.

7.2.1 Mechanism(s) of IpLITR 1.1b WT_{CYT} segment-mediated cross-talk down-regulation of ITAM-driven phagocytosis

The mechanism of IpLITR 1.1b WT_{CYT}-mediated down-regulation of ITAM-driven phagocytosis involves signals from Y⁴⁵³ and Y⁴⁷⁷ that recruit Csk and SHP2, respectively. However, Csk does not appear to play a role, while SHP2 plays only a partial role in the inhibitory cross-talk signaling mechanism, suggesting that alternative signaling molecules are involved. It would be interesting to know if more than one signaling molecule is involved (i.e. one at each motif) or if one signaling molecule is recruited and activated by Y⁴⁵³ and Y⁴⁷⁷, respectively, or vice versa. A potential candidate is the SH2 domain-containing inositol 5'-phosphatase (SHIP), known to bind FcγRIIB and inhibit FcγR-mediated phagocytosis. Interestingly, full inhibitory SHIP signaling may require distinct interactions with the FcγRIIB CYT segments (263), which is similar to the co-operative IpLITR 1.1b WT_{CYT} motif requirements demonstrated here. The Y⁴⁷⁷ (V-I-Y⁴⁷⁷-T-E-L) sequence bears similarity to a SHIP consensus binding motif (i.e. V-A/G/V-Y-T-L/F/M/T/Y-L; 383), but SHIP recruitment to IpLITR 1.1b WT_{CYT} has not been tested. Alternatively, a phosphotyrosine-binding (PTB) domain-containing protein may also be a potential candidate. However, presently characterized PTB binding specificities do not match Y⁴⁵³ nor Y⁴⁷⁷ motif sequences of IpLITR 1.1b WT_{CYT} (436). Unbiased screens for signaling pathway participants may reveal hitherto unpredicted molecules. Two potential approaches include phosphorylation profiling or fingerprinting of unknown molecules by mass spectrometry. In the case of phosphorylation profiling, cellular lysates may be blotted anti-phosphotyrosine (374, 414, 437–439) or cells may be stained by intracellular anti-phosphotyrosine on a flow cytometer (440–442) after receptor co-cross-linking. Mass spectrometry requires the enrichment of potential molecules in a sample that may be

visualized by silver stain. Enrichment may be accomplished by tagging IpLITR 1.1b with a C-terminal biotin ligase enzyme that labels all proteins within close proximity (i.e. in the signalosome) during receptor co-cross-linking. Biotinylated molecules are then purified using anti-streptavidin-coated beads (443). While these screens may identify signaling participants and advance biochemical characterizations, it would also be beneficial to improve the cell system and technical strategy for functional characterizations, as well as perform detailed imaging studies.

Better control of the functional phagocytosis assay may be achieved by using stable IpLITR co-expressing cell lines and an alternative site-directed mutant strategy. Co-expressing these receptors in stable cell lines may enhance reproducibility and limit variability due to receptor expression levels or transfection. In addition, a better site-directed mutagenesis strategy would be to mutate all tyrosine residues that are not thought to be involved in facilitating signaling to control redundant/alternative inhibitory signals. For example, IpLITR 1.1b proximal CYT Y⁴³³ is known to bind the adaptor Nck and while this association was not detectable in pervanadate-stimulated cells, adaptor-dependent inhibitory pathways can still operate downstream of inhibitory receptors, like KIRs (177). Finally, it would be interesting to visualize phagocytic synapse dynamics using super-resolution imaging to track receptor movements and AD293 cells are highly suited to imaging (329). While improving heterologous cell culture systems may provide new information regarding mechanisms of signaling capabilities, these studies have raised questions about the roles of LITRs during fish immune responses.

7.2.2 Potential roles for IpLITR signaling in channel catfish immune cells

IpLITRs clearly possess versatile signaling capabilities in heterologous cell systems, but limited data about the roles IpLITRs may play in catfish immune cells is available. To date, cell

expression data and indirect observations, as well as one direct demonstration, of potential roles have been reported.

Three prototypical IpLITR-types were originally characterized and a subsequent study revealed several isoforms of these receptors are up-regulated on certain catfish immune cells following alloantigen stimulation. IpLITR 1 and 3 cDNAs were identified in a cDNA library generated from an NK-like cell-enriched mixed leukocyte culture while IpLITR 2 cDNA was identified from a macrophage cell line library. In addition, IpLITR 1 mRNA was also detected in catfish macrophages, B cells, T cells and allo-specific CTLs while IpLITR 2 mRNA was detected in B cells, allo-specific CTLs and NK-like cells (2). When two clonal cytotoxic T lymphocyte (CTL) lines, TS32.15 and TS32.17 (444), were stimulated with irradiated allogeneic B cells, several IpLITR 1 and 2 isoforms were up-regulated including two IpLITR 1.1a isoforms (ABI16036.1, ABI16049.1), two IpLITR 1.1b isoforms (ABI16037.1 and ABI16050.1), four IpLITR 1.2a isoforms (ABI16039.1, ABI16040.1, ABI16041.1 and ABI16051.1) and IpLITR 2.6b (ABI23577.1) among others. Interestingly, while these isoforms contain closely related extracellular domains and TM segments with slightly different compositions, four isoforms (including IpLITR 1.1b and a recently discovered isoform IpLITR 1.2.5_1 (328)) contain a proximal CYT segment insert that is not present in any of the other known isoforms (Figure 7.1). This inserted cassette is known to confer inhibitory signaling plasticity to inhibit NK cell-mediated cytotoxicity (6) and phagocytosis (see chapters V and VI), but also functional plasticity to stimulate phagocytosis in RBL-2H3 cells (7, 8). The catfish TS32.15 and TS32.17 CTL lines show differential abilities to lyse target cells. TS32.15 CTLs use only perforin/granzyme pathways to lyse allogeneic 3B11 B cell targets (444, 445) while TS32.17 CTLs use both a perforin/granzyme and another unknown pathway to lyse multiple target cells including 3B11

and 1G8 B cell targets (444). Furthermore, catfish CTL cultures progress through three stages of differentiation: 1) small memory-like CTLs, 2) terminally differentiated effector CTLs and 3) small IgM⁺ senescent CTLs. Like mammalian clonal CD8⁺ CTL cultures, catfish TS32.15 cultures exhibit small non-cytotoxic (marked by CD62L^{hi} in mammals) and large granular cytotoxic (marked by CD62L^{lo} in mammals) cells but do not express CD8 or CD4 message. If left unstimulated, mammalian CTLs apoptose or differentiate into memory CTLs marked by CD45RO, CCR7, CD27, CD28, IL7R α , PD1, perforin (446). While the presence of catfish memory CTLs has been inferred due to faster and longer immune responses after booster vaccinations against channel catfish virus (328), similar markers for memory CTLs in catfish have not been identified. Altogether, these observations indirectly support potential roles for IpLITR signaling in regulating catfish CTL-mediated cytotoxic responses and whether IpLITR isoforms are expressed at different stages of CTL differentiation. Perhaps the insertion of a proximal Csk-binding CYT signaling cassette in IpLITR 1.1b is part of the functional maturation of catfish CTLs, allowing IpLITR 1.1b to play a role in fine-tuning target recognition or cytotoxic synapse-forming signaling pathways by differentially regulating SFK activity (447). Interestingly, infection models have also implicated roles for LITR in catfish immune responses. A bacterial infection with *Flavobacterium columnare* may up-regulate IpLITR 1.1a and IpLITR 3 expression in the gill tissue of channel catfish according to BLAST annotations of sequenced RNA isolated from infected tissue (448). Finally, a direct role for IpLITRs in catfish anti-viral responses has been reported. CC41 mAb staining identifies a subset of CTLs that recognize and lyse channel catfish virus-infected MHC-matched clonal T cells. The primary marker recognized by CC41 is an IpLITR 1.1a isoform that, along with additional IpLITR 1 and 2 isoforms, is up-regulated on anti-viral CTLs. Importantly, pre-incubating these CTLs with CC41 mAb inhibited

lysis of virus-infected targets by ~40%, directly implicating a role for IpLITRs in target recognition and/or activation of cytotoxicity (328). Future investigations will likely confirm that IpLITRs are involved in recognition and/or regulate signaling during immune responses in catfish. However, LITRs may also be potential markers for specific immune cell-types in fish, including memory CTLs, which are critical cellular components for long-term protection from pathogens and may advance the broader field of fish immunity and vaccinology to benefit the fish-farming (i.e. aquaculture) industry.

7.2.3 Potential impact of LITR research on vaccine development and aquaculture

Long-term protection from pathogens in fish is a relatively unexplored aspect of fish immunity from a molecular and cellular perspective. While the use of vaccines has been critical to the success of commercial aquaculture since the 1970s (449–451), enhancing the efficacy of fish vaccines will help increase production to support a growing world population. In 2017, 40% of the world population lived within 100 km of a coast making seafood, including shellfish and finfish, a major source of nutrition (452). Markets are supplied with either captured (i.e. from the ocean) or farmed (i.e. aquaculture) fish. Finfish capture production has plateaued at ~90 million tonnes since 1990 and was 90.91 million tonnes in 2016. In contrast, aquaculture production has increased steadily since 1950, including a 611% increase from 1990-2016 (13.01 to 80.03 million tonnes) that is primarily due to its popularity in developing countries. While Asia accounted for 88% of worldwide aquaculture production, the US and Canada account for 0.45% (453). US finfish aquaculture of catfish, trout, salmon and others produced 196692 tonnes worth \$591 million USD in 2016 (454). Canadian finfish aquaculture of salmon, trout and other fish produced 160054 tonnes worth \$940 million USD in 2016 (455). Parasitic, viral and bacterial

outbreaks can severely limit production and decimate fish stocks, placing disease prevention at the forefront of sustainable, large-scale aquaculture.

In contrast to agriculture, controlling the spread of infectious microbes in water presents several challenges. Microbes are efficiently transmitted through water which cannot be disinfected in large enough quantities at economical costs. In addition, the use of antibiotics in farms, especially those connected to larger bodies of water, would lead to the dissemination of those drugs throughout the environment, leading to concerns of drug resistance and other effects. Therefore, natural or acquired immunity are crucial for maintaining healthy fish stocks and fish vaccines that induce long-term cell-mediated protection are key (451).

Similar to mammals, fish possess two types of long-term immune protection known as memory and trained innate immunity that involve different mechanisms. While memory involves long-lived B and T cells, trained innate immunity includes B/T cell-independent processes, epigenetic changes and altered metabolic profiles in innate immune cells that collectively confer resistance to a previously encountered innate immune challenge (456, 457). This can be triggered by pattern recognition receptor (PRR) activation and MAPK signaling in various innate immune cell-types (458, 459). For example, β -glucan injections protect salmon from subsequent *V. salmonicida* challenge (460). Several theories speculate about the underlying mechanisms of trained innate immunity and the high diversity of PRRs in fish likely plays a central role, but no studies describe the details of trained innate immunity in fish (461, 462). Interestingly, LITRs are involved in protection from viral infection in fry and fingerling catfish (328), they are expressed in anti-viral CTLs as well as several innate immune cell-types (2, 94) and they can activate MAPK signaling in a myeloid (i.e. innate immune) cell-type (5). It would be very interesting to

know if LITRs are also expressed in fish memory B/T cells and if they might play a role in long-term immune protection through memory or trained innate immunity.

The study of LITR biology has been limited to channel catfish, however, several fish genomes encode LITR genes including tilapia, carp, salmon and trout which are commonly farmed species in North America and Asia. However, zebrafish and goldfish also possess LITR genes and offer tractable models for *in/ex vivo* studies.

7.2.4 Establishing LITR-based *in/ex vivo* immune models in zebrafish and goldfish

Complete zebrafish and goldfish genomes are available through the Ensembl database (<https://www.ensembl.org/index.html>). This offers the potential to identify all predicted LITR genes and gain insight into their genomic organization, transcript isoforms, splicing patterns and the structural features of predicted LITR proteins. Whether isoforms arise from different genes or from alternatively spliced genes has not been possible for IpLITRs since no accessible genome was available, although the Ensembl database now contains a channel catfish genome assembly. Once zebrafish and goldfish LITR sequences are identified, each model organism has its own advantages for pursuing different avenues of LITR research.

Zebrafish offers several advantages including a relatively short developmental timeline (~3 months to adulthood) and advanced molecular and imaging techniques to study fish-specific LITR immune biology (463–465). LITR expression during embryonic development may show when and how many different forms of LITRs are expressed. Subsequent tissue expression analyses in adults may then be performed under homeostatic conditions, but also in response to immunological challenges. Several transgenic zebrafish lines with specifically labeled macrophage and neutrophil cells have been established (466). Generating transgenic animals with fluorescently tagged LITRs in combination with whole-animal imaging would allow LITR

expression in specific cell-types during the course of an infection to be tracked in real-time. When a fluorescently tagged LITR gene is expressed, the cell will begin to fluoresce and this may yield interesting insights into potential *in vivo* LITR functions by revealing tissue-specific induction of LITR expression, migratory patterns of an LITR-expressing cell-type or cell-cell interactions where one cell is expressing the fluorescent LITR (467). One limitation to these systems is that transgenic LITR studies would require LITR-specific gene promoters to be identified. Another limitation is that isolating primary cell cultures from zebrafish is challenging and time-consuming (468, 469). Fortunately, primary culture systems are well-established in goldfish.

The *ex vivo* goldfish model has been extensively characterized and offers another opportunity to study cell-specific LITR biology in fish. Goldfish primary cell cultures can be isolated for *in vitro* mixed leukocyte reactions (i.e. *ex vivo* allogeneic or xenogeneic recognition tests) or to study specific innate immune cell-types. Isolating goldfish red blood cell (RBCs) pellets from peripheral blood samples and lysing RBCs results in primary neutrophil-like cultures after 1-2 days. These neutrophils exhibit several functional capabilities including cytokine secretion, degranulation, phagocytosis and reactive oxygen species production (470, 471). It would be interesting to know if LITRs are expressed by these cells and further, if LITRs are involved in regulating any of these functions. Alternatively, supplementing peripheral blood leukocyte cultures with conditioned medium stimulates macrophage differentiation into pro- and anti-inflammatory states and survival for up to ~10 days. It would be interesting to characterize LITR expression and involvement in primary neutrophil development and/or during macrophage differentiation.

7.2.5 Identification of LITR ligands

One major limitation to LITR studies is that their ligands remain unknown. This prevents physiological receptor cross-linking in functional and biochemical characterizations, resulting in a dependence on epitope-tagging and mAb cross-linking approaches. The identification of LITR ligands also directly impacts establishing orthologous evolutionary relationships with other vertebrate immunoregulatory receptor families. Receptor-ligand interactions are primarily determined by extracellular domain structure and IgSF receptors are vastly diversified. Consequently, receptor-ligand interactions are not necessarily conserved from one species to the next and interactions may have simultaneously evolved, expanded and/or contracted.

For example, inhibitory KIRs bind MHC class I on target cells, but KIR2DL4 is an endosomal receptor for the soluble non-classical MHC class I HLA-G (472). Human FcRL4 and FcRL5 bind IgA and IgG, respectively, while FcRL6 binds MHC class II (473–475). Mouse PIRs were identified due to similarities with human Fc α R, yet PIRs bind MHC class I in mice (476–478). Subsequently, CHIRs were discovered due to similarities with PIRs (479). However, CHIR-AB1 is structurally similar to mammalian LILRs which bind classical and non-classical MHC class I ligands yet CHIR-AB1 is an IgY FcR in chickens (480). In teleosts, the IpLITR family contains conserved structural features with mammalian LILRs indicative of a putative MHC class I binding site, however, direct interactions have yet to be demonstrated. In fact, no ligands for immunoregulatory receptor families like LITRs, NITRs or NILTs have been identified in teleost fish, however, two examples have narrowed the scope of potential ligands to two particular cell-types. Channel catfish NITR11 binds to allogeneic 1G8 B cells (481) and IpLITR-types are implicated in the cytotoxic cell-mediated recognition of virus-infected channel catfish T lymphocytes (328). These examples directly suggest that NITR11 binds to a 1G8 B

cell-specific antigen while IpLITR 1.1a-like or IpLITR 2-like receptor-types expressed on cytotoxic cells bind an antigen on channel catfish virus-infected lymphocytes. In any event, ligand identification is difficult due to receptor family diversification and the sheer number of potential interactions.

Given the number of potential ligands, an unbiased high throughput screen is best to begin LITR ligand discovery initiatives. This could include a phage display approach (482–484) or affinity chromatography using Fc fusion proteins that could be used as bait to precipitate potential prey from tissue or cell lysates. By eluting purified proteins and separating them by SDS-PAGE, specific protein bands may be excised and identified by mass spectrometry (485, 486). After identifying candidate ligands, reporter cell assays (481) or yeast two-hybrid (487, 488) approaches could be used to confirm binding interactions. The identification of LITR ligands opens avenues of *in vivo* research within fish models, like goldfish and zebrafish, to begin characterizing specific roles of LITRs during infection, development and immune cell differentiation to expand our fundamental understanding of innate immunity.

7.3 Concluding remarks

Innate immunity is conserved across vertebrate lineages and teleost immunoregulatory receptors are excellent models for exploring innate immune cell biology. Teleost IpLITRs have contributed new insights into the regulation of innate immune cell effector responses. Traditionally, immunoregulatory receptors are categorized as stimulatory or inhibitory types based on the presence of structural features in their TM segments and CYT regions. However, a growing category of vertebrate ITIM-containing receptors have demonstrated versatile signaling potential and functional plasticity.

Previously, the our lab showed that the inhibitory ITIM-containing IpLITR 1.1b mediated versatile signaling and functional plasticity. For example, in NK cells, IpLITR 1.1b facilitates inhibitory signaling via two independent pathways to abrogate NK cell-mediated cytotoxicity. However, when expressed in the myeloid RBL-2H3 cells, IpLITR 1.1b facilitates two independent stimulatory signaling pathways to capture and phagocytose targets via membrane proximal and distal CYT motif-dependent pathways, respectively. Importantly, IpLITR 1.1b WT_{CYT} evokes different functional outcomes by switching its signaling potential depending on cell-type expression. A widely accepted approach for studying molecular details of receptor biology is to establish a heterologous expression system because gain-of-function in a cell-type downstream of a non-endogenously expressed receptor strongly supports the ‘true’ functional, and therefore, signaling potential of said receptor. Heterologous expression approaches for immune receptors often employ non-immune cell-types since these cell-types do not express immune co-receptors and express limited signaling components (e.g. reduced SFK repertoire) relative to immune cell-types. However, IpLITR 1.1b WT_{CYT} has not been stably expressed in a non-immune cell system. In addition, non-immune cells are highly conducive to transfection and transduction techniques allowing efficient expression of several receptor constructs, selection of stable transfectants and efficient signaling molecule knockdowns for detailed molecular studies.

Therefore, my thesis research aimed to establish a non-immune AD293 cell model to further characterize the cellular context-dependent signaling versatility of IpLITR 1.1b WT_{CYT}. The IpLITR 1.1b CYT binds several stimulatory signaling molecules in AD293 cellular lysates, however IpLITR 1.1b does not activate phagocytosis in intact cells. Furthermore, IpLITR 1.1b CYT recruited the inhibitory signaling molecules Csk and SHP2 in physiologically activated cells, suggesting this receptor may mediate inhibitory signaling within an AD293 cellular

context. Conversely, the stimulatory ITAM-containing IpFcR γ -L CYT activated phagocytosis in AD293 cells, representing a ‘bona fide’ phagocytic signaling potential. This work set the stage for studying IpLITR 1.1b CYT-mediated cross-talk modulation of ITAM-dependent phagocytosis. Using a novel imaging flow cytometry-based phagocytosis assay, the IpLITR 1.1b CYT down-regulates ITAM-dependent phagocytosis. IpLITR 1.1b CYT uses a novel cooperative proximal and distal CYT segment-dependent inhibitory mechanism to inhibit ITAM-dependent phagocytosis. These observations have expanded the versatile signaling capabilities of IpLITR 1.1b, including the first report of signaling cross-talk within a teleost immunoregulatory receptor family and uncovered a new mechanism that may regulate how cells decide which targets to eat (Figure 7.2). Overall, my thesis has extended novel observations of the conservation of signaling versatility in vertebrates using teleost immunoregulatory receptors and provided a basis for using teleost receptor models to expand the current understanding of innate immune processes in vertebrates.

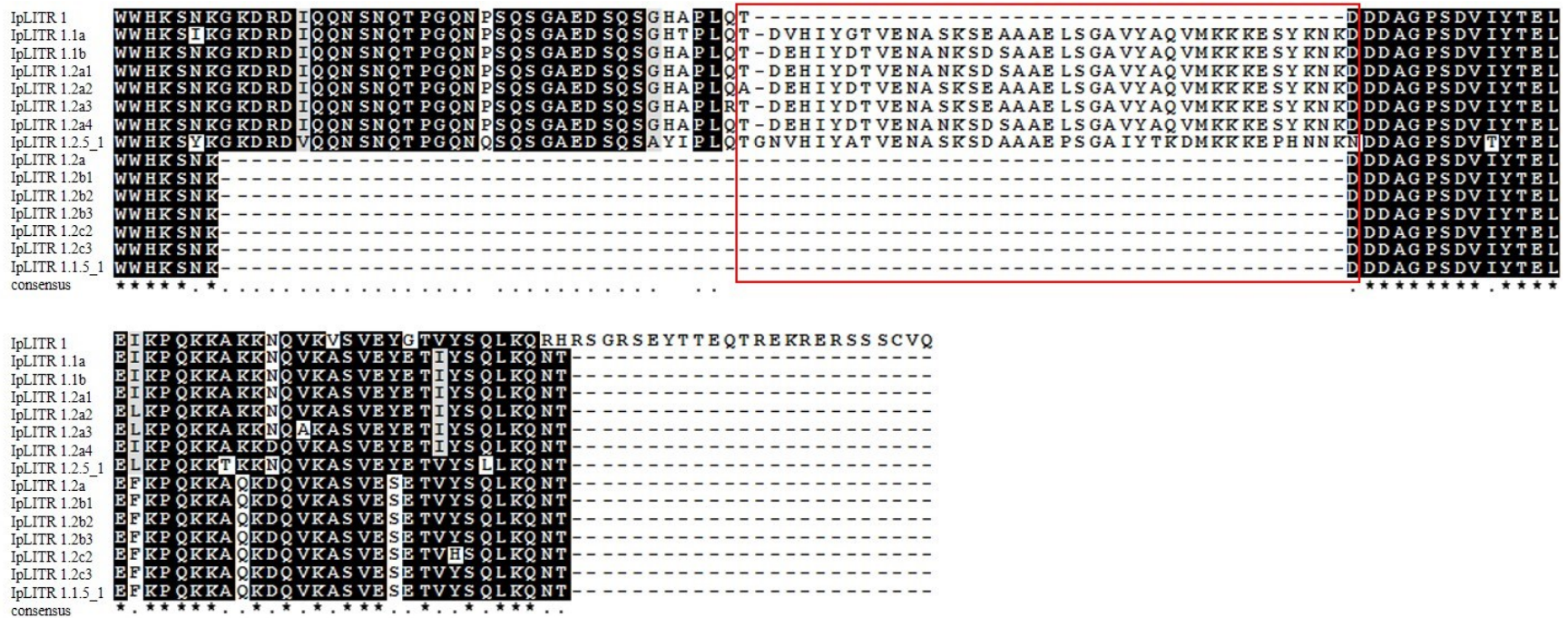


Figure 7.1. Select inhibitory IpLITR isoforms contain an inserted proximal cytoplasmic tail (CYT) segment signaling cassette. GenBank sequences downloaded from the NCBI website were aligned using Jalview and shaded using BoxShade (https://embnet.vital-it.ch/software/BOX_form.html). The red box highlights a proximal CYT segment signaling cassette. Consensus sequence similarity is indicated by ‘*’ or ‘.’ symbols. Black or grey shading indicates identical residues or similar (e.g. hydrophobic, charged, polar) residues in a column, respectively. GenBank accessions for the IpLITR CYT sequences are: IpLITR 1 (AAW82352.1), IpLITR 1.1a (ABI16036.1), IpLITR 1.1b (ABI16050.1), IpLITR 1.2a1 (ABI16039.1), IpLITR 1.2a2 (ABI16040.1), IpLITR 1.2a3 (ABI16041.1), IpLITR 1.2a4 (ABI16042.1), IpLITR 1.2.5_1 (AMK06384.1), IpLITR 1.2a (ABI16051.1), IpLITR 1.2b1 (ABI16043.1), IpLITR 1.2b2 (ABI16044.1), IpLITR 1.2b3 (ABI16045.1), IpLITR 1.2c2 (ABI16047.1), IpLITR 1.2c3 (ABI16048.1), IpLITR 1.1.5_1 (AMK06382.1).

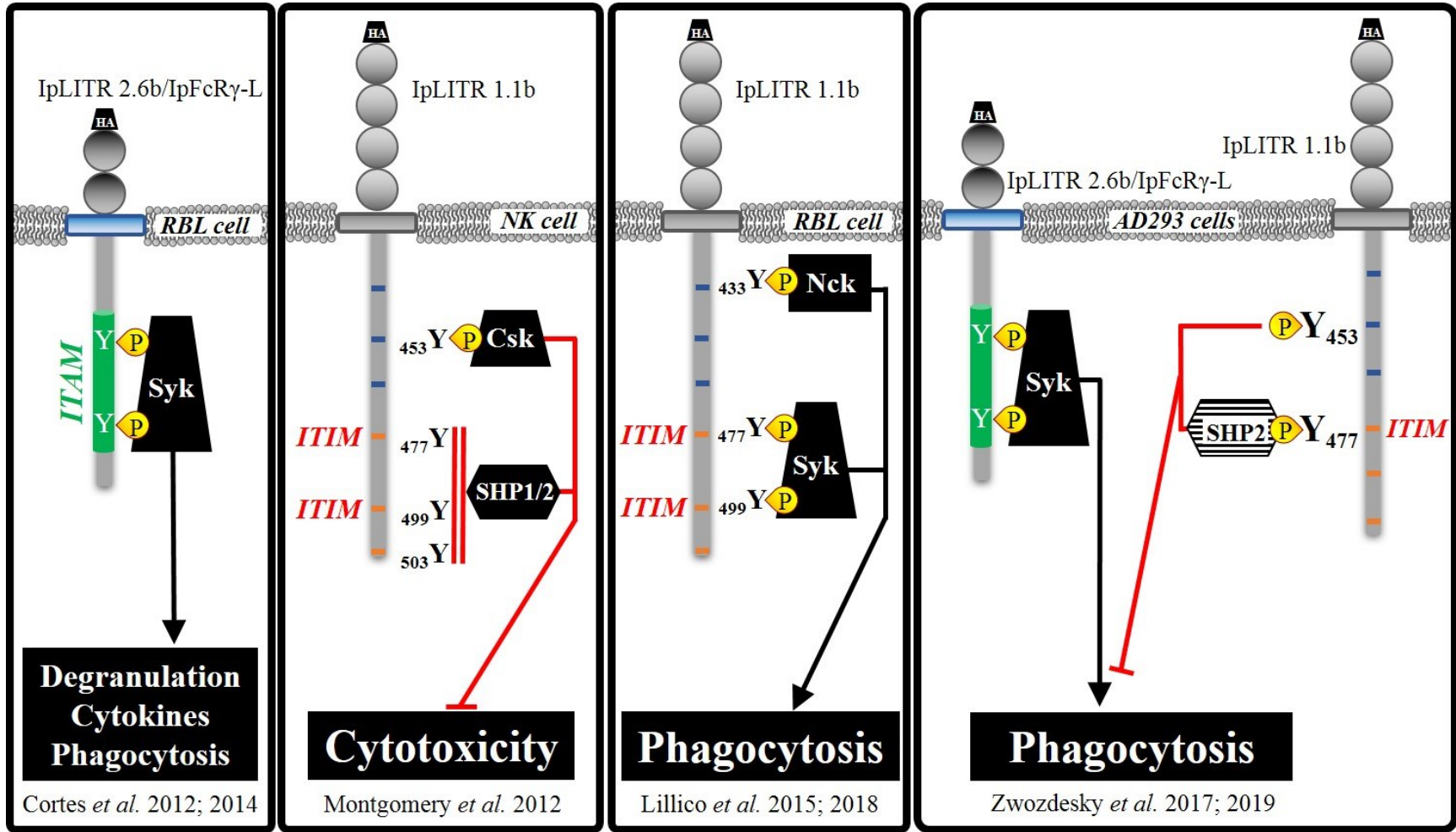


Figure 7.2. Versatility of IpLITR cytoplasmic tail (CYT)-mediated signal transduction capabilities includes cross-talk potential. Heterologous expression of N-terminal hemagglutinin (HA) epitope-tagged IpLITRs in mammalian immune cells allows receptor-specific activation of signal transduction by antibody-mediated cross-linking. Conserved aspects of IpLITR-mediated control of effector responses include the activation of stimulatory responses (e.g. phagocytosis, left panel) and the inhibition of cytotoxicity (middle left panel) through ITAM (green) Syk-dependent and ITIM (red) SHP-dependent pathways, respectively. Two unique aspects of IpLITR-mediated control of effector responses include: 1) inhibitory signaling plasticity through an ITIM-independent, Csk-dependent membrane proximal cytoplasmic tail (CYT) segment pathway (middle left panel) and 2) functional plasticity via activation of phagocytosis through a co-operative ITAM-independent Nck- and Syk-dependent pathway (middle right panel). IpLITR-mediated cross-talk during the down-regulation of ITAM-driven phagocytosis has revealed a novel partially SHP2-dependent inhibitory mechanism (right panel). This work has expanded the versatility of IpLITR CYT-mediated capabilities to include modulation of signaling through one another for the first time within a teleost immunoregulatory receptor family.

REFERENCES

1. Lim, W., B. Mayer, and T. Pawson. 2014. *Cell signaling: principles and mechanisms*,. Taylor & Francis Group, New York.
2. Stafford, J. L., E. Bengtén, L. Du Pasquier, R. D. McIntosh, S. M. Quiniou, L. W. Clem, N. W. Miller, and M. Wilson. 2006. A novel family of diversified immunoregulatory receptors in teleosts is homologous to both mammalian Fc receptors and molecules encoded within the leukocyte receptor complex. *Immunogenetics* 58: 758–773.
3. Mewes, J., K. Verheijen, B. C. S. Montgomery, and J. L. Stafford. 2009. Stimulatory catfish leukocyte immune-type receptors (IpLITRs) demonstrate a unique ability to associate with adaptor signaling proteins and participate in the formation of homo- and heterodimers. *Mol Immunol* 47: 318–331.
4. Cortes, H. D., B. C. S. Montgomery, K. Verheijen, E. García-García, and J. L. Stafford. 2012. Examination of the stimulatory signaling potential of a channel catfish leukocyte immune-type receptor and associated adaptor. *Dev Comp Immunol* 36: 62–73.
5. Cortes, H. D., D. M. E. Lillico, M. A. Zwozdesky, J. G. Pemberton, A. O'Brien, B. C. S. Montgomery, L. Wiersma, J. P. Chang, and J. L. Stafford. 2014. Induction of phagocytosis and intracellular signaling by an inhibitory channel catfish leukocyte immune-type receptor: Evidence for immunoregulatory receptor functional plasticity in teleosts. *J Innate Immun* 6: 435–55.
6. Montgomery, B. C., H. D. Cortes, D. N. Burshtyn, and J. L. Stafford. 2012. Channel catfish leukocyte immune-type receptor mediated inhibition of cellular cytotoxicity is facilitated by SHP-1-dependent and -independent mechanisms. *Dev Comp Immunol* 37: 151–163.
7. Lillico, D. M. E., M. A. Zwozdesky, J. G. Pemberton, J. M. Deutscher, L. O. Jones, J. P. Chang, and J. L. Stafford. 2015. Teleost leukocyte immune-type receptors activate distinct phagocytic modes for target acquisition and engulfment. *J Leukoc Biol* 98: 235–248.
8. Lillico, D. M. E., J. G. Pemberton, and J. L. Stafford. 2018. Selective regulation of cytoskeletal dynamics and filopodia formation by teleost leukocyte immune-type receptors differentially contributes to target capture during the phagocytic process. *Front Immunol* 9: 1144.
9. Fritz, J. H., L. Le Bourhis, J. G. Magalhaes, and D. J. Philpott. 2008. Innate immune recognition at the epithelial barrier drives adaptive immunity: APCs take the back seat. *Trends Immunol* 29: 41–9.
10. Lei-Leston, A. C., A. G. Murphy, and K. J. Maloy. 2017. Epithelial cell inflammasomes in intestinal immunity and inflammation. *Front Immunol* 8: 1168.
11. Indik, Z., C. Kelly, P. Chien, A. I. Levinson, and A. D. Schreiber. 1991. Human Fc γ RII, in the absence of other Fc γ receptors, mediates a phagocytic signal. *J Clin Invest* 88: 1766–1771.
12. Indik, Z. K., J.-G. Park, X. Q. Pan, and A. D. Schreiber. 1995. Induction of phagocytosis by a protein tyrosine kinase. *Blood* 85: 1175–80.
13. Indik, Z. K., J.-G. Park, S. Hunter, and A. D. Schreiber. 1995. The molecular dissection of Fc γ receptor mediated phagocytosis. *Blood* 86: 4389–99.
14. Hutchinson, M. J., and J. M. Allen. 1996. The functional role of the gamma-chain cysteine in

- Fc γ RI-mediated phagocytosis using co-transfected COS-7 cells. *Biochem Soc Trans* 24: 114S.
15. Socolovsky, M., A. R. Hockaday, and J. M. Allen. 1994. Human high-affinity Fc IgG receptor (Fc γ RI)-mediated phagocytosis and pinocytosis in COS cells. *Eur J Cell Biol* 64: 29–44.
 16. Davis, W., P. T. Harrison, M. J. Hutchinson, and J. M. Allen. 1995. Two distinct regions of Fc γ RI initiate separate signalling pathways involved in endocytosis and phagocytosis. *EMBO J* 14: 432–41.
 17. Mitchell, M. A., M.-M. Huang, P. Chien, Z. K. Indik, X. Q. Pan, and A. D. Schreiber. 1994. Substitutions and deletions in the cytoplasmic domain of the phagocytic receptor Fc γ RIIA: effect on receptor tyrosine phosphorylation and phagocytosis. *Blood* 84: 1753–9.
 18. Hutchinson, M. J., P. T. Harrison, and J. M. Allen. 1995. Transmembrane association with gamma-chain is required for Fc γ RI-mediated phagocytosis in transfected COS cells. *Biochem Soc Trans* 23: 121S.
 19. Ward, A. E., and B. M. Rosenthal. 2014. Evolutionary responses of innate immunity to adaptive immunity. *Infect Genet Evol* 21: 492–6.
 20. Riera Romo, M., D. Perez-Martinez, and C. Castillo Ferrer. 2016. Innate immunity in vertebrates: an overview. *Immunology* 148: 125–39.
 21. Gordon, S. 2016. Phagocytosis: An immunobiologic process. *Immunity* 44: 463–75.
 22. Underhill, D. M., S. Gordon, B. A. Imhof, G. Núñez, and P. Bousso. 2016. Élie Metchnikoff (1845-1916): celebrating 100 years of cellular immunology and beyond. *Nat Rev Immunol* 16: 651–656.
 23. Gordon, S. 2016. Phagocytosis: the legacy of Metchnikoff. *Cell* 166: 1065–1068.
 24. Danilova, N. 2006. The evolution of immune mechanisms. *J Exp Zool B Mol Dev Evol* 306: 496–520.
 25. Boehm, T. 2012. Evolution of vertebrate immunity. *Curr Biol* 22: R722-32.
 26. Buchmann, K. 2014. Evolution of innate immunity: clues from invertebrates via fish to mammals. *Front Immunol* 5: 459.
 27. Berry, R., and M. E. Call. 2017. Modular activating receptors in innate and adaptive immunity. *Biochemistry* 56: 1383–402.
 28. Bauer, B., and A. Steinle. 2017. HemITAM: A single tyrosine motif that packs a punch. *Sci Signal* 10: ean3676.
 29. Underhill, D. M., and H. S. Goodridge. 2007. The many faces of ITAMs. *Trends Immunol* 28: 66–73.
 30. Billadeau, D. D., and P. J. Leibson. 2002. ITAMs versus ITIMs: striking a balance during cell regulation. *J Clin Invest* 109: 161–168.
 31. Burshtyn, D. N., and E. O. Long. 1997. Regulation through inhibitory receptors: lessons from natural killer cells. *Trends Cell Biol* 7: 473–9.
 32. van Rees, D. J., K. Szilagyi, T. W. Kuijpers, H. L. Matlung, and T. K. van den Berg. 2016. Immunoreceptors on neutrophils. *Semin Immunol* 28: 94–108.
 33. Long, E. O., H. S. Kim, D. Liu, M. E. Peterson, and S. Rajagopalan. 2013. Controlling natural killer cell responses: integration of signals for activation and inhibition. *Annu Rev*

Immunol 31: 227–58.

34. Kawamoto, H., and Y. Katsura. 2009. A new paradigm for hematopoietic cell lineages: revision of the classical concept of the myeloid-lymphoid dichotomy. *Trends Immunol* 30: 193–200.
35. Koonin, E. V, and M. Krupovic. 2015. Evolution of adaptive immunity from transposable elements combined with innate immune systems. *Nat Rev Genet* 16: 184–192.
36. Sire, J.-Y., and M.-A. Akimenko. 2004. Scale development in fish: a review, with description of sonic hedgehog (shh) expression in the zebrafish (*Danio rerio*). *Int J Dev Biol* 48: 233–47.
37. Alibardi, L. 2006. Structural and immunocytochemical characterization of keratinization in vertebrate epidermis and epidermal derivatives. *Int Rev Cytol* 253: 177–259.
38. Castro, R., and C. Tafalla. 2015. Overview of fish immunity. In *Mucosal Health in Aquaculture* B. H. Beck, and E. Peatman, eds. Academic Press, Madrid. 3–54.
39. Gomez, D., J. O. Sunyer, and I. Salinas. 2013. The mucosal immune system of fish: the evolution of tolerating commensals while fighting pathogens. *Fish Shellfish Immunol* 35: 1729–39.
40. Xu, Z., D. Parra, D. Gómez, I. Salinas, Y.-A. Zhang, L. von Gersdorff Jørgensen, R. D. Heinecke, K. Buchmann, S. LaPatra, and J. O. Sunyer. 2013. Teleost skin, an ancient mucosal surface that elicits gut-like immune responses. *Proc Natl Acad Sci U S A* 110: 13097–102.
41. Benhamed, S., F. A. Guardiola, M. Mars, and M. Á. Esteban. 2014. Pathogen bacteria adhesion to skin mucus of fishes. *Vet Microbiol* 171: 1–12.
42. Murphy, K., P. Travers, M. Walport, and C. Janeway. 2008. *Janeway's Immunobiology*, 7th ed. Garland Science, New York.
43. DeFranco, A. L., R. M. Locksley, and M. Robertson. 2007. *Immunity: the immune response in infectious and inflammatory disease*. New Science Press in association with Oxford University Press and Sinauer Associates, London.
44. Daimon, T., and A. Caxton-Martins. 1977. Electron microscopic and enzyme cytochemical studies on granules of mature chicken granular leucocytes. *J Anat* 123: 553–62.
45. Cannon, M. S., H. H. Mollenhauer, T. E. Eurell, D. H. Lewis, A. M. Cannon, and C. Tompkins. 1980. An ultrastructural study of the leukocytes of the channel catfish, *Ictalurus punctatus*. *J Morphol* 164: 1–23.
46. Carvalho, M. P. N., N. G. T. Queiroz-Hazarbassanov, C. O. Massoco, S. Rossi, S. S. Sant'Anna, J. L. Catão-Dias, and K. F. Grego. 2016. Flow cytometric characterization of peripheral blood leukocyte populations of 3 neotropical snake species: *Boa constrictor*, *Bothrops jararaca*, and *Crotalus durissus*. *Vet Clin Pathol* 45: 271–80.
47. Secombes, C. J., and J. Zou. 2017. Evolution of interferons and interferon receptors. *Front Immunol* 8: 209.
48. Zou, J., and C. J. Secombes. 2016. The function of fish cytokines. *Biology (Basel)* 5: 23.
49. Hansen, J. D., L. Du Pasquier, M.-P. Lefranc, V. Lopez, A. Benmansour, and P. Boudinot. 2009. The B7 family of immunoregulatory receptors: a comparative and evolutionary perspective. *Mol Immunol* 46: 457–72.

50. Ashfaq, H., H. Soliman, M. Saleh, and M. El-Matbouli. 2019. CD4: a vital player in the teleost fish immune system. *Vet Res* 50: 1.
51. Litman, G. W., M. K. Anderson, and J. P. Rast. 1999. Evolution of antigen binding receptors. *Annu Rev Immunol* 17: 109–47.
52. Wilson, A. B. 2017. MHC and adaptive immunity in teleost fishes. *Immunogenetics* 69: 521–8.
53. Scapigliati, G. 2013. Functional aspects of fish lymphocytes. *Dev Comp Immunol* 41: 200–8.
54. Fink, I. R., E. L. Benard, T. Hermsen, A. H. Meijer, M. Forlenza, and G. F. Wiegertjes. 2015. Molecular and functional characterization of the scavenger receptor CD36 in zebrafish and common carp. *Mol Immunol* 63: 381–93.
55. Barreda, D. R., H. R. Neely, and M. F. Flajnik. 2016. Evolution of myeloid cells. *Microbiol Spectr* 4: MCHD-0007-2015.
56. Neulen, M.-L., B. C. Viertlboeck, C. Straub, and T. W. Göbel. 2015. Identification of novel chicken CD4⁺ CD3⁻ blood population with NK cell like features. *Dev Comp Immunol* 49: 72–8.
57. Chen, C.-Y., Q.-M. Xie, Y. Xue, J. Ji, S. Chang, J.-Y. Ma, and Y.-Z. Bi. 2013. Characterization of cytotoxicity-related gene expression in response to virulent Marek's disease virus infection in the bursa of Fabricius. *Res Vet Sci* 94: 496–503.
58. Jansen, C. A., D. A. van Haarlem, B. Sperling, P. J. van Kooten, E. de Vries, B. C. Viertlboeck, L. Vervelde, and T. W. Göbel. 2016. Identification of an activating chicken Ig-like receptor recognizing avian influenza viruses. *J Immunol* 197: 4696–703.
59. Wu, Z., L. Rothwell, J. R. Young, J. Kaufman, C. Butter, and P. Kaiser. 2010. Generation and characterization of chicken bone marrow-derived dendritic cells. *Immunology* 129: 133–45.
60. Rath, N. C., M. S. Parcells, H. Xie, and E. Santin. 2003. Characterization of a spontaneously transformed chicken mononuclear cell line. *Vet Immunol Immunopathol* 96: 93–104.
61. Rath, N. C., G. R. Huff, J. M. Balog, and W. E. Huff. 1998. Fluorescein isothiocyanate staining and characterization of avian heterophils. *Vet Immunol Immunopathol* 64: 83–95.
62. Chuammitri, P., J. Ostojic, C. B. Andreasen, S. B. Redmond, S. J. Lamont, and D. Palic. 2009. Chicken heterophil extracellular traps (HETs): novel defense mechanism of chicken heterophils. *Vet Immunol Immunopathol* 129: 126–31.
63. Goyos, A., and J. Robert. 2009. Tumorigenesis and anti-tumor immune responses in *Xenopus*. *Front Biosci* 14: 167–76.
64. de Carvalho, M. P. N., N. G. T. Queiroz-Hazarbassanov, C. de Oliveira Massoco, S. S. Sant'Anna, M. M. Lourenço, G. Levin, M. C. Sogayar, K. F. Grego, and J. L. Catão-Dias. 2017. Functional characterization of neotropical snakes peripheral blood leukocytes subsets: Linking flow cytometry cell features, microscopy images and serum corticosterone levels. *Dev Comp Immunol* 74: 144–53.
65. Lu, Y., J. Li, H. Yu, X. Xu, J. Liang, Y. Tian, D. Ma, G. Lin, G. Huang, and R. Lai. 2006. Two families of antimicrobial peptides with multiple functions from skin of rufous-spotted torrent frog, *Amolops loloensis*. *Peptides* 27: 3085–91.
66. Rossinholi, G. M., and I. Vugman. 1983. Toad (*Bufo paracnemius*) mast cell degranulation

- by compound 48/80 and by chlorpromazine: a non-lytic process. *Eur J Pharmacol* 96: 133–5.
67. Hoole, D., and J. B. Mitchell. 1984. Gorgoderina vitelliloba: interaction with frog leucocytes in vivo and in vitro. *Exp Parasitol* 57: 225–33.
68. Horton, T. L., P. Ritchie, M. D. Watson, and J. D. Horton. 1996. NK-like activity against allogeneic tumour cells demonstrated in the spleen of control and thymectomized Xenopus. *Immunol Cell Biol* 74: 365–73.
69. Nakanishi, T., H. Toda, Y. Shibasaki, and T. Somamoto. 2011. Cytotoxic T cells in teleost fish. *Dev Comp Immunol* 35: 1317–23.
70. Grayfer, L., B. Kerimoglu, A. Yaparla, J. W. Hodgkinson, J. Xie, and M. Belosevic. 2018. Mechanisms of fish macrophage antimicrobial immunity. *Front Immunol* 9: 1105.
71. Praveen, K., J. H. Leary III, D. L. Evans, and L. Jaso-Friedmann. 2006. Nonspecific cytotoxic cells of teleosts are armed with multiple granzymes and other components of the granule exocytosis pathway. *Mol Immunol* 43: 1152–62.
72. Quiniou, S. M. A., M. Sahoo, E.-S. Edholm, E. Bengten, and M. Wilson. 2011. Channel catfish CD8 α and CD8 β co-receptors: characterization, expression and polymorphism. *Fish Shellfish Immunol* 30: 894–901.
73. Haynes, L., and E. C. McKinney. 1991. Shark spontaneous cytotoxicity: characterization of the regulatory cell. *Dev Comp Immunol* 15: 123–34.
74. Esteban, M. Á., A. Cuesta, E. Chaves-Pozo, and J. Meseguer. 2015. Phagocytosis in teleosts. Implications of the new cells involved. *Biology (Basel)* 4: 907–22.
75. Rieger, A. M., and D. R. Barreda. 2011. Antimicrobial mechanisms of fish leukocytes. *Dev Comp Immunol* 35: 1238–45.
76. Katzenback, B. A., F. Katakura, and M. Belosevic. 2016. Goldfish (*Carassius auratus* L.) as a model system to study the growth factors, receptors and transcription factors that govern myelopoiesis in fish. *Dev Comp Immunol* 58: 68–85.
77. Belosevic, M., P. C. Hanington, and D. R. Barreda. 2006. Development of goldfish macrophages in vitro. *Fish Shellfish Immunol* 20: 152–71.
78. Li, J., D. R. Barreda, Y.-A. Zhang, H. Boshra, A. E. Gelman, S. LaPatra, L. Tort, and J. O. Sunyer. 2006. B lymphocytes from early vertebrates have potent phagocytic and microbicidal abilities. *Nat Immunol* 7: 1116–24.
79. Parra, D., A. M. Rieger, J. Li, Y.-A. Zhang, L. M. Randall, C. A. Hunter, D. R. Barreda, and J. O. Sunyer. 2012. Peritoneal cavity B-1 B cells have phagocytic and microbicidal capacities and present phagocytosed antigen to CD4 $^{+}$ T cells. *J Leukoc Biol* 91: 525–36.
80. Sunyer, J. O. 2012. Evolutionary and functional relationships of B cells from fish and mammals: insights into their novel roles in phagocytosis and presentation of particulate antigen. *Infect Disord Drug Targets* 12: 200–12.
81. Fillatreau, S., A. Six, S. Magadan, R. Castro, J. O. Sunyer, and P. Boudinot. 2013. The astonishing diversity of Ig classes and B cell repertoires in teleost fish. *Front Immunol* 4: 28.
82. Wilson, M., E. Hsu, A. Marcuz, M. Courtet, L. Du Pasquier, and C. Steinberg. 1992. What limits affinity maturation of antibodies in Xenopus--the rate of somatic mutation or the ability to

select mutants? *EMBO J* 11: 4337–47.

83. Wu, L., S. Fu, X. Yin, W. Leng, Z. Guo, A. Wang, and J. Ye. 2018. Affinity maturation occurs in channel catfish (*Ictalurus punctatus*) following immunization with a T-cell dependent antigen. *Fish Shellfish Immunol* 84: 781–6.

84. Shen, L., T. B. Stuge, H. Zhou, M. Khayat, K. S. Barker, S. M. A. Quiniou, M. Wilson, E. Bengten, V. G. Chinchar, L. W. Clem, and N. W. Miller. 2002. Channel catfish cytotoxic cells: a mini-review. *Dev Comp Immunol* 26: 141–9.

85. Oumouna, M., L. Jaso-Friedmann, and D. L. Evans. 2002. Activation of nonspecific cytotoxic cells (NCC) with synthetic oligodeoxynucleotides and bacterial genomic DNA: binding, specificity and identification of unique immunostimulatory motifs. *Dev Comp Immunol* 26: 257–69.

86. Yoder, J. A. 2004. Investigating the morphology, function and genetics of cytotoxic cells in bony fish. *Comp Biochem Physiol Part C, Toxicol Pharmacol* 138: 271–80.

87. Bishop, G. R., S. Taylor, L. Jaso-Friedmann, and D. L. Evans. 2002. Mechanisms of nonspecific cytotoxic cell regulation of apoptosis: cytokine-like activity of Fas ligand. *Fish Shellfish Immunol* 13: 47–67.

88. Evans, D. L., J. H. Leary III, and L. Jaso-Friedmann. 2001. Nonspecific cytotoxic cells and innate immunity: regulation by programmed cell death. *Dev Comp Immunol* 25: 791–805.

89. Volff, J.-N. 2005. Genome evolution and biodiversity in teleost fish. *Heredity (Edinb)* 94: 280–94.

90. Maisey, K., and M. Imarai. 2011. Diversity of teleost leukocyte molecules: role of alternative splicing. *Fish Shellfish Immunol* 31: 663–72.

91. Dixon, B., and R. J. M. Stet. 2001. The relationship between major histocompatibility receptors and innate immunity in teleost fish. *Dev Comp Immunol* 25: 683–99.

92. Rast, J. P., R. N. Haire, R. T. Litman, S. Pross, and G. W. Litman. 1995. Identification and characterization of T-cell antigen receptor-related genes in phylogenetically diverse vertebrate species. *Immunogenetics* 42: 204–12.

93. Stet, R. J. M., T. Hermsen, A. H. Westphal, J. Jukes, M. Engelsma, B. M. Lidy Verburg-van Kemenade, J. Dortmans, J. Aveiro, and H. F. J. Savelkoul. 2005. Novel immunoglobulin-like transcripts in teleost fish encode polymorphic receptors with cytoplasmic ITAM or ITIM and a new structural Ig domain similar to the natural cytotoxicity receptor NKp44. *Immunogenetics* 57: 77–89.

94. Stafford, J. L., E. Bengtén, L. Du Pasquier, N. W. Miller, and M. Wilson. 2007. Channel catfish leukocyte immune-type receptors contain a putative MHC class I binding site. *Immunogenetics* 59: 77–91.

95. Fei, C., J. G. Pemberton, D. M. E. Lillico, M. A. Zwozdesky, and J. L. Stafford. 2016. Biochemical and functional insights into the integrated regulation of innate immune cell responses by teleost leukocyte immune-type receptors. *Biology (Basel)* 5: 13.

96. Bhattacharyya, R. P., A. Reményi, B. J. Yeh, and W. A. Lim. 2006. Domains, motifs, and scaffolds: the role of modular interactions in the evolution and wiring of cell signaling circuits.

Annu Rev Biochem 75: 655–80.

97. Dueber, J. E., B. J. Yeh, R. P. Bhattacharyya, and W. A. Lim. 2004. Rewiring cell signaling: the logic and plasticity of eukaryotic protein circuitry. *Curr Biol Struct Biol* 14: 690–9.
98. Sudol, M. 1998. From Src homology domains to other signaling modules: proposal of the “protein recognition code.” *Oncogene* 17: 1469–74.
99. Herberman, R. B., D. Char, R. Oldham, P. Levine, B. G. Leventhal, J. L. McCoy, H. C. Ho, and J. C. W. Chau. 1975. Cell-mediated immunity in human acute leukemia. *Bibl Haematol* 649–56.
100. Catalona, W. J., R. K. Oldham, J. Y. Djeu, R. B. Herberman, and G. B. Cannon. 1975. Specificity of in vitro cellular cytotoxicity against transitional cell carcinoma cell line T-24. *Surg Forum* 26: 122–4.
101. Moretta, A., C. Bottino, D. Pende, G. Tripodi, G. Tambussi, O. Viale, A. Orengo, M. Barbaresi, A. Merli, E. Ciccone, and L. Moretta. 1990. Identification of four subsets of human CD3-CD16+ natural killer (NK) cells by the expression of clonally distributed functional surface molecules: correlation between subset assignment of NK clones and ability to mediate specific alloantigen recognition. *J Exp Med* 172: 1589–98.
102. Moretta, A., G. Tambussi, C. Bottino, G. Tripodi, A. Merli, E. Ciccone, G. Pantaleo, and L. Moretta. 1990. A novel surface antigen expressed by a subset of human CD3-CD16+ natural killer cells. Role in cell activation and regulation of cytolytic function. *J Exp Med* 171: 695–714.
103. Colonna, M., T. Spies, J. L. Strominger, E. Ciccone, A. Moretta, L. Moretta, D. Pende, and O. Viale. 1992. Alloantigen recognition by two human natural killer cell clones is associated with HLA-C or a closely linked gene. *Proc Natl Acad Sci U S A* 89: 7983–5.
104. Ciccone, E., D. Pende, O. Viale, A. Than, C. Di Donato, A. M. Orengo, R. Biassoni, S. Verdiani, A. Amoroso, A. Moretta, and L. Moretta. 1992. Involvement of HLA class I alleles in natural killer (NK) cell-specific functions: expression of HLA-Cw3 confers selective protection from lysis by alloreactive NK clones displaying a defined specificity (specificity 2). *J Exp Med* 176: 963–71.
105. Moretta, A., M. Vitale, C. Bottino, A. M. Orengo, L. Morelli, R. Augugliaro, M. Barbaresi, E. Ciccone, and L. Moretta. 1993. P58 molecules as putative receptors for major histocompatibility complex (MHC) class I molecules in human natural killer (NK) cells. Anti-p58 antibodies reconstitute lysis of MHC class I-protected cells in NK clones displaying different specificities. *J Exp Med* 178: 597–604.
106. Moretta, A., S. Sivori, M. Vitale, D. Pende, L. Morelli, R. Augugliaro, C. Bottino, and L. Moretta. 1995. Existence of both inhibitory (p58) and activatory (p50) receptors for HLA-C molecules in human natural killer cells. *J Exp Med* 182: 875–84.
107. Long, E. O., M. Colonna, and L. L. Lanier. 1996. Inhibitory MHC class I receptors on NK and T cells: a standard nomenclature. *Immunol Today* 17: 100.
108. Vitale, M., S. Sivori, D. Pende, R. Augugliaro, C. Di Donato, A. Amoroso, M. Malnati, C. Bottino, L. Moretta, and A. Moretta. 1996. Physical and functional independency of p70 and p58 natural killer (NK) cell receptors for HLA class I: their role in the definition of different groups

- of alloreactive NK cell clones. *Proc Natl Acad Sci U S A* 93: 1453–7.
109. Litwin, V., J. Gumperz, P. Parham, J. H. Phillips, and L. L. Lanier. 1994. NKB1: a natural killer cell receptor involved in the recognition of polymorphic HLA-B molecules. *J Exp Med* 180: 537–43.
110. D’Andrea, A., C. Chang, K. Franz-Bacon, T. McClanahan, J. H. Phillips, and L. L. Lanier. 1995. Molecular cloning of NKB1. A natural killer cell receptor for HLA-B allotypes. *J Immunol* 155: 2306–10.
111. Wagtmann, N., R. Biassoni, C. Cantoni, S. Verdiani, M. S. Malnati, M. Vitale, C. Bottino, L. Moretta, A. Moretta, and E. O. Long. 1995. Molecular clones of the p58 NK cell receptor reveal immunoglobulin-related molecules with diversity in both the extra- and intracellular domains. *Immunity* 2: 439–49.
112. Colonna, M., and J. Samaridis. 1995. Cloning of immunoglobulin-superfamily members associated with HLA-C and HLA-B recognition by human natural killer cells. *Science (80-)* 268: 405–8.
113. Biassoni, R., C. Cantoni, M. Falco, S. Verdiani, C. Bottino, M. Vitale, R. Conte, A. Poggi, A. Moretta, and L. Moretta. 1996. The human leukocyte antigen (HLA)-C-specific “activatory” or “inhibitory” natural killer cell receptors display highly homologous extracellular domains but differ in their transmembrane and intracytoplasmic portions. *J Exp Med* 183: 645–50.
114. Selvakumar, A., U. Steffens, and B. Dupont. 1997. Polymorphism and domain variability of human killer cell inhibitory receptors. *Immunol Rev* 155: 183–96.
115. Dupont, B., A. Selvakumar, and U. Steffens. 1997. The killer cell inhibitory receptor genomic region on human chromosome 19q13.4. *Tissue Antigens* 49: 557–63.
116. Bottino, C., M. Vitale, L. Olcese, S. Sivori, L. Morelli, R. Augugliaro, E. Ciccone, L. Moretta, and A. Moretta. 1994. The human natural killer cell receptor for major histocompatibility complex class I molecules. Surface modulation of p58 molecules and their linkage to CD3 ζ chain, Fc ϵ RI γ chain and the p56lck kinase. *Eur J Immunol* 24: 2527–34.
117. Einspahr, K. J., R. T. Abraham, B. A. Binstadt, Y. Uehara, and P. J. Leibson. 1991. Tyrosine phosphorylation provides an early and requisite signal for the activation of natural killer cell cytotoxic function. *Proc Natl Acad Sci U S A* 88: 6279–83.
118. Lanier, L. L., A. M. Le, J. H. Phillips, N. L. Warner, and G. F. Babcock. 1983. Subpopulations of human natural killer cells defined by expression of the Leu-7 (HNK-1) and Leu-11 (NK-15) antigens. *J Immunol* 131: 1789–96.
119. Ståhls, A., M. Heiskala, T. Mustelin, and L. C. Andersson. 1992. Activation of natural killer cells via the Fc γ RIII (CD16) requires initial tyrosine phosphorylation. *Eur J Immunol* 22: 611–4.
120. Ting, A. T., K. J. Einspahr, R. T. Abraham, and P. J. Leibson. 1991. Fc γ receptor signal transduction in natural killer cells. Coupling to phospholipase C via a G protein-independent, but tyrosine kinase-dependent pathway. *J Immunol* 147: 3122–7.
121. Amigorena, S., J. Salamero, J. Davoust, W. H. Fridman, and C. Bonnerot. 1992. Tyrosine-containing motif that transduces cell activation signals also determines internalization and antigen presentation via type III receptors for IgG. *Nature* 358: 337–41.

122. Amigorena, S., C. Bonnerot, J. R. Drake, D. Choquet, W. Hunziker, J.-G. Guillet, P. Webster, C. Sautes, I. Mellman, and W. H. Fridman. 1992. Cytoplasmic domain heterogeneity and functions of IgG Fc receptors in B lymphocytes. *Science* (80-) 256: 1808–12.
123. Doody, G. M., L. B. Justement, C. C. Delibrias, R. J. Matthews, J. Lin, M. L. Thomas, and D. T. Fearon. 1995. A role in B cell activation for CD22 and the protein tyrosine phosphatase SHP. *Science* (80-) 269: 242–4.
124. Muta, T., T. Kurosaki, Z. Misulovin, M. Sanchez, M. C. Nussenzweig, and J. V Ravetch. 1994. A 13-amino-acid motif in the cytoplasmic domain of FcγRIIB modulates B-cell receptor signalling. *Nature* 368: 70–3.
125. Burshtyn, D. N., A. M. Scharenberg, N. Wagtmann, S. Rajagopalan, K. Berrada, T. Yi, J.-P. Kinet, and E. O. Long. 1996. Recruitment of tyrosine phosphatase HCP by the killer cell inhibitor receptor. *Immunity* 4: 77–85.
126. Burshtyn, D. N., W. Yang, T. Yi, and E. O. Long. 1997. A novel phosphotyrosine motif with a critical amino acid at position -2 for the SH2 domain-mediated activation of the tyrosine phosphatase SHP-1. *J Biol Chem* 272: 13066–13072.
127. Burshtyn, D. N., A. S. Lam, M. Weston, N. Gupta, P. A. M. Warmerdam, and E. O. Long. 1999. Conserved residues amino-terminal of cytoplasmic tyrosines contribute to the SHP-1-mediated inhibitory function of killer cell Ig-like receptors. *J Immunol* 162: 897–902.
128. Samelson, L. E. 2002. Signal transduction mediated by the T cell antigen receptor: the role of adapter proteins. *Annu Rev Immunol* 20: 371–94.
129. Pitcher, L. A., and N. S. C. van Oers. 2003. T-cell receptor signal transmission: who gives an ITAM? *Trends Immunol* 24: 554–60.
130. Humphrey, M. B., L. L. Lanier, and M. C. Nakamura. 2005. Role of ITAM-containing adapter proteins and their receptors in the immune system and bone. *Immunol Rev* 208: 50–65.
131. Stanietsky, N., and O. Mandelboim. 2010. Paired NK cell receptors controlling NK cytotoxicity. *FEBS Lett* 584: 4895–900.
132. Long, E. O. 2008. Negative signaling by inhibitory receptors: the NK cell paradigm. *Immunol Rev* 224: 70–84.
133. Liu, B. A., B. W. Engelmann, and P. D. Nash. 2012. The language of SH2 domain interactions defines phosphotyrosine-mediated signal transduction. *FEBS Lett* 586: 2597–2605.
134. Sadowski, I., J. C. Stone, and T. Pawson. 1986. A noncatalytic domain conserved among cytoplasmic protein-tyrosine kinases modifies the kinase function and transforming activity of Fujinami sarcoma virus P130gag-fps. *Mol Cell Biol* 6: 4396–4408.
135. Songyang, Z., S. E. Shoelson, M. Chaudhuri, G. Gish, T. Pawson, W. G. Haser, F. King, T. Roberts, S. Ratnofsky, R. J. Lechleider, B. G. Neel, R. B. Birge, J. E. Fajardo, M. M. Chou, H. Hanafusa, B. Schaffhausen, and L. C. Cantley. 1993. SH2 domains recognize specific phosphopeptide sequences. *Cell* 72: 767–776.
136. Huang, H., L. Li, C. Wu, D. Schibli, K. Colwill, S. Ma, C. Li, P. Roy, K. Ho, Z. Songyang, T. Pawson, Y. Gao, and S. S.-C. Li. 2008. Defining the specificity space of the human SRC homology 2 domain. *Mol Cell Proteomics* 7: 768–784.

137. Engelmann, B. W., Y. Kim, M. Wang, B. Peters, R. S. Rock, and P. D. Nash. 2014. The development and application of a quantitative peptide microarray based approach to protein interaction domain specificity space. *Mol Cell Proteomics* 13: 3647–62.
138. Cussac, D., M. Frech, and P. Chardin. 1994. Binding of the Grb2 SH2 domain to phosphotyrosine motifs does not change the affinity of its SH3 domains for Sos proline-rich motifs. *EMBO J* 13: 4011–4021.
139. Wagner, M. J., M. M. Stacey, B. A. Liu, and T. Pawson. 2013. Molecular mechanisms of SH2- and PTB-domain-containing proteins in receptor tyrosine kinase signaling. *Cold Spring Harb Perspect Biol* 5: a008987.
140. Rojas, M., S. Yao, J. P. Donahue, and Y.-Z. Lin. 1997. An alternative to phosphotyrosine-containing motifs for binding to an SH2 domain. *Biochem Biophys Res Commun* 234: 675–80.
141. Clarke, M., A. J. Lohan, B. Liu, I. Lagkouvardos, S. Roy, N. Zafar, C. Bertelli, C. Schilde, A. Kianianmomeni, T. R. Bürglin, C. Frech, B. Turcotte, K. O. Kopec, J. M. Synnot, C. Choo, I. Paponov, A. Finkler, C. S. H. Tan, A. P. Hutchins, T. Weinmeier, T. Rattei, J. S. C. Chu, G. Gimenez, M. Irimia, D. J. Rigden, D. A. Fitzpatrick, J. Lorenzo-Morales, A. Bateman, C.-H. Chiu, P. Tang, P. Hegemann, H. Fromm, D. Raoult, G. Greub, D. Miranda-Saavedra, N. Chen, P. Nash, M. L. Ginger, M. Horn, P. Schaap, L. Caler, and B. J. Loftus. 2013. Genome of *Acanthamoeba castellanii* highlights extensive lateral gene transfer and early evolution of tyrosine kinase signaling. *Genome Biol* 14: R11.
142. Manning, G., S. L. Young, W. T. Miller, and Y. Zhai. 2008. The protist, *Monosiga brevicollis*, has a tyrosine kinase signaling network more elaborate and diverse than found in any known metazoan. *Proc Natl Acad Sci U S A* 105: 9674–9.
143. Liu, B. A., E. Shah, K. Jablonowski, A. Stergachis, B. Engelmann, and P. D. Nash. 2011. The SH2 domain-containing proteins in 21 species establish the provenance and scope of phosphotyrosine signaling in eukaryotes. *Sci Signal* 4: ra83.
144. Blaikie, P., D. Immanuel, J. Wu, N. Li, V. Yajnik, and B. Margolis. 1994. A region in Shc distinct from the SH2 domain can bind tyrosine-phosphorylated growth factor receptors. *J Biol Chem* 269: 32031–4.
145. Kavanaugh, W. M., and L. T. Williams. 1994. An alternative to SH2 domains for binding tyrosine-phosphorylated proteins. *Science (80-)* 266: 1862–5.
146. Ingham, R. J., H. Okada, M. Dang-Lawson, J. Dinglasan, P. van der Geer, T. Kurosaki, and M. R. Gold. 1999. Tyrosine phosphorylation of shc in response to B cell antigen receptor engagement depends on the SHIP inositol phosphatase. *J Immunol* 163: 5891–5.
147. Jadwin, J. A., D. Oh, T. G. Curran, M. Ogiue-Ikeda, L. Jia, F. M. White, K. Machida, J. Yu, and B. J. Mayer. 2016. Time-resolved multimodal analysis of Src Homology 2 (SH2) domain binding in signaling by receptor tyrosine kinases. *Elife* 2: e11835.
148. Call, M. E., and K. W. Wucherpfennig. 2007. Common themes in the assembly and architecture of activating immune receptors. *Nat Rev Immunol* 7: 841–50.
149. Viertelboeck, B. C., F. A. Habermann, R. Schmitt, M. A. M. Groenen, L. Du Pasquier, and T. W. Göbel. 2005. The chicken leukocyte receptor complex: a highly diverse multigene family

- encoding at least six structurally distinct receptor types. *J Immunol* 175: 385–93.
150. Guselnikov, S. V, T. Ramanayake, A. Y. Erilova, L. V Mechetina, A. M. Najakshin, J. Robert, and A. V Taranin. 2008. The Xenopus FcR family demonstrates continually high diversification of paired receptors in vertebrate evolution. *BMC Evol Biol* 8: 148.
151. Guselnikov, S. V, E. S. Reshetnikova, A. M. Najakshin, L. V Mechetina, J. Robert, and A. V Taranin. 2010. The amphibians *Xenopus laevis* and *Silurana tropicalis* possess a family of activating KIR-related Immunoglobulin-like receptors. *Dev Comp Immunol* 34: 308–15.
152. Carroll-Portillo, A., K. Spendier, J. Pfeiffer, G. Griffiths, H. Li, K. A. Lidke, J. M. Oliver, D. S. Lidke, J. L. Thomas, B. S. Wilson, and J. A. Timlin. 2010. Formation of a mast cell synapse: FcεRI membrane dynamics upon binding mobile or immobilized ligands on surfaces. *J Immunol* 184: 1328–38.
153. Goodridge, H. S., C. N. Reyes, C. A. Becker, T. R. Katsumoto, J. Ma, A. J. Wolf, N. Bose, A. S. H. Chan, A. S. Magee, M. E. Danielson, A. Weiss, J. P. Vasilakos, and D. M. Underhill. 2011. Activation of the innate immune receptor Dectin-1 upon formation of a “phagocytic synapse.” *Nature* 472: 471–475.
154. Dustin, M. L., and E. O. Long. 2010. Cytotoxic immunological synapses. *Immunol Rev* 235: 24–34.
155. Dykstra, M., A. Cherukuri, and S. K. Pierce. 2001. Rafts and synapses in the spatial organization of immune cell signaling receptors. *J Leukoc Biol* 70: 699–707.
156. Dustin, M. L., A. K. Chakraborty, and A. S. Shaw. 2010. Understanding the structure and function of the immunological synapse. *Cold Spring Harb Perspect Biol* 2: a002311.
157. Flannagan, R. S., V. Jaumouillé, and S. Grinstein. 2012. The cell biology of phagocytosis. *Annu Rev Pathol* 7: 61–98.
158. Freeman, S. A., and S. Grinstein. 2014. Phagocytosis: receptors, signal integration, and the cytoskeleton. *Immunol Rev* 262: 193–215.
159. Stuart, L. M., and R. A. B. Ezekowitz. 2005. Phagocytosis: elegant complexity. *Immunity* 22: 539–50.
160. Rosales, C., and E. Uribe-Querol. 2017. Phagocytosis: A fundamental process in immunity. *Biomed Res Int* 2017: 9042851.
161. Ivashkiv, L. B. 2009. Cross-regulation of signaling by ITAM-associated receptors. *Nat Immunol* 10: 340–7.
162. Bakker, A. B. H., J. Wu, J. H. Phillips, and L. L. Lanier. 2000. NK cell activation: distinct stimulatory pathways counterbalancing inhibitory signals. *Hum Immunol* 61: 18–27.
163. Lam, R. A., J. Y. Chwee, N. Le Bert, M. Sauer, E. P. von Strandmann, and S. Gasser. 2013. Regulation of self-ligands for activating natural killer cell receptors. *Ann Med* 45: 384–94.
164. Cheng, J., A. Montecalvo, and L. P. Kane. 2011. Regulation of NF-κB induction by TCR/CD28. *Immunol Res* 50: 113–7.
165. Vivier, E., J. A. Nunès, and F. Vély. 2004. Natural killer cell signaling pathways. *Science (80-)* 306: 1517–9.
166. Dal Porto, J. M., S. B. Gauld, K. T. Merrell, D. Mills, A. E. Pugh-Bernard, and J. Cambier.

2004. B cell antigen receptor signaling 101. *Mol Immunol* 41: 599–613.
167. Maeda, A., M. Kurosaki, and T. Kurosaki. 1998. Paired immunoglobulin-like receptor (PIR)-A is involved in activating mast cells through its association with Fc receptor γ chain. *J Exp Med* 188: 991–5.
168. Wei, S., J. Zhou, X. Chen, R. N. Shah, J. Liu, T. M. Orcutt, D. Traver, J. Y. Djeu, G. W. Litman, and J. A. Yoder. 2007. The zebrafish activating immune receptor Nitr9 signals via Dap12. *Immunogenetics* 59: 813–21.
169. Leibson, P. J. 1997. Signal transduction during natural killer cell activation: inside the mind of a killer. *Immunity* 6: 655–61.
170. Bléry, M., J. Delon, A. Trautmann, A. Cambiaggi, L. Olcese, R. Biassoni, L. Moretta, P. Chavrier, A. Moretta, M. Daëron, and E. Vivier. 1997. Reconstituted killer cell inhibitory receptors for major histocompatibility complex class I molecules control mast cell activation induced via immunoreceptor tyrosine-based activation motifs. *J Biol Chem* 272: 8989–96.
171. Stebbins, C. C., C. Watzl, D. D. Billadeau, P. J. Leibson, D. N. Burshtyn, and E. O. Long. 2003. Vav1 dephosphorylation by the tyrosine phosphatase SHP-1 as a mechanism for inhibition of cellular cytotoxicity. *Mol Cell Biol* 23: 6291–6299.
172. Bruhns, P., P. Marchetti, W. H. Fridman, E. Vivier, and M. Daëron. 1999. Differential roles of N- and C-terminal immunoreceptor tyrosine-based inhibition motifs during inhibition of cell activation by killer cell inhibitory receptors. *J Immunol* 162: 3168–75.
173. Yusa, S., T. L. Catina, and K. S. Campbell. 2004. KIR2DL5 can inhibit human NK cell activation via recruitment of Src homology region 2-containing protein tyrosine phosphatase-2 (SHP-2). *J Immunol* 172: 7385–92.
174. Faure, M., D. F. Barber, S. M. Takahashi, T. Jin, and E. O. Long. 2003. Spontaneous clustering and tyrosine phosphorylation of NK cell inhibitory receptor induced by ligand binding. *J Immunol* 170: 6107–14.
175. Vyas, Y. M., H. Maniar, C. E. Lyddane, M. Sadelain, and B. Dupont. 2004. Ligand binding to inhibitory killer cell Ig-like receptors induce colocalization with Src homology domain 2-containing protein tyrosine phosphatase 1 and interruption of ongoing activation signals. *J Immunol* 173: 1571–8.
176. Matalon, O., S. Fried, A. Ben-Shmuel, M. H. Pauker, N. Joseph, D. Keizer, M. Piterburg, and M. Barda-Saad. 2016. Dephosphorylation of the adaptor LAT and phospholipase C- γ by SHP-1 inhibits natural killer cell cytotoxicity. *Sci Signal* 9: ra54.
177. Peterson, M. E., and E. O. Long. 2008. Inhibitory receptor signaling via tyrosine phosphorylation of the adaptor Crk. *Immunity* 29: 578–88.
178. Liu, D., M. E. Peterson, and E. O. Long. 2012. The adaptor protein Crk controls activation and inhibition of natural killer cells. *Immunity* 36: 600–11.
179. Yusa, S., T. L. Catina, and K. S. Campbell. 2002. SHP-1- and phosphotyrosine-independent inhibitory signaling by a killer cell Ig-like receptor cytoplasmic domain in human NK cells. *J Immunol* 168: 5047–57.
180. Allan, D. S., A. J. McMichael, and V. M. Braud. 2000. The ILT family of leukocyte

receptors. *Immunobiology* 202: 34–41.

181. Rojo, S., D. N. Burshtyn, E. O. Long, and N. Wagtmann. 1997. Type I transmembrane receptor with inhibitory function in mouse mast cells and NK cells. *J Immunol* 158: 9–12.

182. Wang, L. L., I. K. Mehta, P. A. LeBlanc, and W. M. Yokoyama. 1997. Mouse natural killer cells express gp49B1, a structural homologue of human killer inhibitory receptors. *J Immunol* 158: 13–17.

183. Katz, H. R., E. Vivier, M. C. Castells, M. J. McCormick, J. M. Chambers, and K. F. Austen. 1996. Mouse mast cell gp49B1 contains two immunoreceptor tyrosine-based inhibition motifs and suppresses mast cell activation when coligated with the high-affinity Fc receptor for IgE. *Proc Natl Acad Sci U S A* 93: 10809–14.

184. Kuroiwa, A., Y. Yamashita, M. Inui, T. Yuasa, M. Ono, A. Nagabukuro, Y. Matsuda, and T. Takai. 1998. Association of tyrosine phosphatases SHP-1 and SHP-2, inositol 5-phosphatase SHIP with gp49B1, and chromosomal assignment of the gene. *J Biol Chem* 273: 1070–4.

185. Bléry, M., H. Kubagawa, C.-C. Chen, F. Vély, M. D. Cooper, and E. Vivier. 1998. The paired Ig-like receptor PIR-B is an inhibitory receptor that recruits the protein-tyrosine phosphatase SHP-1. *Proc Natl Acad Sci U S A* 95: 2446–51.

186. Viertlboeck, B. C., R. P. M. A. Crooijmans, M. A. M. Groenen, and T. W. F. Göbel. 2004. Chicken Ig-like receptor B2, a member of a multigene family, is mainly expressed on B lymphocytes, recruits both Src homology 2 domain containing protein tyrosine phosphatase (SHP)-1 and SHP-2, and inhibits proliferation. *J Immunol* 173: 7385–93.

187. Yoder, J. A., M. G. Mueller, S. Wei, B. C. Corliss, D. M. Prather, T. Willis, R. T. Litman, J. Y. Djeu, and G. W. Litman. 2001. Immune-type receptor genes in zebrafish share genetic and functional properties with genes encoded by the mammalian leukocyte receptor cluster. *Proc Natl Acad Sci U S A* 98: 6771–6.

188. Montgomery, B. C. S., J. Mewes, C. Davidson, D. N. Burshtyn, and J. L. Stafford. 2009. Cell surface expression of channel catfish leukocyte immune-type receptors (IpLITRs) and recruitment of both Src homology 2 domain-containing protein tyrosine phosphatase (SHP)-1 and SHP-2. *Dev Comp Immunol* 33: 570–582.

189. Torigoe, C., J. K. Inman, and H. Metzger. 1998. An unusual mechanism for ligand antagonism. *Science (80-)* 281: 568–72.

190. Pasquier, B., P. Launay, Y. Kanamaru, I. C. Moura, S. Pfirsch, C. Ruffié, D. Hénin, M. Benhamou, M. Pretolani, U. Blank, and R. C. Monteiro. 2005. Identification of Fc α RI as an inhibitory receptor that controls inflammation: Dual role of FcR γ ITAM. *Immunity* 22: 31–42.

191. Kanamaru, Y., S. Pfirsch, M. Aloulou, F. Vrtovsnik, M. Essig, C. Loirat, G. Deschênes, C. Guérin-Marchand, U. Blank, and R. C. Monteiro. 2008. Inhibitory ITAM signaling by Fc α RI-FcR γ chain controls multiple activating responses and prevents renal inflammation. *J Immunol* 180: 2669–78.

192. Hamerman, J. a, N. K. Tchao, C. a Lowell, and L. L. Lanier. 2005. Enhanced Toll-like receptor responses in the absence of signaling adaptor DAP12. *Nat Immunol* 6: 579–586.

193. Hirsch, I., V. Janovec, R. Stranska, and N. Bendriss-Vermare. 2017. Cross talk between

- inhibitory immunoreceptor tyrosine-based activation motif-signaling and toll-like receptor pathways in macrophages and dendritic cells. *Front Immunol* 8: 394.
194. Wang, L., R. A. Gordon, L. Huynh, X. Su, K.-H. Park Min, J. Han, J. S. Arthur, G. D. Kalliolias, and L. B. Ivashkiv. 2010. Indirect inhibition of Toll-like receptor and type I interferon responses by ITAM-coupled receptors and integrins. *Immunity* 32: 518–30.
195. Kawai, T., and S. Akira. 2006. TLR signaling. *Cell Death Differ* 13: 816–25.
196. Han, C., J. Jin, S. Xu, H. Liu, N. Li, and X. Cao. 2010. Integrin CD11b negatively regulates TLR-triggered inflammatory responses by activating Syk and promoting degradation of MyD88 and TRIF via Cbl-b. *Nat Immunol* 11: 734–42.
197. Fourmentraux-Neves, E., A. Jalil, S. Da Rocha, C. Pichon, S. Chouaib, G. Bismuth, and A. Caignard. 2008. Two opposite signaling outputs are driven by the KIR2DL1 receptor in human CD4+ T cells. *Blood* 112: 2381–9.
198. Faure, M., and E. O. Long. 2002. KIR2DL4 (CD158d), an NK cell-activating receptor with inhibitory potential. *J Immunol* 168: 6208–6214.
199. Miah, S. M. S., T. L. Hughes, and K. S. Campbell. 2008. KIR2DL4 differentially signals downstream functions in human NK cells through distinct structural modules. *J Immunol* 180: 2922–32.
200. Jackson, D. E., K. R. Kupcho, and P. J. Newman. 1997. Characterization of phosphotyrosine binding motifs in the cytoplasmic domain of platelet/endothelial cell adhesion molecule-1 (PECAM-1) that are required for the cellular association and activation of the protein-tyrosine phosphatase, SHP-2. *J Biol Chem* 272: 24868–75.
201. Henshall, T. L., K. L. Jones, R. Wilkinson, and D. E. Jackson. 2001. Src homology 2 domain-containing protein-tyrosine phosphatases, SHP-1 and SHP-2, are required for platelet endothelial cell adhesion molecule-1/CD31-mediated inhibitory signaling. *J Immunol* 166: 3098–106.
202. Udell, C. M., L. A. Samayawardhena, Y. Kawakami, T. Kawakami, and A. W. B. Craig. 2006. Fer and Fps/Fes participate in a Lyn-dependent pathway from FcεRI to platelet-endothelial cell adhesion molecule 1 to limit mast cell activation. *J Biol Chem* 281: 20949–57.
203. Moraes, L. A., N. E. Barrett, C. I. Jones, L. M. Holbrook, M. Spyridon, T. Sage, D. K. Newman, and J. M. Gibbins. 2010. Platelet endothelial cell adhesion molecule-1 regulates collagen-stimulated platelet function by modulating the association of phosphatidylinositol 3-kinase with Grb-2-associated binding protein-1 and linker for activation of T cells. *J Thromb Haemost* 8: 2530–41.
204. Wang, J., Y. Wu, H. Hu, W. Wang, Y. Lu, H. Mao, X. Liu, Z. Liu, and B. guan Chen. 2011. Syk protein tyrosine kinase involves PECAM-1 signaling through tandem immunotyrosine inhibitory motifs in human THP-1 macrophages. *Cell Immunol* 272: 39–44.
205. Proust, R., C. Crouin, L. Y. Gandji, J. Bertoglio, and F. Gesbert. 2014. The adaptor protein SAP directly associates with PECAM-1 and regulates PECAM-1-mediated-cell adhesion in T-like cell lines. *Mol Immunol* 58: 206–13.
206. Chen, J., I. L. Leskov, A. Yurdagul Jr, B. Thiel, C. G. Kevil, K. Y. Stokes, and A. W. Orr.

2015. Recruitment of the adaptor protein Nck to PECAM-1 couples oxidative stress to canonical NF- κ B signaling and inflammation. *Sci Signal* 8: ra20.
207. Álvarez-Errico, D., J. Sayós, and M. López-Botet. 2007. The IREM-1 (CD300f) inhibitory receptor associates with the p85 α subunit of phosphoinositide 3-kinase. *J Immunol* 178: 808–16.
208. Izawa, K., M. Isobe, T. Matsukawa, S. Ito, A. Maehara, M. Takahashi, Y. Tamanishi, A. Kaitani, T. Oki, K. Okumura, T. Kitamura, and J. Kitaura. 2014. Sphingomyelin and ceramide are physiological ligands for human LMIR3/CD300f, inhibiting Fc ϵ RI-mediated mast cell activation. *J Allergy Clin Immunol* 133: 270–3.
209. Izawa, K., Y. Yamanishi, A. Maehara, M. Takahashi, M. Isobe, S. Ito, A. Kaitani, T. Matsukawa, T. Matsuoka, F. Nakahara, T. Oki, H. Kiyonari, T. Abe, K. Okumura, T. Kitamura, and J. Kitaura. 2012. The receptor LMIR3 negatively regulates mast cell activation and allergic responses by binding to extracellular ceramide. *Immunity* 37: 827–39.
210. Matsukawa, T., K. Izawa, M. Isobe, M. Takahashi, A. Maehara, Y. Yamanishi, A. Kaitani, K. Okumura, T. Teshima, T. Kitamura, and J. Kitaura. 2016. Ceramide-CD300f binding suppresses experimental colitis by inhibiting ATP-mediated mast cell activation. *Gut* 65: 777–87.
211. Izawa, K., J. Kitaura, Y. Yamanishi, T. Matsuoka, A. Kaitani, M. Sugiuchi, M. Takahashi, A. Maehara, Y. Enomoto, T. Oki, T. Takai, and T. Kitamura. 2009. An activating and inhibitory signal from an inhibitory receptor LMIR3/CLM-1: LMIR3 augments lipopolysaccharide response through association with Fc γ R in mast cells. *J Immunol* 183: 925–36.
212. Tian, L., S.-C. Choi, Y. Murakami, J. Allen, H. C. Morse III, C.-F. Qi, K. Krzewski, and J. E. Coligan. 2014. p85 α recruitment by the CD300f phosphatidylserine receptor mediates apoptotic cell clearance required for autoimmunity suppression. *Nat Commun* 5: 3146.
213. Viertlboeck, B. C., R. Schmitt, and T. W. Göbel. 2006. The chicken immunoregulatory receptor families SIRP, TREM, and CMRF35/CD300L. *Immunogenetics* 58: 180–90.
214. Tadisio, T. M., A. Sharma, and I. Hordvik. 2011. Analysis of polymeric immunoglobulin receptor- and CD300-like molecules from Atlantic salmon. *Mol Immunol* 49: 462–73.
215. Schmitter, T., S. Pils, V. Sakk, R. Frank, K.-D. Fischer, and C. R. Hauck. 2007. The granulocyte receptor carcinoembryonic antigen-related cell adhesion molecule 3 (CEACAM3) directly associates with Vav to promote phagocytosis of human pathogens. *J Immunol* 178: 3797–805.
216. Pils, S., K. Kopp, L. Peterson, J. D. Tascón, N. J. Nyffenegger-Jann, and C. R. Hauck. 2012. The adaptor molecule Nck localizes the WAVE complex to promote actin polymerization during CEACAM3-mediated phagocytosis of bacteria. *PLoS One* 7.
217. Buntru, A., K. Kopp, M. Voges, R. Frank, V. Bachmann, and C. R. Hauck. 2011. Phosphatidylinositol 3'-kinase activity is critical for initiating the oxidative burst and bacterial destruction during CEACAM3-mediated phagocytosis. *J Biol Chem* 286: 9555–66.
218. Sarantis, H., and S. D. Gray-Owen. 2007. The specific innate immune receptor CEACAM3 triggers neutrophil bactericidal activities via a Syk kinase-dependent pathway. *Cell Microbiol* 9: 2167–80.

219. Kopp, K., A. Buntru, S. Pils, T. Zimmermann, R. Frank, A. Zumbusch, and C. R. Hauck. 2012. Grb14 is a negative regulator of CEACAM3-mediated phagocytosis of pathogenic bacteria. *J Biol Chem* 287: 39158–70.
220. Ariizumi, K., G.-L. Shen, S. Shikano, S. Xu, R. Ritter III, T. Kumamoto, D. Edelbaum, A. Morita, P. R. Bergstresser, and A. Takashima. 2000. Identification of a novel, dendritic cell-associated molecule, dectin-1, by subtractive cDNA cloning. *J Biol Chem* 275: 20157–67.
221. Yokota, K., A. Takashima, P. R. Bergstresser, and K. Ariizumi. 2001. Identification of a human homologue of the dendritic cell-associated C-type lectin-1, dectin-1. *Gene* 272: 51–60.
222. Hermanz-Falcón, P., I. Arce, P. Roda-Navarro, and E. Fernández-Ruiz. 2001. Cloning of human DECTIN-1, a novel C-type lectin-like receptor gene expressed on dendritic cells. *Immunogenetics* 53: 288–95.
223. Brown, G. D. 2006. Dectin-1: a signalling non-TLR pattern-recognition receptor. *Nat Rev Immunol* 6: 33–43.
224. Martin, B., K. Hirota, D. J. Cua, B. Stockinger, and M. Veldhoen. 2009. Interleukin-17-producing $\gamma\delta$ T cells selectively expand in response to pathogen products and environmental signals. *Immunity* 31: 321–30.
225. Taylor, P. R., G. D. Brown, D. M. Reid, J. A. Willment, L. Martinez-Pomares, S. Gordon, and S. Y. C. Wong. 2002. The β -glucan receptor, dectin-1, is predominantly expressed on the surface of cells of the monocyte/macrophage and neutrophil lineages. *J Immunol* 169: 3876–82.
226. Willment, J. A., A. S. J. Marshall, D. M. Reid, D. L. Williams, S. Y. C. Wong, S. Gordon, and G. D. Brown. 2005. The human β -glucan receptor is widely expressed and functionally equivalent to murine dectin-1 on primary cells. *Eur J Immunol* 35: 1539–47.
227. Olynych, T. J., D. L. Jakeman, and J. S. Marshall. 2006. Fungal zymosan induces leukotriene production by human mast cells through a dectin-1-dependent mechanism. *J Allergy Clin Immunol* 118: 837–43.
228. Dennehy, K. M., G. Ferwerda, I. Faro-Trindade, E. Pyż, J. A. Willment, P. R. Taylor, A. Kerrigan, S. V. Tsoni, S. Gordon, F. Meyer-Wentrup, G. J. Adema, B.-J. Kullberg, E. Schweighoffer, V. Tybulewicz, H. M. Mora-Montes, N. A. R. Gow, D. L. Williams, M. G. Netea, and G. D. Brown. 2008. Syk kinase is required for collaborative cytokine production induced through Dectin-1 and Toll-like receptors. *Eur J Immunol* 38: 500–6.
229. Haas, T., S. Heidegger, A. Wintges, M. Bscheider, S. Bek, J. C. Fischer, G. Eisenkolb, M. Schmickl, S. Spoerl, C. Peschel, H. Poeck, and J. Ruland. 2017. Card9 controls dectin-1-induced T-cell cytotoxicity and tumor growth in mice. *Eur J Immunol* 47: 872–9.
230. Brown, G. D., P. R. Taylor, D. M. Reid, J. A. Willment, D. L. Williams, L. Martinez-Pomares, S. Y. C. Wong, and S. Gordon. 2002. Dectin-1 is a major β -glucan receptor on macrophages. *J Exp Med* 196: 407–12.
231. Herre, J., A. S. J. Marshall, E. Caron, A. D. Edwards, D. L. Williams, E. Schweighoffer, V. Tybulewicz, C. Reis e Sousa, S. Gordon, and G. D. Brown. 2004. Dectin-1 uses novel mechanisms for yeast phagocytosis in macrophages. *Blood* 104: 4038–45.
232. Underhill, D. M., E. Rosnagle, C. A. Lowell, and R. M. Simmons. 2005. Dectin-1 activates

- Syk tyrosine kinase in a dynamic subset of macrophages for reactive oxygen production. *Blood* 106: 2543–50.
233. Rogers, N. C., E. C. Slack, A. D. Edwards, M. A. Nolte, O. Schulz, E. Schweighoffer, D. L. Williams, S. Gordon, V. L. Tybulewicz, G. D. Brown, and C. Reis e Sousa. 2005. Syk-dependent cytokine induction by dectin-1 reveals a novel pattern recognition pathway for C type lectins. *Immunity* 22: 507–17.
234. LeibundGut-Landmann, S., O. Groß, M. J. Robinson, F. Osorio, E. C. Slack, S. V. Tsoni, E. Schweighoffer, V. Tybulewicz, G. D. Brown, J. Ruland, and C. Reis e Sousa. 2007. Syk- and CARD9-dependent coupling of innate immunity to the induction of T helper cells that produce interleukin 17. *Nat Immunol* 8: 630–8.
235. Deng, Z., S. Ma, H. Zhou, A. Zang, Y. Fang, T. Li, H. Shi, M. Liu, M. Du, P. R. Taylor, H. H. Zhu, J. Chen, G. Meng, F. Li, C. Chen, Y. Zhang, X.-M. Jia, X. Lin, X. Zhang, E. Pearlman, X. Li, G.-S. Feng, and H. Xiao. 2015. Tyrosine phosphatase SHP-2 mediates C-type lectin receptor-induced activation of the kinase Syk and anti-fungal TH17 responses. *Nat Immunol* 16: 642–52.
236. Shlapatska, L. M., S. V. Mikhalap, A. G. Berdova, O. M. Zelensky, T. J. Yun, K. E. Nichols, E. A. Clark, and S. P. Sidorenko. 2001. CD150 association with either the SH2-containing inositol phosphatase or the SH2-containing protein tyrosine phosphatase is regulated by the adaptor protein SH2D1A. *J Immunol* 166: 5480–7.
237. Veillette, A. 2010. SLAM-family receptors: immune regulators with or without SAP-family adaptors. *Cold Spring Harb Perspect Biol* 2: a002469.
238. Veillette, A., Z. Dong, L.-A. Pérez-Quintero, M.-C. Zhong, and M.-E. Cruz-Munoz. 2009. Importance and mechanism of “switch” function of SAP family adapters. *Immunol Rev* 232: 229–39.
239. Latour, S., and A. Veillette. 2004. The SAP family of adaptors in immune regulation. *Semin Immunol* 16: 409–19.
240. Watzl, C., C. C. Stebbins, and E. O. Long. 2000. NK cell inhibitory receptors prevent tyrosine phosphorylation of the activation receptor 2B4 (CD244). *J Immunol* 165: 3545–48.
241. Valiante, N. M., and G. Trinchieri. 1993. Identification of a novel signal transduction surface molecule on human cytotoxic lymphocytes. *J Exp Med* 178: 1397–406.
242. Parolini, S., C. Bottino, M. Falco, R. Augugliaro, S. Giliani, R. Franceschini, H. D. Ochs, H. Wolf, J.-Y. Bonnefoy, R. Biassoni, L. Moretta, L. D. Notarangelo, and A. Moretta. 2000. X-linked lymphoproliferative disease. 2B4 molecules displaying inhibitory rather than activating function are responsible for the inability of natural killer cells to kill Epstein-Barr virus-infected cells. *J Exp Med* 192: 337–46.
243. Eissmann, P., L. Beauchamp, J. Wooters, J. C. Tilton, E. O. Long, and C. Watzl. 2005. Molecular basis for positive and negative signaling by the natural killer cell receptor 2B4 (CD244). *Blood* 105: 4722–9.
244. Straub, C., B. C. Viertlboeck, and T. W. Göbel. 2013. The chicken SLAM family. *Immunogenetics* 65: 63–73.

245. Straub, C., M.-L. Neulen, B. C. Viertlboeck, and T. W. Göbel. 2014. Chicken SLAMF4 (CD244, 2B4), a receptor expressed on thrombocytes, monocytes, NK cells, and subsets of $\alpha\beta$ -, $\gamma\delta$ - T cells and B cells binds to SLAMF2. *Dev Comp Immunol* 42: 159–68.
246. Upshaw, J. L., L. N. Arneson, R. a Schoon, C. J. Dick, D. D. Billadeau, and P. J. Leibson. 2006. NKG2D-mediated signaling requires a DAP10-bound Grb2-Vav1 intermediate and phosphatidylinositol-3-kinase in human natural killer cells. *Nat Immunol* 7: 524–532.
247. Engels, N., and J. Wienands. 2011. The signaling tool box for tyrosine-based costimulation of lymphocytes. *Curr Opin Immunol* 23: 324–9.
248. Segawa, Y., H. Suga, N. Iwabe, C. Oneyama, T. Akagi, T. Miyata, and M. Okada. 2006. Functional development of Src tyrosine kinases during evolution from a unicellular ancestor to multicellular animals. *Proc Natl Acad Sci U S A* 103: 12021–6.
249. Okada, M. 2012. Regulation of the Src family kinases by Csk. *Int J Biol Sci* 8: 1385–1397.
250. Donella-Deana, A., L. Cesaro, M. Ruzzene, A. M. Brunati, O. Marin, and L. A. Pinna. 1998. Spontaneous autophosphorylation of Lyn tyrosine kinase at both its activation segment and C-terminal tail confers altered substrate specificity. *Biochemistry* 37: 1438–46.
251. Suzuki, T., H. Kono, N. Hirose, M. Okada, T. Yamamoto, K. Yamamoto, and Z. Honda. 2000. Differential involvement of Src family kinases in Fc gamma receptor-mediated phagocytosis. *J Immunol* 165: 472–82.
252. Takeda, H., Y. Kawamura, A. Miura, M. Mori, A. Wakamatsu, J. Yamamoto, T. Isogai, M. Matsumoto, K. I. Nakayama, T. Natsume, N. Nomura, and N. Goshima. 2010. Comparative analysis of human SRC-family kinase substrate specificity in vitro. *J Proteome Res* 9: 5982–93.
253. Songyang, Z., K. L. Carraway III, M. J. Eck, S. C. Harrison, R. A. Feldman, M. Mohammadi, J. Schlessinger, S. R. Hubbard, D. P. Smith, C. Eng, M. J. Lorenzo, B. A. J. Ponder, B. J. Mayer, and L. C. Cantley. 1995. Catalytic specificity of protein-tyrosine kinases is critical for selective signalling. *Nature* 373: 536–9.
254. Hubbard, S. R., L. Wei, L. Ellis, and W. A. Hendrickson. 1994. Crystal structure of the tyrosine kinase domain of the human insulin receptor. *Nature* 372: 746–54.
255. Mayer, B. J., H. Hirai, and R. Sakai. 1995. Evidence that SH2 domains promote processive phosphorylation by protein-tyrosine kinases. *Curr Biol* 5: 296–305.
256. Granum, S., V. Sundvold-Gjerstad, R. P. Gopalakrishnan, T. Berge, L. Koll, G. Abrahamsen, M. Sørli, and A. Spurrkland. 2014. The kinase Itk and the adaptor TSAAd change the specificity of the kinase Lck in T cells by promoting the phosphorylation of Tyr192. *Sci Signal* 7: ra118.
257. Liu, B. A., K. Jablonowski, M. Raina, M. Arcé, T. Pawson, and P. D. Nash. 2006. The human and mouse complement of SH2 domain proteins-establishing the boundaries of phosphotyrosine signaling. *Mol Cell* 22: 851–68.
258. Jin, L. L., L. E. Wybenga-Groot, J. Tong, P. Taylor, M. D. Minden, S. Trudel, C. J. McGlade, and M. F. Moran. 2015. Tyrosine phosphorylation of the Lyn Src homology 2 (SH2) domain modulates its binding affinity and specificity. *Mol Cell Proteomics* 14: 695–706.
259. Klasen, S., F. Pages, J.-F. Peyron, D. A. Cantrell, and D. Olive. 1998. Two distinct regions

- of the CD28 intracytoplasmic domain are involved in the tyrosine phosphorylation of Vav and GTPase activating protein-associated p62 protein. *Int Immunol* 10: 481–9.
260. Pagès, F., M. Ragueneau, S. Klasen, M. Battifora, D. Couez, R. Sweet, A. Truneh, S. G. Ward, and D. Olive. 1996. Two distinct intracytoplasmic regions of the T-cell adhesion molecule CD28 participate in phosphatidylinositol 3-kinase association. *J Biol Chem* 271: 9403–9.
261. Daëron, M., O. Malbec, S. Latour, C. Bonnerot, D. M. Segal, and W. H. Fridman. 1993. Distinct intracytoplasmic sequences are required for endocytosis and phagocytosis via murine Fc γ RII in mast cells. *Int Immunol* 5: 1393–1401.
262. Wiedemann, A., J. C. Patel, J. Lim, A. Tsun, Y. van Kooyk, and E. Caron. 2006. Two distinct cytoplasmic regions of the β 2 integrin chain regulate RhoA function during phagocytosis. *J Cell Biol* 172: 1069–1079.
263. Fong, D. C., A. Brauweiler, S. A. Minskoff, P. Bruhns, I. Tamir, I. Mellman, M. Daeron, and J. C. Cambier. 2000. Mutational analysis reveals multiple distinct sites within Fc γ receptor IIB that function in inhibitory signaling. *J Immunol* 165: 4453–62.
264. Borroto, A., D. Abia, and B. Alarcón. 2014. Crammed signaling motifs in the T-cell receptor. *Immunol Lett* 161: 113–7.
265. López, C. A., A. Sethi, B. Goldstein, B. S. Wilson, and S. Gnanakaran. 2015. Membrane-mediated regulation of the intrinsically disordered CD3 ϵ cytoplasmic tail of the TCR. *Biophys J* 108: 2481–91.
266. Zhang, H., S.-P. Cordoba, O. Dushek, and P. A. van der Merwe. 2011. Basic residues in the T-cell receptor ζ cytoplasmic domain mediate membrane association and modulate signaling. *Proc Natl Acad Sci U S A* 108: 19323–8.
267. Dobbins, J., E. Gagnon, J. Godec, J. Pyrdol, D. A. A. Vignali, A. H. Sharpe, and K. W. Wucherpfennig. 2016. Binding of the cytoplasmic domain of CD28 to the plasma membrane inhibits Lck recruitment and signaling. *Sci Signal* 9: ra75.
268. Paddock, C., B. L. Lytle, F. C. Peterson, T. Holyst, P. J. Newman, B. F. Volkman, and D. K. Newman. 2011. Residues within a lipid-associated segment of the PECAM-1 cytoplasmic domain are susceptible to inducible, sequential phosphorylation. *Blood* 117: 6012–23.
269. Oellerich, T., V. Bremes, K. Neumann, H. Bohnenberger, K. Dittmann, H.-H. Hsiao, M. Engelke, T. Schnyder, F. D. Batista, H. Urlaub, and J. Wienands. 2011. The B-cell antigen receptor signals through a preformed transducer module of SLP65 and CIN85. *EMBO J* 30: 3620–34.
270. Urzainqui, A., J. M. Serrador, F. Viedma, M. Yanez-Mo, A. Rodriguez, A. L. Corbi, J. L. Alonso-Lebrero, A. Luque, M. Deckert, J. Vazquez, and F. Sanchez-Madrid. 2002. ITAM-based interaction of ERM proteins with Syk mediates signaling by the leukocyte adhesion receptor PSGL-1. *Immunity* 17: 401–12.
271. Falet, H., A. Y. Pollitt, A. J. Begonja, S. E. Weber, D. Duerschmied, D. D. Wagner, S. P. Watson, and J. H. Hartwig. 2010. A novel interaction between FlnA and Syk regulates platelet ITAM-mediated receptor signaling and function. *J Exp Med* 207: 1967–79.
272. Barth, N. D., J. A. Marwick, M. Vendrell, A. G. Rossi, and I. Dransfield. 2017. The

- “phagocytic synapse” and clearance of apoptotic cells. *Front Immunol* 8: 1708.
273. Niedergang, F., V. Di Bartolo, and A. Alcover. 2016. Comparative anatomy of phagocytic and immunological synapses. *Front Immunol* 7: 18.
274. Piragyte, I., and C.-D. Jun. 2012. Actin engine in immunological synapse. *Immune Netw* 12: 71–83.
275. Saito, T., and S. Yamasaki. 2003. Negative feedback of T cell activation through inhibitory adapters and costimulatory receptors. *Immunol Rev* 192: 143–60.
276. Bongartz, H., W. Hessenkemper, C. Muller, M. Fensky, J. Fritsch, K. Mandel, I. Behrmann, C. Haan, T. Fischer, S. M. Feller, and F. Schaper. 2017. The multi-site docking protein Gab1 is constitutively phosphorylated independent from its recruitment to the plasma membrane in Jak2-V617F-positive cells and mediates proliferation of human erythroleukaemia cells. *Cell Signal* 35: 37–47.
277. Bartelt, R. R., and J. C. D. Houtman. 2013. The adaptor protein LAT serves as an integration node for signaling pathways that drive T cell activation. *Wiley Interdiscip Rev Syst Biol Med* 5: 101–10.
278. Herzog, S., B. Storch, and H. Jumaa. 2006. Dual role of the adaptor protein SLP-65: organizer of signal transduction and tumor suppressor of pre-B cell leukemia. *Immunol Res* 34: 143–55.
279. Jordan, M. S., and G. A. Koretzky. 2010. Coordination of receptor signaling in multiple hematopoietic cell lineages by the adaptor protein SLP-76. *Cold Spring Harb Perspect Biol* 2: a002501.
280. Yablonski, D., and A. Weiss. 2001. Mechanisms of signaling by the hematopoietic-specific adaptor proteins, SLP-76 and LAT and their B cell counterpart, BLNK/SLP-65. *Adv Immunol* 79: 93–128.
281. Abeyweera, T. P., E. Merino, and M. Huse. 2011. Inhibitory signaling blocks activating receptor clustering and induces cytoskeletal retraction in natural killer cells. *J Cell Biol* 192: 675–90.
282. Kantonen, S., N. Hatton, M. Mahankali, K. M. Henkels, H. Park, D. Cox, and J. Gomez-Cambronero. 2011. A novel phospholipase D2-Grb2-WASp heterotrimer regulates leukocyte phagocytosis in a two-step mechanism. *Mol Cell Biol* 31: 4524–37.
283. Shah, S., A. W. Gibson, C. Ji, E. Darrington, J. Mobley, K. Kojima, J. C. Edberg, and R. P. Kimberly. 2017. Regulation of FcR γ function by site-specific serine phosphorylation. *J Leukoc Biol* 101: 421–8.
284. Freeman, S. A., A. Vega, M. Riedl, R. F. Collins, P. P. Ostrowski, E. C. Woods, C. R. Bertozzi, M. I. Tammi, D. S. Lidke, P. Johnson, S. Mayor, K. Jaqaman, and S. Grinstein. 2018. Transmembrane pickets connect cyto- and pericellular skeletons forming barriers to receptor engagement. *Cell* 172: 305–317.
285. Mylvaganam, S. M., S. Grinstein, and S. A. Freeman. 2018. Picket-fences in the plasma membrane: functions in immune cells and phagocytosis. *Semin Immunopathol* 40: 605–15.
286. Trimble, W. S., and S. Grinstein. 2015. Barriers to the free diffusion of proteins and lipids

- in the plasma membrane. *J Cell Biol* 208: 259–71.
287. Yonemura, S., M. Hirao, Y. Doi, N. Takahashi, T. Kondo, S. Tsukita, and S. Tsukita. 1998. Ezrin/radixin/moesin (ERM) proteins bind to a positively charged amino acid cluster in the juxta-membrane cytoplasmic domain of CD44, CD43, and ICAM-2. *J Cell Biol* 140: 885–95.
288. Nunomura, W., and Y. Takakuwa. 2006. Regulation of protein 4.1R interactions with membrane proteins by Ca²⁺ and calmodulin. *Front Biosci* 11: 1522–39.
289. Nunomura, W., Y. Takakuwa, R. Tokimitsu, S. W. Krauss, M. Kawashima, and N. Mohandas. 1997. Regulation of CD44-protein 4.1 interaction by Ca²⁺ and calmodulin. Implications for modulation of CD44-ankyrin interaction. *J Biol Chem* 272: 30322–8.
290. Beekman, J. M., J. E. Bakema, C. E. van der Poel, J. A. van der Linden, J. G. J. van de Winkel, and J. H. W. Leusen. 2008. Protein 4.1G binds to a unique motif within the FcγRI cytoplasmic tail. *Mol Immunol* 45: 2069–75.
291. Wang, Y., T. Yago, N. Zhang, S. Abdisalaam, G. Alexandrakis, W. Rodgers, and R. P. McEver. 2014. Cytoskeletal regulation of CD44 membrane organization and interactions with E-selectin. *J Biol Chem* 289: 35159–71.
292. Girard, T., M. El-Far, D. Gaucher, O. Acuto, G. Beaulé, F. Michel, W. Mourad, and R.-P. Sékaly. 2012. A conserved polylysine motif in CD86 cytoplasmic tail is necessary for cytoskeletal association and effective co-stimulation. *Biochem Biophys Res Commun* 423: 301–307.
293. Gibson, A. W., X. Li, J. Wu, J. G. Baskin, C. Raman, J. C. Edberg, and R. P. Kimberly. 2012. Serine phosphorylation of FcγRI cytoplasmic domain directs lipid raft localization and interaction with protein 4.1G. *J Leukoc Biol* 91: 97–103.
294. Lopes, F. B., Š. Bálint, S. Valvo, J. H. Felce, E. M. Hessel, M. L. Dustin, and D. M. Davis. 2017. Membrane nanoclusters of FcγRI segregate from inhibitory SIRPα upon activation of human macrophages. *J Cell Biol* 216: 1123–41.
295. Jaumouillé, V., Y. Farkash, K. Jaqaman, R. Das, C. A. Lowell, and S. Grinstein. 2014. Actin cytoskeleton reorganization by Syk regulates Fcγ receptor responsiveness by increasing its lateral mobility and clustering. *Dev Cell* 29: 534–46.
296. Jaqaman, K., H. Kuwata, N. Touret, R. Collins, W. S. Trimble, G. Danuser, and S. Grinstein. 2011. Cytoskeletal control of CD36 diffusion promotes its receptor and signaling function. *Cell* 146: 593–606.
297. Akula, S., S. Mohammadamin, and L. Hellman. 2014. Fc receptors for immunoglobulins and their appearance during vertebrate evolution. *PLoS One* 9: e96903.
298. Jackson, T. A., C. L. Haga, G. R. A. Ehrhardt, R. S. Davis, and M. D. Cooper. 2010. FcR-like 2 inhibition of B cell receptor-mediated activation of B cells. *J Immunol* 185: 7405–12.
299. Shabani, M., A. A. Bayat, M. Jeddi-Tehrani, H. Rabbani, M. Hojjat-Farsangi, C. Ulivieri, Z. Amirghofran, C. T. Baldari, and F. Shokri. 2014. Ligation of human Fc receptor like-2 by monoclonal antibodies down-regulates B-cell receptor-mediated signalling. *Immunology* 143: 341–53.
300. Kochi, Y., K. Myouzen, R. Yamada, A. Suzuki, T. Kurosaki, Y. Nakamura, and K.

- Yamamoto. 2009. FCRL3, an autoimmune susceptibility gene, has inhibitory potential on B-cell receptor-mediated signaling. *J Immunol* 183: 5502–10.
301. Li, F. J., D. M. Schreeder, R. Li, J. Wu, and R. S. Davis. 2013. FCRL3 promotes TLR9-induced B-cell activation and suppresses plasma cell differentiation. *Eur J Immunol* 43: 2980–92.
302. Sohn, H. W., P. D. Krueger, R. S. Davis, and S. K. Pierce. 2011. FcRL4 acts as an adaptive to innate molecular switch dampening BCR signaling and enhancing TLR signaling. *Blood* 118: 6332–42.
303. Liu, Y., K. Bezverbnaya, T. Zhao, M. J. Parsons, M. Shi, B. Treanor, and G. R. A. Ehrhardt. 2015. Involvement of the HCK and FGR src-family kinases in FCRL4-mediated immune regulation. *J Immunol* 194: 5851–60.
304. Dement-Brown, J., C. S. Newton, T. Ise, B. Damdinsuren, S. Nagata, and M. Tolnay. 2012. Fc receptor-like 5 promotes B cell proliferation and drives the development of cells displaying switched isotypes. *J Leukoc Biol* 91: 59–67.
305. Zhu, Z., R. Li, H. Li, T. Zhou, and R. S. Davis. 2013. FcRL5 exerts binary and compartment-specific influence on innate-like B-cell receptor signaling. *Proc Natl Acad Sci U S A* 110: E1282-90.
306. Kulemzin, S. V., A. Y. Zamoshnikova, M. Y. Yurchenko, N. Y. Vitak, A. M. Najakshin, S. A. Fayngerts, N. A. Chikaev, E. S. Reshetnikova, N. M. Kashirina, M. M. Peclo, P. N. Rutkevich, A. Y. Shevelev, E. V Yanushevskaya, K. O. Baranov, M. Mamonkin, T. N. Vlasik, S. P. Sidorenko, A. V Taranin, and L. V Mechetina. 2011. FCRL6 receptor: expression and associated proteins. *Immunol Lett* 134: 174–82.
307. Wilson, T. J., R. M. Presti, I. Tassi, E. T. Overton, M. Cella, and M. Colonna. 2007. FcRL6, a new ITIM-bearing receptor on cytolytic cells, is broadly expressed by lymphocytes following HIV-1 infection. *Blood* 109: 3786–93.
308. Hayakawa, K., R. R. Hardy, D. R. Parks, and L. A. Herzenberg. 1983. The “Ly-1 B” cell subpopulation in normal immunodeficient, and autoimmune mice. *J Exp Med* 157: 202–18.
309. Popi, A. F. 2015. B-1 phagocytes: the myeloid face of B-1 cells. *Ann N Y Acad Sci* 1362: 86–97.
310. Davis, R. S. 2015. FCRL regulation in innate-like B cells. *Ann N Y Acad Sci* 1362: 110–16.
311. Pampolina, C., and A. McNicol. 2005. Streptococcus sanguis-induced platelet activation involves two waves of tyrosine phosphorylation mediated by FcγRIIA and αIIbβ3. *Thromb Haemost* 93: 932–9.
312. Cario, E., and D. K. Podolsky. 2005. Intestinal epithelial TOLLerance versus inTOLLerance of commensals. *Mol Immunol* 42: 887–93.
313. Cario, E., and D. K. Podolsky. 2006. Toll-like receptor signaling and its relevance to intestinal inflammation. *Ann N Y Acad Sci* 1072: 332–8.
314. Günther, J., and H.-M. Seyfert. 2018. The first line of defence: insights into mechanisms and relevance of phagocytosis in epithelial cells. *Semin Immunopathol* 40: 555–65.
315. Ryeom, S. W., J. R. Sparrow, and R. L. Silverstein. 1996. CD36 participates in the

- phagocytosis of rod outer segments by retinal pigment epithelium. *J Cell Sci* 109: 387–95.
316. McCaffrey, L. M., and I. G. Macara. 2012. Signaling pathways in cell polarity. *Cold Spring Harb Perspect Biol* 4: a009654.
317. Nadatani, Y., X. Huo, X. Zhang, C. Yu, E. Cheng, Q. Zhang, K. B. Dunbar, A. Theiss, T. H. Pham, D. H. Wang, T. Watanabe, Y. Fujiwara, T. Arakawa, S. J. Spechler, and R. F. Souza. 2016. NOD-like receptor protein 3 inflammasome priming and activation in Barrett's epithelial cells. *Cell Mol Gastroenterol Hepatol* 2: 439–53.
318. Burton, E. A., S. Hunter, S. C. Wu, and S. M. Anderson. 1997. Binding of src-like kinases to the beta-subunit of the interleukin-3 receptor. *J Biol Chem* 272: 16189–95.
319. Simcox, M. E., A. Huvar, T. G. Simcox, and Q. Vega. 1994. TK E. coli strains for producing tyrosine-phosphorylated proteins in vivo. *Strateg Mol Biol* 7: 68–9.
320. Weiner, M. P., C. Anderson, B. Jerpseth, S. Wells, B. Johnson Browne, and P. Vaillancourt. 1994. pET system vectors and hosts. *Strateg Mol Biol* 7: 41–3.
321. Pearson, J. D., J. Zhang, Z. Wu, K. D. Thew, K. J. Rowe, J. T. C. Bacani, and R. J. Ingham. 2014. Expression of granzyme B sensitizes ALK+ ALCL tumour cells to apoptosis-inducing drugs. *Mol Cancer* 13: 199.
322. Zhang, J., Z. Wu, A. Savin, M. Yang, Y.-H. R. Hsu, E. Jantuan, J. T. C. Bacani, and R. J. Ingham. 2018. The c-Jun and JunB transcription factors facilitate the transit of classical Hodgkin lymphoma tumour cells through G1. *Sci Rep* 8: 16019.
323. Barrilleaux, B., and P. Knoepfler. 2011. Transduction of human cells with polymer-complexed ecotropic lentivirus for enhanced biosafety. *J Vis Exp* e2822.
324. Höfig, I., M. J. Atkinson, S. Mall, A. M. Krackhardt, C. Thirion, and N. Anastasov. 2012. Poloxamer synperonic F108 improves cellular transduction with lentiviral vectors. *J Gene Med* 14: 549–60.
325. Schindelin, J., I. Arganda-Carreras, E. Frise, V. Kaynig, M. Longair, T. Pietzsch, S. Preibisch, C. Rueden, S. Saalfeld, B. Schmid, J.-Y. Tinevez, D. J. White, V. Hartenstein, K. Eliceiri, P. Tomancak, and A. Cardona. 2012. Fiji: an open-source platform for biological-image analysis. *Nat Methods* 9: 676.
326. Zwozdesky, M. A., C. Fei, D. M. E. Lillico, and J. L. Stafford. 2017. Imaging flow cytometry and GST pulldown assays provide new insights into channel catfish leukocyte immune-type receptor-mediated phagocytic pathways. *Dev Comp Immunol* 67: 126–138.
327. Fei, C., D. M. E. Lillico, B. Hall, A. M. Rieger, and J. L. Stafford. 2017. Connected component masking accurately identifies the ratio of phagocytosed and cell-bound particles in individual cells by imaging flow cytometry. *Cytom Part A* 91: 372–381.
328. Taylor, E. B., M. Moulana, T. B. Stuge, S. M. A. Quiniou, E. Bengten, and M. Wilson. 2016. A leukocyte immune-type receptor subset is a marker of antiviral cytotoxic cells in channel catfish, *Ictalurus punctatus*. *J Immunol* 196: 2677–89.
329. Flannagan, R. S., J. Canton, W. Furuya, M. Glogauer, and S. Grinstein. 2014. The phosphatidylserine receptor TIM4 utilizes integrins as coreceptors to effect phagocytosis. *Mol Biol Cell* 25: 1511–22.

330. Vojtěchová, M., Z. Tuháčková, J. Hlaváček, J. Velek, and V. Sovová. 2004. The v-Src and c-Src tyrosine kinases immunoprecipitated from Rous sarcoma virus-transformed cells display different peptide substrate specificities. *Arch Biochem Biophys* 421: 277–82.
331. Huyer, G., S. Liu, J. Kelly, J. Moffat, P. Payette, B. Kennedy, G. Tsaprailis, M. J. Gresser, and C. Ramachandran. 1997. Mechanism of inhibition of protein-tyrosine phosphatases by vanadate and pervanadate. *J Biol Chem* 272: 843–51.
332. Ibarrola, I., P. J. M. Vosseveld, C. H. E. Homburg, M. Thelen, D. Roos, and A. J. Verhoeven. 1997. Influence of tyrosine phosphorylation on protein interaction with FcγRIIa. *Biochim Biophys Acta* 1357: 348–58.
333. Schulze, W. X., L. Deng, and M. Mann. 2005. Phosphotyrosine interactome of the ErbB-receptor kinase family. *Mol Syst Biol* 1: 2005.0008.
334. Hanke, S., and M. Mann. 2009. The phosphotyrosine interactome of the insulin receptor family and its substrates IRS-1 and IRS-2. *Mol Cell Proteomics* 8: 519–34.
335. Yaoi, T., S. Chamnongpol, X. Jiang, and X. Li. 2006. Src homology 2 domain-based high throughput assays for profiling downstream molecules in receptor tyrosine kinase pathways. *Mol Cell Proteomics* 5: 959–68.
336. Liu, B. A., K. Jablonowski, E. E. Shah, B. W. Engelmann, R. B. Jones, and P. D. Nash. 2010. SH2 domains recognize contextual peptide sequence information to determine selectivity. *Mol Cell Proteomics* 9: 2391–2404.
337. Frese, S., W.-D. Schubert, A. C. Findeis, T. Marquardt, Y. S. Roske, T. E. B. Stradal, and D. W. Heinz. 2006. The phosphotyrosine peptide binding specificity of Nck1 and Nck2 Src homology 2 domains. *J Biol Chem* 281: 18236–18245.
338. Kinchen, J. M., and K. S. Ravichandran. 2010. Phagocytic signaling: you can touch, but you can't eat. *Curr Biol* 18: R521-4.
339. Chalifour, A., J. Roger, S. Lemieux, and P. Duplay. 2003. Receptor/ligand avidity determines the capacity of Ly49 inhibitory receptors to interfere with T-cell receptor-mediated activation. *Immunology* 109: 58–67.
340. Olsson-Alheim, M. Y., M. Salcedo, H.-G. Ljunggren, K. Kärre, and C. L. Sentman. 1997. NK cell receptor calibration: effects of MHC class I induction on killing by Ly49A^{high} and Ly49A^{low} NK cells. *J Immunol* 159: 3189–94.
341. Frazier, W. R., N. Steiner, L. Hou, S. Dakshanamurthy, and C. K. Hurley. 2013. Allelic variation in KIR2DL3 generates a KIR2DL2-like receptor with increased binding to its HLA-C ligand. *J Immunol* 190: 6198–208.
342. Thomas, S. M., and J. S. Brugge. 1997. Cellular functions regulated by Src family kinases. *Annu Rev Cell Dev Biol* 13: 513–609.
343. Yadav, S. S., and W. T. Miller. 2008. The evolutionarily conserved arrangement of domains in SRC family kinases is important for substrate recognition. *Biochemistry* 47: 10871–10880.
344. Zhao, B., P. H. Tan, S. S. C. Li, and D. Pei. 2013. Systematic characterization of the specificity of the SH2 domains of cytoplasmic tyrosine kinases. *J Proteomics* 81: 56–69.
345. Brown, M. T., and J. A. Cooper. 1996. Regulation, substrates and functions of src. *Biochim*

Biophys Acta 1287: 121–49.

346. Yanagi, S., R. Inatome, J. Ding, H. Kitaguchi, V. L. J. Tybulewicz, and H. Yamamura. 2001. Syk expression in endothelial cells and their morphologic defects in embryonic Syk-deficient mice. *Blood* 98: 2869–71.
347. Mikhalap, S. V., L. M. Shlapatska, A. G. Berdova, C.-L. Law, E. A. Clark, and S. P. Sidorenko. 1999. CDw150 associates with src-homology 2-containing inositol phosphatase and modulates CD95-mediated apoptosis. *J Immunol* 162: 5719–27.
348. Parolini, O., A. Weinhäusel, B. Kagerbauer, J. Sassmann, W. Holter, H. Gadner, O. A. Haas, and W. Knapp. 2003. Differential methylation pattern of the X-linked lymphoproliferative (XLP) disease gene SH2D1A correlates with the cell lineage-specific transcription. *Immunogenetics* 55: 116–21.
349. Latour, S., G. Gish, C. D. Helgason, R. K. Humphries, T. Pawson, and A. Veillette. 2001. Regulation of SLAM-mediated signal transduction by SAP, the X-linked lymphoproliferative gene product. *Nat Immunol* 2: 681–90.
350. Dong, Z., D. Davidson, L. A. Pérez-Quintero, T. Kurosaki, W. Swat, and A. Veillette. 2012. The adaptor SAP controls NK cell activation by regulating the enzymes Vav-1 and SHIP-1 and by enhancing conjugates with target cells. *Immunity* 36: 974–85.
351. Jaumouillé, V., and S. Grinstein. 2011. Receptor mobility, the cytoskeleton, and particle binding during phagocytosis. *Curr Opin Cell Biol* 23: 22–9.
352. Goodridge, H. S., D. M. Underhill, and N. Touret. 2012. Mechanisms of Fc receptor and dectin-1 activation for phagocytosis. *Traffic* 13: 1062–71.
353. Legg, J. W., and C. M. Isacke. 1998. Identification and functional analysis of the ezrin-binding site in the hyaluronan receptor, CD44. *Curr Biol* 8: 705–8.
354. Vachon, E., R. Martin, J. Plumb, V. Kwok, R. W. Vandivier, M. Glogauer, A. Kapus, X. Wang, C. W. Chow, S. Grinstein, and G. P. Downey. 2006. CD44 is a phagocytic receptor. *Blood* 107: 4149–4158.
355. Vachon, E., R. Martin, V. Kwok, V. Cherepanov, C.-W. Chow, C. M. Doerschuk, J. Plumb, S. Grinstein, and G. P. Downey. 2007. CD44-mediated phagocytosis induces inside-out activation of complement receptor-3 in murine macrophages. *Blood* 110: 4492–502.
356. Roskoski Jr, R. 2005. Src kinase regulation by phosphorylation and dephosphorylation. *Biochem Biophys Res Commun* 331: 1–14.
357. Boulven, I., P. Robin, C. Desmyter, S. Harbon, and D. Leiber. 2002. Differential involvement of Src family kinases in pervanadate-mediated responses in rat myometrial cells. *Cell Signal* 14: 341–9.
358. Xie, J., C. M. Tato, and M. M. Davis. 2013. How the immune system talks to itself: the varied role of synapses. *Immunol Rev* 251: 65–79.
359. Franz, K. M., and J. C. Kagan. 2017. Innate immune receptors as competitive determinants of cell fate. *Mol Cell* 66: 750–60.
360. Akira, S., S. Uematsu, and O. Takeuchi. 2006. Pathogen recognition and innate immunity. *Cell* 124: 783–801.

361. Lowell, C. A. 2011. Src-family and Syk kinases in activating and inhibitory pathways in innate immune cells: signaling cross talk. *Cold Spring Harb Perspect Biol* 3: a002352.
362. Blázquez-Moreno, A., S. Park, W. Im, M. J. Call, M. E. Call, and H. T. Reyburn. 2017. Transmembrane features governing Fc receptor CD16A assembly with CD16A signaling adaptor molecules. *Proc Natl Acad Sci U S A* 114: E5645-54.
363. Moradi, S., R. Berry, P. Pymm, C. Hitchen, S. A. Beckham, M. C. J. Wilce, N. G. Walpole, C. S. Clements, H. H. Reid, M. A. Perugini, A. G. Brooks, J. Rossjohn, and J. P. Vivian. 2015. The structure of the atypical killer cell immunoglobulin-like receptor, KIR2DL4. *J Biol Chem* 290: 10460–71.
364. Kargas, V., J. K. Marzinek, D. A. Holdbrook, H. Yin, R. C. Ford, and P. J. Bond. 2017. A polar SxxS motif drives assembly of the transmembrane domains of Toll-like receptor 4. *Biochim Biophys Acta* 1859: 2086–95.
365. Wagtmann, N., S. Rajagopalan, C. C. Winter, M. Peruni, and E. O. Long. 1995. Killer cell inhibitory receptors specific for HLA-C and HLA-B identified by direct binding and by functional transfer. *Immunity* 3: 901–909.
366. Köhler, K., S. Xiong, J. Brzostek, M. Mehrabi, P. Eissmann, A. Harrison, S.-P. Cordoba, S. Oddos, V. Miloserdov, K. Gould, N. J. Burroughs, P. A. van der Merwe, and D. M. Davis. 2010. Matched sizes of activating and inhibitory receptor/ligand pairs are required for optimal signal integration by human natural killer cells. *PLoS One* 5: e15374.
367. Yamauchi, S., K. Kawauchi, and Y. Sawada. 2012. Myosin II-dependent exclusion of CD45 from the site of Fc γ receptor activation during phagocytosis. *FEBS Lett* 586: 3229–35.
368. Maxson, M. E., X. Naj, T. R. O’Meara, J. D. Plumb, L. E. Cowen, and S. Grinstein. 2018. Integrin-based diffusion barrier separates membrane domains enabling the formation of microbiostatic frustrated phagosomes. *Elife* 7: e34798.
369. Flannagan, R. S., R. E. Harrison, C. M. Yip, K. Jaqaman, and S. Grinstein. 2010. Dynamic macrophage “probing” is required for the efficient capture of phagocytic targets. *J Cell Biol* 191: 1205–1218.
370. Züllig, S., and M. O. Hengartner. 2004. Tickling macrophages, a serious business. *Science* (80-) 304: 1123–4.
371. Somersan, S., and N. Bhardwaj. 2001. Tethering and tickling: a new role for the phosphatidylserine receptor. *J Cell Biol* 155: 501–4.
372. Bezbradica, J. S., and R. Medzhitov. 2012. Role of ITAM signaling module in signal integration. *Curr Opin Immunol* 24: 58–66.
373. May, R. C., E. Caron, A. Hall, and L. M. Machesky. 2000. Involvement of the Arp2/3 complex in phagocytosis mediated by Fc γ R or CR3. *Nat Cell Biol* 2: 246–8.
374. Okazawa, H., S. Motegi, N. Ohyama, H. Ohnishi, T. Tomizawa, Y. Kaneko, P.-A. Oldenborg, O. Ishikawa, and T. Matozaki. 2005. Negative regulation of phagocytosis in macrophages by the CD47-SHPS-1 system. *J Immunol* 174: 2004–11.
375. Oldenborg, P., H. D. Gresham, and F. P. Lindberg. 2001. CD47-signal regulatory protein α (SIRP α) regulates Fc γ and complement receptor-mediated phagocytosis. *J Exp Med* 193: 855–

62.

376. Nakamura, K., A. Malykhin, and K. M. Coggeshall. 2002. The Src homology 2 domain-containing inositol 5-phosphatase negatively regulates Fc γ receptor-mediated phagocytosis through immunoreceptor tyrosine-based activation motif-bearing phagocytic receptors. *Blood* 100: 3374–3382.
377. Huang, Z., S. Hunter, M.-K. Kim, Z. K. Indik, and A. D. Schreiber. 2003. The effect of phosphatases SHP-1 and SHIP-1 on signaling by the ITIM- and ITAM-containing Fc γ receptors Fc γ RIIB and Fc γ RIIA. *J Leukoc Biol* 73: 823–829.
378. Syam, S., P. Mero, T. Pham, C. A. McIntosh, P. Bruhns, and J. W. Booth. 2010. Differential recruitment of activating and inhibitory Fc γ RII during phagocytosis. *J Immunol* 184: 2966–73.
379. Hilton, H. G., L. A. Guethlein, A. Goyos, N. Nemat-Gorgani, D. A. Bushnell, P. J. Norman, and P. Parham. 2015. Polymorphic HLA-C receptors balance the functional characteristics of KIR haplotypes. *J Immunol* 195: 3160–70.
380. Sanchez-Lockhart, M., A. V Rojas, M. M. Fettis, R. Bauserman, T. R. Higa, H. Miao, R. E. Waugh, and J. Miller. 2014. T cell receptor signaling can directly enhance the avidity of CD28 ligand binding. *PLoS One* 9: e89263.
381. Freedman, B. D., Q.-H. Liu, S. Somersan, M. I. Kotlikoff, and J. A. Punt. 1999. Receptor avidity and costimulation specify the intracellular Ca²⁺ signaling pattern in CD4+CD8+ thymocytes. *J Exp Med* 190: 943–52.
382. Vigano, S., D. T. Utzschneider, M. Perreau, G. Pantaleo, D. Zehn, and A. Harari. 2012. Functional avidity: a measure to predict the efficacy of effector T cells? *Clin Dev Immunol* 2012: 153863.
383. Ioannidou, K., P. Baumgaertner, P. O. Gannon, M. F. Speiser, M. Allard, M. Hebeisen, N. Rufer, and D. E. Speiser. 2017. Heterogeneity assessment of functional T cell avidity. *Sci Rep* 7: 44320.
384. Hilton, H. G., J. H. Blokhuis, L. A. Guethlein, P. J. Norman, and P. Parham. 2017. Resurrecting KIR2DP1: a key intermediate in the evolution of human inhibitory NK cell receptors that recognize HLA-C. *J Immunol* 198: 1961–73.
385. Smith, E. M., and J. D. Mueller. 2012. The statistics of protein expression ratios for cellular fluorescence studies. *Eur Biophys J* 41: 341–52.
386. Zhang, K., X. Li, Y. Ma, S. Zou, L. Yang, and M. Zhang. 2010. A curve fitting method of quantifying green fluorescent protein expression level in Escherichia coli. *J Microbiol Methods* 80: 172–7.
387. Lo, C.-A., I. Kays, F. Emran, T.-J. Lin, V. Cvetkovska, and B. E. Chen. 2015. Quantification of protein levels in single living cells. *Cell Rep* 13: 2634–44.
388. Zhu, J. W., T. Brdicka, T. R. Katsumoto, J. Lin, and A. Weiss. 2008. Structurally distinct phosphatases CD45 and CD148 both regulate B cell and macrophage immunoreceptor signaling. *Immunity* 28: 183–96.
389. Sendide, K., N. E. Reiner, J. S. I. Lee, S. Bourgoin, A. Talal, and Z. Hmama. 2005. Cross-talk between CD14 and complement receptor 3 promotes phagocytosis of mycobacteria:

- regulation by phosphatidylinositol 3-kinase and cytohesin-1. *J Immunol* 174: 4210–9.
390. Alloatti, A., F. Kotsias, A.-M. Pauwels, J.-M. Carpier, M. Jouve, E. Timmerman, L. Pace, P. Vargas, M. Maurin, U. Gehrman, L. Joannas, O. I. Vivar, A.-M. Lennon-Duménil, A. Savina, K. Gevaert, R. Beyaert, E. Hoffmann, and S. Amigorena. 2015. Toll-like receptor 4 engagement on dendritic cells restrains phago-lysosome fusion and promotes cross-presentation of antigens. *Immunity* 43: 1087–100.
391. Underhill, D. M. 2007. Collaboration between the innate immune receptors dectin-1, TLRs, and Nods. *Immunol Rev* 219: 75–87.
392. Kagan, J. C., and A. Iwasaki. 2012. Phagosome as the organelle linking innate and adaptive immunity. *Traffic* 13: 1053–61.
393. Kim, T. K., and J. H. Eberwine. 2010. Mammalian cell transfection: the present and the future. *Anal Bioanal Chem* 397: 3173–8.
394. Bacolla, A., G. Wang, A. Jain, N. A. Chuzhanova, R. Z. Cer, J. R. Collins, D. N. Cooper, V. A. Bohr, and K. M. Vasquez. 2011. Non-B DNA-forming sequences and WRN deficiency independently increase the frequency of base substitution in human cells. *J Biol Chem* 286: 10017–26.
395. Homann, S., C. Hofmann, A. M. Gorin, H. C. X. Nguyen, D. Huynh, P. Hamid, N. Maithel, V. Yacoubian, W. Mu, A. Kossyvakis, S. Sen Roy, O. O. Yang, and T. Kelesidis. 2017. A novel rapid and reproducible flow cytometric method for optimization of transfection efficiency in cells. *PLoS One* 12: e0182941.
396. Joshi, T., L. P. Ganesan, X. Cao, and S. Tridandapani. 2006. Molecular analysis of expression and function of hFcγRIIb1 and b2 isoforms in myeloid cells. *Mol Immunol* 43: 839–50.
397. Chen, J., M.-C. Zhong, H. Guo, D. Davidson, S. Mishel, Y. Lu, I. Rhee, L.-A. Pérez-Quintero, S. Zhang, M.-E. Cruz-Munoz, N. Wu, D. C. Vinh, M. Sinha, V. Calderon, C. A. Lowell, J. S. Danska, and A. Veillette. 2017. SLAMF7 is critical for phagocytosis of haematopoietic tumour cells via Mac-1 integrin. *Nature* 544: 493–7.
398. Greenberg, S., P. Chang, D.-C. Wang, R. Xavier, and B. Seed. 1996. Clustered syk tyrosine kinase domains trigger phagocytosis. *Proc Natl Acad Sci U S A* 93: 1103–7.
399. Bakalar, M. H., A. M. Joffe, E. M. Schmid, S. Son, M. Podolski, and D. A. Fletcher. 2018. Size-dependent segregation controls macrophage phagocytosis of antibody-opsonized targets. *Cell* 174: 131–42.
400. Alakoskela, J.-M., A. L. Koner, D. Rudnicka, K. Kohler, M. Howarth, and D. M. Davis. 2011. Mechanisms for size-dependent protein segregation at immune synapses assessed with molecular rulers. *Biophys J* 100: 2865–74.
401. Jaiswal, S., C. H. M. Jamieson, W. W. Pang, C. Y. Park, M. P. Chao, R. Majeti, D. Traver, N. van Rooijen, and I. L. Weissman. 2009. CD47 is upregulated on circulating hematopoietic stem cells and leukemia cells to avoid phagocytosis. *Cell* 138: 271–85.
402. Neher, J. J., U. Neniskyte, J.-W. Zhao, A. Bal-Price, A. M. Tolkovsky, and G. C. Brown. 2011. Inhibition of microglial phagocytosis is sufficient to prevent inflammatory neuronal death.

J Immunol 186: 4973–83.

403. Brown, G. C., and J. J. Neher. 2012. Eaten alive! Cell death by primary phagocytosis: “phagoptosis.” *Trends Biochem Sci* 37: 325–32.

404. Hayashi, T., H. Morohashi, and M. Hatakeyama. 2013. Bacterial EPIYA effectors - where do they come from? What are they? Where are they going? *Cell Microbiol* 15: 377–85.

405. Uribe-Querol, E., and C. Rosales. 2017. Control of phagocytosis by microbial pathogens. *Front Immunol* 8: 1368.

406. Van Avondt, K., N. M. van Sorge, and L. Meyaard. 2015. Bacterial immune evasion through manipulation of host inhibitory immune signaling. *PLoS Pathog* 11: e1004644.

407. Chan, K. R., E. Z. Ong, H. C. Tan, S. L.-X. Zhang, Q. Zhang, K. F. Tang, N. Kaliaperumal, A. P. C. Lim, M. L. Hibberd, S. H. Chan, J. E. Connolly, M. N. Krishnan, S. M. Lok, B. J. Hanson, C.-N. Lin, and E. E. Ooi. 2014. Leukocyte immunoglobulin-like receptor B1 is critical for antibody-dependent dengue. *Proc Natl Acad Sci U S A* 111: 2722–7.

408. Underhill, D. M., and A. Ozinsky. 2002. Phagocytosis of microbes: complexity in action. *Annu Rev Immunol* 20: 825–852.

409. Myster, F., L. Palmeira, O. Sorel, F. Bouillenne, E. DePauw, I. Schwartz-Cornil, A. Vanderplasschen, and B. G. Dewals. 2015. Viral semaphorin inhibits dendritic cell phagocytosis and migration but is not essential for gammaherpesvirus-induced lymphoproliferation in malignant catarrhal fever. *J Virol* 89: 3630–47.

410. Nainu, F., A. Shiratsuchi, and Y. Nakanishi. 2017. Induction of apoptosis and subsequent phagocytosis of virus-infected cells as an antiviral mechanism. *Front Immunol* 8: 1220.

411. Ren, Y., F. A. Khan, N. S. Pandupuspitasari, and S. Zhang. 2017. Immune evasion strategies of pathogens in macrophages: the potential for limiting pathogen transmission. *Curr Issues Mol Biol* 21: 21–40.

412. Fanger, N. A., D. Cosman, L. Peterson, S. C. Braddy, C. R. Maliszewski, and L. Borges. 1998. The MHC class I binding proteins LIR-1 and LIR-2 inhibit Fc receptor-mediated signaling in monocytes. *Eur J Immunol* 28: 3423–34.

413. Ikeda, H., H. Okazawa, H. Ohnishi, Y. Murata, P.-A. Oldenburg, and T. Matozaki. 2006. Mutational analysis of the mechanism of negative regulation by SRC homology 2 domain-containing protein tyrosine phosphatase substrate-1 of phagocytosis in macrophages. *J Immunol* 177: 3123–32.

414. Tsai, R. K., and D. E. Discher. 2008. Inhibition of “self” engulfment through deactivation of myosin-II at the phagocytic synapse between human cells. *J Cell Biol* 180: 989–1003.

415. Gitik, M., R. Kleinhaus, S. Hadas, F. Reichert, and S. Rotshenker. 2014. Phagocytic receptors activate and immune inhibitory receptor SIRP α inhibits phagocytosis through paxillin and cofilin. *Front Cell Neurosci* 8: 104.

416. Sayós, J., A. Martínez-Barriocanal, F. Kitzig, T. Bellón, and M. López-Botet. 2004. Recruitment of C-terminal Src kinase by the leukocyte inhibitory receptor CD85j. *Biochem Biophys Res Commun* 324: 640–7.

417. Verbrugge, A., E. S. K. Rijkers, T. de Ruiter, and L. Meyaard. 2006. Leukocyte-associated

Ig-like receptor-1 has SH2 domain-containing phosphatase-independent function and recruits C-terminal Src kinase. *Eur J Immunol* 36: 190–8.

418. Dodd, D. A., R. G. Worth, M. K. Rosen, S. Grinstein, N. S. C. van Oers, and E. J. Hansen. 2014. The *Haemophilus ducreyi* LspA1 protein inhibits phagocytosis by using a new mechanism involving activation of C-terminal Src kinase. *MBio* 5: e01178-14.

419. Safari, F., N. Murata-Kamiya, Y. Saito, and M. Hatakeyama. 2011. Mammalian Pragmin regulates Src family kinases via the Glu-Pro-Ile-Tyr-Ala (EPIYA) motif that is exploited by bacterial effectors. *Proc Natl Acad Sci U S A* 108: 14938–43.

420. Senda, Y., N. Murata-Kamiya, and M. Hatakeyama. 2016. C-terminal Src kinase-mediated EPIYA phosphorylation of Pragmin creates a feed-forward C-terminal Src kinase activation loop that promotes cell motility. *Cancer Sci* 107: 972–80.

421. Northrop, J. P., M. J. Pustelnik, A. T. Lu, and J. R. Grove. 1996. Characterization of the roles of SH2 domain-containing proteins in T-lymphocyte activation by using dominant negative SH2 domains. *Mol Cell Biol* 16: 2255–63.

422. Sweeney, M. C., A.-S. Wavreille, J. Park, J. P. Butchar, S. Tridandapani, and D. Pei. 2005. Decoding protein-protein interactions through combinatorial chemistry: sequence specificity of SHP-1, SHP-2, and SHIP SH2 domains. *Biochemistry* 44: 14932–47.

423. Hays, J. L., and S. J. Watowich. 2004. Oligomerization-dependent changes in the thermodynamic properties of the TPR-MET receptor tyrosine kinase. *Biochemistry* 43: 10570–8.

424. Swanson, J. A., and A. D. Hoppe. 2004. The coordination of signaling during Fc receptor-mediated phagocytosis. *J Leukoc Biol* 76: 1093–103.

425. Futosi, K., and A. Mócsai. 2016. Tyrosine kinase signaling pathways in neutrophils. *Immunol Rev* 273: 121–39.

426. Yanagi, S., R. Inatome, T. Takano, and H. Yamamura. 2001. Syk expression and novel function in a wide variety of tissues. *Biochem Biophys Res Commun* 288: 495–8.

427. Fenteany, G., and M. Glogauer. 2004. Cytoskeletal remodeling in leukocyte function. *Curr Opin Hematol* 11: 15–24.

428. dos Remedios, C. G., D. Chhabra, M. Kekic, I. V Dedova, M. Tsubakihara, D. A. Berry, and N. J. Nosworthy. 2003. Actin binding proteins: regulation of cytoskeletal microfilaments. *Physiol Rev* 83: 433–73.

429. Sarkar, P., and A. Chattopadhyay. 2019. Exploring membrane organization at varying spatiotemporal resolutions utilizing fluorescence-based approaches: implications in membrane biology. *Phys Chem Chem Phys* 21: 11554–63.

430. Diakowski, W., M. Grzybek, and A. F. Sikorski. 2006. Protein 4.1, a component of the erythrocyte membrane skeleton and its related homologue proteins forming the protein 4.1/FERM superfamily. *Folia Histochem Cytobiol* 44: 231–48.

431. Hoover, K. B., and P. J. Bryant. 2000. The genetics of the protein 4.1 family: organizers of the membrane and cytoskeleton. *Curr Opin Cell Biol* 12: 229–34.

432. Scott, C., G. W. Phillips, and A. J. Baines. 2001. Properties of the C-terminal domain of 4.1 proteins. *Eur J Biochem* 268: 3709–17.

433. Baines, A. J., H.-C. Lu, and P. M. Bennett. 2014. The protein 4.1 family: hub proteins in animals for organizing membrane proteins. *Biochim Biophys Acta* 1838: 605–619.
434. Lu, H. K., C. Rentero, M. J. Raftery, L. Borges, K. Bryant, and N. Tedla. 2009. Leukocyte Ig-like receptor B4 (LILRB4) is a potent inhibitor of FcγRI-mediated monocyte activation via dephosphorylation of multiple kinases. *J Biol Chem* 284: 34839–48.
435. Park, M., M. J. Raftery, P. S. Thomas, C. L. Geczy, K. Bryant, and N. Tedla. 2016. Leukocyte immunoglobulin-like receptor B4 regulates key signalling molecules involved in FcγRI-mediated clathrin-dependent endocytosis and phagocytosis. *Sci Rep* 6: 35085.
436. Sain, N., G. Tiwari, and D. Mohanty. 2016. Understanding the molecular basis of substrate binding specificity of PTB domains. *Sci Rep* 6: 31418.
437. Ninomiya, N., K. K. Hazeki, Y. Fukui, T. Seya, T. Okada, O. Hazeki, and M. Ui. 1994. Involvement of phosphatidylinositol 3-kinase in Fcγ receptor signaling. *J Biol Chem* 269: 22732–7.
438. Utomo, A., X. Cullere, M. Glogauer, W. Swat, and T. N. Mayadas. 2006. Vav proteins in neutrophils are required for FcγR-mediated signaling to Rac GTPases and nicotinamide adenine dinucleotide phosphate oxidase component p40(phox). *J Immunol* 177: 6388–97.
439. Vaillancourt, M., S. Levasseur, M.-L. Tremblay, L. Marois, E. Rollet-Labelle, and P. H. Naccache. 2006. The Src homology 2-containing inositol 5-phosphatase 1 (SHIP1) is involved in CD32a signaling in human neutrophils. *Cell Signal* 18: 2022–32.
440. Desplat, V., V. Lagarde, F. Belloc, C. Chollet, T. Leguay, J.-M. Pasquet, V. Praloran, and F.-X. Mahon. 2004. Rapid detection of phosphotyrosine proteins by flow cytometric analysis in Bcr-Abl-positive cells. *Cytom Part A* 62: 35–45.
441. Lösing, M., I. Goldbeck, B. Manno, T. Oellerich, T. Schnyder, H. Bohnenberger, B. Stork, H. Urlaub, F. D. Batista, J. Wienands, and M. Engelke. 2013. The Dok-3/Grb2 protein signal module attenuates Lyn kinase-dependent activation of Syk kinase in B cell antigen receptor microclusters. *J Biol Chem* 288: 2303–13.
442. Osborne, D. G., and S. A. Wetzel. 2012. Trogocytosis results in sustained intracellular signaling in CD4+ T cells. *J Immunol* 189: 4728–39.
443. Roux, K. J., D. I. Kim, and B. Burke. 2013. BioID: A screen for protein-protein interactions. *Curr Protoc Protein Sci* 1–14.
444. Stuge, T. B., M. R. Wilson, H. Zhou, K. S. Barker, E. Bengtén, G. Chinchar, N. W. Miller, and L. W. Clem. 2000. Development and analysis of various clonal alloantigen-dependent cytotoxic cell lines from channel catfish. *J Immunol* 164: 2971–7.
445. Zhou, H., T. B. Stuge, N. W. Miller, E. Bengten, J. P. Naftel, J. M. Bernanke, V. G. Chinchar, L. W. Clem, and M. Wilson. 2001. Heterogeneity of channel catfish CTL with respect to target recognition and cytotoxic mechanisms employed. *J Immunol* 167: 1325–32.
446. Vasconcelos, Z., S. Müller, D. Guipouy, W. Yu, C. Christophe, S. Gadat, S. Valitutti, and L. Dupré. 2015. Individual human cytotoxic T lymphocytes exhibit intraclonal heterogeneity during sustained killing. *Cell Rep* 11: 1474–85.
447. Rahmouni, S., T. Vang, A. Alonso, S. Williams, M. van Stipdonk, C. Soncini, M.

- Moutschen, S. P. Schoenberger, and T. Mustelin. 2005. Removal of C-terminal SRC kinase from the immune synapse by a new binding protein. *Mol Cell Biol* 25: 2227–41.
448. Sun, F., E. Peatman, C. Li, S. Liu, Y. Jiang, Z. Zhou, and Z. Liu. 2012. Transcriptomic signatures of attachment, NF- κ B suppression and IFN stimulation in the catfish gill following columnaris bacterial infection. *Dev Comp Immunol* 38: 169–80.
449. Evelyn, T. P. 1997. A historical review of fish vaccinology. *Dev Biol Stand* 90: 3–12.
450. Van Muiswinkel, W. B., and M. Nakao. 2014. A short history of research on immunity to infectious diseases in fish. *Dev Comp Immunol* 43: 130–50.
451. Gudding, R., and W. B. Van Muiswinkel. 2013. A history of fish vaccination: science-based disease prevention in aquaculture. *Fish Shellfish Immunol* 35: 1683–8.
452. Nations, U. 2017. Factsheet: people and oceans. In *The Ocean Conference* New York. 1–7.
453. FAO. 2018. *The state of world fisheries and aquaculture 2018 - meeting the sustainable development goals*, 2018th ed. Rome.
454. Service, N. M. F. 2018. *Fisheries of the United States, 2017*, 2017th ed. (M. Liddel, and M. Yench, eds).
455. Canada, D. of fisheries and oceans. 2018. Aquaculture - production quantities and values. .
456. Zhang, Z., H. Chi, and R. A. Dalmo. 2019. Trained innate immunity of fish is a viable approach in larval aquaculture. *Front Immunol* 10: 42.
457. Arts, R. J. W., L. A. B. Joosten, and M. G. Netea. 2018. The potential role of trained immunity in autoimmune and autoinflammatory disorders. *Front Immunol* 9: 298.
458. Ifrim, D. C., J. Quintin, L. A. B. Joosten, C. Jacobs, T. Jansen, L. Jacobs, N. A. R. Gow, D. L. Williams, J. W. M. van der Meer, and M. G. Netea. 2014. Trained immunity or tolerance: opposing functional programs induced in human monocytes after engagement of various pattern recognition receptors. *Clin Vaccine Immunol* 21: 534–45.
459. Lau, C. M., N. M. Adams, C. D. Geary, O.-E. Weizman, M. Rapp, Y. Pritykin, C. S. Leslie, and J. C. Sun. 2018. Epigenetic control of innate and adaptive immune memory. *Nat Immunol* 19: 963–72.
460. Dalmo, R. A., B. Martinsen, T. E. Horsberg, A. Ramstad, C. Syvertsen, R. Seljelid, and K. Ingebrigtsen. 1998. Prophylactic effect of $\beta(1,3)$ -D-glucan (laminaran) against experimental *Aeromonas salmonicida* and *Vibrio salmonicida* infections. *J Fish Dis* 21: 459–62.
461. Petit, J., and G. F. Wiegertjes. 2016. Long-lived effects of administering β -glucans: indications for trained immunity in fish. *Dev Comp Immunol* 64: 93–102.
462. Rojo-Cebreros, A. H., L. Ibarra-Castro, and J. M. Martínez-Brown. 2018. Immunostimulation and trained immunity in marine fish larvae. *Fish Shellfish Immunol* 80: 15–21.
463. Yoder, J. A., M. E. Nielsen, C. T. Amemiya, and G. W. Litman. 2002. Zebrafish as an immunological model system. *Microbes Infect* 4: 1469–78.
464. Traver, D., P. Herbomel, E. E. Patton, R. D. Murphey, J. A. Yoder, G. W. Litman, A. Catic, C. T. Amemiya, L. I. Zon, and N. S. Trede. 2003. The zebrafish as a model organism to study development of the immune system. *Adv Immunol* 81: 253–330.

465. Crowhurst, M. O., J. E. Layton, and G. J. Lieschke. 2002. Developmental biology of zebrafish myeloid cells. *Int J Dev Biol* 46: 483–92.
466. Astin, J. W., P. Keerthisinghe, L. Du, L. E. Sanderson, K. E. Crosier, P. S. Crosier, and C. J. Hall. 2017. Innate immune cells and bacterial infection in zebrafish. *Methods Cell Biol* 138: 31–60.
467. Dee, C. T., R. T. Nagaraju, E. I. Athanasiadis, C. Gray, L. F. del Ama, S. A. Johnston, C. J. Secombes, A. Cvejic, and A. F. L. Hurlstone. 2016. CD4-transgenic zebrafish reveal tissue-resident Th2- and regulatory T cell-like populations and diverse mononuclear phagocytes. *J Immunol* 197: 3520–30.
468. Choorapoikayil, S., J. Overvoorde, and J. der Hertog. 2013. Deriving cell lines from zebrafish embryos and tumors. *Zebrafish* 10: 316–25.
469. Bradford, C. S., L. Sun, P. Collodi, and D. W. Barnes. 1994. Cell cultures from zebrafish embryos and adult tissues. *J Tissue Cult Methods* 16: 99–107.
470. Katzenback, B. A., and M. Belosevic. 2009. Isolation and functional characterization of neutrophil-like cells, from goldfish (*Carassius auratus* L.) kidney. *Dev Comp Immunol* 33: 601–11.
471. Hodgkinson, J. W., J.-Q. Ge, B. A. Katzenback, J. J. Havixbeck, D. R. Barreda, J. L. Stafford, and M. Belosevic. 2015. Development of an in vitro model system to study the interactions between *Mycobacterium marinum* and teleost neutrophils. *Dev Comp Immunol* 53: 349–57.
472. Rajagopalan, S., and E. O. Long. 2012. KIR2DL4 (CD158d): an activation receptor for HLA-G. *Front Immunol* 3: 258.
473. Wilson, T. J., A. Fuchs, and M. Colonna. 2012. Human FcRL4 and FcRL5 are receptors for IgA and IgG. *J Immunol* 188: 4741–5.
474. Franco, A., B. Damdinsuren, T. Ise, J. Dement-Brown, H. Li, S. Nagata, and M. Tolnay. 2013. Human Fc receptor-like 5 binds intact IgG via mechanisms distinct from those of Fc receptors. *J Immunol* 190: 5739–46.
475. Schreeder, D. M., J. P. Cannon, J. Wu, R. Li, M. A. Shakhmatov, and R. S. Davis. 2010. FcR-like 6 is an MHC class II receptor. *J Immunol* 185: 23–7.
476. Kubagawa, H., P. D. Burrows, and M. D. Cooper. 1997. A novel pair of immunoglobulin-like receptors expressed by B cells and myeloid cells. *Proc Natl Acad Sci U S A* 94: 5261–5266.
477. Nakamura, A., E. Kobayashi, and T. Takai. 2004. Exacerbated graft-versus-host disease in *Pirb*^{-/-} mice. *Nat Immunol* 5: 623–9.
478. Hayami, K., D. Fukuta, Y. Nishikawa, Y. Yamashita, M. Inui, Y. Ohyama, M. Hikida, H. Ohmori, and T. Takai. 1997. Molecular cloning of a novel murine cell-surface glycoprotein homologous to killer cell inhibitory receptors. *J Biol Chem* 272: 7320–7.
479. Glynn Jr, D., H. Kubagawa, and M. D. Cooper. 2000. Paired Ig-like receptor homologs in birds and mammals share a common ancestor with mammalian Fc receptors. *Proc Natl Acad Sci U S A* 97: 13245–50.
480. Viertlboeck, B. C., S. Schweinsberg, M. A. Hanczaruk, R. Schmitt, L. Du Pasquier, F. W.

- Herberg, and T. W. Göbel. 2007. The chicken leukocyte receptor complex encodes a primordial, activating, high-affinity IgY Fc receptor. *Proc Natl Acad Sci U S A* 104: 11718–23.
481. Cannon, J. P., R. N. Haire, A. T. Magis, D. D. Eason, K. N. Winfrey, J. A. H. Prada, K. M. Bailey, J. Jakoncic, G. W. Litman, and D. A. Ostrov. 2008. A bony fish immunological receptor of the NITR multigene family mediates allogeneic recognition. *Immunity* 29: 228–37.
482. Caberoy, N. B., G. Alvarado, J.-L. Bigcas, and W. Li. 2012. Galectin-3 is a new MerTK-specific eat-me signal. *J Cell Physiol* 227: 401–7.
483. Beppler, J., S. Ben Mkaddem, J. Michaloski, R. V. Honorato, I. T. Velasco, P. S. L. de Oliveira, R. J. Giordano, R. C. Monteiro, and F. Pinheiro da Silva. 2016. Negative regulation of bacterial killing and inflammation by two novel CD16 ligands. *Eur J Immunol* 46: 1926–35.
484. Li, W. 2012. Eat-me signals: keys to molecular phagocyte biology and “appetite” control. *J Cell Physiol* 227: 1291–7.
485. Yabe, R., H. Tateno, and J. Hirabayashi. 2010. Frontal affinity chromatography analysis of constructs of DC-SIGN, DC-SIGNR and LSECTin extend evidence for affinity to agalactosylated N-glycans. *FEBS J* 277: 4010–26.
486. Savas, J. N., J. De Wit, D. Comoletti, R. Zemla, A. Ghosh, and J. R. Yates 3rd. 2014. Ecto-Fc MS identifies ligand-receptor interactions through extracellular domain Fc fusion protein baits and shotgun proteomic analysis. *Nat Protoc* 9: 2061–74.
487. Aebersold, R., M. Babu, V. Bhandari, S. Bowden, C. Bundalovic-Torma, C. Calmettes, C. S. Chan, T. N. Chernikova, C. A. Cooper, V. Deineko, K. Dufresne, A. Emili, P. N. Golyshin, A. Gagarinova, O. V Golyshina, W. A. Houry, A. Judd, A. Kumar, M. J. Lemieux, I. Libourel, I. L. Mainprize, T. F. Moraes, G. Moreno-Hagelsieb, H. Mori, A. Muto, N. N. Nickerson, Y. Otsuka, R. Panigrahi, C. Paradis-Bleau, J. Parkinson, L. Parts, A. Popovic, S. V. Rajagopala, G. Santoya, O. T. Schubert, R. Takeuchi, A. Tchigvintsev, H. Tran, R. J. Turner, J. Vlasblom, J. T. Wade, O. Wagih, B. L. Wanner, M. M. Yakimov, A. F. Yakunin, and K. Yokoyama. 2015. *Prokaryotic systems biology*, (N. J. Krogan, and M. Babu, eds). Springer International Publishing Switzerland, London, United States.
488. Felgueiras, J., J. V. Silva, and M. Fardilha. 2018. Adding biological meaning to human protein-protein interactions identified by yeast two-hybrid screenings: a guide through bioinformatics tools. *J Proteomics* 171: 127–40.